Research Insights

Attractors and Higher Dimensions in Population and Molecular Biology

Emerging Research and Opportunities

Gennadiy Vladimirovich Zhizhin

Attractors and Higher Dimensions in Population and Molecular Biology:

Emerging Research and Opportunities

Gennadiy Vladimirovich Zhizhin
Russian Academy of Natural Sciences, Russia

A volume in the Advances in Bioinformatics and Biomedical Engineering (ABBE) Book Series

Published in the United States of America by
IGI Global
Engineering Science Reference (an imprint of IGI Global)
701 E. Chocolate Avenue
Hershey PA, USA 17033
Tel: 717-533-8845
Fax: 717-533-8661
E-mail: cust@igi-global.com
Web site: http://www.igi-global.com

Library of Congress Cataloging-in-Publication Data

Names: Zhizhin, G. V. (Gennadi?i Vladimirovich), author.
Title: Attractors and higher dimensions in population and molecular biology : emerging research and opportunities / by Gennadiy Vladimirovich Zhizhin.
Description: Hershey PA : Engineering Science Reference, [2020] | Includes bibliographical references.
Identifiers: LCCN 2019005485| ISBN 9781522596516 (hardcover) | ISBN 9781522596530 (ebook) | ISBN 9781522596523 (softcover)
Subjects: LCSH: Mendel's law. | Genetics. | Hybridization. | Plant hybridization.
Classification: LCC QH430 .Z45 2020 | DDC 576.5/2--dc23 LC record available at https://lccn.loc.gov/2019005485

This book is published in the IGI Global book series Advances in Bioinformatics and Biomedical Engineering (ABBE) (ISSN: 2327-7033; eISSN: 2327-7041)

British Cataloguing in Publication Data
A Cataloguing in Publication record for this book is available from the British Library.

Advances in Bioinformatics and Biomedical Engineering (ABBE) Book Series

ISSN:2327-7033
EISSN:2327-7041

Editor-in-Chief: Ahmad Taher Azar, Benha University, Egypt

MISSION

The fields of biology and medicine are constantly changing as research evolves and novel engineering applications and methods of data analysis are developed. Continued research in the areas of bioinformatics and biomedical engineering is essential to continuing to advance the available knowledge and tools available to medical and healthcare professionals.

The **Advances in Bioinformatics and Biomedical Engineering (ABBE) Book Series** publishes research on all areas of bioinformatics and bioengineering including the development and testing of new computational methods, the management and analysis of biological data, and the implementation of novel engineering applications in all areas of medicine and biology. Through showcasing the latest in bioinformatics and biomedical engineering research, ABBE aims to be an essential resource for healthcare and medical professionals.

COVERAGE

- Bayesian Methods
- Databases
- Molecular Engineering
- Biomechanical Engineering
- Tissue Engineering
- Artificial Organs
- Orthopedic Bioengineering
- Genetic Engineering
- Biomedical Sensors
- Genetics

IGI Global is currently accepting manuscripts for publication within this series. To submit a proposal for a volume in this series, please contact our Acquisition Editors at Acquisitions@igi-global.com or visit: http://www.igi-global.com/publish/.

The Advances in Bioinformatics and Biomedical Engineering (ABBE) Book Series (ISSN 2327-7033) is published by IGI Global, 701 E. Chocolate Avenue, Hershey, PA 17033-1240, USA, www.igi-global.com. This series is composed of titles available for purchase individually; each title is edited to be contextually exclusive from any other title within the series. For pricing and ordering information please visit http://www.igi-global.com/book-series/advances-bioinformatics-biomedical-engineering/73671. Postmaster: Send all address changes to above address.

Titles in this Series

For a list of additional titles in this series, please visit:
https://www.igi-global.com/book-series/advances-bioinformatics-biomedical-engineering/73671

Computational Models for Biomedical Reasoning and Problem Solving
Chung-Hao Chen (Old Dominion University, USA) and Sen-Ching Samson Cheung (University of Kentucky, USA)
Medical Information Science Reference • ©2019 • 353pp • H/C (ISBN: 9781522574675) • US $275.00

Medical Data Security for Bioengineers
Butta Singh (Guru Nanak Dev University, India) Barjinder Singh Saini (Dr. B. R. Ambedkar National Institute of Technology, India) Dilbag Singh (Dr. B. R. Ambedkar National Institute of Technology, India) and Anukul Pandey (Dumka Engineering College, India)
Medical Information Science Reference • ©2019 • 340pp • H/C (ISBN: 9781522579526) • US $365.00

Examining the Causal Relationship Between Genes, Epigenetics, and Human Health
Oscar J. Wambuguh (California State University – East Bay, USA)
Medical Information Science Reference • ©2019 • 603pp • H/C (ISBN: 9781522580669) • US $295.00

Expert System Techniques in Biomedical Science Practice
Prasant Kumar Pattnaik (KIIT University, India) Aleena Swetapadma (KIIT University, India) and Jay Sarraf (KIIT University, India)
Medical Information Science Reference • ©2018 • 280pp • H/C (ISBN: 9781522551492) • US $205.00

Nature-Inspired Intelligent Techniques for Solving Biomedical Engineering Problems
Utku Kose (Suleyman Demirel University, Turkey) Gur Emre Guraksin (Afyon Kocatepe University, Turkey) and Omer Deperlioglu (Afyon Kocatepe University, Turkey)
Medical Information Science Reference • ©2018 • 381pp • H/C (ISBN: 9781522547693) • US $255.00

For an entire list of titles in this series, please visit:
https://www.igi-global.com/book-series/advances-bioinformatics-biomedical-engineering/73671

701 East Chocolate Avenue, Hershey, PA 17033, USA
Tel: 717-533-8845 x100 • Fax: 717-533-8661
E-Mail: cust@igi-global.com • www.igi-global.com

Dedicated to my parents

Table of Contents

Preface

Back in 1905 S.S. Chetverikov (1905) in the *Diary of the Zoological Department of the Imperial Society of Lovers of Natural Science, Anthropology and Ethnography* noted that locust invasions into Russia are waves of life, thus emphasizing the important property of living matter - the ability to spread in waves. The mathematical study of the question of the propagation of the waves of biological populations originates from the work of A.N. Kolmogorov, I.G. Petrovsky, & N.S. Piskunova (Kolmogorov, Petrovsky, & Piskunov, 1937). In this work, the nonstationary diffusion equation with the source term modeling the reproduction process of a biological population was studied, and the diffusion corresponded to the chaotic mobility of individuals. The possibility of applying this work it is limited by the framework of a very simple model of the biological population: the process of feeding of organisms was not taken into account, the possibility of their directional movement (taxis), the patterns of reproduction and dying were taken in the simplest form. The formation of the waves of biological populations is the result of the manifestation of the important quality of living nature - its self - organization. Waves of biological populations can be of two types: a wave of territory conquest and a solitary wave (soliton). The wave of conquest is necessary for the resettlement of organisms over a large area. A solitary wave is the search for food for a multitude of individuals forming a population of finite size when it moves across the territory.

A vivid example of a wave of conquest in nature can be the spread of blue - green algae over the surface of the Earth several billion years ago when they emerge from the ocean (Elenkin, 1936; Zavarzin, 2002). This ensured the development of life on Earth. The flight of the gregarious locust is a vivid example of a solitary wave of a population.

Mathematical models of wave propagation of the various biological populations (communities of biological organisms) were built and studied in the number works (Zhizhin & Bolshakova, 2000 a, b, c; Zhizhin, 2004, 2005,

2012, 2014; Zhizhin, & Selikhovkin, 2012). This monograph presents studies of stationary waves of conquest and solitary waves in logistic populations and populations of Ollie, as well as a study of the flight model of the herd locust.

Nonlinear waves, which include waves of biological populations, are mobile dissipative structures (Svirezhev, 1987). The dissipative structures support themselves at the expense of energy consumption from the environment. Dissipative structures can also be fixed. They can have a different form and are called generally attractors. These are the formations that systems seeking over time (including stationary standing and traveling waves). The desire for living matter to equilibrium is also an important feature of them. An attractor can be a special point in the phase space of the system - the equilibrium position. It can be a limit cycle on which the trajectories of the phase space are wound, and it can be a torus. Attractors can form continuous manifolds of dimension n. In 1971 the term strange attractor appeared. They denote the attractor, to which the trajectories of the phase space tend in a chaotic way, approaching and moving away from it. This is accompanied by bifurcation of the special points of the phase space. The system of equations studied in 1971 was a model of turbulence (the Lorentz equations). With some form of functions included in the Lorentz equations, the system describes the dynamics of the biological population consisting of predators and preys (Volterra, 1931). Currently, a large scientific literature is devoted to the mathematical study of the strange attractors (see, for example, Marsden, & McCracken, 1976; Kolmogorov, & Novikov, 1981). Affinity by its nature is affirmed of the strange attractors and fractal attractors (Mandelbrot, 2004).

Thus, in the populations of living organisms in which they are born and die due to death from other organisms or adverse climatic conditions, an equilibrium occurs sooner or later, i.e. the system tends to attractor. In some cases, this attractor may be strange. However, what happens in populations if conditions are created that significantly reduce the likelihood of death of organisms? G. Mendel created such conditions, when in 1865 he conducted his experiments on the crossing of plants with different (constant - different) characters (Mendel, 1965). Naturally, under these conditions, the number of hybrids increases from generation to generation. This was the reason for Hardy to believe that there is no equilibrium position in this system. To get it, Hardy introduced a number of strong, unsupported assumptions (Hardy, 1908). It is known that the experiments of G. Mendel became the basis for the creation of genetics as a science. In this paper, for the first time, a mathematical model of G. Mendel's experiments on hybridization of plants with an arbitrary number of constant - distinct characters for any number of

generations was constructed. This greatly expands the ability to determine the asymptotic nature of the sequence of experiments that G. Mendel could not afford. It has been shown that with an increase in the number of generations in a plant population, the number of phenotypes of organisms with different sets of genes quickly level up. With the increase in the number of generations and the absence of the death of organisms, these quantities increase synchronously, remaining almost equal to each other. This can be considered as establishing an equilibrium between plant phenotypes. In this case, the trajectories of the process in a multidimensional phase space with coordinates in the form of inverse quantities of phenotypes tend to an isolated stable equilibrium position of the node type at the origin.

If the death of organisms is possible, then equilibrium in general is achieved with final concentrations of the organisms. The book considers temporal and spatial dissipative structures in the systems of marine and oceanic phytoplankton and zooplankton, since plankton has a significant impact on the formation of climate on Earth. It is proved that the widespread mechanistic models of plankton, equating the mobility of individuals of the plankton population with the turbulent diffusion coefficient of seas and oceans, do not correspond to reality. It is shown that in violation of the processes of self - regulation between plankton populations, caused, for example, by eutrophication, the extinction regime of a population begins. Bifurcation analysis of the equations describing the spatial distribution of the concentrations of plankton components found that the most interesting area of the system parameters is a cloud in which the equilibrium position of plankton has two pairs of conjugate purely imaginary eigenvalues. See, the system of equations even after linearization in the neighborhood of the equilibrium position, in contrast to the problem considered by V. I. Arnold (Arnold, 1976) does not break up into two systems. There are no methods for analyzing such points in the modern theory of dynamical systems (Katok, & Hasselblat, 1999). These points were initially excluded from the analysis in the works of A. M. Lyapunov (Lyapunov, 1935), A. A. Andronov (Andronov and others, 1966, 1967), N. N. Bautin (Bautin, 1984).

A numerical study of trajectories in the four - dimensional phase space in a sufficiently large neighborhood of such equilibrium states revealed the existence of a strange attractor of previously unknown form (Zhizhin, 2005). It is a multilayer attractor, each layer of which is also a strange attractor with two characteristic points for a given layer, common to all trajectories of this layer. Each layer of the multilayer strange attractor corresponds to the dissipative structure of plankton, covering the surface of the aquatic environment.

It can be said that another important property of living systems, as it was established in the last monographs of author (Zhizhin, 2017, 2008), is the creation of a space of higher dimensionality due to the higher dimension of their constituent molecules. It should be emphasized that here we are not talking about Euclidean space, which by definition is infinite and three - dimensional. Based on the definition of the dimension of convex polytopes using the Euler – Poincaré formula (Poincaré, 1895), one can calculate the dimension of a convex body (in this case, a molecule), counting each atom (or functional group) as the vertices of the polytope. Then almost all compounds formed by chemical elements have the highest dimension (Zhizhin, 2017). This is especially important for biomolecules that have a complex structure. The geometry of B. Riemann is applicable here. In his famous lecture "On the Hypotheses that Lie at The Foundations of Geometry" (Riemann, 1854) he introduces the concept of n – extended manifold. It is essential, that n – dimensional extension it is determined by Riemann without introduction of infinite spaces.

Thus, the existence of closed objects of higher dimension (molecules) in a space of lower dimension does not contradict Riemann`s geometry, which assumes the boundedness of a space with a given dimension. Therefore, all studies in molecular biology in this work take into account this fact. The dimensions of the compounds of biogenic elements have been calculated, i.e. chemical elements present in living organisms and necessary for them to live. The dimensions of various types of biomolecules, including nucleic acid molecules, are calculated. A simplified three - dimensional model of this molecule and a simplified three - dimensional model of nucleic acids were built for the first time on the basis of a five - carbon sugar molecule model having dimension 12. This is important for visualizing the structure of nucleic acids. The calculations of the basic geometric characteristics of nucleic acid molecules according to this model are in good agreement with the experimental data obtained by Watson and Crick (1953). It has been proven that five - carbon sugar molecules bound by nitrogenous bases and located in two helices of one nucleic acid molecule (DNA or RNA) form a 13 - dimension polytope with anti - parallel edges. Moreover, this polytope has exactly 12 free coordinate planes in which exactly 12 possible compounds of nitrogenous bases can be located. Thus, the arrangement of nitrogenous bases in nucleic acids obtained a geometrical basis and specification. This circumstance translates the question of the genetic code into a space of higher dimension, which is considered in the last chapter of the monograph.

The concept of Big Data has become widespread in computer science in recent times (Kosrapohr, 2003; Hughes, 2011; Rodger, 2015). The higher dimensionality of molecules can be considered as an example of Big Data. Apparently, a description using spaces of higher dimensionality can be considered as an alternative to existing mathematical methods for solving problems in a domain Big Data.

REFERENCES

Andronov, A. A., Leontovich, E. A., Gordon, I. I., & Mayer, A. G. (1966). *Qualitative theory of second - order dynamical systems*. Moscow: Science.

Andronov, A. A., Leontovich, E. A., Gordon, I. I., & Mayer, A. G. (1967). *Theory of bifurcations of dynamical systems on the plane*. Moscow: Science.

Arnold, V. I. (1976). *Mathematical methods of classical mechanics*. Moscow: Science.

Bautin, N. N. (1984). *Behavior of dynamic systems in the limits of the zone of stability*. Moscow: Science.

Chetverikov, S. S. (1905). Waves of life. From lepidopetrological observations of the summer of 1903. *Diary of the Zoological Department of the Imperial Society of Lovers of Natural Science*. *Anthropology and Ethnography*, *3*(6), 106–111.

Elenkin, A. A. (1936). *Blue - green algae USSR*. Moscow: USSR Academy of Sciences.

Hardy, G. H. (1908). Mendelian proportions in a mixed population. *Science*, *28*(706), 49–50. doi:10.1126cience.28.706.49 PMID:17779291

Hughes, G. (2011). *How big is "big data" in healthcare?* Retrieved from http://blogs. Sas.com/content//hls/2011/10/21/how – big – is – data – in –healthcare/

Katok, A. V., & Hasselblatt, B. (1999). *Introduction to the modern theory of dynamical systems*. Moscow: Factorial.

Kolmogorov, A. N., & Novikov, S. P. (Eds.). (1981). *Strange attractors*. Moscow: World.

Kolmogorov, A. N., Petrovsky, I. G., & Piskunov, N. S. (1937). The study of the diffusion equation, combined with an increase in the amount of substance, and its application to a single biological problem. MSU Bulletin, series A. *Mathematics and Mechanics*, *1*(1), 1–26.

Kosrapohr. (Ed). (2003). *Managing data mining technologies in organizations: techniques and applications.* Hershey, PA: Idea Group Publishing.

Mandelbrot, B. B. (2004). *Fractals and Chaos. The Mandelbrot Set and Beyond*. New Haven, CT: Springer. doi:10.1007/978-1-4757-4017-2

Marsden, J. E., & McCracken, M. (1976). *The Hopf Bifurcation and its Applications*. New York: Springer – Verlag. doi:10.1007/978-1-4612-6374-6

Mendel, G. (1965). *Experiments on plant hybrids*. Moscow: Science.

Poincare, A. (1895). Analysis Situs. *J.de e`Ecole Polytechnique*, *1*, 1 – 121.

Riemann, B. (1854). *On the Hypotheses Which Lie at the Foundations of Geometry*. Gottingen: Gottingen Observatory.

Rodger, J. A. (2015). Discovery of medical Big Data analytics: Improving the prediction of traumatic brain injury survival rates by data mining Patient Informatics Processing Software Hybrid Hadoop Hive. *Informatics in Medicine Unlocked*, *1*, 17–26. doi:10.1016/j.imu.2016.01.002

Ruelle, D., & Takens, F. (1971). On the Nature of Turbulence. *Communications in Mathematical Physics*, *20*(3), 167–192. doi:10.1007/BF01646553

Svirezhev, Yu. M. (1987). *Nonlinear waves, dissipative structures and disasters in ecology*. Moscow: Science.

Volterra, V. (1931). *Lecons sur la Theorie Mathematique de La Lutte Pour la Vie*. Paris: Gautheer – Villars.

Zavarzin, G. A. (2002). *Bacterial paleontology*. Moscow: PIN.

Zhizhin, G. V. (2004). *Self - regulating waves of chemical reactions and biological populations*. St. Petersburg: Science.

Zhizhin, G. V. (2005). *Dissipative structures in chemical, geological and ecological systems*. St. Petersburg: Science.

Zhizhin, G. V. (2012). Mathematical model of a solitary wave of a population of beetles - bark beetles. *Proceedings of the St. Petersburg State Forestry Academy*, *196*, 153 - 162.

Zhizhin, G. V. (2014). Mathematical model of flight of the gregarious locust. *Biosphere*, *6*(2), 112–117.

Zhizhin, G. V. (2017). *Chemical Compound Structures and Higher Dimension of Molecules: Emerging Research and Opportunities*. Hershey, PA: IGI Global.

Zhizhin, G. V. (2018). *The Geometry of Higher – Dimensional Polytopes*. Hershey, PA: IGI Global.

Zhizhin, G. V., & Bolshakova, N. N. (2000a). Single waves in populations of multicellular animal organisms. *Mathematical Modelling*, *12*(12), 55–65.

Zhizhin, G. V., & Bolshakova, N. N. (2000b). Mathematical model of a solitary wave of biocenosis. In *Mathematical methods in engineering and technology*. St. Petersburg: St. Petersburg State Institute of Technology (TU).

Zhizhin, G. V., & Bolshakova, N. N. (2000c). The method of semi - infinite reaction zone to determine the speed and structure of solitary waves of biological populations. In *Mathematical methods in engineering and technology*. St. Petersburg: St. Petersburg State Institute of Technology (TU).

Zhizhin, G. V., & Selikhovkin, A. V. (2012). *Mathematical modeling of the development and distribution of insect populations - stem pests in the forests of Russia.* St. Petersburg State Forestry University.

Chapter 1
Equilibrium in the Population of the Plants

ABSTRACT

On the basis Mendel's experiments, a mathematical model is constructed that describes the results of these experiments in a wide range of parameters. This model is compared with the Hardy-Weinberg logistic model based only on probabilistic ideas about the presence of dominant and recessive alleles in the chromosomes of living organisms. There is shown that in the mathematical model of Mendel's experiments, based on real patterns of plant development, there are equilibrium positions between the dominant and recessive forms. It consists in the fact that with an increase in the number of generations all dominant and recessive phenotypes of organisms, with any number of sings, quickly equalize and then synchronously (in the absence of death of organisms) increase together, seeking asymptotically to a stable isolated equilibrium position of the type of a multidimensional node. This newly discovered behavior of the dominant and recessive forms in the vicinity of the equilibrium position (true) differs significantly from the logistic equilibrium position in the Hardy-Weinberg principle, built without taking into account the real patterns in the plant population.

INTRODUCTION

In 1865, Mendel made a presentation at the Society of Naturalists in Brynn about experiments on plant hybrids (Mendel, 1965). This presentation gave birth to the development of genetics as a science, although not immediately the content of the speech became of known to the scientific community and

DOI: 10.4018/978-1-5225-9651-6.ch001

was appreciated (Gaisinovich, 1988). Understanding of its significant results took place in the struggle of opposing scientific trends and was accompanied by dramatic events in human relations. At different times, scientists have seen in these experiments different, sometimes opposite, results. More than 30 years after this speech, when the results works of Mendel were reopened and confirmed experimentally in the works of Correns (Correns, 1900), and De Vries (De Vries, 1904).

Over the past 150 years after the speech of Mendel, a chromosome theory of heredity was created, which gave a molecular explanation to the results of the experiments of Mendel (Weismann, 1885; Johannsen, 1933; Morgan, 1937; Koltsov, 1935; Chetverikov, 1926; Watson & Crick, 1953; Zhizhin, 2016, 2017, 2018). The same time after of the second discovery of Mendel's experiments, there appeared works in which it was noted that in Mendel's experiments there was a steady increase in the number of dominant alleles in populations, which indicated the absence of equilibrium positions in plant populations that obeyed Mendel's law.

In this regard, Yule (Yule, 1902) purely mathematically proved that in the case of free crossing in the population of heterozygous forms, there is an equilibrium between the number of dominant and recessive forms. Continued these studies Hardy (Hardy, 1908), who derived the formula for the distribution of genotypes in freely crossbreeding populations. Regardless of him and even earlier, Weinberg (Weinberg, 1908) established the same formula. This formula was called as principle the Hardy - Weinberg and became widespread. However, for the mathematical derivation of this formula, very strong assumptions are used: lack of choice in organisms, infinity of the population, accidental crossing of the population's organisms with each other, uniform distribution of male and female individuals, absence of mutation and genetic drift. The totality of these assumptions precludes the possibility of realizing such populations in nature. Therefore, this principle cannot be confirmed experimentally. Its only advantage is that it has equilibrium positions (a finite ratio of the numbers of dominant and recessive forms). However, these equilibrium positions are formed for any initial contents of these forms. Consequently, the set of equilibrium positions is a continuous manifold, and therefore they are asymptotically unstable, since any small perturbation can translate the system from one equilibrium position to another (Zhizhin, 1972, 2004a). The combination of necessary mathematical conditions in the derivation of the Hardy -Weinberg formula does not alleviate this advantage.

In this Chapter, a mathematical analysis of the sequences of obtaining the values of the number of phenotypes of organisms in Mendel's experiments was carried out. It is found that the patterns of inheritance of constant - differing sings, experimentally established by Mendel, are described by special algebraic relations, the basis of which are geometric progressions. Mendel and subsequent researchers did not pay attention to this. Naturally, Mendel could not trace the patterns of inheritance on experiments with a large number of generations. However, the mathematical model obtained in this Chapter (Zhizhin, 2019), accurately confirmed by Mendel's opaque in the field of conditions of their conduct, allows one to cram into the inheritance processes of sings with a large number of generations. A numerical and qualitative analysis of the equations of the mathematical model with an increase in the number of generations with an arbitrary number of pairs of constant - differing features was carried out.

There is shown that in the mathematical model of Mendel's experiments, based on real patterns of plant development, there are equilibrium positions between the dominant and recessive forms. It is shown that with an increase in the number of generations of the number all of dominant and recessive phenotypes of organisms with any number of sings quickly equalize and then synchronously (in the absence of death of organisms) increase together. In this case, the system asymptotically strive to achieve an isolated stable equilibrium position of the node type in a multidimensional space with coordinates in the form of quantities inversely proportional to the number of different phenotypes of organisms.

Thus, for finding equilibrium positions there is no need to use such stringent conditions which definition of the Hardy – Weinberg principle. Moreover, the regularities obtained by Mendel are based on clear biological processes in cells, in chromosomes. Moreover, the behavior of the system in the vicinity of the equilibrium position of the mathematical model of Mendel's experiments has a clear physical meaning. While one of the authors of the Hardy -Weinberg principle wrote that, a purely mathematical probabilistic description of random crossing is caused by the impossibility of having any physical justification for it (Yule, 1902).

In the experiments of Mendel, the plants were pollinated of the self – pollination, since many plants are pollinated by this method (Takhtadzhyan, 1980). In addition, recently in the neurobiology of plants convincingly shown (Mancuso, & Viola, 2013) that even in cross - pollination, for example, bees, insects pollinate plants not in a random way. The so - called "law of place" appears. The bees pollinate the plants of the species from which they started

to pollinate in the early morning. This manifests the intellectual ability of plants to manage the surrounding nature for their needs (Pollan, 2001; Pereira et al., 2012).

MONO - HYBRID CROSSING

Mendel carefully selected plants so that they consistently had differing signs (constant -distinguishing signs) to determine the inheritance patterns of plant sings. Now can to say that, in accordance with the chromosome theory of heredity, two homozygous organisms were crossed, the homologous chromosomes of each of which contain two identical genes. One pair of genes (*AA*) in one organism corresponds to one sing (dominant), and the other pair of genes (*aa*) in another organism corresponds to another sing (recessive). This crossing is called monohybrid. In accordance with Mendel's first law, when crossing homozygous parent forms that differ in one pair of sings, all hybrids of the first generation will be uniform both in genotype (gene composition, *Aa*) and in phenotype (appearance). When the first generation hybrids are crossed in accordance with the second Mendelian law, the predominance of the dominant sing over the recessive one in the ratio 3: 1 for the phenotype and 1: 2: 1 for the genotype will be observed in the offspring. This means that organisms of the first generation F_1 are characterized by a pair of *Aa* genes, and the second generation F_2 is characterized by pairs *AA, Aa, aa* in the ratio 1: 2: 1. Moreover, organisms with *AA* and *Aa* genes have the same phenotype, since the influence of recessive genes affects only when there are two, and not one, in homologous chromosomes.

Suppose that in the generation of F_1 there are m organisms and their mean fecundity is ν. Then in the generation of F_2 there are $m\nu$ organisms. Taking into account Mendel's second law is necessary to conclude that $m\nu$ is a multiple of four. Then in the generation of F_2 there are $\frac{m\nu}{4}$ homozygous organisms with *AA* genes, as many homozygous organisms with genes *aa* and $\frac{m\nu}{2}$ of heterozygous organisms with genes *Aa*

$$F_2 = \frac{m\nu}{4} AA + \frac{m\nu}{2} Aa + \frac{m\nu}{4} aa.$$

Each of the constituent parts of the second generation gives offspring to the next generation F_3. At the same time, homozygous organisms have homozygous organisms in the progeny, but the total number of corresponding organisms increases by a factor of ν. The heterozygous organisms, which have both dominant and recessive genes, also breed homozygous and heterozygous organisms. Taking into account the number of heterozygous organisms in the generation F_2 and their fertility, one have

$$\frac{m\nu}{2}Aa \to \frac{m\nu^2}{8}AA + \frac{m\nu^2}{4}Aa + \frac{m\nu^2}{8}aa.$$

In sum, homozygous and heterozygous organisms of generation F_2 give the following distribution of organisms in generation F_3

$$F_3 = m\nu^2(\frac{1}{4} + \frac{1}{8})AA + \frac{m\nu^2}{4}Aa + m\nu^2(\frac{1}{4} + \frac{1}{8})aa.$$

It is easy to determine that the ratio of the number of organisms of the dominant phenotype to the number of organisms of the recessive phenotype in this generation is 5: 3. In the generation F_4, heterozygous organisms also breed homozygous and heterozygous organisms

$$\frac{m\nu^2}{4}Aa \to \frac{m\nu^3}{16}AA + \frac{m\nu^3}{8}Aa + \frac{m\nu^3}{16}aa.$$

Homozygous organisms increase their numbers according to their fertility. In the sum in generation four, the following distribution of progeny is obtained

$$F_4 = m\nu^3(\frac{1}{4} + \frac{1}{8} + \frac{1}{16})AA + \frac{m\nu^3}{8}Aa + m\nu^3(\frac{1}{4} + \frac{1}{8} + \frac{1}{16})aa.$$

The ratio of the numbers of the dominant and recessive phenotypes in this generation is 9: 7.

In the *n* generation, arguing in a similar way, one get the following expression for the distribution of organisms

$$F_n = m\nu^{n-1}(\frac{1}{2^2}+\frac{1}{2^3}+...+\frac{1}{2^n})AA+\frac{m\nu^{n-1}}{2^{n-1}}Aa+m\nu^{n-1}(\frac{1}{2^2}+\frac{1}{2^3}+...+\frac{1}{2^n})aa.$$

The numbers of the dominant N_{df} and recessive N_{rf} phenotypes in the generation *n* are determined by the following equalities

$$N_{df}(n) = m\nu^{n-1}\frac{1+2+2^2+...+2^{n-2}+2}{2^n},$$

$$N_{rf}(n) = m\nu^{n-1}\frac{1+2+2^2+...+2^{n-2}}{2^n}.$$

The numerator on the right - hand side of the last equality is a geometric progression

$$\sum_{k=1}^{n-1}2^{k-1} = 2^{n-1}-1.$$

It should be noted that in the book A.E. Gaisinovich (Gaisinovich, 1988) mistakenly asserted that the numbers of phenotypes of organisms in Mendel's law are expressed in terms of Bin Newton. In accordance with the last equality, the numbers of the dominant and recessive phenotype are equal, respectively

$$N_{df}(n) = m\nu^{n-1}\frac{2^{n-1}+1}{2^n}, N_{rf}(n) = m\nu^{n-1}\frac{2^{n-1}-1}{2^n}. \quad (1)$$

The ratio of these numbers is

$$\frac{N_{df}}{N_{rf}} = \delta_1(n) = \frac{2^{n-1}+1}{2^{n-1}-1}. \quad (2)$$

Equation (2) represents a general expression for the ratio of the numbers of the dominant and recessive phenotypes in a mono - hybrid crossing for any number of generation $n > 1$. It depends only on *n*. When $n = 2$, the ratio (2) is 3: 1, which corresponds to Mendel's second law. It follows from (1),

(2) when the number of the generation increases, the numbers of the dominant and recessive phenotypes quite quickly occur (their ratio tends to unity). Absolute values of these numbers grow steadily with increasing number of generation. This is natural, since conditions that are not too remote from the initial state are considered, when the death of organisms is not taken into account due to external influences (aggression of surrounding, climatic and seasonal causes (Zhizhin, 2004b, 2005). The number of hybrids $m\left(\frac{\nu}{2}\right)^{n-1}$, which is a component of the number of dominant phenotypes, also grows steadily as the number of the generation increases (ν is usually greater than 2). Thus, the assertion that with the passage of time there is a restoration of parental populations and the disappearance of hybrids is erroneous.

Since the numbers of phenotypes grow with increasing n, it is convenient to go over to variables, inverses of the numbers of phenotypes, in order to analyze the nature of the desire of the system for the equilibrium position. The set of solutions of the system for various initial values of the number of organisms m and the constant value of fecundity ν in these variables are represented by trajectories in the phase plane (N_{df}^{-1}, N_{rf}^{-1}) (Figure 1).

Figure 1. Phase diagram of changes in the numbers of dominant and recessive phenotypes in coordinates of inverses numbers of phenotypes N_{df}^{-1} *and* N_{rf}^{-1}

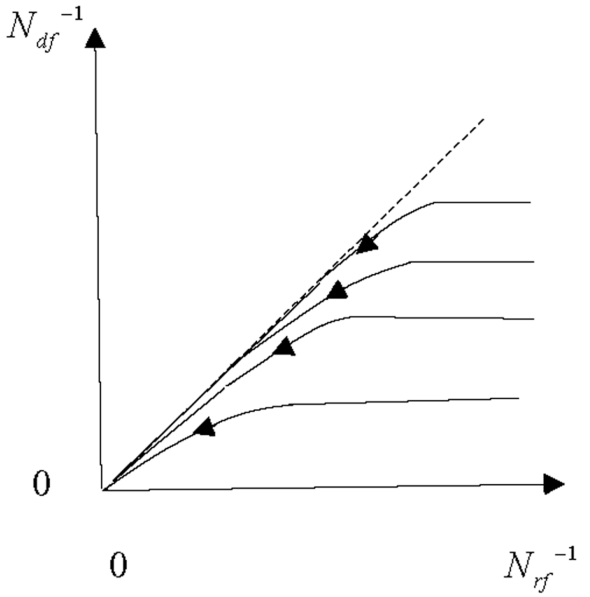

From which we see that the ratio (2) defines in this plane an intrinsic direction, along which the solutions tend to the equilibrium position at the origin of coordinates of the phase plane. The equilibrium position is isolated, stable and has a node type.

BE – HYBRID CROSSING

Let the organisms have two pairs of constant - differing signs. In one pair, the A_1A_1 genes correspond to the dominant sign, and the genes a_1a_1 correspond to the recessive sign. In another pair, the A_2A_2 genes correspond to the dominant sign, and the genes a_2a_2 correspond to the recessive sign. In each pair of signs, Mendel's second law is independent and at the same time acts

$$A_1a_1 \to \left(A_1A_1 + 2A_1a_1 + a_1a_1\right)$$
$$A_2a_2 \to \left(A_2A_2 + 2A_2a_2 + a_2a_2\right).$$

This corresponds to the product of expansions

$$\left(A_1A_1 + 2A_1a_1 + a_1a_1\right)\left(A_2A_2 + 2A_2a_2 + a_2a_2\right), \tag{3}$$

since the probability of the product of independent events is equal to the product of the probability of these events. The result of this work are 16 terms

$$A_1A_1A_2A_2 + A_1A_1a_2a_2 + a_1a_1A_2A_2 + a_1a_1a_2a_2 + 2A_1A_1A_2a_2 + 2a_1a_1A_2a_2 +$$

$$+2A_1a_1A_2A_2 + 2A_1a_1a_2a_2 + 4A_1a_1A_2a_2. \tag{4}$$

Therefore, if in the first generation F_1 there are m hybrid organisms $A_1a_1A_2a_2$, then in the second generation F_2, taking into account their fertility ν, there are $m\nu$ organisms and this number must be a gradual number 16. Consequently, the second generation is the sum of the following organisms

$$F_2 = \frac{m\nu}{16} A_1A_1A_2A_2 + \frac{m\nu}{16} A_1A_1a_2a_2 + \frac{m\nu}{16} a_1a_1A_2A_2 + \frac{m\nu}{16} a_1a_1a_2a_2 +$$
$$+ \frac{m\nu}{8} A_1A_1a_2a_2 + \frac{m\nu}{8} a_1a_1A_2a_2 + \frac{m\nu}{8} A_1a_1A_2A_2 + \frac{m\nu}{8} A_1a_1a_2a_2 + \frac{m\nu}{4} A_1a_1A_2a_2. \quad (5)$$

One distinguish among the 16 terms in (4) those terms that correspond to organisms with the phenotype on the sing of A_1A_1 genes. Such terms are 12

$$A_1A_1A_2A_2, A_1A_1a_2a_2, 2A_1A_1A_2a_2, 2A_1a_1A_2A_2, 2A_1a_1a_2a_2, 4A_1a_1A_2a_2.$$

In (4) are terms that correspond to organisms with the phenotype on the sing of a_1a_1 genes. This are 4 terms $a_1a_1A_2A_2, a_1a_1a_2a_2, 2a_1a_1A_2a_2$. Thus, the ratio of the number of organisms in the second generation (5) with the A_1A_1 phenotype and with the phenotype a_1a_1 is the same as in the mono - hybrid crossing 3:1. Obviously, the same 3: 1 ratio of the number of organisms with phenotypes of A_2A_2 and of a_2a_2. This manifests the third law of Mendel, discovered by him in experiments with bi - hybrid crossing: the law of independent splitting of sings in the ratio of 3: 1 in the second generation. In this Chapter, this law follows from a mathematical treatment of bi - hybrid crossing. From the same consideration follows the second part of the third law of Mendel.

Indeed, if one select the terms corresponding to the organisms with the phenotype for the A_1A_2 genes from the sum (4), then there are nine such terms

$$A_1A_1A_2A_2, 2A_1A_1A_2a_2, 2A_1a_1A_2A_2, 4A_1a_1A_2a_2.$$

The terms in (4) corresponding to the organisms with the phenotype in the product a_1A_2 are three $a_1a_1A_2A_2, 2a_1a_1A_2a_2$. The same number of terms in (4) for phenotype a_2A_1. These are the terms $A_1A_1a_2a_2, 2A_1a_1a_2a_2$. One term in (4), corresponding to the organisms with phenotype a_1a_2, this is $a_1a_2\ a_1a_2$. Thus, in the second generation (5), the ratio of the number of organisms to the simultaneous presence of some two of the four sings is 9: 3: 3: 1. This is the second part of the third law of Mendel, observed by him in the experiments on bi - hybrid crossing in the second generation.

Mendel did not succeed in elucidating the regularity of bi - hybrid crossing in the following after the second generation. This can be done using a mathematical description, the correctness of which has already been proved. In the transition to the third generation, heterozygous organisms A_1a_1, A_2a_2 in (3) are split according to Mendel's second law. If we focus on the ratio of the phenotype counts by the dominant A_1A_1 gene and the recessive a_1a_1 gene, then after splitting the heterozygous organism A_1a_1 in the first bracket of the product (3), this product takes the form $\left(3A_1A_1 + 4A_1a_1 + 3a_1a_1\right)f$ where, for brevity, f denotes the second bracket in (3) $f = \left(A_2A_2 + 2A_2a_2 + a_2a_2\right)$. It follows that the ratio of the number of organisms in the phenotypes A_1A_1 and a_1a_1 in the third generation is 7: 3.

Similarly, in the fourth generation, the product (3) takes the form $\left(7A_1A_1 + 8A_1a_1 + 7a_1a_1\right)f$, that is, in the fourth generation, the ratio of the numbers of organisms according to the phenotypes A_1A_1 and a_1a_1 is 15: 7 and so on. Expanding the sequence of the obtained digits in the relationship, one conclude that in the generation *n* the number of organisms according to the phenotype A_1A_1 in the product (3) is a geometric progression

$$1 + 2 + 2^2 + ... + 2^{n-1} = \sum_{k=1}^{n} 2^{k-1} = 2^n - 1,$$

In addition, the number of organisms according to the phenotype a_1a_1 is a geometric progression

$$1 + 2 + 2^2 + ... + 2^{n-2} = \sum_{k=1}^{n-1} 2^{k-1} = 2^{n-1} - 1.$$

Thus, one obtain that the ratio of the number of organisms in the generation *n* according to the phenotypes A_1A_1 and a_1a_1 in the bi - hybrid crossing is

$$\delta_2(n) = \frac{2^n - 1}{2^{n-1} - 1}. \tag{6}$$

It is clear that this formula is also suitable for the ratio of the numbers of organisms according to the phenotypes A_2A_2 and a_2a_2 in the bi - hybrid crossing

in the generation *n*, in view of the equality of rights of brackets in the product (3).

If it is necessary to consider the ratio of the number of organisms to phenotypes with the simultaneous presence of two pairs of sings in the generation after the second, then it is necessary to split both brackets in the product (3) sequentially. Denote the organisms by the phenotype A_1A_1 by the symbol φ_{A_1}. These organisms include organisms with A_1A_1 and A_1a_1 genes. Similarly, φ_{A_2} denotes the organisms according to the phenotype of A_2A_2, φ_{a_1} - organisms according to the phenotype of a_1a_1, φ_{a_2} - organisms according to the phenotype of a_2a_2. The number of organisms with a phenotype A_iA_i is equal to the sum of the number of organisms with genes A_iA_i and the number of organisms with genes A_ia_i, ($i = 1, 2$). Then, expression (3) in the third generation takes the form

$$\left(7\varphi_{A_1} + 3\varphi_{a_1}\right)\left(7\varphi_{A_2} + 3\varphi_{a_2}\right) = 7^2\varphi_{A_1}\varphi_{A_2} + 7\cdot 3\varphi_{a_1}\varphi_{A_2} + 7\cdot 3\varphi_{A_1}\varphi_{a_2} + 3^2\varphi_{a_1}\varphi_{a_2}.$$

From this it follows that the ratio of the number of organisms according to the phenotypes A_1A_1 and A_2A_2, a_1a_1 and A_2A_2, a_2a_2 and A_1A_1, a_1a_1 and a_2a_2 in the third generation is $7^2 : 7\cdot 3 : 7\cdot 3 : 3^2$.

In the fourth generation, the ratio of the number of organisms by the same phenotypes is obtained similarly when the brackets are split in expression (3)

$$\left(15\varphi_{A_1} + 7\varphi_{a_1}\right)\left(15\varphi_{A_2} + 7\varphi_{a_2}\right) =$$
$$15^2\varphi_{A_1}\varphi_{A_2} + 15\cdot 7\varphi_{a_1}\varphi_{A_2} + 15\cdot 7\varphi_{A_1}\varphi_{a_2} + 7^2\varphi_{a_1}\varphi_{a_2}.$$

From this it follows that the ratio of the number of organisms according to the phenotypes A_1A_1 and A_2A_2, a_1a_1 and A_2A_2, a_2a_2 and A_1A_1, a_1a_1 and a_2a_2 in the fourth generation is

$$15^2 : 15\cdot 7 : 15\cdot 7 : 7^2.$$

The construction of these relations continues in the next generation. The numbers participating in the relationships (1, 3, 7, 15,...) are numerators and denominators (6) for the corresponding values of *n*. The indicators and

the number of repetitive products in the relationship indicate the number of independent feature pairs (in this case 2). This leads to the following ratios of the number of organisms according to the phenotypes, with the simultaneous presence of two pairs of characters for an arbitrary generation number *n*

$$(2^n-1)^2 : (2^n-1)(2^{n-1}-1) : (2^n-1)(2^{n-1}-1) : (2^{n-1}-1)^2. \quad (7)$$

We introduce the notation of the absolute numbers of organisms in the generation *n* and phenotypes with two dominant genes $N_{d_1d_2}$, with one dominant and one recessive gene $N_{d_1r_2}$ and $N_{d_2r_1}$, and with two recessive genes $N_{d_1r_2}$. These numbers, according to (7), are equal

$$N_{d_1d_2} = m\nu^{n-1}\frac{(2^n-1)^2}{2^{2n}}, N_{d_1r_2} = N_{d_2r_1}$$
$$= m\nu^{n-1}\frac{(2^n-1)(2^{n-1}-1)}{2^{2n}}, N_{r_1r_2} = m\nu^{n-1}\frac{(2^{n-1}-1)^2}{2^{2n}}.$$

For large values of *n*, these numbers tend to the same value $m\nu^n$, that is, there is an alignment of the number of organisms with purely dominant genes, purely recessive genes and hybrid genes. Just as with mono - hybrid crossing in the case of bi - hybrid crossings, solutions with an increase in the number of generations can be represented in space with coordinates in the form of inverse numbers $N^{-1}_{d_1d_2}, N^{-1}_{d_1r_2}, N^{-1}_{d_2r_1}, N^{-1}_{r_1r_2}$. In this case, there are four such coordinates. The equilibrium position of the given system is the origin of the coordinates of the four - dimensional space. This is a special point of the type of a considerate four - dimensional node. The solutions of the system enter into a position of equilibrium in its own direction, defined by the equality of a unit of relation pairwise coordinates of space.

POLY-HYBRID CROSSING

If organisms with more than two pairs of characteristics are crossing, for example, *t* pairs, then the distribution of organisms in the progeny can be obtained from the product of *t* factors

$$\left(A_1A_1 + 2A_1a_1 + a_1a_1\right)\left(A_2A_2 + 2A_2a_2 + a_2a_2\right)\ldots\left(A_tA_t + 2A_ta_t + a_ta_t\right). \tag{8}$$

If the ratio of the numbers of phenotype organisms according to the dominant and recessive members of one of the *i* pairs of sings is of interest $(1 \le i \le t)$, then in the second generation the product (8) can be written in the form $\left(A_iA_i + 2A_ia_i + a_ia_i\right)f$, where *f* includes all the other factors of the product (8). From this expression, it follows that in the second generation the ratio of the numbers of organisms according to the dominant and recessive members of the pair *i* is a ratio of 3: 1. When splitting heterozygous organisms A_ia_i with formed of a third generation the ratio of the number of organisms to phenotypes A_iA_i and a_ia_i is 7: 3 and so on. Therefore, the ratio of the numbers of organisms in the generation *n* to the phenotypes A_iA_i and a_ia_i in the case of poly - hybrid crossing has the same form as in the mono - hybrid crossing

$$\delta_t(n) = \frac{2^n - 1}{2^{n-1} - 1}. \tag{9}$$

This ratio is valid for any pair of sings *i* from *t* pairs due to their independence.

If it is necessary to consider the ratio of the number of organisms to a phenotype with the simultaneous presence of several pairs of sings, then it is necessary to split all the brackets in the product (8) sequentially. For example, in the case of three pairs of sings ($t = 3$), using the notations introduced in the previous section, product (8) takes in this case the form

$$\left(3\varphi_{A_1} + \varphi_{a_1}\right)\left(3\varphi_{A_2} + \varphi_{a_2}\right)\left(3\varphi_{A_3} + \varphi_{a_3}\right) = 27\varphi_{A_1}\varphi_{A_2}\varphi_{A_3} + 9\varphi_{a_1}\varphi_{A_2}\varphi_{A_3} + 9\varphi_{A_1}\varphi_{a_2}\varphi_{A_3} + 9\varphi_{A_1}\varphi_{A_2}\varphi_{a_3} + 3\varphi_{A_1}\varphi_{a_2}\varphi_{a_3} + 3\varphi_{a_1}\varphi_{A_2}\varphi_{a_3} + 3\varphi_{a_1}\varphi_{a_2}\varphi_{A_3} + \varphi_{a_1}\varphi_{a_2}\varphi_{a_3}. \tag{10}$$

It follows from equality (10) that in the case of crossing with three pairs of characteristics in the second generation, the ratio between the numbers of organisms according to the phenotypes of different possible pairs of genes has the form

$$3^3 : 3^2 : 3^2 : 3^2 : 3 : 3 : 3 : 1.$$

In the third generation, the product (8) is transformed so

$$\begin{aligned}&\left(7\varphi_{A_1}+3\varphi_{a_1}\right)\left(7\varphi_{A_2}+3\varphi_{a_2}\right)\left(7\varphi_{A_3}+3\varphi_{a_3}\right)=\\&7^3\varphi_{A_1}\varphi_{A_2}\varphi_{A_3}+7^2\cdot 3\varphi_{a_1}\varphi_{A_2}\varphi_{A_3}+7^2\cdot 3\varphi_{A_1}\varphi_{a_2}\varphi_{A_3}+\\&7^2\cdot 3\varphi_{A_1}\varphi_{A_2}\varphi_{a_3}+7\cdot 3^2\varphi_{A_1}\varphi_{a_2}\varphi_{a_3}+\\&7\cdot 3^2\varphi_{a_1}\varphi_{A_2}\varphi_{a_3}+7\cdot 3^2\varphi_{a_1}\varphi_{a_2}\varphi_{A_3}+3^3\varphi_{a_1}\varphi_{a_2}\varphi_{a_3}.\end{aligned}$$

From the last expression, it follows that the relationship between the numbers of organisms with different genes when crossing organisms with three pairs of characters in generation 3 has the form

$$7^3:(7^2\cdot 3):(7^2\cdot 3):(7^2\cdot 3):(7\cdot 3^2):(7\cdot 3^2):(7\cdot 3^2):3^3.$$

In the fourth generation, the product (8) is transformed so

$$\begin{aligned}&\left(15\varphi_{A_1}+7\varphi_{a_1}\right)\left(15\varphi_{A_2}+7\varphi_{a_2}\right)\left(15\varphi_{A_3}+7\varphi_{a_3}\right)=\\&15^3\varphi_{A_1}\varphi_{A_2}\varphi_{A_3}+15^2\cdot 7\varphi_{a_1}\varphi_{A_2}\varphi_{A_3}+15^2\cdot 7\varphi_{A_1}\varphi_{a_2}\varphi_{A_3}+\\&15^2\cdot 7\varphi_{A_1}\varphi_{A_2}\varphi_{a_3}+15\cdot 7^2\varphi_{A_1}\varphi_{a_2}\varphi_{a_3}+\\&15\cdot 7^2\varphi_{a_1}\varphi_{A_2}\varphi_{a_3}+15\cdot 7^2\varphi_{a_1}\varphi_{a_2}\varphi_{A_3}+7^3\varphi_{a_1}\varphi_{a_2}\varphi_{a_3}.\end{aligned}$$

From the last expression, it follows that the relationship between the numbers of organisms with different genes when crossing organisms with three pairs of characters in generation 3 has the form

$$5^3:(15^2\cdot 7):(15^2\cdot 7):(15^2\cdot 7):(15\cdot 7^2):(15\cdot 7^2):(15\cdot 7^2):7^3$$

In the same way, it is possible to obtain the corresponding ratios of the numbers of organisms in the crossing of organisms with 3 pairs of characters in the generation of *n*

$$\begin{aligned}&(2^n-1)^3:\left[(2^n-1)^2(2^{n-1}-1)\right]_1:\left[(2^n-1)^2(2^{n-1}-1)\right]_2:\left[(2^n-1)^2(2^{n-1}-1)\right]_3:\\&\left[(2^n-1)\ (2^{n-1}-1)^2\right]_1:\left[(2^n-1)\ (2^{n-1}-1)^2\right]_2:\left[(2^n-1)\ (2^{n-1}-1)^2\right]_3:(2^{n-1}-1)^3.\end{aligned}$$

Here, the subscript in square brackets shows that the number of repetitions of identical expressions is equal to the number of pairs of constant - distinct characters.

By indexing repetitive products by the number of pairs of attributes, these relations take the form

$$(2^n-1)^t : \left[(2^n-1)^{t-1}(2^{n-1}-1)\right]_1 : \left[(2^n-1)^{t-1}(2^{n-1}-1)\right]_2 : \ldots : \left[(2^n-1)^{t-1}(2^{n-1}-1)\right]_t :$$
$$\left[(2^n-1)^{t-2}(2^{n-1}-1)^2\right]_1 : \left[(2^n-1)^{t-2}(2^{n-1}-1)^2\right]_2 : \ldots : \left[(2^n-1)^{t-2}(2^{n-1}-1)^2\right]_t : \ldots :$$
$$\left[(2^n-1)(2^{n-1}-1)^{t-1}\right]_1 : \left[(2^n-1)(2^{n-1}-1)^{t-1}\right]_2 : \ldots : \left[(2^n-1)(2^{n-1}-1)^{t-1}\right]_t : (2^{n-1}-1)^t. \quad (11)$$

Just as in the case of bi – hybrid crossing, here it is possible to introduce inverse numbers of organisms according to phenotypes with different sets of genes. As can be seen from the expression (11), the number of these variables in the general case is (t - 1) t + 2. Each of the variables is proportional to $\frac{1}{m\nu^{n-1}}$ and tends to zero as the number of generations increases. The ratio of the pairs of any two variables with increasing n tends to unity. Therefore, in poly - hybrid crossing, with increasing n, the number of organisms is equalized by phenotypes with different sets of genes. Solutions for different values of m tend in the space of the reciprocal numbers of organisms to the proper direction of the equilibrium position at the origin, which has the type of an isolated multidimensional stable node.

Thus, it is shown that the patterns of inheritance of features of organisms in their crossing are based on a special kind of the mathematical relationships that allow us to derive algebraically the experimental patterns studied 150 years ago by Mendel. The core of these relations are geometric progressions. An expression is obtained for the general relationship between the numbers of organisms with different phenotypes for any number of pairs of constant - distinct characters and any number of generations. Using these relationships is possible to predict and investigate the inheritance processes outside the intervals of the initial data of Mendel's experiments (for any number of pairs of constant - distinguishing signs and any number of generations). The general formulas obtained are transformed continuously into the relations of Mendel in the conditions of the experiments carried out by him.

It has been established that with an increase in the number of generations in a plant population, the phenotypes of organisms in different gene sets are leveled quickly. These numbers, with an increase in the number of generations

and the absence of death of organisms, synchronously increase while remaining practically equal to each other. Mathematically, this can be represented by trajectories in a multidimensional phase space with coordinates in the form of inverse numbers of phenotypes of organisms. These trajectories tend along their own direction to an isolated stable equilibrium position of the type of a multidimensional node at the origin. With the results obtained, based on G. Mendel's experiments, the Hardy - Weinberg principle is fundamentally inconsistent, constructed purely logistically without taking into account the real laws in living nature.

REFERENCES

Chetverikov, S. S. (1926). About some moments of the evolutionary process from the point of view of modern genetics. *Journal of Experimental Biology A*, *2*, 3–54.

Correns, C. (1900). Mendel's Regel über das Verhalten der Nachkommenschaft der Rassenbastarde. *Berichte der Deutschen Botanischen Gesellschaft*, *18*, 158–168.

De Vries, G. (1904). Mutation theory: Mutations and mutational periods in the origin of species. In *Development Theory*. St. Petersburg: Brockhaus and Efron.

Gaisinovich, A. E. (1988). *Origin and development of genetics*. Moscow: Science.

Hardy, G. H. (1908). Mendelian proportions in a mixed population. *Science*, *28*(706), 49–50. doi:10.1126cience.28.706.49 PMID:17779291

Johannsen, V. L. (1933). *Elements of the exact doctrine of variability and heredity with the basics of biological variation statistics*. Leningrad: Sel'khozgiz.

Koltsov, N. K. (1935). Hereditary molecules. *Science and Life*, *5*, 4–13.

Mancuso, S., & Viola, A. (2013). *Verde Brillante. Sensibilita e Intellidenza Del Mondo Vegetale*. Firenze, Milano: Giunti Editore.

Mendel, G. (1965). *Experiments on plant hybrids*. Moscow: Science.

Morgan, T. G. (1937). *Selected works on genetics*. Moscow: Sel'khozgiz.

Pereira, C. G. (2012). Underground Leavers of Philcoxia Trap and Digest Nematodes. *Proceedings of the National Academy of Science of the United States of America*.

Pollan, M. (2001). *The Botany of Desire: A Plant's – Eye View of the World*. New York: Random House.

Takhtadzhyan, A. L. (1980). Life of plants. T. 5. Flowering plants. Moscow: Education.

Watson, J. D., & Crick, F. H. C. (1953). Molecular structure of nucleic acids. *Nature*, *171*(4356), 728–740. doi:10.1038/171737a0 PMID:13054692

Weinberg, W. (1908). Ueber den Nachweis der Vererbung beim Menschen. *Jahreshefte Verreins vaterländ, 64*, 368 – 382.

Weismann, A. (1885). *Die Continuität des Keimplasmas als Grundlage einer Theore der Vererbung*. Jena: Fisheri.

Yule, G. U. (1902). Mendel's laws and their probable relations to intra-racial heredity. *The New Phytologist*, *1*(9), 193–207, 222–238. doi:10.1111/j.1469-8137.1902.tb06590.x

Zhizhin, G. V. (1972). *Qualitative investigation of one - dimensional stationary flows* (Thesis). Leningrad: Polytechnic Institute.

Zhizhin, G.V. (2004 a). Synergetics of flows. *Life and Safety*, *2 – 3*, 366 – 385.

Zhizhin, G. V. (2004 b). *Self - regulating waves of chemical reactions and biological populations*. St. - Petersburg: Science.

Zhizhin, G. V. (2005). The Dissipative Structures in Chemical, Geological and Ecological Systems. St. - Petersburg. *Science*.

Zhizhin, G. V. (2016). The Structure, Topological, and Functional Dimension of Biomolecules. *International Journal of Chemoinformatics and Chemical Engineering*, *5*(2), 44–58. doi:10.4018/IJCCE.2016070104

Zhizhin, G. V. (2017). *Chemical Compound Structures and the Higher Dimension of Molecules: Emerging Research and Opportunities*. Hershey, PA: IGI Global.

Zhizhin, G. V. (2019). About the True Equilibrium in the Population of the Plants. *Journal of Biochemistry and Molecular Biology Research*, *4*(1), 214–224.

KEY TERMS AND DEFINITIONS

Dominant Traits: The traits that predominate in the first generation.

Gene: A hereditary factor; functionally indivisible unit of genetic material; section of the DNA molecule encoding the primary structure of the polypeptide.

Genotype: A set of genes of a given cell or organism.

Heterozygous Individuals: The individuals that produce cleavage in the offspring.

Homozygous Individuals: The individuals that do not produce cleavage in the offspring.

Monohybrid Crossing: A crossing in which the manifestation of only one trait is examined.

Phenotype: The totality of all traits and properties of an individual that are formed in the process of interaction between its genetic structure and the external environment.

Polyhybrid Crossing: A crossing in which explores the manifestation of several signs.

Recessive Traits: The traits that do not appear in the first generation.

Chapter 2
Waves in Biological Populations

ABSTRACT

Self-regulating nonlinear waves in various biological populations are considered as moving attractors in excitable media. Mathematically, waves in populations are solutions of nonstationary parabolic systems of differential diffusion equations with source terms, and the velocity of the wave is an eigenvalue of the problem, and its profile is an eigenvalue function of the problem. There is no general exact method for solving such a problem. An approximate method for its solution is proposed (the semi-infinite reaction zone method), which essentially reduces to solving an algebraic system of equations. The method is used to calculate the waves in various biological populations. It is shown that there are two types of waves: a wave of conquest and a solitary wave. In all cases considered, formulas for calculating the velocity of the wave and its profile were obtained. One of the important examples considered is the analysis of solitary waves in populations of the herd locust.

WAVES IN THE LOGISTIC BIOLOGICAL POPULATIONS

To study the waves of biological populations, one will use the semi - infinite reaction zone method developed by the author in the study of the polymerization waves and combustion waves (Zhizhin, 1982, 1988, 1992, 1997 a, b, 2004a,b, 2008; Zhizhin, & Poritskaya, 1994; Zhizhin, & Larina, 1994).

DOI: 10.4018/978-1-5225-9651-6.ch002

The nonstationary equation for the change in the concentration N of individuals in the logistic population in a one - dimensional range, taking into account the chaotic mobility μ of individuals, has the form (Svirezhev, 1987)

$$\frac{\partial N}{\partial t} = \mu \frac{\partial^2 N}{\partial x^2} + F(N). \tag{1}$$

Here F (N) is the function describing the local law of the population growth, and

$$F(N) = (B - D)N, \tag{2}$$

where B and D are the fertility and mortality functions.

Equation (2) describes the fact that the local law of the population growth is determined by two processes — birth and death. In the model of the logistic population it is assumed, that mortality D is a linearly increasing function of the concentration of individuals

$$D(N) = \alpha_1 + \alpha_2 N, \alpha_1 > 0, \alpha_2 > 0.$$

Here α_1 is natural mortality. Increase in mortality with increasing concentration N is due to increased competition with limited resources (food, space, etc.). In addition, it is assumed that the fertility function B it is determined only by the physiological limits of fertility and is independent of N, i.e. $B = m =$ constant, where m is the so - called natural fertility or fecundity. Given these assumptions and equation (2), equation (1) takes the form

$$\frac{\partial N}{\partial t} = \mu \frac{\partial^2 N}{\partial x^2} + \alpha N(1 - N / N_+). \tag{3}$$

Here $\alpha = m - \alpha_1$ is Malthusian parameter, and $N_+ = (m - \alpha_1) / \alpha_2$ is the capacity of the medium, i.e. maximum possible concentration of individuals in the environment.

If the competition between individuals of the population is completely absent $(\alpha_2 = 0)$, $N_+ = \infty$, then the law of the local population growth takes

a simple form $F(N) = \alpha N$. In this case, the population density increases indefinitely (the Malthus model of exponential growth) and the wave solution, as a transition from one equilibrium position to another, does not exist $(\alpha > 0)$.

To find the stationary wave solution of equation (3), one can introduce the wave coordinate $z = ut - x$, here *u* is the wave velocity. One also introduce dimensionless variables $n = N / N_{+}, \varsigma = z(\alpha / \mu)^{1/2}, w = u(\alpha\mu)^{-1/2}$. Then equation (3) can be written as a system

$$\frac{dp}{d\varsigma} = wp - F(n), F(n) = (1-n)n, \tag{4}$$

$$\frac{dn}{d\varsigma} = p. \tag{5}$$

The solutions of the autonomous system (4), (5) can be represented by trajectories in the phase plane (p, n) . Their locations are determined by the zero isocline $p = n(1-n) / w$, on which $dp / d\varsigma = 0$, the zero isocline $p = 0$, on which $dn / d\varsigma = 0$, as well as by special points $a(0,0), b(0,1)$. The eigenvalues in the special point *a* (the initial equilibrium position) are equal to the eigendirections at this point

$$\lambda_{1,2} = w / 2 \pm \sqrt{w^2 / 4 - 1} = (dp / dn)_{1,2}, \tag{6}$$

and the eigenvalues at the special point *b* (the final equilibrium position) are equal to the eigendirections at the special point *b*

$$\lambda_{3,4} = w / 2 \pm \sqrt{w^2 / 4 + 1} = (dp / dn)_{3,4}. \tag{7}$$

Let us consider in more detail than in the well - known work of A.N. Kolmogorov, I.G. Petrovsky, N.S. Piskunov (Kolmogorov, Petrovsky, Piskunov, 1937), the behavior of trajectories in the phase plane, omitting the already known details. From (7) it follows that the final equilibrium position is of a saddle type, since $\lambda_1 > 0, \lambda_2 < 0$.

From (6) it follows that the initial equilibrium position can be of the type of an unstable node with $w \geq 2$ or a focus with $w < 2$. Since at $w < 2$

trajectories will fall into the region of negative concentrations, this area of parameters is not of interest. One confine ourselves to the values of speed $w \geq 2$. Then the point *a* has the type of an unstable node, since $\lambda_{1,2} > 0$ and has two proper directions, and both are located in the quadrant $p > 0, n > 0$. The wave solution leaves the point *a* and enters point *b*, i.e. boundary conditions must be satisfied $p = n = 0$ at $\varsigma \to -\infty$ and $p = 0, n = 1$ at $\varsigma \to +\infty$. Obviously, for any value of speed, there is a trajectory emanating from point *a,* and entering point *b* (Figure 1).

However, with which eigenvalues λ_1 or λ_2 the trajectory leaves point *a,* if it enters point *b*, is not known in advance, since both options are may be. In the first case, the trajectories emanating from point *a* along its own direction 2 intersect the zero isocline $p = n(1-n)/w$ and, without entering point *b*, intersect the axis $p = 0$. In this case, one of the trajectories emanating from point *a* along its own direction 1 enters point *b*. In the second case, the trajectories emanating from point *a* in its own direction 1, not reaching point

Figure 1. Phase diagram of waves in the logistic population

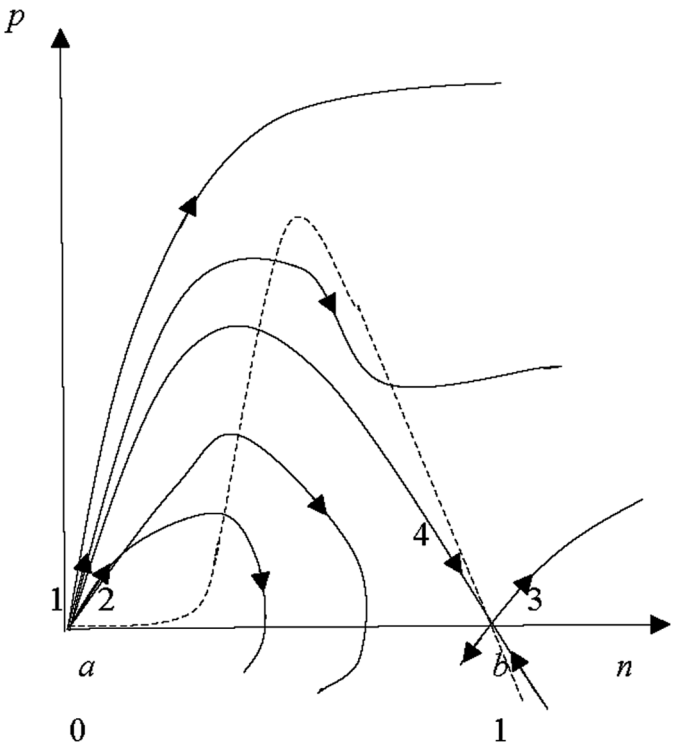

b, leave in their own direction3 points *b*. For $w = 2$ the eigenvalues of the point *a* coincide; their own directions coincide, and the point *a* has the type of a degenerate unstable node. Figure 1 shows the case when the trajectory emanating from point *a* in its own direction 1 enters the special point *b* along the own direction 4. The corresponding integral curve is shown in Figure 2.

It represents the conquest wave profile since the wave, moving along the spatial coordinate *x,* with a speed *u*, fills the space with the maximum concentration of individuals N_+ (according to the introduced wave coordinate, the directions *x* and *z* are opposite). One divide the wave into three zones (Figure 2). In zone 1 $(-\infty < \varsigma < 0)$, one consider the solution of the system linearized in the vicinity of the initial equilibrium state *a* to be fair

$$n = n_f \exp(\lambda_{1,2}\varsigma). \tag{8}$$

Figure 2. Wave profile of conquering the logistic population: n_f is the concentration of individuals at the wave front ($\varsigma = 0$), n_Δ is the concentration of individuals at the bound of zone 2 ($\varsigma = \Delta$)

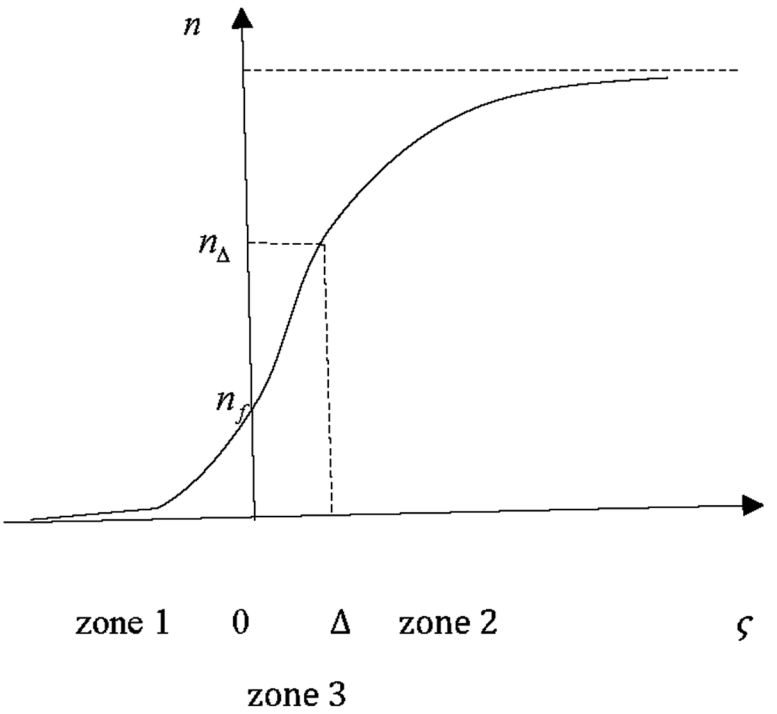

Here n_f is the concentration of individuals at the wave front $\varsigma = 0$, $\lambda_{1,2}$ is the eigenvalue at the point *a* (which of them will be established later).

In zone 2 $(\Delta \le \varsigma < +\infty)$, one consider the solution of the system linearized in the vicinity of the final equilibrium state *b* to be valid

$$n = 1 - (1 - n_{\Delta}) \exp(\lambda_4(\varsigma - \Delta)). \tag{9}$$

The conditions in zone 1 and zone 2 ensure that the approximate solution of the system emerges from the initial equilibrium position and enters the final equilibrium position with almost the same eigenvalues and proper directions as the exact solution of system (4), (5).

In zone 3, one linearize the right - hand side of equation (4) in the vicinity of the maximum of the trajectory in the phase plane (expand the right - hand side of (4) into the Taylor series in the vicinity of the maximum and limit the first nonzero member of the series)

$$\frac{dp}{d\varsigma} = (2n_m - 1)(n - n_m). \tag{10}$$

Here n_m is concentration at maximum of trajectory.

One integrate (10) in view of (5)

$$(n - n_m)(1 - 2n_m)^{1/2} \,/\, p_m = \sin((1 - 2n_m)^{1/2}\varsigma + A). \tag{11}$$

Here

$$A = \arcsin((n_f - n_m)(1 - 2n_m)^{1/2} \,/\, p_m), \tag{12}$$

$$p_m = n_m(1 - n_m) \,/\, w\,. \tag{13}$$

is sense of *p* at maximum of trajectory

Put in (11) $\varsigma = \Delta$, then one have

$$(n_{\Delta} - n_m)(1 - 2n_m)^{1/2} \,/\, p_m = \sin((1 - 2n_m)^{1/2}\Delta + A). \tag{14}$$

Here n_Δ is sense of n at $\varsigma = \Delta$.

Differentiating (8), (9) once, one equate the first derivatives on the border of zones 1 - 3 and 2 – 3

$$n_f^2\lambda_{1,2}^2 = p_m^2 - (1-2n_m)(n_f - n_m)^2, \tag{15}$$

$$\lambda_4^2(1-n_\Delta)^2 = p_m^2 - (1-2n_m)(n_\Delta - n_m)^2. \tag{16}$$

Differentiating (8), (9) twice, one equate the second derivatives on the border of zones 1 - 3 and 2 – 3

$$n_f\lambda_{1,2}^2 = (2n_m - 1)(n_f - n_m), \tag{17}$$

$$\lambda_4^2(1-n_\Delta) = (1-2n_m)(\mathrm{n}_\Delta - n_m). \tag{18}$$

So, one have a system of nine algebraic equations (6), (7), (12) - (18) with respect to nine unknowns $n_f, n_m, n_\Delta, p_m, A, \lambda_{1,2}, \lambda_4, w, \Delta$, i.e. system is closed. Solving it, can to get the equation to determine the speed of the wave

$$\lambda_4^2(4w^2(-K_{1,2} \pm T_{1,2} - 1)^2 - (-K_{1,2} \pm T_{1,2})^{-1}) = 1. \tag{19}$$

Here

$$K_{1,2} = 0.5(\lambda_4^2 + \lambda_{1,2}^2 - w^2\lambda_{1,2}^2 + w\lambda_4^2), T_{1,2} = (K_{1,2}^2 + (w^2-1)\lambda_{1,2}^2\lambda_4^2).$$

After finding the velocity in (19), the remaining parameters are determined by the equations already obtained.

The results of the calculation of the left side of equation (19) (*Y)* as functions of speed are shown in Figure 3.

The branches of the function *Y* (*w*), corresponding to the values of λ_1, are designated 1. The branches of the function *Y* (*w*), corresponding to the values of λ_2, are designated 2. The signs "+" and "-"at 1 and 2 correspond to the signs $T_{1,2}$. From Figure 3 it follows that equation (19) satisfies only the branch

Figure 3. Decision of equation (19) 1 - $Y(w,\lambda_1)$, 2 - $Y(w,\lambda_2)$

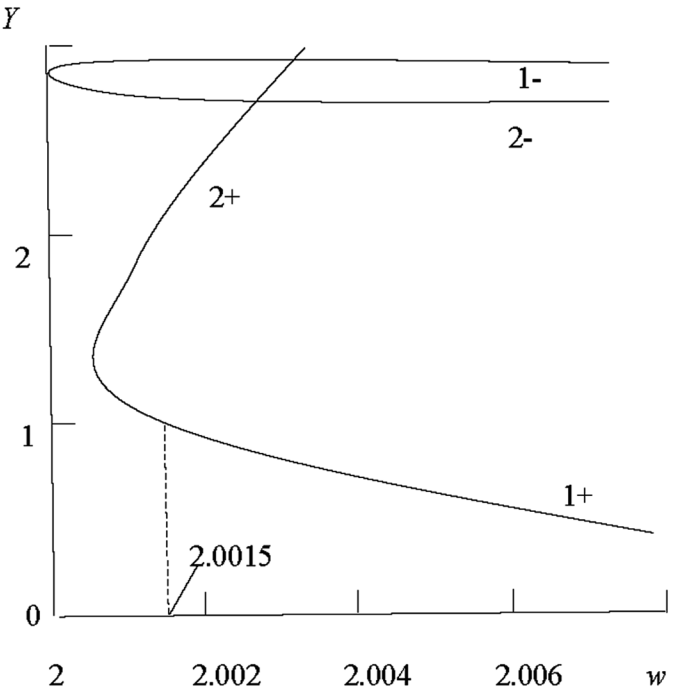

$Y(w)$, corresponding to the eigenvalue λ_1 at the sign "+" at T_1.The value of speed satisfying equation (19) is 2.0015. It is very close to the speed value of 2, found by A.N. Kolmogorov, I.G. Petrovsky, & N.S. Piskunov as a result of a complex analysis of the nonstationary equation (3).

The main attention in this work was paid to determining the shape and velocity of a population wave in a stationary mode. With the help of a mathematical study of the nonstationary equation (1), they shown that over time the initial perturbation of the concentration of a population in the form of a step transforms and the population wave takes a stationary form of a hollowed out step. For it the wave propagation velocity tends to a constant value — the minimum of all possibility the values of the diffusion coefficient and the coefficient of proportionality in the law of reproduction of the population. Unfortunately, the possibility of applying the results of A.N. Kolmogorov, I.G. Petrovsky, N. S. Piskunov is limited by the framework of a very simple model of biological population and accepted form of the initial

perturbation of the concentration. In the monograph by A.A. Samara et al. (Samara, Galaktionov, Kurdyumov, & Mikhailov, 1987) showed that if the initial concentration perturbation is different from the step, then the propagation velocity of a stationary wave may differ from the minimum. Therefore, it should be considered incorrect the assumptions of some authors (for example, Svirezhev, 1987; Ivanov, 1984), who consider more modern models of the population, that the wave propagation velocity has a minimum value of 2. In each case, the wave propagation velocity of the biological population and in the study of equations of mathematical physics (Polozhiy, 1964), it must be determined on the basis of this particular system of equations, as an eigenvalue of the problem. Moreover, this eigenvalue must correspond to the solution of the problem of the profile of the population wave, as an eigenvalue function.

Many authors generally do not set the task of determining the wave velocity of a biological population (see, for example, Keller, & Segel, 1971; Ivanitsky, Medvedinsky, & Tsyganov, 1991; Kerner, & Osipov, 1991), considering it to be an unknown parameter, and classify possible solutions (Berezovsky, & Karev, 1999) depending on wave velocity values. At the same time, it is as if they forget that the speed of wave propagation is a function of the conditions in which the population is located and the characteristics of the population itself. All these conditions and characteristics should be included in the equations of the population under consideration, and thus these equations themselves should determine the value of the wave velocity. Only those profiles can be considered in the wave, which correspond to the found speed values. The reason for this situation is the lack of methods for determining the speed of stationary propagation of a wave of a biological population.

The semi - infinite reaction zone method (Zhizhin, 2004), given in this section, allows finding the agreed values of the wave velocity of a biological population and its structure. This makes it possible to solve problems on the speed and structure of waves of biological populations of various models, in essence, by algebraic methods. It should be noted that the solution of the question of the velocity and structure of the wave of a biological population by the method proposed by A.N. Kolmogorov, I.G. Petrovsky, & N.S. Piskunov. However, this method is so complex that so far no one has been able to extend it to solve the problems of the population wave with more complex models. The theory of autosolitons (Kerner, & Osipov, 1991), which proposed methods for finding the speed and structure of autosolitons, does not describe a wave of populations of living organisms (Zhizhin, 2004).

MODEL OF A SOLITARY WAVE OF UNICELLULAR ORGANISMS TAKING INTO ACCOUNT THEIR NUTRITION, REPRODUCTION AND DEATH

In the mid - 60s of the last century, Adler and his students conducted a series of experimental studies of the propagation of waves of a population of bacteria in capillary tubes containing a nutrient medium (Adler, 1966; Adler, & Templeton, 1967; Adler, & Dahl, 1967). The experiments were carried out on bacteria *Escherichia coli* in a nutrient medium containing various salts. When bacteria were launched on one side of the tube, a wave of population (wave of conquest) was observed as it ran through the tube. When methionine was added to the nutrient medium in experiments, a different mode of wave propagation was observed — an antinode of bacterial concentration was formed, which moved along the tube. This means that a solitary wave of a population of bacteria was observed. The mechanism that leads to the formation of a solitary wave of a population in experiments has remained unclear. Keller and Segel (Keller, & Segel, 1971) suggested that the cause of the formation of a solitary population wave is the chemotaxis of bacteria, i.e. directional movement of bacteria towards an increase in the gradient of the nutrient resource, which naturally occurs due to the absorption of the resource by bacteria in the place of their appearance. The mathematical model of a solitary wave constructed by them did not take into account the multiplication of bacteria and their death, which contradicts the possibility of a wave being formed. An analysis of the possible effects of chemotaxis on the formation of a solitary wave conducted by the author (Zhizhin, 2004) showed that the established opinion in the scientific literature on the leading role of chemotaxis in the formation of a solitary population wave (Ivanitsky, Medvedinsky, & Tsyganov, 1991, 1994) is hyperbolized. Kennedy and Aris (Kennedy, & Aris, 1980) for the first time showed that a solitary population wave can exist without chemotaxis, if one take into account the chaotic mobility of individuals, the reproduction of the population, the death of individuals, the change in the concentration of the resource due to the feeding of individuals. The velocity of the wave, however, in this work and in its continuation (Lauffenburger, Kennedy, & Aris, 1984) was assumed minimal and the dependence of the velocity on the parameters was not established. In this regard, in the book consider the population model proposed by Kennedy and Aris, disregarding chemotaxis, and apply the semi - infinite reaction zone method to determine the wave velocity and its dependence on parameters.

The system of non - stationary equations describing in a one - dimensional formulation the change in the concentrations of unicellular organisms *N* and the resource *R* will be written as

$$\frac{\partial N}{\partial t} = \mu \frac{\partial^2 N}{\partial x^2} + N(\eta \tau_f^{-1} + \tau_e^{-1}), \tag{20}$$

$$\frac{\partial R}{\partial t} = -N / \tau_f. \tag{21}$$

Here τ_e is the effective lifetime of unicellular organisms, which will be considered permanent ($\tau_e = \tau_{e0}$); η is coefficient of resource processing into biomass of single - cell organisms; $\tau_f = \tau_{f0}(K_p + R)R^{-1}$ is effective time for feeding unicellular organisms (equation of Manod (Manod, 1950)) ; τ_{f0} is characteristic time of food with an excess of resource; resource concentration at which the food process time is twice as long τ_{f0}.

In equations (20), (21), the increase in the amount of biomass of a population due to reproduction is proportional to the amount of the resource consumed by it (proportionality factor η). Thus, it is possible to enter the characteristic time of reproduction of the population $\tau_p = \tau_f / \eta$. One also introduce the wave coordinate $z = u\,t - x$, dimensionless variables and parameters

$$r = R / K_p, \varepsilon = \tau_{e0} / \tau_{p0}, n = \varepsilon N(\eta K_p)^{-1}, \varsigma = (\tau_{e0}\mu)^{-1/2}, w = u(\tau_{e0} / \mu)^{1/2}.$$

Then the system (20), (21) is reduced to a system of three ordinary differential equations of the first order

$$\frac{dp}{d\varsigma} = wp + n(1 - \varepsilon r(1 + r)^{-1}), \tag{22}$$

$$\frac{dr}{d\varsigma} = -nrw^{-1}(1 + r)^{-1}, \tag{23}$$

$$\frac{dn}{d\varsigma} = p. \tag{24}$$

Solutions of the autonomous system (22) - (24) can be represented by trajectories in a three -dimensional phase space. It has the following four zero surfaces (Figure 4)

$F_1 : p = nw^{-1}(\varepsilon r(1+r)^{-1} - 1),$

in its points

$dp \,/\, d\varsigma = 0;$

$F_2 : p = 0,$

Figure 4. The phase space of the system (22) – (24)

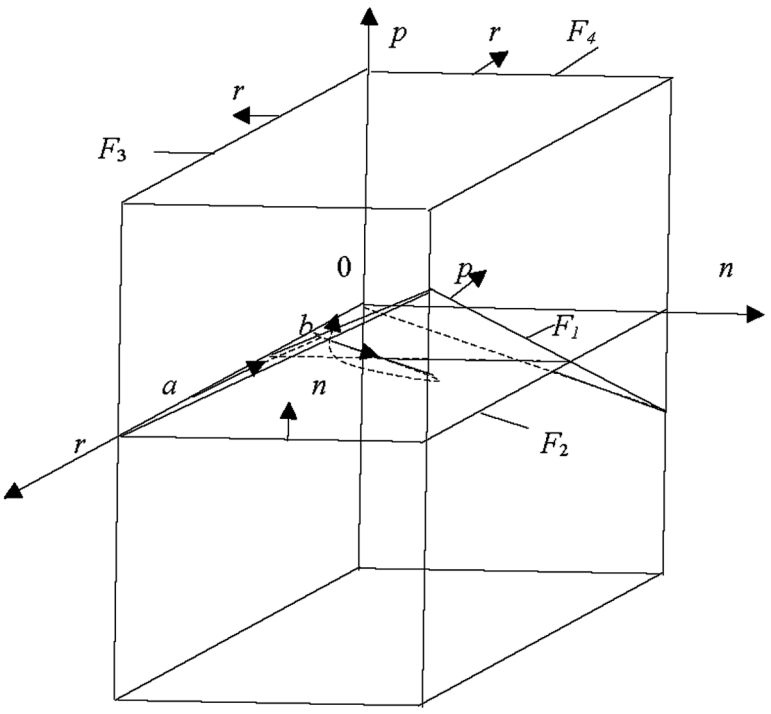

in its points

$dn / d\varsigma = 0;$

F_3

and

$F_4 : n = 0$

and

$r = 0$,

in its points $dr / d\varsigma = 0.$

The phase space has a line of equilibrium positions $p = 0, n = 0$, axis *r*. In the neighborhood of each point ($r_s > 0$) of this line, the trajectories are located in a plane. Moreover, depending on the values *w*, ε, r_s there are three possible locations of the trajectories. From the discriminant of equations (22), (23) can to find that the eigenvalues are equal to their own directions

$$\lambda_{1,2} = (dp / dn)_{1,2} = w / 2 \pm \sqrt{w^2 / 4 + 1 - \varepsilon r_s (1 + r_s)^{-1}}. \quad (25)$$

From (25) it follows that with $\varepsilon < (1 + r_s) / r_s$ special points of the axis are of the saddle type $(\lambda_1 > 0, \lambda_2 < 0)$, with $(1 + r_s) / r_s$ the special points have the type of unstable knot $(\lambda_1 > 0, \lambda_2 > 0)$, and with $\varepsilon > (w^2 / 4 + 1)(1 + r_s) / r_s$ - the focus. The desired wave solution can leave the initial equilibrium position only in an unstable proper direction $(\lambda_i > 0, i = 1,2)$. From the above it is clear, that two variants of the wave solution are provided. 1) A trajectory emerging from the initial equilibrium position of the saddle type along the separatrix S_1, and entering into the final equilibrium position of the saddle type along the separatrix S_2. 2) Trajectories emerging from the initial equilibrium position of a knot type along one of its own directions and entering the final equilibrium position of a saddle type along the separatrix S_2. Since at $r_s < (\varepsilon - 1)^{-1}$ the equilibrium positions are of saddle type, but the zero

surface F_1 is located in the negative octant (on p) of the phase space, the separatrix S_1, leaving the saddle equilibrium position in the positive octant of the phase space, cannot fall into the negative octant of this space. Therefore, it cannot enter the saddle position of equilibrium in a stable proper direction, located in the negative octant. Thus, the first variant of the wave solution cannot be implemented. There is only the second option. Indeed, in the region of the existence of a nodal equilibrium position, the zero surface F_1 is located in the positive octant of the phase space and trajectories emerging from the initial equilibrium position can first cross the zero surface F_1 and then the zero surface F_2 and get into the negative octant. After that, the trajectories can again cross the zero surface F_1, located already in the negative octant, and one of them can enter the saddle equilibrium position in a stable proper direction.

The integral curves corresponding to this wave solution are presented in Figure 5.

As follows from the graphs, the concentration of the population first grows along the wave coordinate and then one decreases. Thus, the wave solution has the form of a solitary population wave. It should be noted that in this case there was no chemotaxis.

Figure 5. The structure of the wave solution in the population with regard to nutrition, reproduction, death and the absence of chemotaxis

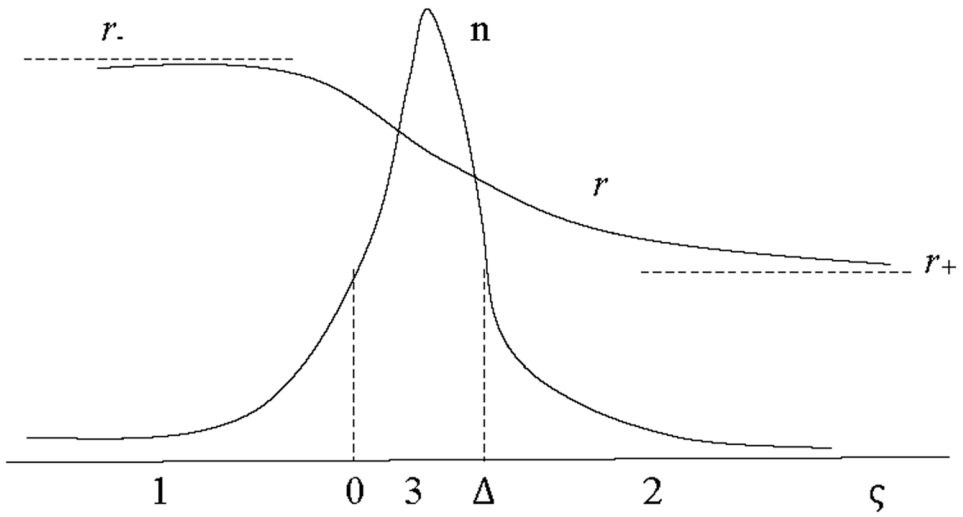

To obtain an approximate analytical solution, one apply the semi-infinite reaction zone method. Divide the wavelength into three zones (Figure 5). In the first zone $(-\infty < \varsigma < 0)$, one consider the solution of the system (22) – (24) linearized in the vicinity of the initial equilibrium state *a* to be fair

$$r = r_{-} - (r_{-} - r_{f}) \exp(\lambda_{1,2-}\varsigma), \tag{26}$$

$$n = n_{f} \exp(\lambda_{1,2-}\varsigma). \tag{27}$$

Here r_{-} is the initial concentration of the resource, r_{f} and n_{f} are the concentration of the resource and population at the wave front at $\varsigma = 0$,

$$\lambda_{1,2-} = w / 2 \pm \sqrt{w^2 / 4 + 1 - \varepsilon r_{-}(1 + r_{-})^{-1}}. \tag{28}$$

In the second zone $(\Delta < \varsigma < +\infty)$, one consider the solution of the system (22) – (24) linearized in the vicinity of finite equilibrium state *b* to be fair

$$r = r_{+} - (r_{\Delta} - r_{+}) \exp(\lambda_{2+}(\varsigma - \Delta)), \tag{29}$$

$$n = n_{\Delta} \exp(\lambda_{2+}(\varsigma - \Delta)). \tag{30}$$

Here r_{+} is concentration of the resource at point *b,* r_{Δ} and n_{Δ} are the concentrations of the resource and the population at the border of zones 2 and 3 at $\varsigma = \Delta$,

$$\lambda_{2+} = w / 2 - \sqrt{w^2 / 4 + 1 - \varepsilon r_{+}(1 + r_{+})^{-1}}. \tag{31}$$

In the zone 3 $(0 < \varsigma < \Delta)$ one used of the first integral of the system (22) – (24)

$$dn / d\varsigma = wn - (\varepsilon - 1)w(r_{-} - r) + w \ln(r_{-} / r). \tag{32}$$

One linearize the right - hand side of (32) in the neighborhood of the maximum of the trajectory *n*(*r*). Expanding the right - hand side of (32) into a Taylor series in the vicinity of the maximum ($n = n_m, r = r_m$), one confine ourselves to the first non - zero term

$$dn \,/\, d\varsigma = \beta_m (r - r_m). \tag{33}$$

Here

$$\beta_m = (\varepsilon - 1)w - w \,/\, r_m > 0, \tag{34}$$

$$n_m = (\varepsilon - 1)(r_- - r_m) - \ln(r_- \,/\, r_m). \tag{35}$$

In view of the finiteness of zone 3, one take the linear law of variation of *r* in this zone

$$r = r_f - (r_f - r_\Delta)\varsigma \,/\, \Delta. \tag{36}$$

Then, one integrated (33) with account (36)

$$n = -0.5\Delta\beta_m (r - r_m)^2 \,/\, (r_f - r_\Delta) + n_m. \tag{37}$$

Using the condition of continuity of concentrations at the zone boundary from (37) can to obtain

$$n_f = -0.5\Delta\beta_m (r_f - r_m)^2 \,/\, (r_f - r_\Delta) + n_m, \tag{38}$$

$$n_\Delta = -0.5\Delta\beta_m (r_\Delta - r_m)^2 \,/\, (r_f - r_\Delta) + n_m. \tag{39}$$

Using the condition of continuity of the first derivatives on the zone boundary from (26), (27), (29), (30), (36), (37) one get

$$\Delta(r_- - r_f)\lambda_{1,2-} = r_f - r_\Delta, \tag{40}$$

$$n_f \lambda_{1,2-} = (r_f - r_m)\beta_m, \tag{41}$$

$$\Delta(r_\Delta - r_+)\lambda_{2+} = r_\Delta - r_f, \tag{42}$$

$$n_\Delta \lambda_{2+} = (r_\Delta - r_m)\beta_m. \tag{43}$$

One assume that the linear section in the profile $r(\varsigma)$ is chosen so that the sum of the second derivatives $d^2r \,/\, d\varsigma^2$ at $\varsigma = 0$ on the left and at $\varsigma = \Delta$ on the right is zero. Differentiating (26), (29), one have

$$(r_\Delta - r_+)\lambda_{2+}^2 = (r_- - r_f)\lambda_{1,2-}^2. \tag{44}$$

Equate the right side of equation (22) to zero on the border at $\varsigma = \Delta$

$$w\lambda_{2+} + 1 - \varepsilon r_\Delta \,/\, (1 + r_\Delta) = 0. \tag{45}$$

So, one have 12 equations (28), (31), (34), (35), (38) - (45) and 12 unknowns

$$\lambda_{1,2-}, \lambda_{2+}, w, n_m, r_m, \Delta, r_f, r_\Delta, r_+, n_f, n_\Delta, \beta_m.$$

The resulting system of equations is resolved (Zhizhin, 2004) and leads to one equation for the speed

$$(r_f - r_m)(2r_- - r_f - r_m)\beta_m \,/\, \lambda_{1,2-} = 2n_m(r_- - r_f). \tag{46}$$

All quantities in the last equation (46) are functions of speed. After determining the velocity value by (46), the remaining parameters are determined by the already obtained equations.

As rally from (33) with

$$r_- = r_+ = r_f = r_\Delta = (\varepsilon - 1)^{-1}, w = 0\,,$$

this equation holds. The ratio $r_- = (\varepsilon - 1)^{-1}$ defines a line in the plane of control parameters (r_-, ε) (Figure 6).

This line (1) is the lower boundary of the domain of existence of solutions. It corresponds to the complete degeneration of the wave. The upper limit of the domain of existence of solutions is line 2 (Figure 6), on which $r_+ = 0$. The equation of this line is obtained after substituting $r_+ = 0$ into the analytical solution. It responds to the mode of complete consumption of the resource in the wave. On this line, the wave velocity at the given ε is maximum. The value of the wave velocity decreases to zero, if one move in a straight line ε = *constant* across the region of existence of solutions, from line 2 to line 1. The wave velocity along line 2 smoothly increases with increasing ε. Calculations of concentration profiles of a population and a resource with

Figure 6. Area of existence of a solitary wave of unicellular organisms: 1- the lower boundary of the domain of existence of solutions (complete degeneration of the wave), 2 - complete consumption of the resource in the wave

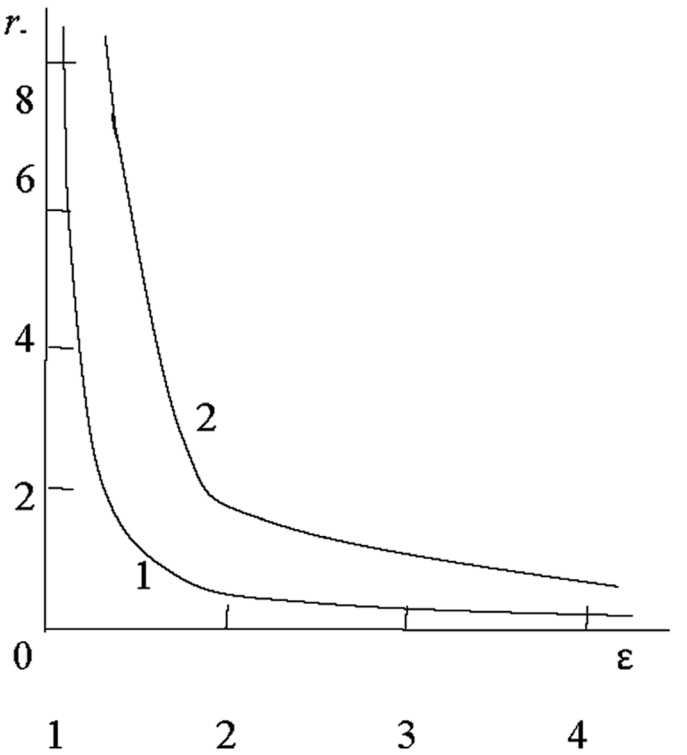

specific values of control parameters (Zhizhin, 2004) confirmed the appearance of the graphs in Figure 5, obtained as a result of a qualitative study of the original system of differential equations.

THE WAVES IN POPULATIONS ALLEE

When considering the logistic population, it was assumed that the fertility function B in the local law of growth is determined only by the physiological limits of fertility and does not depend on the concentration of the population. For many species of multicellular organisms that migrate freely across their range and reproduce sexually, this is not entirely true. At low population densities, reproduction is determined rather by the probability of meeting the mating partners, and not by physical fertility. In these cases, the B (N) relationship has the form shown in Figure 7 as an example of the butterfly population.

In this figure, the number of eggs laid by one butterfly *Anagasta kuhniella* (Svirezhev, 1987; Ullyet, 1945) is plotted on the ordinate axis, depending on

Figure 7. Dependence of the fertility function on the population concentration in the Allee populations

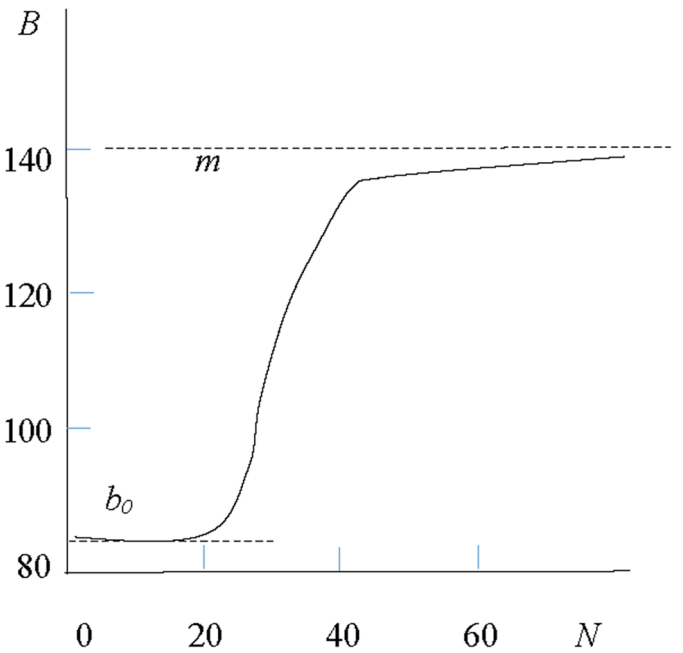

the concentration of butterflies. Populations with this type of dependence *B* (*N*) are called Allee populations (Allee, 1951).

The peculiarity of this dependence for such populations is the saturability of *B* with increasing *N* and the finiteness of *B* at low concentrations of *N*. The dependence that asymptotically tends to some limiting values for large and small values of the argument can be expressed, as in the theory of combustion, by an exponential function

$$B(N) = b_0 + b_1 \exp(-\alpha_0 / N). \tag{47}$$

Here $b_1 + b_0 = m$ is physiological birth rate.

Assuming that mortality linearly depends on the concentration of the pupil, the function describing the local law of population growth in the nonstationary diffusion equation (1) has the form

$$F(N) = b + b_1 \exp(-\alpha_0 / N) - \alpha_2 N. \tag{48}$$

Here $b = b_0 - \alpha_1 > 0$.

Introducing the scaled concentration of the population $n = N / \alpha_0$, related to the parameter α_0, characterizing the rate of increase of *B* with increasing *N*, as well as the wave coordinate $z = ut - x$, one write the differential equation of diffusion in total derivatives

$$wdn / d\varsigma = d^2 n / d\varsigma^2 + (1 + a \exp(-1 / n) - cn. \tag{49}$$

Here $\varsigma = z(b / \mu)^{1/2}, w = u(\mu b)^{1/2}, a = b_1 / b, c = \alpha_2 \alpha_0 / b.$

Equation (49) may be write in form of system

$$dp / d\varsigma = wp - F(n), \tag{50}$$

$$dn / d\varsigma = p. \tag{51}$$

Here

$$F(n) = n(1 + aexp(-1 / n) - cn). \tag{52}$$

It should be noted that the representation of the local law of population growth $F(n)$ in the form of a polynomial of *n*, proposed in some works (Kerner, & Osipov, 1991), does not reflect the main feature of the Allee population - the saturability of the birth function at large *n*. Accounting for this feature leads to a function (52) that is not a polynomial.

The solution of system (50), (51) can be represented by trajectories in the phase plane (p, n) . Their location is determined by zero isoclines $p = 0$, on which $dn / d\varsigma = 0$, and

$$p = (1 + a\exp(-1 / n) - cn)n / w, \tag{53}$$

on which $dp / d\varsigma = 0$.

The equilibrium positions of the system (50) – (52) are the intersections of the zero isoclines, i.e. they are the roots of the equation $0 = (1 + a\exp(-1 / n) - cn)n$. Obviously, one root of this equation is $n = 0$. Other roots are determined by the equality

$$a\exp(-1 / n) = cn - 1. \tag{54}$$

The number of roots of equality (54) depends on the values of the parameters *a*, *c*. It can be equal to 1 or 3 according to the number of intersections of the right and left side of (54). The boundary value of the roots (54) is equal to two, one of which corresponds to the touch of the right and left parts of (54). Equating the derivatives of the right and left parts of (54) with the simultaneous fulfillment of equality (54) itself, one can find an expression for the boundary line in the plane (*a, c*) separating the parameter regions with two and four equilibrium positions

$$a = (c(0.5 \pm \sqrt{0.25 - c^{-1}}) - 1\exp(0.5 \pm \sqrt{0.25 - c^{-1}})^{-1}. \tag{55}$$

The graph of this line (*l*) is presented in Figure 8.

It consists of two branches (l_+ and l_-) corresponding to the signs in front of the root in (55). In region 1 between of branches of the line *l*, there are four equilibrium positions. In area 2, including the *c* axis, the system has two equilibrium positions. On the line (55) itself, the system has three equilibrium positions, one of which is not coarse and disappears with a small wiggling of the system. On the axis *a*, the system has one equilibrium position when

Figure 8. Bifurcation system diagram (50)-(52): 1 – region of four equilibrium positions, 2 – region of two equilibrium positions

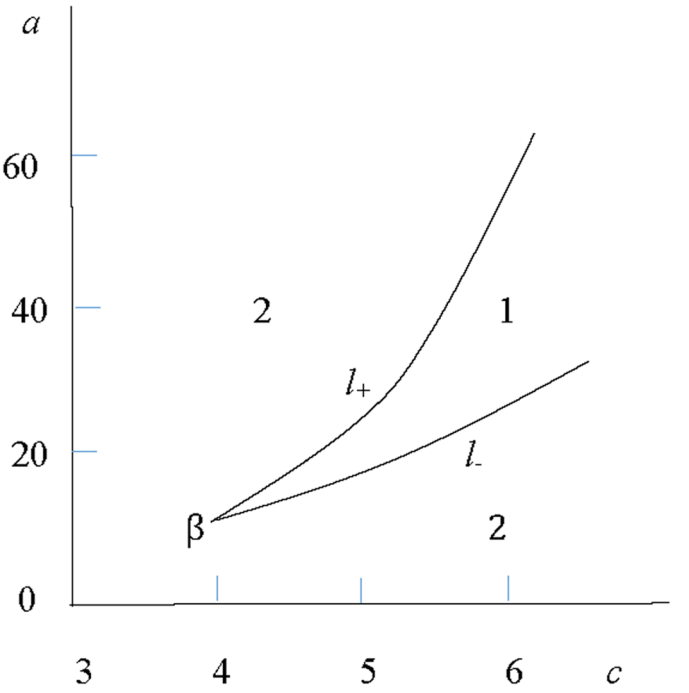

$n = 0$. The β point with the coordinates $a = e^2 = 7.389, c = 4$ in which both branches of the line are connected is a catastrophe point of the system (50) – (52). Since $F(n)$ is not a polynomial, this point cannot be attributed to any of the elemental catastrophe (Breker, & Lander, 1977), but its neighborhood is close to a neighborhood of a hyperbolic ombelic catastrophe at a constant value of one of the deformation parameters. Of greatest interest is the case when the system (50) – (52) has four equilibrium positions, as in this case there is the greatest number of solutions (Zhizhin, 2004).

Here there are topologically distinct phase diagrams of the system (50) – (52), having as a solution conquest waves, solitary waves and switching waves (transitions from one equilibrium position to another, each of which is different from the origin) (Zhizhin, 2004). Choose one of them, containing waves of conquest and solitary waves (Figure 9).

It contains the equilibrium positions $e_i, i = 1 \div 4$. The types of special points (equilibrium positions) are determined from the discriminant of the

Figure 9. Phase diagram of system (50) - (52) with four equilibrium positions

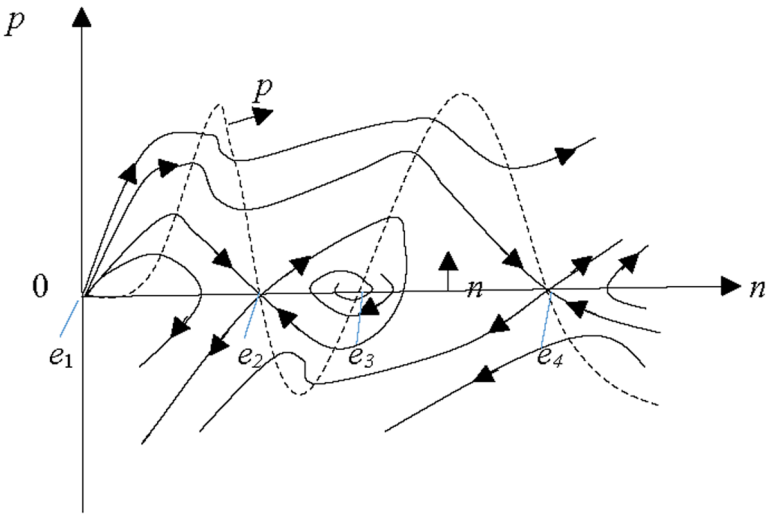

system in the neighborhood of each of the special points. In the vicinity of the point $e_1(0,0)$ one have

$$\lambda_{1,2e_1} = 0.5w \pm \sqrt{0.25w^2 - 1}, \tag{56}$$

for $w > 2$ the point e_1 has the type of an unstable node. In the vicinity of points $e_i, i = 2,3,4$ one have

$$\lambda_{1,2e_i} = 0.5w \pm \sqrt{0.25w^2 - F^{'}(n)}, \mathrm{i} = 2,3,4. \tag{57}$$

Here

$$F^{'}(n) = 1 - 2cn + (1 + 1/n)\exp(-1/\mathrm{n}). \tag{58}$$

Since $F^{'}(n) < 0$ in point e_3, so this point has the type of an unstable focus or an unstable node.

However, in topological terms, this difference is insignificant, which determines the topological equivalence of phase diagrams in these cases. Since at points $e_2, e_4 F^{'}(n) > 0$ these points are of saddle type. To solve the problem of the existence of wave solutions, it is necessary to construct the

entire system of trajectories on the phase plane so that the assumed location in the neighborhood of a particular point does not contradict the location of the trajectories in the neighborhood of other special points. This excludes some of the solutions found (Svirezhev, 1987) without considering this condition. From the phase diagram in Figure 9 it follows that the trajectory that goes from the equilibrium position e_1 to the equilibrium position e_2 corresponds to the wave of conquest. The solitary wave corresponds to the trajectory out of the equilibrium position e_2 and entering the equilibrium position e_2.

Consider the waves of conquest. Using the semi - infinite reaction zone method, one divide the wave into three zones. In the first zone $(-\infty < \varsigma < 0)$, one consider the solution of the system in the vicinity of the equilibrium state e_1 to be fair

$$n = n_f \exp(\lambda_{1,2e_1}\varsigma). \tag{59}$$

Here n_f is the concentration value of the population at the wave front at $\varsigma = 0$.

In the second zone $(\Delta < \varsigma < +\infty)$, one consider the solution of the system in the vicinity of the e_2 point to be fair

$$n = n_2 - (n_2 - n_\Delta)\exp(\lambda_{2e_2}(\varsigma - \Delta)). \tag{60}$$

Here n_Δ is the concentration value of the population for $\varsigma = \Delta$.

In the third zone, one linearize the right - hand side of (50) in the vicinity of the maximum of the trajectory of the phase plane (p, n)

$$dp \,/\, d\varsigma = -F'_m(n - n_m), F'_m = F'_n(n_m). \tag{61}$$

One integrate (61) with account (51)

$$(n - n_m)p_m^{-1}(-F'_m)^{1/2} = \sin((-F'_m)^{1/2}\varsigma + A), \tag{62}$$

$$A = \arcsin((n_f - n_m)p_m^{-1}(-F'_m)^{1/2}), \tag{63}$$

$$p_m = F_m / w. \tag{64}$$

One put in (62) $\varsigma = \Delta$

$$(n_\Delta - n_m)p_m^{-1}(-F_m^{'})^{1/2} = \sin((-F_m^{'})^{1/2}\Delta + A). \tag{65}$$

Differentiating (59), (60), (65) once, one equate the first derivatives on the border of zones 1 - 3, 2 – 3

$$n_f^2\lambda_{1,2e_1}^2 = p_m^2 - F_m^{'}(n_f - n_m)^2, \tag{66}$$

$$\lambda_{2e_2}^2(n_2 - n_\Delta)^2 = p_m^2 - F_m^{'}(n_\Delta - n_m)^2. \tag{67}$$

Differentiating (59), (60) twice taking into account (61), one equate the second derivatives on the border of zones 1 - 3, 2 - 3

$$n_f^2\lambda_{1,2e_1}^2 = -F_m^{'}(n_f - n_m), \tag{68}$$

$$\lambda_{2e_2}^2(n_2 - n_\Delta) = -F_m^{'}(n_\Delta - n_m). \tag{69}$$

Solving the resulting system of algebraic equations, one obtain two equations for determining the velocity of the wave *w* and the concentration of the population at the maximum of the trajectory n_m

$$1 = \lambda_{1,2e_1}^2(w^2 n_m^2 F_m^{-2} - 1 / F_m^{'}), \tag{70}$$

$$F_m^{'}\lambda_{2e_2}^{-2} = F_m^{-2}(F_m^{'})^{-1}w^2(\lambda_{2e_2}^2(n_2 - 1) + (n_2 - n_m)F_m^{'})^2 - 1. \tag{71}$$

The solution obtained can be considered as a general solution of the problem of the conquest wave for an arbitrary function *F* (*n*) in equation (50).

Similarly, using the semi - infinite reaction zone method, analytical solutions can also be obtained for other wave solutions in the Allee populations.

MATHEMATICAL MODEL OF FLIGHT OF THE GREGARIOUS LOCUST

The propagation of wave in populations of animal organisms complicated by many accompanying processes. Such processes include changes in the concentration of the nutritional resource for the organisms of the population, environmental pollution with waste products of organisms, the desire for the herd of animal organisms, the interaction of animal populations and populations of plant organisms. Mathematical models of waves in populations of multicellular organisms taking into account changes in the concentration of nutrient resources and environmental pollution by products of vital activity of organisms are constructed and investigated in the already mentioned monograph (Zhizhin, 2004) and in work (Zhizhin, Bolshakova, 2000). The influence of the bark beetle herd in the process of attacking the forests in the form of a solitary wave has been studied in works (Zhizhin, 2011; Zhizhin, & Selikhovkin, 2012). In this section, the flight pattern of the gregarious locust will be investigated, since the locust still causes enormous damage to vegetation in many parts of the earth.

Many works have been devoted to the description of mass locust breeding and migration of its flocks (Bei - Bienko, & Mishchenko, 1951; Kopaneva, & Stebaev, 1985; Chetverikov, 1905; Shcherbinovsky, 1952, 1958). Well - known entomologist B.P. Uvarov in the 20s of the last century showed (Bey - Bienko, 1970) that the phenomenon of so - called phase variation is characteristic of the locust: depending on the density of the group and the concentration of food, either single forms or herd larvae form. A single form of larvae is formed when there is enough feed. This form of the locust characterized by inconspicuous coloring and calm behavior. With a lack of food and large crowding, a gregarious locust form is formed. This form is characterized by bright color, great mobility and aggressiveness. Processes, causing the dynamics of the number of any insects, associated with the interaction of the two kingdoms living organisms: plants and animals. External influences — abiotic, biotic, and man - made — are multifaceted, and the response of bio – geo – cenosis is difficult to foresee, which requires the use of mathematical methods to describe and analyze them.

Existing work on the mathematical description of the behavior of insects includes questions of mathematical modeling of the distribution of locust populations over the territory. Topaz et al. (2012) consider a model of the locust transition to the active phase. Taylor (1979) assumes that the locust migration is completely determined by the flow of air. Topaz et al. (2008) raise of a model creeping locust migration.

In this section, a mathematical model of the flight of the gregarious locust is built over long distances when the locust is removed from the earth's surface at distances significantly exceeding the size of insects, as this is probably the most dangerous option for the environment to spread locusts in space.

This regime is not consistent with the locust migration crawling model. A model that considers locusts at the flight stage as inert dust particles in an air stream contradicts the established notions of aggressiveness and high mobility of the herd locust. Following the concept of S.S. Chetverikov (Chetverikov, 1905) one will consider the process of locust propagation as the propagation of living matter in space in the form of waves of life. Then, to describe the flight of the locust flock, parabolic systems of equations can be used, as soon as they describe the propagation of nonlinear waves in space in various excitable media (Kolmogorov et al., 1937; Svirezhev, 1987; Zhizhin, 2004, 2005, 2008).

The system of non - stationary equations describing in a one - dimensional formulation the change in the concentration of the biological population $N(x,t)$ and the food supply $R(x,t)$, averaging the discrete flight process of the herd locust in space and time, can be written as

$$\frac{\partial N}{\partial t} = \frac{\partial}{\partial x}\mu\frac{\partial N}{\partial x} + F(N), \tag{72}$$

$$\frac{\partial R}{\partial t} = -\tau_f^{-1}N. \tag{73}$$

Here *t* is a time, *x* is a spatial coordinate, μ is locust mobility coefficient, τ_f is characteristic locust feeding time, $F(N)$ is a function describing a local change in locust population concentration.

A local decrease in the concentration of locust individuals in flight occurs for various reasons (diseases, their swallowing up by birds and even other individuals of the flock). Locusts do not breed during the flight, but locust has

another way to combine the natural decline of the flock - this is attracting the locust to the flock from the environment through special chemical products released by insects.

In connection with this, equation (72) can be rewritten as

$$\frac{\partial N}{\partial t} = \frac{\partial}{\partial x}\mu\frac{\partial N}{\partial x} + (\tau_c^{-1} - \tau_e^{-1})N. \tag{74}$$

Here τ_e is the characteristic time of life of individuals of the population, τ_c is the characteristic time of replenishment of the population due to the desire of individuals of the locust to unite in a flock. One assume τ_e, τ_c, τ_f as constants. The mobility coefficient of locust individuals increases with a decrease in the concentration of food supply (Kopaneva, & Stebaev, 1985). This behavior of locusts can be described as a first approximation by an inversely proportional relationship, considering the degree of the concentration of the food supply to be equal to one, $\mu \sim A / R$. The coefficient of proportionality *A* in this relationship must have the dimension of the product $[\mu][R]$. Therefore, *A* can be represented as a product of two constants, one of which has the dimension of the concentration of food supply, and the other has the dimension of mobility of locust individuals, that is,

$$\mu = \frac{\mu_0 K_R}{R}. \tag{75}$$

Let us call K_R the unit concentration of the food base and μ_0 the mobility coefficient of the individuals at a single concentration of the food base.

The constants in formulas (73) - (75) obviously depend on the locust species, as well as on temperature as a parameter.

One will consider the stationary mode of locust population spread by the wave. If to introduce the wave coordinate $z = ut - x$, where *u* is the unknown wave propagation velocity (determined during the solution of the problem), as well as dimensionless variables and parameters

$$r = \frac{R}{K_R}, n = \frac{N}{K_R}, \varsigma = z\tau_0\mu_0 / 2, \mathrm{w} = u(\tau_0 / \mu_0)^{1/2}, \varepsilon = \tau_0 / \tau_f, \tau_0 = \frac{\tau_c\tau_e}{\tau_e - \tau_c},$$

then equations (74), (73) take the following form

$$w\frac{dn}{d\varsigma} = \frac{d}{d\varsigma}(\frac{1}{r}\frac{dn}{d\varsigma}) + n, \tag{76}$$

$$w\frac{dr}{d\varsigma} = -\varepsilon n. \tag{77}$$

Equation (76) with regard to (77) and the boundary condition $n = 0, \frac{dn}{d\varsigma} = 0$ for $r = r_{-}$ (the initial concentration of the food supply) has the first integral

$$\frac{dn}{d\varsigma} = rw(n - \frac{r_{-} - r}{\varepsilon}). \tag{78}$$

The system (78), (77) is autonomous and has in the phase plane (n, r) zero isoclines $r = 0, n = \frac{r_{-} - r}{\varepsilon}$, on which $\frac{dn}{d\varsigma} = 0$, and $n = 0$, on which $\frac{dr}{d\varsigma} = 0$, as well as two special points α(0,0), β(0, r_{-}). From the discriminant of the system in the neighborhood of a point β one find the eigenvalues of this special point

$$\lambda_{1,2} = 0.5r_{-}w \pm \sqrt{(0.5r_{-}w)^2 - r_{-}}. \tag{79}$$

From (79) it follows that with $(0.5r_{-}w)^2 - r_{-} > 0$ the point β has the type of an unstable node, and with $(0.5r_{-}w)^2 - r_{-} < 0$ an unstable focus. Since we are looking for a solution that describes the change in the concentration of locust glands along the wave coordinate from zero to zero, one assume that the radical expression in (79) is positive. Then the point β will have the type of an unstable node, and from it the trajectories emanate from its own directions $(\frac{dn}{dr})_{1,2} = -\lambda_{1,2}w / \varepsilon$, one of which corresponds to the desired wave solution.

From the discriminant of system (77), (78) in the vicinity of a point α, it follows that a point α has a saddle type with eigenvalues $\lambda_{3,4} = -r_{-}^{1/2}$, and the proper direction $\lambda_4 = -r_{-}^{1/2}$ in which the trajectory enters the point α is

located in the positive quadrant of the plane. The sought solution leaves the point β along one of the separatrices of the node and enters the point α along the separatrix of the saddle (Figure 10), crossing the zero isocline $n = \frac{r_- - r}{\varepsilon}$.

The arrows at the zero isoclines indicate the regions of positive values of the corresponding derivatives (Figure 10). The integral curves corresponding to this wave solution are shown in Figure 11.

It can be seen that the concentration profile of the locust population has the form of a solitary wave (soliton), and the concentration profile of the food supply has the form of a nonlinear wave. Both proper directions in a point β are located above the zero isocline $n = \frac{r_- - r}{\varepsilon}$ and it is not possible to decide from qualitative analysis in which proper direction the wave solution leaves the special point β.

To solve this question, one apply the semi - infinite reaction zone method. Imagine that a wave consists of five zones. In the first zone $(-\infty < \varsigma < 0)$,

Figure 10. The phase plane of solitary wave of the locust population

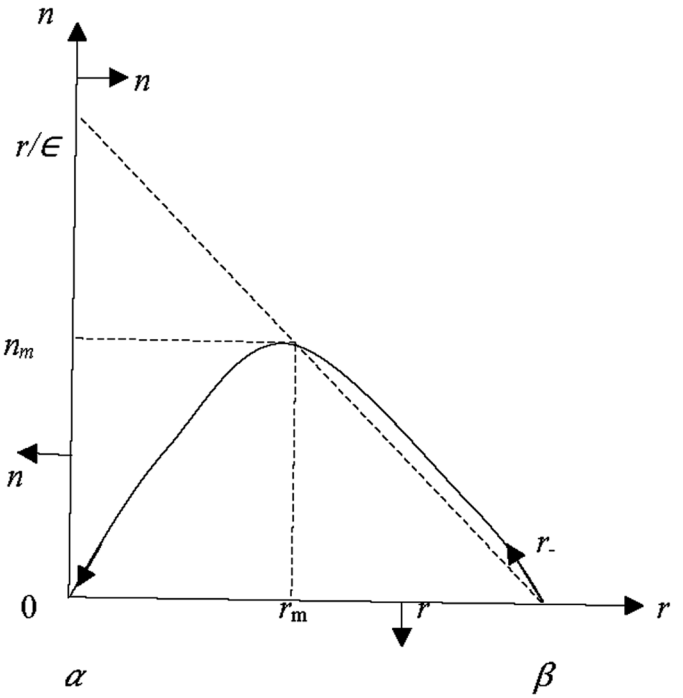

Figure 11. Qualitative view of the integral curves of the system (77), (78)

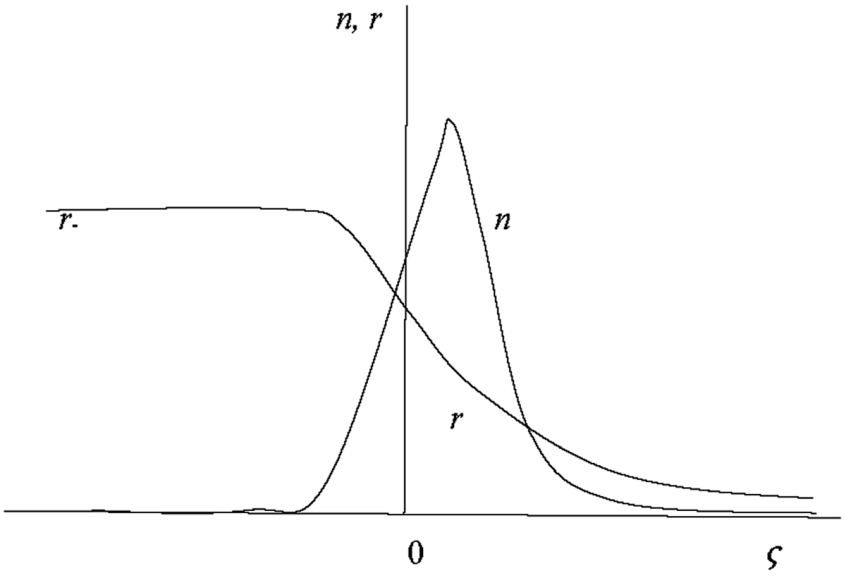

one consider the solution of the system (77), (78) in the neighborhood of the point β to be fair. In the second zone $(\Delta < \varsigma < +\infty)$, one consider the solution of the system in the neighborhood of the point α to be fair. In the third zone $(0 < \varsigma < \Delta)$, due to its limited nature, one will take a linear dependence of the concentration of the food base on the spatial coordinate. Then the equations for the concentrations in the first zone have the form

$$r = r_{-} - (r_{-} - r_{f}) \exp(\lambda_{1,2}\varsigma), \tag{80}$$

$$n = n_{f} \exp(\lambda_{1,2}\varsigma), \tag{81}$$

and in the second zone this form

$$r = r_{\Delta} \exp(-r_{-}^{1/2}(\varsigma - \Delta)), \tag{82}$$

$$n = n_{\Delta} \exp(-r_{-}^{1/2}(\varsigma - \Delta)). \tag{83}$$

Here r_f, n_f are concentrations of the foot base and locust population on the front wave for $\varsigma = 0$; r_f, n_f are concentrations of the foot base and locust population on the bound second and third zones for $\varsigma = \Delta$. In the third zone equation for concentration of the foot base have form

$$r = r_f - \frac{(r_f - r_\Delta)\varsigma}{\Delta}. \tag{84}$$

In order to obtain an equation for locust population concentration in the third zone, expand the right - hand side of equation (78) into a Taylor series in the vicinity of the soliton maximum $(n = n_m, r = r_m)$ and confine ourselves to the first term of the expansion

$$\frac{dn}{d\varsigma} = r_m n_m (\varsigma - \varsigma_m). \tag{85}$$

With (78) one have

$$n_m = \frac{r_- - r_m}{\varepsilon}. \tag{86}$$

Integrating (84), can to get

$$n = n_m - 0.5 r_m n_m (\varsigma - \varsigma_m)^2. \tag{87}$$

The set of boundary conditions includes:

1. the equalities of concentrations of the locust population on both sides of the boundaries of the first and third zones at $\varsigma = 0$, as well as the boundaries of the second and second and third zones at $\varsigma = \Delta$
2. $n_f = n_m - 0.5 r_m n_m \varsigma_m^2,$ (88)

$$n_\Delta = n_m - 0.5 r_m n_m (\Delta - \varsigma_m)^2; \tag{89}$$

3. the equalities of the first derivatives of the concentrations of the components on ς with both sides of the boundaries of the first and third zones, as well as the boundaries of the second and third zones

$$(r_{-} - r_f)\lambda_{1,2} = \frac{r_f - r_\Delta}{\Delta}, \tag{90}$$

$$n_f \lambda_{1,2} = r_m n_m \varsigma_m, \tag{91}$$

$$r_\Delta r_{-}^{1/2} = \frac{r_f - r_\Delta}{\Delta}, \tag{92}$$

$$n_\Delta r_{-}^{1/2} = r_m n_m (\Delta - \varsigma_m); \tag{93}$$

4. the equality of the second derivative to zero of the n on ς in equation (76) in point $\varsigma = 0$, which leads to equation

$$w = \frac{r_f - r_\Delta}{\Delta r_f^2} + \frac{n_f}{r_m n_m \varsigma_m}. \tag{94}$$

In addition, from the equation (84) follows

$$r_m = r_f - \frac{(r_f - r_\Delta)\varsigma_m}{\Delta}. \tag{95}$$

The system of ten algebraic equations (79), (86), (88) – (95) is closed with respect to ten unknown parameters $\lambda_{1,2}, w, \Delta, r_m, r_\Delta, n_m, n_\Delta, r_f, n_f, \varsigma_m$. .

Solving this system (Zhizhin, 2014), can to obtain an equation for calculating the wave propagation velocity

$$[r_f - (r_- - r_f)\lambda_{1,2}\varsigma_m](\varsigma_m / \lambda_{1,2} + 0.5\varsigma_m^2) = 1. \tag{96}$$

Here

$$\varsigma_m = b\frac{r_-^{-1/2} + 0.5b}{b + r_-^{-1/2} + \lambda_{1,2}^{-1}}, \tag{97}$$

$$b = \frac{r_f - (r_- - r_f)\lambda_{1,2}r_-^{-1/2}}{(r_- - r_f)\lambda_{1,2}}, \tag{98}$$

Figure 12. Dependencies of the characteristics of the solitary locust wave on the initial concentration of the food supply (ε = 0.1): a) speed, b) own number of the initial equilibrium position, c) locust concentration at the soliton maximum

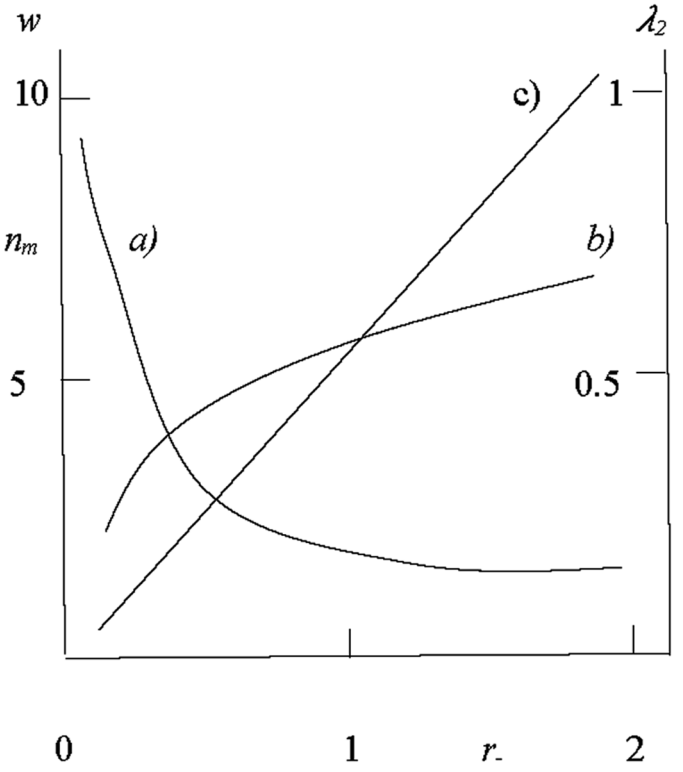

$$r_f = 0.5\lambda_{1,2}\frac{-\lambda_{1,2} + \sqrt{\lambda_{1,2}^2 + 4r_-(w\lambda_{1,2} - 1)}}{w\lambda_{1,2} - 1}. \quad (99)$$

To calculate the system, it is necessary to set the values of two parameters characterizing the initial concentration of the feed base and the ratio of the characteristic process times. A well-studied study showed that equation (96) has a solution if one of two eigenvalues $\lambda_{1,2}$ is chosen λ_2. Thus, the desired wave solution has its own number λ_2 and goes in its own direction $n = \frac{r_- - r}{\varepsilon}$, closest to the zero isocline. Figure 12 shows as an example the graphs of the functions calculated by the solution obtained.

Figure 13 presents the results of the calculation of locust concentration profiles and the food resource in the wave.

It can be seen that the locust concentration profile has the form of a soliton, and the food resource concentration profile has the form of a nonlinear switching wave from the initial final value to zero. Thus, the resulting solution is a solitary wave of the biological population.

Figure 13. Concentration profiles in the secluded locust population wave

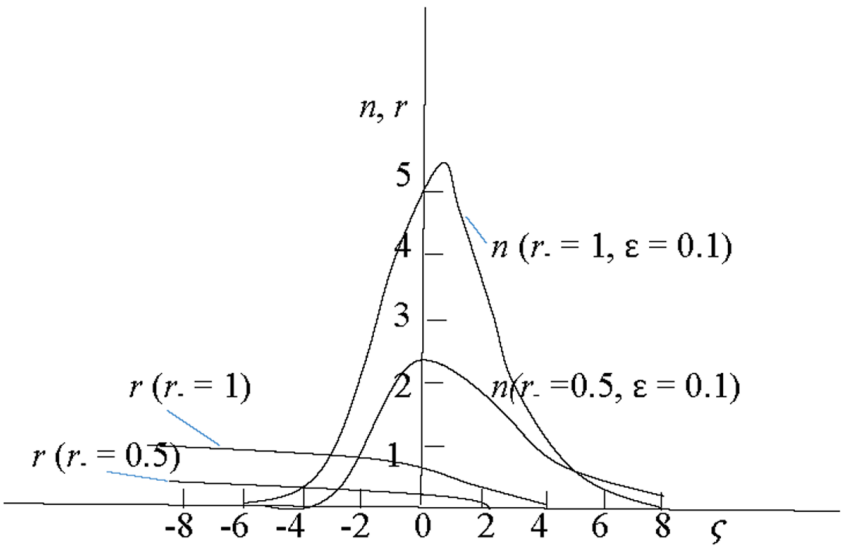

Numerical studies have shown that the rate of a solitary population wave of locusts increases dramatically with a decrease in the initial concentration of the food supply. While the wave profile is stretched. This effect was also observed in other solitary population waves (Zhizhin, 2005).

REFERENCES

Adler, J. (1966). Chemotaxis in bacteria. *Science*, *153*(3737), 708–716. doi:10.1126cience.153.3737.708 PMID:4957395

Adler, J., & Dahl, M. M. (1967). Method for Measuring the Motility of Bacteria and for Comparing Random and Non-random Motility. *Journal of General Microbiology*, *46*(2), 161–173. doi:10.1099/00221287-46-2-161 PMID:5339791

Adler, J., & Templeton, B. (1967). The Effect of Environmental Conditions on the Motility of Escherichia coli. *Journal of General Microbiology*, *46*(2), 175–184. doi:10.1099/00221287-46-2-175 PMID:4961758

Allee, W. C. (1951). *Cooperation among animals with human implications*. N.Y. Shuman.

Berezovskaya, E.S., & Karev, G.P. (1999). Bifurcations of traveling waves in population taxis models. *Advances in Physical Sciences*, *169*(9), 1011-1024.

Bey-Bienko, G.Y., & Mishchenko, L.L. (1951). Locust fauna of the USSR. Part 1 Determinants of fauna. 38. Moscow: Ed. Academy of Sciences of the USSR.

Bey-Bienko, G.Y. (1970). B.P. Uvarov (1889 - 1970) and his contribution to science and practice. *Entomological Review*, *49*(4), 915–922.

Chetverikov, S. S. (1905). Waves of life. From lepidopetrological observations of the summer of 1903. *Diary of the Zoological Department of the Imperial Society of Lovers of Natural Science*, *Anthropology and Ethnography*, *3*(6), 106–111.

Isaev, A. S. (2001). *Population dynamics of forest insects*. Moscow: Science.

Isaev, A. S., Nedorezov, L. V., & Khlebopros, R. G. (1979). Mathematical model of escape in the interaction of a predator and a prey. In *Mathematical analysis of the components of forest biocenoses* (pp. 74–82). Novosibirsk: Science.

Ivanitsky, G.R., Medvedinsky, A.B., & Tsyganov, M.A. (1991). From disorder to orderliness - on the example of the movement of microorganisms. *Advances in Physical Sciences, 161*(3), 13 – 71.

Ivanov, N.N. (1984). Solitary waves in the theory of populations. *News of the USSR Academy of Sciences. Biological Series, 5*, 656 – 663.

Keller, E. F., & Segel, L. A. (1971). Traveling bands of chemotaxis bacteria: A theoretical analysis. *Journal of Theoretical Biology*, *30*(2), 238–248. doi:10.1016/0022-5193(71)90051-8

Kennedy, C. R., & Aris, R. (1980). Traveling waves in a simple population model involving growth and death. *Bulletin of Mathematical Biology*, *42*(3), 397–429. doi:10.1007/BF02460793 PMID:7378612

Kolmogorov, A. N., Petrovsky, I. G., & Piskunov, N. S. (1937). The study of the diffusion equation, combined with an increase in the amount of substance, and its application to a single biological problem. *MSU Bulletin, series A. Mathematics and Mechanics*, *1*(1), 1–26.

Kopaneva, L. M., & Stebaev, I. V. (1985). *Locust life*. Moscow: Agropromizdat.

Lauffenburger, D., Kennedy, R., & Aris, R. (1984). Traveling bands of Chemotaxis Bacteria in the Context of Population Growth. *Bulletin of Mathematical Biology*, *46*(1), 19–40. doi:10.1007/BF02463721

Manod, J. (1950). La technique de culture continue, theorie et applicationes. *Ann. Inst. Paster.*, 79.

Polozhiy, G. N. (1964). *Equations of mathematical physics*. Moscow: High School.

Samara, A. A., Galaktionov, V. A., Kurdyumov, S. P., & Mikhailov, L. P. (1987). *Modes with aggravation in problems for quasilinear parabolic equations*. Moscow: Science.

Scherbinovsky, N.S. (1952). *Desert Locust Schistocerka*. Moscow: State ed. rural - host lit.

Scherbinovsky, N. S. (1958). The main laws of mass breeding of the desert locust and the migration of its flocks. *9th International Conference on Plant Quarantine and Plant Protection from Pests and Diseases.*

Svirezhev, Yu. M. (1987). *Nonlinear waves, dissipative structures and disasters in ecology*. Moscow: Science.

Taylor, R. A. J. (1979). A simulation model of locust migratory behavior. *J. Anim. Ecob*, *48*(2), 577–602. doi:10.2307/4181

Topaz, C. M., Bernoff, A. J., Logan, S., & Toolson, W. (2008). A model for rolling swarms of locusts. *The European Physical Journal. Special Topics*, *157*(1), 92–109. doi:10.1140/epjst/e2008-00633-y

Topaz, C.M., D`Orsogua, M.R., Edelstein-Keshet, L., & Bernoff, J. (2012). Locust dynamics: Behavioral phase change and swarming. *PLOS Comput. Biol., 8*.

Ullyet, G. C. (1945). Oviposition by Ephestia kukniella. *Zell. J. Ent. Soc. S. Africa*, *8*, 53–59.

Volterra, V. (1931). *Lecons sur la Theorie Mathematique de La Lutte Pour la Vie*. Paris: Gautheer – Villars.

Zhizhin, G. V. (1982). The structure of the wave front of the polymerization. *Reports of the USSR Academy of Sciences*, *263*(6), 1399–1402.

Zhizhin, G. V. (1988). Autowave processes of distribution of chemical reactions in a dispersion medium. *Journal of Applied Mechanics and Technical Physics*, *6*, 35–43.

Zhizhin, G. V. (1992). *Macrokinetics of frontal polymerization reactors*. St. Petersburg: Polytechnica.

Zhizhin, G. V. (1997a). *Mathematical models of waves radical polymerization*. St. Petersburg: Publishing Northwestern Correspondence Polytechnic Institute.

Zhizhin, G. V. (1997b). Stationary waves reversible radical polymerization. *Chemical Physics*, *3*, 114–123.

Zhizhin, G. V. (2004a). *Self - regulating waves of chemical reactions and biological populations*. St. Petersburg: Science.

Zhizhin, G. V. (2004b). Model of a wave of ideal solid-flame combustion with a variable surface of chemical interaction. *Chemical Physics*, *40*(1), 95–102.

Zhizhin, G. V. (2005). *Dissipative structures in chemical, geological and ecological systems*. St. Petersburg: Science.

Zhizhin, G. V. (2008). *Combustion waves with distributed zones of chemical reactions (nonasymptotic combustion theory)*. St. Petersburg: Publishing Werner Regen.

Zhizhin, G. V. (2012). Mathematical model of a solitary wave of a population of beetles - bark beetles. *Proceedings of the St. Petersburg State Forestry Academy*, *196*, 153 - 162.

Zhizhin, G. V. (2014). Mathematical model of flight of the gregarious locust. *Biosphere*, *6*(2), 112–117.

Zhizhin, G. V., & Bolshakova, N. N. (2000a). Single waves in populations of multicellular animal organisms. *Mathematical Modelling*, *12*(12), 55–65.

Zhizhin, G. V., & Larina, T. I. (1994). Standing waves gas chemical reactions in porous inert media. *Combust*, *4*, 11–20.

Zhizhin, G. V., & Poritskaya, I. J. (1994). Self-regulating chemical reactions of n - th order in condensed matter. *Combust*, *6*, 61–68.

Zhizhin, G. V., & Selikhovkin, A. V. (2012). *Mathematical modeling of the development and distribution of insect populations - stem pests in the forests of Russia.* St. Petersburg State Forestry University.

KEY TERMS AND DEFINITIONS

Gregarious Locust: The state of the locust in which the locust forms large flocks capable of long flights; the gregarious locust is characterized by bright coloration and aggressive behavior.

Semi-Infinite Reaction Zone Method: A method that assumes a low reaction rate to the reaction front and a significant reaction rate after the reaction front to infinity.

Separatrix: A trajectory that separates qualitatively different types of trajectories from each other.

Solitary Wave: Wave motion that at each time instant is localized in a finite region of space and rapidly decreases with distance from this region.

Special Point: The point at which the first derivatives of all phase variables with respect to the independent variable are equal to zero.

Zero Isocline: The line at the points of which the first derivative of some phase variable with respect to the independent variable is zero.

Chapter 3
Plankton Models and Its Attractors in a Local Approximation

ABSTRACT

The previously accepted models of plankton consisting of two interacting populations—phytoplankton and zooplankton—are considered in a local approximation. The analysis of models is carried out with the help of a qualitative study of systems of differential equations as a whole (i.e., in the entire phase space of systems, not limited to a neighborhood of equilibrium positions). Analytical conditions for the occurrence of a Hopf bifurcation are obtained for each model using the Lyapunov stability theory. A comparison of various models is given, and their shortcomings associated with the incompleteness of research are indicated. It has been established that in some cases the loss of stability of the equilibrium position does not lead to the formation of a limit cycle (Hopf bifurcation) but to the formation of a limit continuum with a chaotic behavior of the trajectories in a large part of the phase space. It is shown that the parameters significantly influencing the dynamics of the development of plankton are the natural mortality of populations as an environmental characteristic of the environment.

DOI: 10.4018/978-1-5225-9651-6.ch003

PLANKTON MODELS

Plankton is a collection of floating organisms belonging to many types and living in the oceans, seas, freshwater bodies and major rivers. The functional classification of plankton organisms is based on their place in the food chain, their size and distribution in nature (Erhard, & Seguin, 1978; Kiselev, 1982). By size, picoplankton is distinguished (2 μm), micro - plankton (0.2 - 2 mm), macro - plankton (more than 20 mm). Phytoplankton are microscopic plants that largely determine the development of all marine communities and the life within them. Due to the fact that the growth of phytoplankton is due to photosynthesis, the global phytoplankton reserves produce half the amount of oxygen that humanity needs to maintain its existence, and absorb half the amount of carbon that could trigger global warming. Along with oxygen and carbon, there are other elements and substances, which are regenerated by phytoplankton. These include, above all, phosphorus and nitrogen - containing compounds. Thus, phytoplankton, in general, is one of the main factors for the development of climate on Earth. Zooplankton are planktonic animals. In the marine zooplankton can be found both herbivores and predators. At the same time, herbivores feed on phytoplankton and are food for zooplankton predators. In the complex, phytoplankton and zooplankton are the basis of all trophic chains and networks in the ocean. In turn, the reproduction of species forming plankton is determined by many factors, such as ambient temperature, sunlight intensity, availability of nutrients, etc. An increase in the concentrations of certain substances (mainly nitrogen and phosphorus), which are a food product for algae, leads to a significant increase in the concentration of algae, i.e. to eutrophication, and, as a result, to the accumulation of organic matter in water, water pollution, the spread of infections and the gradual withering away of all life. For this reason, eutrophication should be classified as an environmental risk caused by an excessive increase in the concentration of nutrients as pathogenic elements (Slepyan, 2002). The increase in nutrients in water can be the result of natural processes or targeted actions. In the latter case, these actions can be considered as acts of environmental terrorism (Slepyan, 2003).

The beginning of the mathematical modeling of the processes underlying the formation of plankton was laid in the work of R. Fleming (Fleming, 1939). He proposed to describe the change in the number of phytoplankton by a differential equation

$$du_1 / dt = (F - R - G)u_1. \quad (1)$$

Here u_1 is the concentration of phytoplankton in water; *F* is speed of the photosynthesis; *R* is speed of the breath; *G* is phytoplankton excretion rate by zooplankton.

In the future, this simplest model became more complicated in two directions. First, the kinetics of phytoplankton development was refined, taking into account its interaction with zooplankton. Secondly, the influence of the mobility of the waters of the seas and oceans and the mobility of individuals of planktonic populations on the distribution of phytoplankton and zooplankton over the space of these waters was considered. Numerous studies of the distribution of plankton for a long time discovered the heterogeneity (mosaic) of the distribution of plankton in both horizontal and vertical (i.e. in depth) directions in lakes, seas and oceans (Beklemishev, 1969; Kiselev, 1982; Erhard, & Sezhen, 1978; Zenkevich, 1951; Kamshilov, Zelikman, & Rouhiyainen, 1958; Morozova - Vodyanitskaya, 1948; Vinogradov, 1968: Sirenko, & Gavrilenko, 1978).

Moreover, this heterogeneity (structure) exists in certain seasons long enough and steadily. Visually heterogeneity in the horizontal direction is expressed in the so - called phytoplankton spotting. The formation of phytoplankton spots is primarily associated with transfer processes. Moreover, many who study the turbulence of ocean waters believe that turbulence is responsible for the appearance of phytoplankton spots, and the intrinsic mobility of phytoplankton and zooplankton organisms does not matter in the transfer processes (Ozmidov, 1968, 1983, 1998; Petrovsky et al., 1998; Medvedinsky et al., 2002; Medvedinskiy et al., 2003). It is difficult to agree with this opinion. Firstly, it is not confirmed by anything. Secondly, estimates of the velocities of the pulsating motion of moles of water in the turbulent regime in the ocean and the pulsations of the proper movement of individuals of plankton indicate the opposite. Moreover, this heterogeneity (structure) exists in certain seasons long enough and steadily. With developed turbulent fluid motion, the velocity of turbulent pulsations is approximately 0.6 m / s at the boundary of the jet of a co - current flow striking at a high speed, and this velocity rapidly decreases with retreat from this boundary (Loitsyansky, 1957). Measurements of the velocity of turbulent pulsations, for example in the Caspian Sea, are much smaller (approximately 0.2 m / s) (Ozmidov, 1968). Pulsations of the unicellular ciliated infusoria proper movement, as one of the most widespread representatives of zooplankton, can reach 1 m /

s (Shmagina, 1948). Extensive scientific literature is devoted to the analysis of the movement of various organisms that form plankton (Shmagina, 1948; Zaitsev, 1970; Seravin, 1967; Kozlov, 1983; Rudakov, 1972). Such forms of movement are distinguished as contractile, rowing, ameboid, flagellate, ciliary. A well - known reactive mode of motion jellyfish. I.A. Kiselev (Kiselev, 1982) emphasized the huge role of the active movement of almost all representatives of zooplankton and the ability of these movements to self - regulate. It is known that many representatives of zooplankton can quickly rise from great depths to the ocean surface (daily migration of zooplankton). With even greater speed individuals descend into the ocean. For example, copepods with the onset of darkness rise at a speed of 17–30 m / h, and ephausiids at a speed of 100 m / h. At dawn, the reverse movement begins. Moreover, the immersion rate is even higher: 50 m / h in copepods and 140 m / h in ephausiids (Erhard, & Sazhen, 1978). But if there is an ability to move relative to the vertical direction, then what prevents zooplankton individuals from using this ability to move at a certain angle to the vertical, if this allows them to find better living conditions? It is this ability to move allows many representatives of zooplankton to withstand the internal waves in the ocean waters (Petrovsky, Vinogradov, & Moroz, 1998). All of the above suggests that ignoring the mobility of representatives of, at least, zooplankton in the preparation of mathematical models of the development of plankton communities should be considered as a purely mechanistic approach that does not take into account the characteristics of living organisms. These abilities are manifested most clearly in the layer of water immediately adjacent to the ocean surface. Living organisms in the layer, which is called neuston, are attached to the surface of the water, which at the expense of surface tension has viscosity and elasticity. The mobility of organisms in this layer is reduced to their movement over the surface of the water, and the effect of turbulence on such movements is very small. Neuston plays an important role in the formation of plankton throughout the ocean (Zaitsev, 1970).

Accounting for transfer processes in the aquatic environment leads to mathematical models in the form of systems of parabolic differential equations. In a one - dimensional formulation, in each of the equations of the system there is a second - order partial derivative with respect to the spatial variable of the concentration of the corresponding component of plankton. These derivatives contain a multiplier characterizing the mobility of individuals of a given population. For two populations of phytoplankton and zooplankton, such a system of equations has the form

$$\partial u_1 / \partial t = D_1 \partial^2 u_1 / \partial x^2 + M(u_1) - E(u_1, u_2), \quad (2)$$

$$\partial u_2 / \partial t = D_2 \partial^2 u_2 / \partial x^2 + kE(u_1, u_2) - \mu(u_2)u_2. \quad (3)$$

Here u_2 is concentration of zooplankton; x is a spatial coordinate;

$M(u_1)$ is a function expressing a change in the concentration of phytoplankton due to the reproduction and natural death of individuals;

$E(u_1, u_2)$ is phytoplankton digestion by zooplankton (trophic function);

$\mu(u_2)$ is zooplankton natural death function; k is phytoplankton biomass conversion rate into zooplankton biomass;

D_1, D_2 are mobility coefficients of individuals of phyto - and zooplankton, respectively (in the framework of the mechanistic approach, these coefficients are assumed to be equal to the coefficient of turbulent diffusion).

To express the function $M(u_1)$ it is used number functions.

1. The Malthus function (Volterra, 1976; Barbasheva et al., 1991)

$$M = au_1. \quad (4)$$

There a is a Malthusian parameter, in which the rate of phytoplankton deposition can be entered (Barbasheva et al., 1991).

2. The logistic law ((Petrovsky, Vinogradov, & Moroz, 1998; Medvedinsky et al., 2002; Medvedinskiy et al., 2003)

$$M = (a / b)u_1(b - u_1). \quad (5)$$

Here b is phytoplankton saturability.

3. The function $M = \alpha(u_1)u_1$. (6)

There $\alpha(u_1) = a + bu_1 + cu_1^2$ is Allee function (Allee, 1951); *a, b, c* are constants (Svirezev, 1987). In particular, Segel and Levin (1976) suggested counting c from zero.

A number of functions are also used as a function $E(u_1, u_2)$.

1. Ivlev trophic function (Petrovsky, Vinogradov, & Frost, 1998)

$$E = u_2 G\,, \tag{7}$$

which proportional to Ivlev function (Ivlev, 1945)

$$G = G_{\max}(1 - e^{-\xi u_1})\,. \tag{8}$$

Here $G_{\max}$ is the maximum rate of the consumption of phytoplankton by zooplankton,
ξ is a parameter.

2. Volterra function (Volterra, 1976; Svirezhev, 1987; Segel, & Levin, 1976)

$$E = \gamma u_1 u_2, \gamma \text{ is constant.} \tag{9}$$

3. The trophic Manod function, proportional to the Manod function (Medvedinsky et al., 2002, 2003)

$$E = \gamma u_1 u_2 (u_1 + H)^{-1}. \tag{10}$$

Here H is concentration equal to half the maximum phytoplankton concentration.

4. Modified trophic Manod function, proportional to the modified Manod function (Barbasheva et al., 1991)

$$E = \gamma (u_1 - K)(u_1 + H)^{-1}. \tag{11}$$

Here K is the minimum concentration of phytoplankton, such that at a lower concentration there is no digestion of phytoplankton by zooplankton.

The natural mortality function of zooplankton μ is either considered constant (Petrovsky, Vinogradov, & Moroz, 1998; Medvedinsky et al., 2002, 2003), or proportional to the first degree of zooplankton concentration (Svtrezhev, 1987; Segel, & Levin, 1976)

$$\mu = mu_2. \tag{12}$$

In the next paragraphs of the chapter, a number of plankton models will be considered in a local approximation, taking into account the fact that the variables in equations (2), (3) do not depend on the spatial variable *x*, since the data on the study of such plankton models are either not available or contradictory.

Autocatalytic Model With Voltaire Trophic Function

In the work of Segel and Levin (1976), it was stated that the plankton model with growth function (6) with $c = 0$ (the authors called it the autocatalytic model) and the Volterra trophic function (9) with different coefficients $D_1 \neq D_2$ and $\mu = mu_2$ describe the plankton blotch, t. e. leads to the existence of a spatial dissipative structure. However, Segel and Levin did not provide confirmation of this statement. In the section will be consider this model in a local approximation (its research in spatial coordinates will be carried out in the next chapter).

The equations (2), (3) of the adopted model in the local approximation are

$$du_1 / dt = au_1 + bu_1^2 - \gamma u_1 u_2, \tag{13}$$

$$du_2 / dt = k\gamma u_1 u_2 - mu_2^2. \tag{14}$$

System (13), (14) is autonomous, and its solutions can be represented by trajectories in the phase plane (u_1, u_2) (there is no such study in Segel and Levin (1976)). One introduce dimensionless variables and parameters

$$x_1 = (b / \mathrm{a})u_1, x_2 = mb(k\gamma a)^{-1}u_2, \tau = at, \alpha_1 = \gamma^2 k(mb)^{-1}, \alpha_2 = k\gamma / b.$$

Then the system (13), (14) takes the form

$$dx_1 / d\tau = x_1(1 + x_1 - \alpha_1 x_2), \tag{15}$$

$$dx_2 / d\tau = \alpha_2 x_2(x_1 - x_2). \tag{16}$$

The system (15), (16) has four zero isoclines on which the derivatives of the phase coordinates change sign,

$x_1 = 0, x_2 = (1 + x_1) / \alpha_1,$ on them is $dx_1 / d\tau = 0;$
$x_2 = 0, x_1 = x_2,$ on them is $dx_2 / d\tau = 0.$

Zero isocline separates the phase plane on regions with constant signs of derivatives. The regions of positive values of the derivatives are indicated by arrows at the corresponding zero isoclines (Figure 1).

Figure 1. Phase portrait of the system (15), (16)

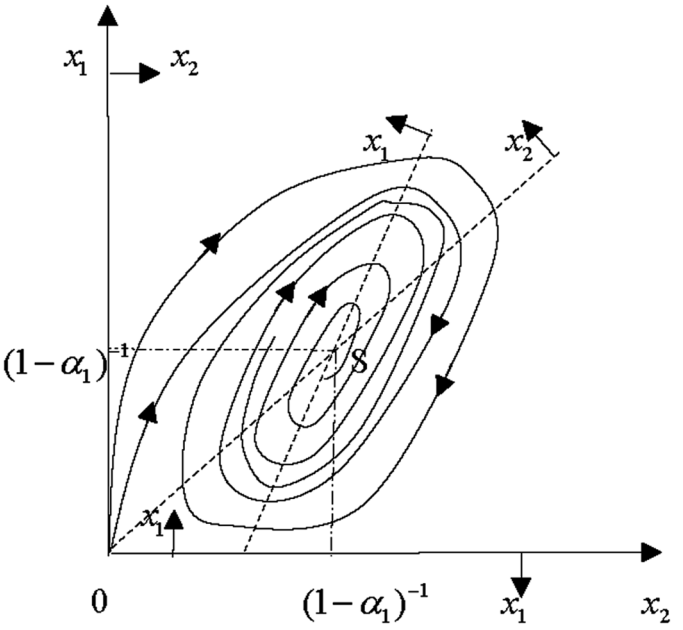

In the positive quadrant of the plane, there are two intersection points of zero isoclines representing equilibrium positions: the origin $(x_1 = 0, x_2 = 0)$ and the point *S* with the coordinate $x_{1s} = x_{2s} = (1-\alpha_1)^{-1}$.

It follows that in order for the system to have equilibrium positions with positive concentrations of phytoplankton and zooplankton, the parameter value α_1 must be less than one. From the discriminant of the system (15), (16) in the neighborhood of the equilibrium position *S* one find the eigenvalues of this equilibrium position

$$\lambda_{1,2} = 0.5\frac{1+\alpha_2}{1-\alpha_1} \pm \sqrt{\frac{(1+\alpha_2)^2}{4\left(1-\alpha_1\right)^2} - \alpha_2\frac{1+\alpha_1}{(1-\alpha_1)^2}}. \qquad (17)$$

Based on equation (17), one can construct a bifurcation diagram of the equilibrium position *S* (Figure 2).

The areas of possible values of the parameters are shaded in Figure 2. The solid line corresponds to the vanishing of the radicand, on it is $\alpha_1 = \dfrac{\alpha_2^2 - 2\alpha_2 + 1}{4\alpha_2}$.

Figure 2. Bifurcation diagram of the equilibrium position S: in area 2 the equilibrium position S has the type of a stable focus, in areas 1 and 3 the equilibrium position S has the type of a stable node

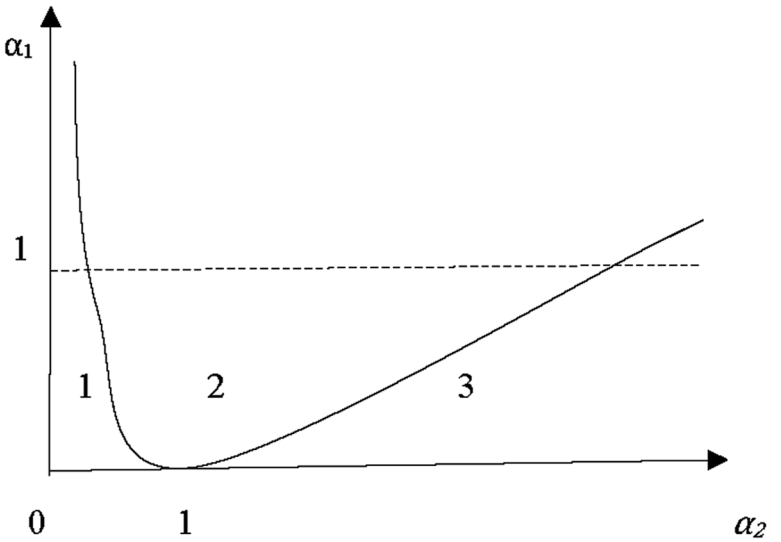

In accordance with equation (17), in regions 1 and 3 of the bifurcation diagram, the equilibrium position *S* has the type of a stable node, and in area 2 - the type of a stable focus. There is no purely imaginary eigenvalue of the equilibrium *S*. Therefore, the possibility of the birth of a limiting cycle disappears.

The origin is a complex special point. Qualitatively, the location of the trajectories in the vicinity of this equilibrium state can be determined from zero isoclines. Until the zero isocline $dx_2 / d\tau = 0$, the trajectories cannot enter or exit the origin. Above the zero isocline $dx_2 / d\tau = 0$, the existence of trajectories emerging from the origin of coordinates is possible. Figure 1 shows the phase portrait of the system with the values of the parameters from region 2 of the bifurcation diagram. If the values of the parameters belong to areas 1 or 3, then the phase portrait changes slightly, since the stable focus and the stable node are topologically equivalent.

Thus, in accordance with accepted assumptions, this model has solutions with an increase in phytoplankton and zooplankton concentrations from zero and a tendency toward an equilibrium position (attractor *S*) with final and equal phytoplankton and zooplankton concentrations. Moreover, this desire may be accompanied by damped fluctuations in the concentrations of both populations.

Logistic Model With Trophic Function Ivleva

Petrovsky, Vinogradov, and Moroz (1998) considered the equilibrium positions of the logistic model with the Ivlev trophic function in a local approximation. Without evidence, the possibility of the formation of a limiting cycle in the vicinity of one of the equilibrium positions of this model was asserted. Let us check this possibility and conduct a qualitative study of the model as a whole, i.e. one will construct a phase portrait of the system, since such a study is absent in this work.

Equations (2), (3) under the accepted conditions with the logistic function (5), the trophic function (8) and the constant function of mortality $\mu(u_2) = m$ are

$$du_1 / dt = (a / b)u_1(b - u_1) - \gamma(1 - e^{-u_1/H})u_2, \tag{18}$$

$$du_2 / dt = k\gamma(1 - e^{-u_1/H})u_2 - mu_2. \quad (19)$$

One introduce dimensionless variables and parameters

$$x_1 = u_1 / H, x_2 = u_2 / (kH), \tau = ta, \alpha_1 = H / b, \alpha_2 = k\gamma / a, \alpha_3 = m / a.$$

Then the system (18), (19) has a form

$$dx_1 / d\tau = x_1(1 - \alpha_1 x_1) - \alpha_2 x_2(1 - e^{-x_1}), \quad (20)$$

$$dx_2 / d\tau = \alpha_2 x_2(1 - e^{-x_1}) - \alpha_3 x_2. \quad (21)$$

Solutions of the system (20), (21) due to its autonomy can be represented by trajectories in the phase plane, whose location is determined by zero isoclines

$$dx_1 / d\tau = 0 : x_1 = 0, x_2 = x_1(1 - \alpha_1 x_1)\alpha_2^{-1}(1 - e^{-x_1})^{-1}, \quad (22)$$

$$dx_2 / d\tau = 0 : x_2 = 0, x_1 = -\ln(1 - \alpha_3 / \alpha_2). \quad (23)$$

As follows from equations (20) - (23), the coordinate axes of the phase plane are simultaneously the solutions of the system (i.e., trajectories) and zero isoclines. The zero isocline $x_1 = -\ln(1 - \alpha_3 / \alpha_2)$ is present in the positive quadrant of the phase plane (representing a straight line) only for $\alpha_3 / \alpha_2 < 1$. The zero isocline

$$x_2 = x_1(1 - \alpha_1 x_1)\alpha_2^{-1}(1 - e^{-x_1})^{-1}$$

is located in the positive quadrant and passes through the points with coordinates $x_1 = 0, x_2 = 1 / \alpha_2$ and $x_1 = 1 / \alpha_1, x_2 = 0$. If $\alpha_3 / \alpha_2 \geq 1$, then there is no other zero isocline in the open part of the positive quadrant of the phase plane and the system has three equilibrium positions on the coordinate axes

$a_1(x_1 = 0, x_2 = 0), a_2(x_1 = 0, x_2 = 1/\alpha_2), a_3(x_1 = 1/\alpha_1, x_2 = 0)$.

Denoting the right -hand sides of (20) and (21), respectively, Φ_1 and Φ_2, one have

$$\begin{aligned} &\partial\Phi_1 / \partial x_1 = 1 - 2\alpha_1 x_1 - \alpha_2 x_2 e^{-x_1}, \partial\Phi_1 / \partial x_2 = -\alpha_2(1 - e^{-x_1} 0, \\ &\partial\Phi_2 / \partial x_1 = \alpha_2 x_2 e^{-x_1}, \partial\Phi_2 / \partial x_2 = \alpha_2(1 - e^{-x_1}) - \alpha_3. \end{aligned} \tag{24}$$

Substituting in (24) the values of the coordinates of the equilibrium positions, from the discriminants of the system in the vicinity of the equilibrium positions can to find their eigenvalues. Thus, the equilibrium state a_1 has eigenvalues $(\lambda_{a_1})_1 = 1, (\lambda_{a_1})_2 = -\alpha_3$, this corresponds to the equilibrium position of the saddle type. The equilibrium state a_2 has eigenvalues $(\lambda_{a_2})_1 = 0, (\lambda_{a_2})_2 = -\alpha_3$, this corresponds to a degenerate equilibrium position. The equilibrium position a_3 has eigenvalues

$$(\lambda_{a_3})_1 = -1, (\lambda_{a_3})_2 = \alpha_2(1 - e^{-1/\alpha_1}) - \alpha_3 < 0,$$

this corresponds to the equilibrium position of the type of stable node. The corresponding system of trajectories is depicted in Figure 3 (the zero isocline (22) is constructed for the values $\alpha_1 = 0.2, \alpha_2 = 4$).

Considering the above, we can conclude that all decisions ultimately lead to the disappearance of zooplankton and the desire of the phytoplankton concentration to $1/\alpha_1$.

If $\alpha_3 / \alpha_2 < 1$, then a zero isocline (23) arises in the phase plane, on which

$$x_1 = x_{1s} = -\ln(1 - \alpha_3 / \alpha_2). \tag{25}$$

If $x_{1s} > 1/\alpha_1$, then this leads to arise new equilibrium state a_4 in which $x_1 = x_{1s}, x_2 = 0$.

This is a state of equilibrium, as is easily seen, as is the equilibrium state a_2 degenerate. If $x_{1s} < 1/\alpha_1$, then two additional equilibrium positions appear in the phase plane (Figure 4) a_4 and a_5 with coordinates

Figure 3. Phase portrait of the system (20), (21) for $\alpha_3 / \alpha_2 < 1$

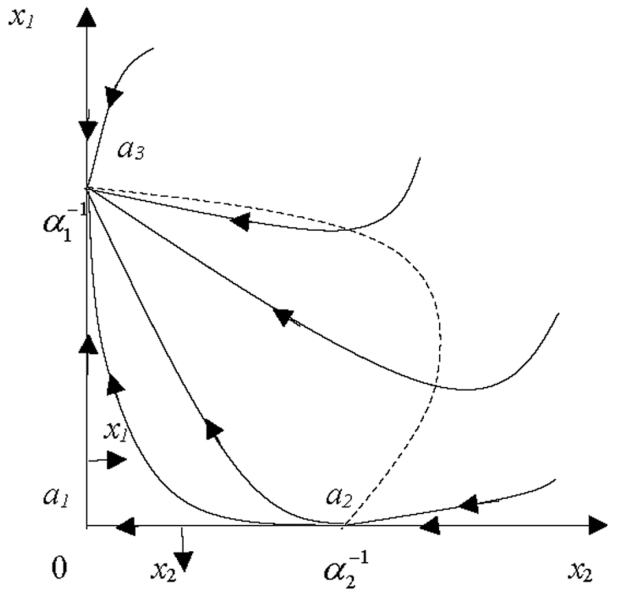

Figure 4. The phase portrait of system (20), (21) for $x_{1s} < 1 / \alpha_1$*, state of equilibrium* a_5 *is stable node*

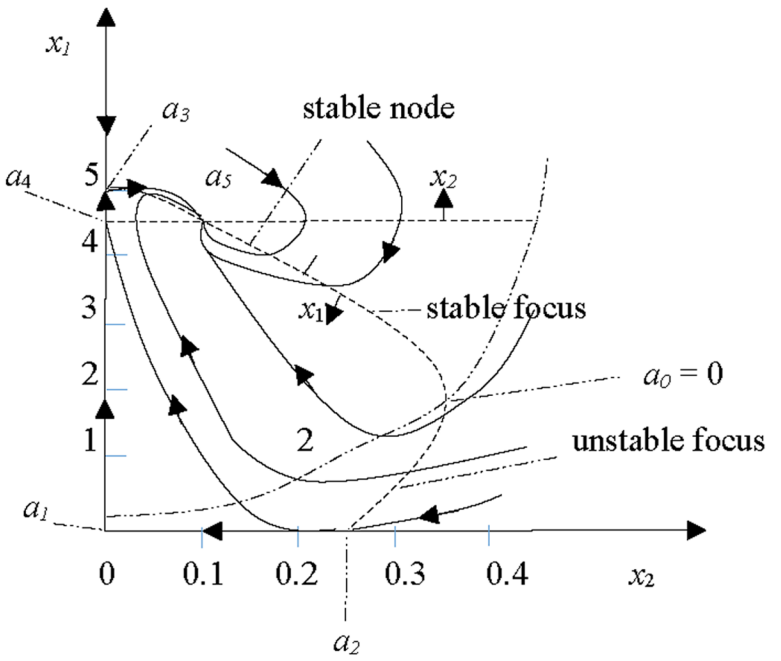

$$x_1 = x_{1s}, x_2 = x_{2s} = -\alpha_3^{-1}[1 + \alpha_1 \ln(1 - \alpha_3 / \alpha_2)]\ln(1 - \alpha_3 / \alpha_2). \quad (26)$$

Thus, the maximum number of equilibrium positions in the system is five, not three, as Petrovsky, Vinogradov, and Moroz (1998) claimed. Moreover, and this is significant, the equilibrium position a_5 with the final values of the concentrations of populations exists only when the number of equilibrium positions is five. It is around him, as will be seen later, that a limiting cycle can be formed.

When there is a_5, then $\alpha_3 / \alpha_2 < 1$ and $(\lambda_{a_3})_2$ changed its sign. Therefore, the equilibrium position a_3 has become a saddle. Substituting the coordinates of the equilibrium position a_5 from equations (26), (25) into system (24), from the discriminant of the system in the vicinity of this equilibrium position we obtain the characteristic equation

$$\lambda^2 - a_0\lambda - c_0 b_0 = 0. \quad (27)$$

Here

$$a_0 = 1 - 2\alpha_1 x_{1s} - \alpha_2 x_{2s} e^{-x_{1s}}, b_0 = -\alpha_2(1 - e^{-x_{1s}}), c_0 = \alpha_2 x_{2s} e^{-x_{1s}}. \quad (28)$$

By the condition of Routh - Hurwitz, the equilibrium state a_5 is stable if $a_0 < 0, c_0 b_0 < 0$. The second of these inequalities, according to equations (24), (25), (28), is satisfied for any values of the parameters within the accepted conditions. The boundary of stability, therefore, is equality $a_0 = 0$. Substituting the value x_{1s}, x_{2s} into this equality, one obtain the expression of this condition through the parameters of the problem

$$\alpha_1 = \frac{(1 - \alpha_2 / \alpha_3)\ln(1 - \alpha_3 / \alpha_2)}{[2 - (1 - \alpha_3 / \alpha_2)\ln(1 - \alpha_3 / \alpha_2)]\ln(1 - \alpha_3 / \alpha_2)}. \quad (29)$$

The line graph (29) on the bifurcation diagram (Figure 5) divides the parameter plane into two regions.

Under the line $a_0 = 0$, the equilibrium position a_5 is unstable, and above the line $a_0 = 0$ the equilibrium position a_5 is stable. Point $a_0 = 0$ is the dividing zero isocline (22) (Figure 3) into two parts. Above this point along the zero

Figure 5. The bifurcation diagram of system (20), (21):1 is region in which $a_0 < 0$, a_5 *is stable; 2 is region in which* $a_0 > 0$, a_5 *is unstable*

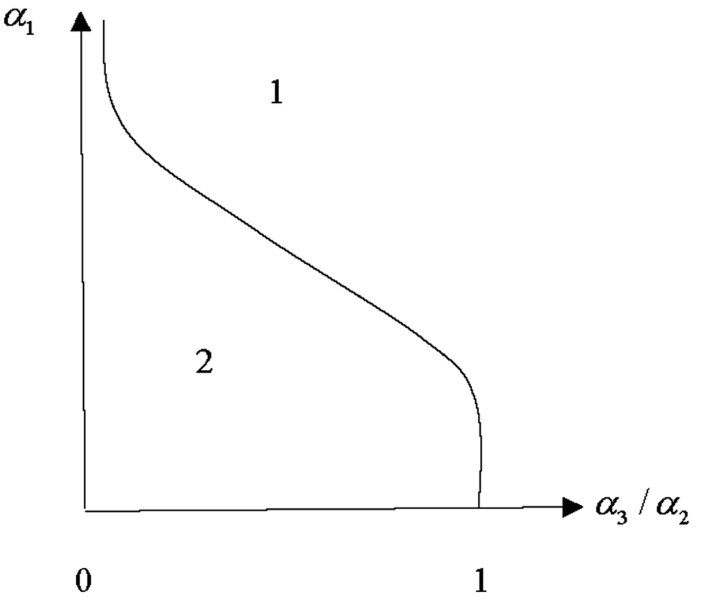

isocline (at this point $dx_1 / dx_2 = \infty$) $a_0 < 0$, below $a_0 > 0$. Moreover, on the part of the zero isocline adjacent to point a_3, the equilibrium position a_5 has of the type of stable node (Figure 4). On the remaining part of the zero isocline to the point $a_0 = 0$, the equilibrium position has of the type of stable focus (Figure 6), and after the point $a_0 = 0$ - of an unstable focus.

Parameters α_1, α_2 determine the location of the zero isocline (22) on the phase plane and this zero isocline does not depend on the parameter α_3. Moreover, moving along the zero isocline, for example, from point a_2 to point a_3, the value of parameter α_3 is steadily increasing (line 2 in Figures 4, 6). The results obtained allow us to give the following interpretation of the evolution of the system with a change in the mortality *m* (since the parameter α_3 is the dimensionless characteristic rate of natural death of zooplankton). With a high natural mortality of zooplankton (adverse conditions), the process of interaction of phytoplankton and zooplankton ends with the complete extinction of zooplankton and the passage of some equilibrium phytoplankton concentration. With a decrease in the natural mortality of zooplankton in the system, a stable equilibrium position occurs with the final concentrations of

Figure 6. The phase portrait of system (20), (21) for $x_{1s} < 1/\alpha_1$, *state of equilibrium* a_5 *is stable focus*

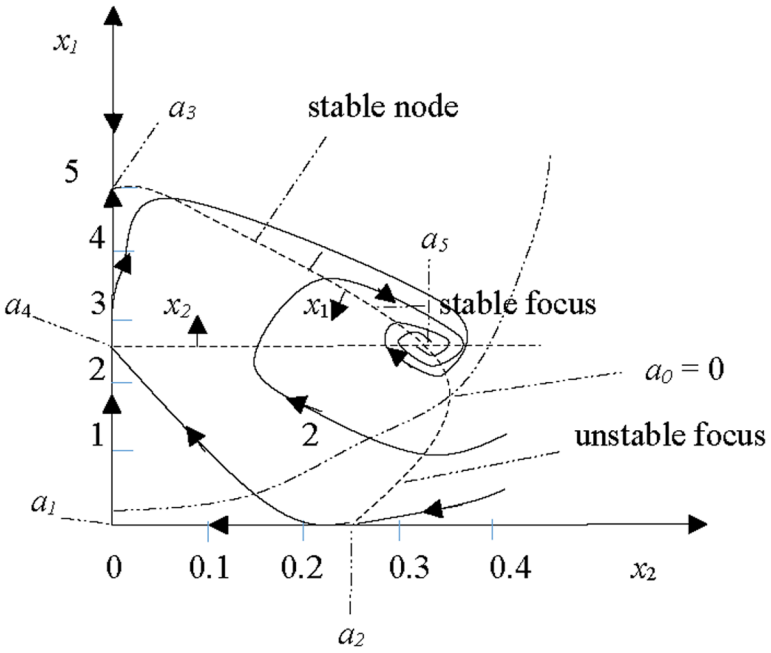

both populations. Moreover, the lower the natural mortality of zooplankton, the lower the concentration of phytoplankton and the greater the concentration of zooplankton in this equilibrium position. A further decrease in the natural mortality of zooplankton leads to a change in the type of stable equilibrium. Its type becomes a stable focus instead of a stable node. In this case, the desire for an equilibrium position is accompanied by damped fluctuations in concentrations. A further decrease in the natural mortality of zooplankton leads to a loss of steady state of equilibrium. It acquires a type of unstable focus and retains this type until the phytoplankton completely disappears, while the concentration of zooplankton decreases.

The transition from stable equilibrium to unstable equilibrium states is accompanied by the transition of the eigenvalues of the characteristic equation (27) through a pair of purely imaginary values of the eigenvalues. Therefore, it is necessary to verify the possibility of the formation of limiting cycles around the a_5 equilibrium position after losing its stability. For this one will use the method of N.N. Bautin (Bautin, 1984), constructed on the basis of

the stability theorems of A.M. Lyapunov. One represent the right - hand sides of equations (20), (21) in the vicinity of the equilibrium position a_5 as a Taylor series, including terms up to terms of the third order of smallness

$$dx_1 / d\tau = a_0(x_1 - x_{1s}) + b_0(x_2 - x_{2s}) + a_{20}(x_1 - x_{1s})^2 + a_{11}(x_1 - x_{1s})(x_2 - x_{2s}) + a_{02}(x_2 - x_{2s})^2 + a_{30}(x_1 - x_{1s})^3 + a_{21}(x_1 - x_{1s})^2(x_2 - x_{2s}) + a_{12}(x_1 - x_{1s})(x_2 - x_{2s})^2 + a_{03}(x_2 - x_{2s})^3,$$

$$dx_2 / d\tau = c_0(x_1 - x_{1s}) + d_0(x_2 - x_{2s}) + b_{20}(x_1 - x_{1s})^2 + b_{11}(x_1 - x_{1s})(x_2 - x_{2s}) + b_{02}(x_2 - x_{2s})^2 + b_{30}(x_1 - x_{1s})^3 + b_{21}(x_1 - x_{1s})^2(x_2 - x_{2s}) + b_{12}(x_1 - x_{1s})(x_2 - x_{2s})^2 + b_{03}(x_2 - x_{2s})^3.$$

Here

$$d_0 = \alpha_2(1 - e^{-x_{1s}}) - \alpha_3, a_{ik} = \frac{1}{i!k!}\frac{\partial^{i+k}\Phi_1}{\partial x_1^i \partial x_2^k}, b_{ik} = \frac{1}{i!\,k!}\frac{\partial^{i+k}\Phi_2}{\partial x_1^i \partial x_2^k}.$$

Taking into account that the values of derivatives are taken in the equilibrium position a_5 with $a_0 = 0$, one get

$$d_0 = 0, a_{20} = -\alpha_1 + 0.5\alpha_2 x_{2s} e^{-x_{1s}}, a_{11} = 0, a_{30} = -x_{2s} e^{x_{1s}}\alpha_2 / 6, a_{21} = 0.5\alpha_2 e^{-x_{1s}}, a_{12} = 0, a_{03} = 0, b_{20} = -x_{2s} e^{x_{1s}}\alpha_2 / 2, b_{11} = \alpha_2 e^{-x_{1s}}, b_{02} = 0, b_{30} = x_{2s} e^{-x_{1s}}\alpha_2 / 6, b_{21} = -e^{-x_{1s}}\alpha_2 / 2, b_{12} = 0, b_{03} = 0. \quad (30)$$

According to Bautin's theory (Bautin, 1984), when passing through the value of the parameter a_{30}, which meets the condition $a_0 = 0$, the limiting cycle will be born in the vicinity of the unstable equilibrium position a_5, if at this point the first Lyapunov coefficient is negative

$$L_1(\alpha_{30}) = -\pi 0.25 b_0^{-1}(\alpha_3\alpha_2 x_{2s} e^{-x_{1s}})^{-3/2}\{a_0c_0(a_{11}^2 + a_{11}b_{02} + a_{02}b_{11}) + a_0b_0(b_{11}^2 + a_{20}b_{11} + a_{11}b_{20}) + c_0^2(a_{11}a_{02} + 2a_{02}b_{02}) - 2a_0c_0(b_{02}^2 - a_{20}a_{02}) - 2a_0b_0(a_{20}^2 - b_{20}b_{02}) - b_0^2(2a_{20}b_{20} + b_{11}b_{20}) + (b_0c_0 - 2a_0^2)(b_{11}b_{02} - a_{11}a_{20}) - (a_0^2 + b_0c_0)[3(c_0b_{02} - b_0a_{30}) + 2a_0(a_{21} + b_{12}) + c_0a_{12} - b_0b_{21}]\}. \quad (31)$$

Substituting the coefficients from equations (30) into (31), taking into account expressions (24), (25) and the equality $a_0 = 0$, one obtain after transformations

$$L_1 = 0.25\pi x_{1s} e^{-x_{1s}} (\alpha_3 \alpha_2 x_{2s} e^{-x_{1s}})^{-3/2} (0.5\alpha_2^2 x_{2s} e^{-x_{1s}} - \alpha_1 \alpha_2 - \alpha_1 \alpha_3). \quad (32)$$

Using the obtained expressions it can be shown that with $\alpha_3 / \alpha_2 < 1$ the last bracket in the right side of equation (32) is always negative. This proves that when moving from stable equilibrium states a_5 to unstable equilibrium states a_5 a stable limiting cycle (attractor) is formed. Thus, damped fluctuations in the concentrations of phytoplankton and zooplankton change to stationary fluctuations in the concentrations of populations (Figure 7).

In the system, a stable temporal heterogeneity is formed, i.e. temporal dissipative structure (Zizhin, 2005).

Thus, a qualitative study of the system as a whole allowed us to determine the evolution of the system depending on the values of the parameters, where the parameter characterizing the natural mortality of zooplankton was decisive.

Figure 7. Phase portrait of system (20), (21) with a stable limiting cycle (attractor)

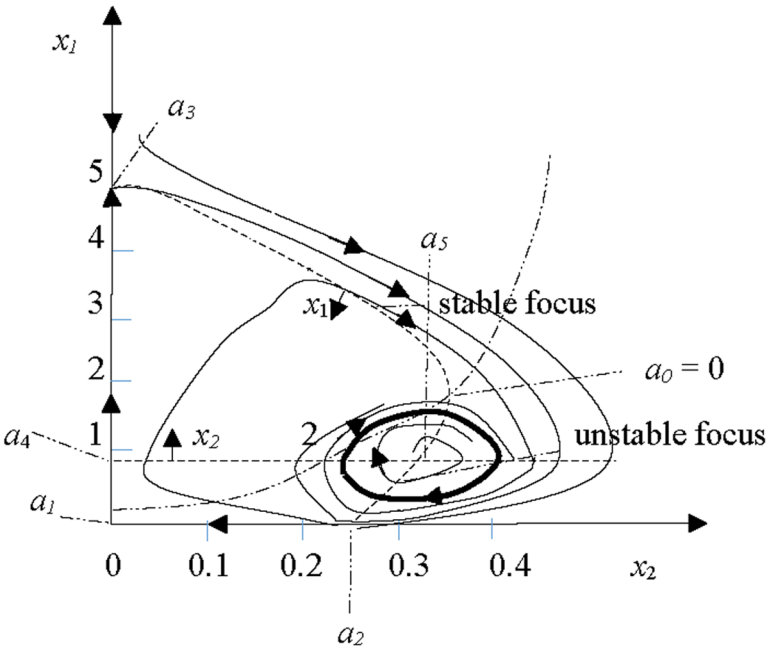

Logistic Model With Trophic Function Monod

In the works of Medvedinsky, Tikhonov and others (Medvedinsky et al., 2002, 2003), a plankton model was proposed in which the growth of the phytoplankton population was described by a logistic law, and the consumption of phytoplankton by zooplankton was taken into account by Mano's law. It was argued without proof that this model leads to the formation of a limiting cycle. Let us verify the validity of this statement by conducting a qualitative study on the whole of this model in a local approximation, determining the sign of the first Lyapunov value. Equations (2), (3) in these conditions with the logistic function (5) and trophic function (10) with constant natural mortality m

$$du_1 / dt = (a / b)u_1(b - u_1) - \gamma u_1(u_1 + H)^{-1}u_2, \tag{33}$$

$$du_2 / dt = k\gamma u_1(u_1 + H)^{-1}u_2 - mu_2. \tag{34}$$

One introduce dimensionless variables and parameters

$$x_1 = u_1 / H, x_2 = u_2 / (kH), \tau = ta, \alpha_1 = H / b, \alpha_2 = k\gamma / a, \alpha_3 = m / a.$$

Then the system (33), (34) has a form

$$dx_1 / d\tau = x_1(1 - \alpha_1 x_1) - \alpha_2 x_2 x_1(1 + x_1)^{-1}, \tag{35}$$

$$dx_2 / d\tau = \alpha_2 x_2 x_1(1 + x_1)^{-1} - \alpha_3 x_2. \tag{36}$$

Solutions of the system (35), (36) due to its autonomy can be represented by trajectories in the phase plane, whose location is determined by zero isoclines

$$dx_1 / d\tau = 0 : x_1 = 0, x_2 = (1 + x_1)(1 - \alpha_1 x_1)\alpha_2^{-1}, \tag{37}$$

$$dx_2 / d\tau = 0 : x_2 = 0, x_1 = (\alpha_2 / \alpha_3 - 1)^{-1}. \quad (38)$$

Here, as well as in the previous model, there are three equilibrium positions in the phase plane (x_1, x_2), if $\alpha_3 / \alpha_2 > 1$, and all of them are located on the coordinate axes: $a_1(0,0), a_2(0, \alpha_2^{-1}), a_3(\alpha_1^{-1}, 0)$. The equilibrium position α_1 has of a saddle type, a_2 is a degenerate equilibrium position, and α_3 has a type of stable knot. In general, the phase diagram is not very different from the phase diagram in Figure 3. All solutions lead to the disappearance of zooplankton. There are differences in the zero isocline (37). It becomes significant when the zero isocline appears in the phase plane and intersects the zero isocline (37), i.e. for $\alpha_3 / \alpha_2 < (1 + \alpha_1)^{-1}$. In the interval $(1 + \alpha_1)^{-1} < \alpha_3 / \alpha_2 < 1$ in the phase plane, in addition to a_1, a_2, a_3, there is another degenerate equilibrium state $a_4((a_2 / \alpha_3 - 1)^{-1}, 0)$. With $a_3 / a_2 < (1 + \alpha_1)^{-1}$ the phase plane has five equilibrium positions. An equilibrium position of a_5 is added with the final concentrations of the two populations with coordinates

$$x_{1s} = \alpha_3(\alpha_2 - \alpha_3)^{-1}, x_{2s} = (\alpha_2 - \alpha_1\alpha_3 - \alpha_3)(\alpha_2 - \alpha_3)^{-2}.$$

The eigenvalues of the equilibrium position a_5 are from the discriminant of the system in the vicinity of this equilibrium position

$$\lambda^2 - a_0\lambda + \alpha_3\alpha_2^{-1}(\alpha_2 - \alpha_1\alpha_3 - \alpha_3) = 0. \quad (39)$$

The Routh – Hurwitz condition in this case reduces to inequality

$$a_0 < 0, a_0 = \alpha_3\alpha_2^{-1}(\alpha_2 - \alpha_3)^{-1}(\alpha_2 - \alpha_2\alpha_1 - \alpha_3 - \alpha_3\alpha_1),$$

i.e. with $\alpha_3 < \alpha_2(1 - \alpha_1)(1 + \alpha_1)^{-1} = \alpha_{30}$, the equilibrium position becomes unstable. The zero isocline (37) is given by the parameters α_1, α_2, and when moving the equilibrium position α_5 along it, the parameter a_3 changes. The area $\alpha_3 > \alpha_{30}$ on the zero isocline is divided into two parts. In the first part, adjacent to the equilibrium position a_3, the equilibrium position α_5 is of the type of stable knot, and in the second part, adjacent to the point where $a_3 = a_{30}$,

α_5 has type of stable focus. With $\alpha_3 < \alpha_{30}$, the equilibrium position is of the type of unstable focus. The transition through a point $a_3 = a_{30}$ is accompanied by the transition of the eigenvalues of the equilibrium position through a pair of purely imaginary values. Does this form a stable limiting cycle around an unstable focus? The answer to this question is given by the definition of the sign of the first Lyapunov value. Performing for the system (35), (36) the transformations described in the previous section, one obtain

$$L_1(\alpha_{30}) = (\alpha_2 - \alpha_3\alpha_1 - \alpha_3)(\alpha_2 - \alpha_3)A,$$
$$A = \alpha_1[(\alpha_2 - \alpha_3)^2 - 2\alpha_3] - [(\alpha_2 - \alpha_3)^2\alpha_2^{-2} - \alpha_1\alpha_3\alpha_2^{-2}(\alpha_2 - \alpha_3)][1 + (\alpha_2 - \alpha_3)^2]. \quad (40)$$

Given that at a point $a_3 = a_{30}$ $a_0 = 0$, can to find the expression for a_1 and substitute it into equation (40). After the transformations, can to get that

$$A = \alpha_2^2 - \alpha_2\alpha_3^{-1}(1 + 2\alpha_3 + 2\alpha_3^2) + \alpha_3^2 + 1,$$

then $L_1 < 0$ for

$$\alpha_3 < \alpha_2 < 0.5\alpha_3^{-1}(1 + 2\alpha_3 + 2\alpha_3^2 + \sqrt{1 + 4\alpha_3 + 4\alpha_3^2 + 8\alpha_3^3}). \quad (41)$$

In Figure 8 it is presented the calculated (41) area of parameters 2 (hatched), in which the unstable equilibrium state is surrounded by a stable limiting cycle, is presented.

The phase diagram of the system in this case is close to the phase diagram in Figure 7. If the values of the parameters do not belong to this region, then the limit cycle in the vicinity of the unstable equilibrium state is not formed. In this case, the trajectories do not remain in the neighborhood of the a_5 equilibrium position. However, they cannot go to infinity, since the entire region of existence of these trajectories is limited by the separatrix of the equilibrium position a_3 and the axes of coordinates, which themselves are composed of trajectories. In this case, the so-called limiting continuum is formed (Andronov et al., 1966) (Figure 9).

The limiting continuum (attractor) consists of separatrixes of equilibrium positions $a_1, a_2, a_3, a_4,$ located on the axes of the phase plane and going from one equilibrium position to another (Figure 9), as well as these same equilibrium

Figure 8. Parameter domain 2 (hatched), in which the equilibrium position a_5 of the system (35), (36) is surrounded by a limiting cycle

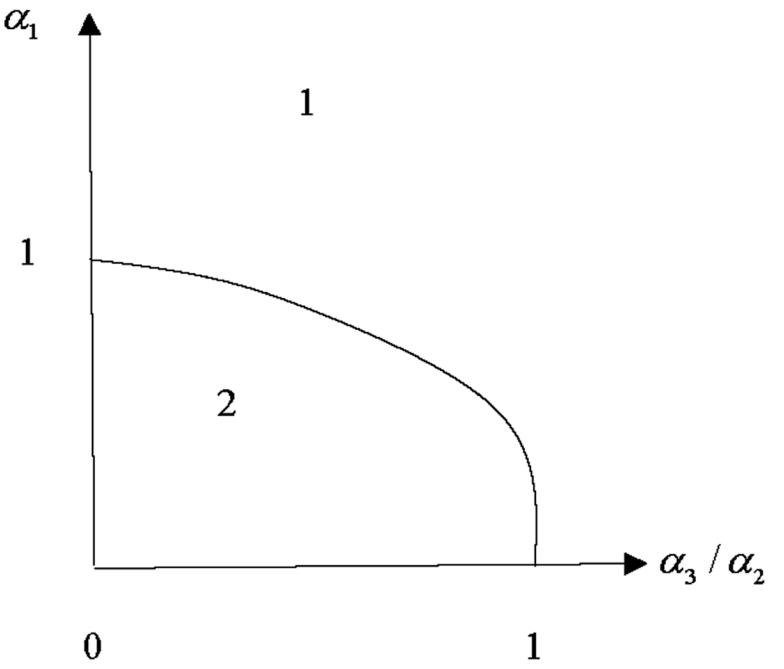

positions. This leads to the existence of a temporal dissipative structure with chaotic behavior, since the trajectories encounter degenerate equilibrium states a_2, a_4 on their way and for some time the state of the system may linger around these equilibria, but any small disturbances deduce the system from their neighborhood. Thus, in the works of Medvedinsky et al. (2002, 2003), it was erroneously stated that if an unstable equilibrium state of focus type is formed in the system, then it is necessarily surrounded in its vicinity by a stable limiting cycle (Hopf bifurcation).

Model of Plankton With Phytoplankton Subsidence and Explosive Trophic Function

In a local simulation model of the dynamics of the plankton community of the Kandalksh Bay of the White Sea (Barbashina et al., 1991), the interaction of zooplankton with phytoplankton is considered taking into account the increase in phytoplankton biomass under the influence of photosynthesis,

Figure 9. Phase portrait of system (35), (36) with a limiting continuum in the absence of a limit cycle around an unstable focus equilibrium state a_5

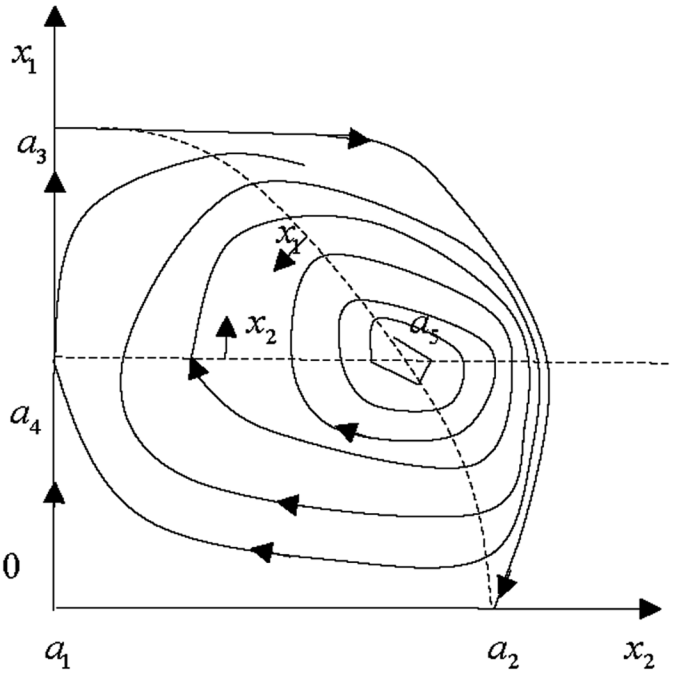

solar radiation, temperature, concentration of mineral phosphorus and mineral nitrogen. In addition, phytoplankton cell sedimentation and zooplankton mortality are taken into account. The release of phytoplankton by zooplankton is described by a discontinuous trophic function. It is assumed that when the concentration of phytoplankton is less than some critical zooplankton ceases to feed on phytoplankton. If the concentration of phytoplankton exceeds this critical value, then the consumption of phytoplankton obeys the modified Monod equation. The model was identified on the basis of long - term studies of plankton in the Kandalksh Bay of the White Sea and is recommended for any other ecosystems. However, this model was not investigated even in the local approximation using the methods of qualitative study of differential equations. According to this model, the function $M(u_1)$ in equation (2) is expressed as $(\alpha - s)u_1$, where

$$\alpha = \alpha_m \varphi_1(I)\varphi_2(N)\varphi_3(P)\varphi_4(T)$$

is the phytoplankton biomass growth rate due to photosynthesis. Here

$$\varphi_2(N) = N / (K_N + N)$$

takes into account the effect on the phytoplankton biomass growth of nitrogen concentration *N*; K_N is constant. Here $\varphi_3(P) = P / (K_P + P)$ takes into account the effect on the phytoplankton biomass growth of phosphor concentration *P*; K_P is constant. Here

$$\varphi_4(T) = c \exp(-\sigma(T - T_m)^2) - d$$

takes into account the effect temperature *T* on the phytoplankton biomass (*c, σ, d* are constants). Here

$$\varphi_1(I) = \Omega^{-1} \ln \frac{I + K_I}{I \exp(-\Omega) + K_I}$$

takes into account the effect on photosynthesis of illumination; $\Omega = a + bu_1$; *I* is average daily solar radiation; *s* is phytoplankton cell sedimentation rate (K_I, α_m, a, b are constants).

As follows from the above expressions, $\varphi_1(I)$ depends on the concentration of phytoplankton u_1. However, in the event of a final change in u_1, this function is weak and it can be assumed that $\varphi_1(I)$ is a variable parameter. According to the model in question, in equations (2), (3) μ is constant, and function $E(u_1, u_2)$ has form $\gamma f(u_1)u_2$. Here γ is constant, and K_u is constant.

$$f = \begin{cases} 0, u_1 \le u_{10} \\ (u_1 - u_{10}) / (u_1 + K_u), u_1 \ge u_{10} \end{cases} \tag{42}$$

The equations (2), (3) under the accepted conditions in the local approximation take the form

$$du_1 / dt = u_1(\alpha - s) - \gamma f(u_1)u_2, \tag{43}$$

$$du_2 / dt = k\gamma f(u_1)u_2 - \mu u_2. \tag{44}$$

One assume that $\alpha > s$, since otherwise, the concentration of phytoplankton can only decrease, and this is unrealistic.

One introduce dimensionless variables and parameters

$$x_1 = u_1 / u_{10}, x_2 = u_2 / (ku_{10}), \tau = tk\gamma,$$
$$\alpha_1 = (\alpha - s) / (k\gamma), \alpha_2 = \mu / (k\gamma), \alpha_3 = K_u / u_{10}.$$

One rewrite the system (43), (44) with regard to (42) in new variables with $x_1 > 1$

$$dx_1 / d\tau = \alpha_1 x_1 - x_2(x_1 - 1) / (x_1 + \alpha_3), \tag{45}$$

$$dx_2 / d\tau = x_2(x_1 - 1) / (x_1 + \alpha_3) - \alpha_2 x_2. \tag{46}$$

The same system with $x_1 < 1$ has the form

$$dx_1 / d\tau = \alpha_1 x_1, dx_2 / d\tau = -\alpha_2 x_2. \tag{47}$$

Solutions of system (45), (46) are represented by trajectories in the phase plane (x_1, x_2) . Their location is determined by zero isoclines (Figure 10)

$$dx_1 / d\tau = 0 : x_2 = \alpha_1 x_1(x_1 + \alpha_3) / (x_1 - 1), \tag{48}$$

$$dx_2 / d\tau = 0 : x_2 = 0, x_1 = (1 + \alpha_2\alpha_3) / (1 - \alpha_2). \tag{49}$$

The arrows at the zero isoclines indicate regions of positive values of the derivatives of the corresponding phase variables. The system (45), (46) has one equilibrium position with coordinates

$$x_1 = (1 + \alpha_2\alpha_3) / (1 - \alpha_2) = x_{1s}, x_2 = x_{1s}\alpha_1 / \alpha_2 = x_{2s}, (\alpha_2 < 1).$$

Figure 10. Faces portrait of the system (45), (46)

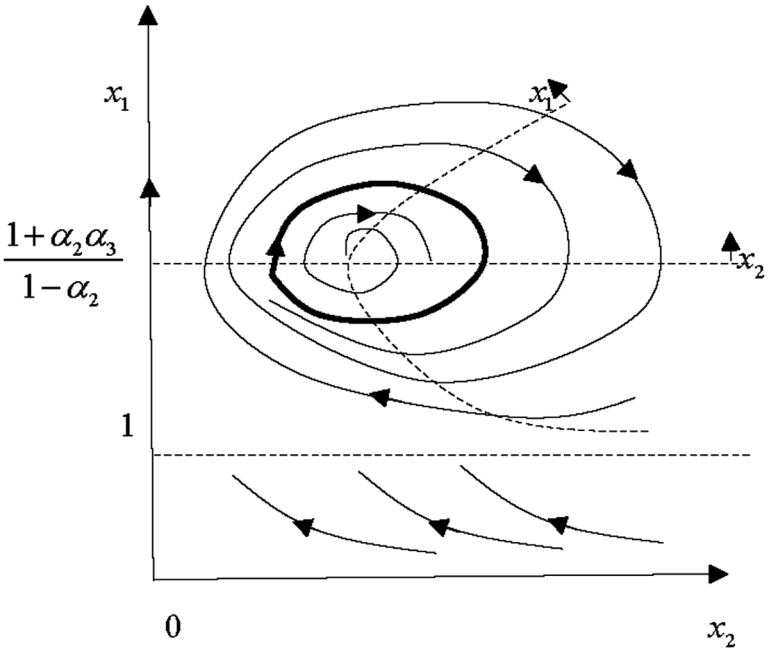

Linearize system (45), (46) in the vicinity of the equilibrium position

$$\frac{dx_1}{d\tau} = -\frac{\alpha_1}{\alpha_2}\frac{1-2\alpha_2-\alpha_2^2\alpha_3}{1+\alpha_3}(x_1 - x_{1s}) - \alpha_2(x_2 - x_{2s}), \tag{50}$$

$$\frac{dx_2}{d\tau} = \alpha_1\frac{1-\alpha_2}{\alpha_2}\frac{\alpha_2\alpha_3+1}{1+\alpha_3}(x_1 - x_{1s}). \tag{51}$$

From the discriminant of the system (50), (51) one find the eigenvalues of the equilibrium position

$$\lambda_{1,2} = -\frac{\alpha_1}{2\alpha_2}\frac{1-2\alpha_2-\alpha_2^2\alpha_3}{1+\alpha_3} \pm \sqrt{\frac{\alpha_1^2}{4\alpha_2^2}\frac{(1-2\alpha_2-\alpha_2^2\alpha_3)^2}{(1+\alpha_3)^2} - \alpha_1(1-\alpha_2)\frac{1+\alpha_2\alpha_3}{1+\alpha_3}}. \tag{52}$$

From equation (52) it follows that at $\alpha_3 < (1-2\alpha_2)\alpha_2^{-2}$ the equilibrium position is stable. Moreover, if in this case

$$\alpha_1 > \frac{(1-\alpha_2)(\alpha_2\alpha_3+1)4\alpha_2^2(1+\alpha_3)}{(1-2\alpha_2-\alpha_2^2\alpha_3)^2} = \alpha_0,$$

then the equilibrium position has the type of a stable node, and if $\alpha_1 < \alpha_0$, then the equilibrium position has the type of a stable focus. In the neighborhood of the zero isocline point (48), in which equality

$$\alpha_3 = (1-2\alpha_2)\alpha_2^{-2}, (\alpha_2 < 1/2)$$

takes place and the eigenvalues of the equilibrium position are purely imaginary, a transition from a stable equilibrium state of focus type to an unstable equilibrium state of focus type occurs. Since the zero isocline is defined by parameters α_1, α_3, the displacement of the equilibrium position along the zero isocline (48) can be considered as result of a change in parameter α_2, which characterizes the mortality of zooplankton. It is clear from equation (49) that α_2 (i.e., mortality) grows along the zero isocline (48) with increasing x_{1s}. In this case, an analysis of the follow function and determining the sign of the first Lyapunov value. Expanding the right - hand sides of equations (45), (46) into a Taylor series in a neighborhood of the equilibrium position, limiting ourselves to terms of the order of up to the third order of smallness, we calculate the value of the first Lyapunov value

$$L_1(\alpha_{20}) = \frac{\pi}{4\alpha_{20}q^{3/2}}\left[-\alpha_1^2(\alpha_{20}\alpha_3+1)\frac{1-\alpha_{20}(1-\alpha_{20})^2}{1+\alpha_3(1+\alpha_3)^2}\right]. \quad (53)$$

Here $\alpha_{20} = (1+\sqrt{1+\alpha_3})\alpha_3^{-1}$ is value α_2, at which the eigenvalues (52) are purely imaginary,

$$q = \alpha_1(1-\alpha_{20})(\alpha_{20}\alpha_3+1)(1+\alpha_3)^{-1}.$$

From equation (53) it follows that under the accepted conditions and. This proves that when passing eigenvalues through a pair of pure imaginary

roots in the vicinity of an unstable equilibrium state, a stable limiting cycle (attractor) is born. Figure 10 shows the system of trajectories in the phase plane with at, corresponding to this case.

The limiting cycle corresponds to the appearance in the system of a temporal dissipative structure — stable fluctuations in time of phytoplankton and zooplankton concentrations. Figure 10 also shows the trajectories of system (47) in the region. The only equilibrium position of system (47) is the origin of the coordinates of the phase plane. This equilibrium position is of saddle type with separatrixes coinciding with the axes of coordinates. From the qualitative analysis in the phase plane as a whole, it follows that, since the asymptote of the zero isocline (48) is the straight line, the trajectories of a part of the phase plane when it can neither leave the part of the phase plane with nor enter it. Therefore, the condition for the rupture of a trophic function (Barbasheva et al., 1991) is impracticable: there is no continuous transition of solutions from one area to another.

Comparison of Plankton Models in the Local Approximation

Comparing the considered models of plankton in the local approximation, it should be noted that the model proposed by Segel and Levin (Segel, & Levin, 1976) is the only model that does not take into account a decrease in the phytoplankton concentration due to natural death (or subsidence) in the growth function . It seems unnatural. In all other models, the growth functions contain the terms of phytoplankton loss due to their natural death. In this regard, in the model of Segel and Levin, the equilibrium position with the final phytoplankton and zooplankton content is always stable (either the node or the focus). In all other models, the growth functions of which contain the phytoplankton loss terms, under certain conditions, there are unstable equilibrium positions (unstable focus) with final concentrations of both populations. The transition from a stable equilibrium position to an unstable focus equilibrium state is accompanied, as a rule, by the formation of a stable limiting cycle in a neighborhood of an equilibrium position (Hopf bifurcation). However, from the conducted qualitative research it follows that in the logistic model with the Mono trophic function under certain conditions (these conditions are determined) there are regimes when the transition to unstable equilibrium positions is not accompanied by the formation of a

limiting cycle. This is proved using the Lyapunov A.M. stability theory. In these cases, in accordance with the Andronov A.A. theory, a limiting continuum (attractor) is born, consisting of entire trajectories that limit the region of finding the trajectories emerging from an unstable focus. This leads to the chaotic behavior of the trajectories in a large part of the phase plane. Such behavior should be distinguished from the behavior of trajectories in a strange attractor, in which the trajectories randomly tend to the equilibrium position. This was established thanks to a qualitative study of systems of differential equations as a whole, i.e. in the entire phase plane, in not only in the vicinity of the equilibrium position, as it was in the works of previous researchers. It was found that in models with trophic functions of Ivlev and Monod there are 5 equilibrium positions (and not three, as previously thought). It was established that not only the natural mortality of phytoplankton, but also the natural mortality of zooplankton have a significant impact on the dynamics of plankton. With a high natural mortality of zooplankton (adverse conditions) in all models with natural mortality of phytoplankton there are no equilibrium positions with the final concentrations of both populations. A consistent decrease in the natural mortality of zooplankton leads to the appearance of an equilibrium position with the final concentrations of both populations (an attractor). At the beginning, the concentration of zooplankton in the equilibrium position is close to zero, and with further decrease in the natural mortality of zooplankton, its concentration in the equilibrium position increases, and the concentration of phytoplankton in the equilibrium position decreases. A gradual decrease in the zooplankton mortality, moreover, leads to a change in the type of equilibrium position with the final concentrations of both populations: from a stable node to a stable focus, and then to an unstable focus. This process of evolution is observed in all models with natural phytoplankton mortality. The difference in growth laws and trophic function affects only quantitative results, in particular, the conditions for the occurrence of the Hopf bifurcation. These conditions are defined in the work exactly for each model using the Lyapunov stability theory.

It should be noted that the model of plankton with a discontinuous trophic function proposed by Barbashev et al. (1991) contradicts the condition for the continuous development of plankton, since it was found that there is no connection between the solutions before and after rupture of the trophic function. Solutions from one area of the gap can not go to another area and back.

REFERENCES

Allee, W. C. (1951). *Cooperation among animals with human implications*. N.Y. Shuman.

Andronov, A. A., Leontovich, E. A., Gordon, I. I., & Mayer, A. G. (1967). *Theory of bifurcations of dynamical systems on the plane*. Moscow: Science.

Barbasheva, Y. M. (1991). The simulation model of the dynamics of the plankton community of the Kandalaksha Bay of the White Sea. In I. Ya. Agarov & E. Yu. Gupalo (Eds.), *Investigations of phytoplankton in the monitoring system of the Baltic Sea and other seas of the USSR*. Moscow: Gidrometioizdat.

Bautin, N. N. (1984). *The behavior of dynamic systems near the boundaries of the stability region*. Moscow: Science.

Beklemishev, K. V. (1969). *Ecology and biogeography Pelagaley*. Moscow: Science.

Erhard, J. P., & Seguin, G. (1978). *Composition, ecologie, pollution*. Gauthier Villars.

Ivlev, V.S. (1945). Biological productivity of reservoirs. *Successes of Modern Biology*, *19*, 98-120.

Kamshilov, M. M., Zelikman, E. A., & Roukhinyainen, M. I. (1958). Plankton of the Murman coast. In M. M. Kamshilov (Ed.), *Patterns of accumulation and migration of commercial fish in the coastal zone of Murman and their relationship with biological, hydrological and hydrochemical processes*. Moscow: Ed. Academy of Sciences of the USSR.

Kiselev, I.A. (1982). *Plankton of the seas and continental waters*. T.2.Москва: Science.

Kozlov, L. F. (1983). *Theoretical biohydrodynamics*. Kiev: High School.

Lyapunov, A. M. (1935). *The general problem of motion stability*. Moscow: ONTI.

Medvedinsky, A.B., Petrovsky, S.V., & Tikhonova, I.A. (2002). Formation of space-time structures, fractals and chaos in conceptual ecological models on the example of the dynamics of interacting populations of plankton and fish. *Successes of Physical Sciences*, *172*(1), 31 - 66.

Medvedinsky, A. B., Tikhonova, I. A., & Lee, B.-L (2003). The interdependence of the distribution of plankton in space and changes in the biomass of plankton over time: Mathematical modeling. *Biophysics*, *48*(1), 104–110.

Morozova-Vodyanitskaya, N.V. (1948). Phytoplankton of the Black Sea. *Proceedings of the Sevastopol Biological Station.*

Ozmidov, R. V. (1968). *Horizontal turbulence and turbulent exchange in the ocean*. Moscow: Science.

Ozmidov, R. V. (1983). Vertical exchange processes in the ocean with intermittent turbulence. Moscow: Preprint No. 52 of the USSR Academy of Sciences.

Ozmidov, R. V. (1988). Phytoplankton patches in the ocean under various regimes of oceanic turbulence. *Oceanology (Moscow)*, *38*(1), 7–15.

Rudakov, D. V. (1972). *Schooling of fish as an ecological phenomenon*. Moscow: Science, Leningrad Branch.

Segel, L. A., & Levin, S. A. (1976). Hypothesis for origin planktonic patchiness. *Nature*, *259*(26), 659. PMID:814470

Seravin, L. N. (1967). *Propulsion systems of the simplest*. Moscow: Science.

Shmagina, A. P. (1948). *Atrial motion*. Moscow: Medgiz.

Sirenko, L. A., & Gavrilenko, M. M. (1978). *Water bloom and eutrophication*. Kiev: Naukova Dumka.

Slepyan, E.I. (2002). Ecological risk. *Regional Ecology*, *1 - 2*, 62 - 82.

Slepyan, E.I. (2003). Ecological terrorism: the nature, consequences and conditions of liquidation of their consequences. *Regional Ecology*, *3 - 4*, 23 - 34.

Svirezhev, Yu. M. (1987). *Nonlinear waves, dissipative structures and disasters in ecology*. Moscow: Science.

Vinogradov, M. E. (1968). *Vertical distribution of ocean zooplankton*. Moscow: Science.

Volterra, V. (1931). *Lecons sur la Theorie Mathematique de La Lutte Pour la Vie*. Paris: Gautheer – Villars.

Zaitsev, Yu. P. (1970). *Marine Neustonology*. Kiev: Naukova Dumka.

Zenkevich, L.A. (1951). *Fauna and biological productivity of the sea*. Moscow: Soviet Science.

Zhizhin, G. V. (2005). *Dissipative structures in chemical, geological and ecological systems*. St. Petersburg: Science.

KEY TERMS AND DEFINITIONS

Neuston: The layer in the water are attached to the surface of the water inhabited by living organisms.

Phytoplankton: A collection of plants inhabiting a series of sea and fresh waters passively carried by currents.

Trophic Function: The rate of phytoplankton eating by zooplankton.

Zooplankton: A collection of animals that inhabit the stratum of sea and fresh water carried by currents.

Chapter 4
Spatial Dissipative Structures in Excitable Media (Plankton, Soil Bacteria. . . .)

ABSTRACT

A general, the simplest model of a spatial dissipative structure arising in an excitable medium is constructed, containing at least two components interacting with each other with their own mobility. One of these components (active) uses the other component as food. It is shown that such a model leads to a stationary stable spatial distribution of the components in the form of Liesegang bands. As specific examples of the formation of spatial dissipative structures, structures arising in plankton consisting of phytoplankton and zooplankton and in the soil containing the bacterial population and the nutrient substrate are considered. Bifurcation diagrams are constructed in the parameter space, characteristic for each of the considered excitable media, which determine the conditions for the formation of dissipative structures in these media. The existence in the plankton of a strange attractor of a previously unknown shape in four-dimensional phase space has been discovered.

GENERAL FORMULATION OF THE PROBLEM OF SPATIAL DISSIPATIVE STRUCTURE IN AN EXCITABLE MEDIUM

The problem of energy dissipation, dissipative structures is one of the unconditionally significant fundamental problems of natural science. Of paramount importance are the phenomenological special dissipative structures arising from the initially uniform distribution of matter. An example of such

DOI: 10.4018/978-1-5225-9651-6.ch004

structures are the famous Liesegang bands (Liesegang, 1896, 1911a, b, 1923, 1924). Attempts to explain the Liesegang bands have been undertaken for more than 100 years (Ostwald, 1899; Nell, 1905; Hatshchek, 1911, 1914; Brandford, 1916; Jablczynski, 1923; Dogadkin, 1928). The establishment of physical, chemical, as well as, as it became obvious (Kravchenko et al., 1998a, b, c) biological mechanisms for the occurrence of Liezegang fields and the development of a mathematical apparatus that reflects the essence of these mechanisms is extremely important. A convincing explanation for the Liezegang bands suggested by G.V. Zhizhin (Zhizhin, 2004a, b, 2005). The explanation is based on solutions of systems of parabolic differential equations taking into account the provisions of chemical kinetics, diffusion, and reversibility of chemical reactions.

It was possible to establish that solutions describing stationary dissipative structures comparable to Liesegang bands form a new class of stationary composite solutions of differential parabolic equations.

This research direction is connected with the law of V.V. Dokuchaeva on the zonality of the distribution of living organisms in nature: plants, animals, bacteria in the soil, etc. (Mishustin, 1982). It is significant that the diversity of soils and the composition of bacteria in them, even in small areas of the earth's surface, is extremely large (Dobrovolsky, 2001). Zonal (spotty) distribution is also characteristic of plankton. It occurs whenever there are interacting components in the medium. This interaction excites the system, launching self - regulation processes. They lead to the formation of dissipative stable systems. In the previous chapter, it was shown on the example of plankton consisting of phytoplankton and zooplankton that the interaction of these components in the local approximation leads to the achievement of an attractor, that is, an equilibrium position as a point in phase space, or a limit cycle, or a limit set. If we take into account the distribution of the substance (in this case, living matter) in space, then the processes of self - regulation lead to the zone distribution of the components.

In the previous chapter, a system of parabolic differential equations for phytoplankton and zooplankton was recorded, taking into account the mobility of individuals of populations, changes in the concentrations of the components in time and spatial coordinate (equations (2), (3) of Chapter 3). The source terms in these equations take into account the reproduction of phytoplankton and zooplankton individuals, their death and feeding processes. Leaving the principal construction of source terms in equations (2), (3) of Chapter 3, distracting from their specific type associated with the characteristic features of these populations, can to formulate a model problem leading to

a rhythmically striped structure of the distribution of the concentrations of the components along the spatial coordinate.

One consider stationary solutions and their stability of a system of two parabolic equations of second order. Each of the equations describes the change in time and space of the concentration of one of the two components of the medium. Among these two components one single out the one that increases its mass content in the medium by reducing the mass content of the other component. The first will be called the active component, the second - passive. The active component has a high mobility coefficient compared to the passive one. The reduction in the mass content of the second is coordinated with the increase in the mass content of the first, so that the source terms in the equations for the concentrations of active and passive components differ only in sign. They have the form of the product of the concentration of the active component on the function of the concentration of the passive component.

This reflects the leading role of the first component in the process of their interaction. It is believed that convective motion of the medium is absent, i.e. the environment as a whole can be considered stagnant.

The equations describing the changes in the concentrations of active u_1 and passive u_2 components in a one - dimensional space over time, taking into account the accepted assumptions, can be written in the following form

$$\partial u_1 / \partial t = D_1 \partial^2 u_1 / \partial x^2 + u_1 \varphi(u_2), \tag{1}$$

$$\partial u_2 / \partial t = D_2 \partial^2 u_2 / \partial x^2 - u_1 \varphi(u_2). \tag{2}$$

Here D_i is the mobility coefficient ($i = 1, 2$); t is the time; x is the special coordinate; $\varphi(u_2)$ is a function of class C^2 which changes sign at a certain equilibrium value of $u_2 = u_{2s}, (\varphi(u_{2s}) = 0)$, and

$$(d\varphi / du_2)_{u_2 = u_{2s}} > 0, (\varphi(u_2 < u_{2s}) < 0, \varphi(u_2 > u_{2s}) > 0).$$

The above conditions for φ are consistent with the equality of the rates of increase and decrease in the concentration of the active component at a certain equilibrium concentration of the passive component. Moreover, if the concentration of the passive component is less than the equilibrium concentration, then the rate of decrease in the concentration of the active

component exceeds the rate of increase in the concentration of the active component. On the functions $u_1(t,x), u_2(t,x)$ imposed conditions of boundedness and continuity. They can vanish for some finite values of independent variables *t* and *x* in the domain Ω of the task of equations (1), (2). On the boundary of the region Ω, one set the derivatives to zero along the normal to the boundary

$$\partial u_i / \partial x = 0, i = 1,2 \text{ at } \partial\Omega \times (0,\infty). \quad (3)$$

System (1) - (3) has two trivial solutions

$$\text{I: } u_1 = 0; u_2 = u_{20} \text{ - constant,} \quad (4)$$

$$\text{II: } u_2 = u_{2s}, u_1 = u_{10} \text{ - constant.} \quad (5)$$

One investigate the stability of trivial solutions, assuming that the region Ω has size l.

Theorem 1: Solution I is the asymptotically stable trivial stationary solution of system (1) - (3) if $\varphi(u_{20}) = \varphi_0 < D_1\pi^2 / l^2$.

Proof: Consider the solution of system (1) - (3), lying in the neighborhood of solution I and differing from it in each of the variables u_1 and u_2 by a small amount, depending on the variables *t* and *x*

$$u_1 = \nu_1(t,x), \quad (6)$$

$$u_2 = u_{20} + \nu_2(t,x). \quad (7)$$

The set of variables ν_1, ν_2 can be interpreted as a fluctuation around a trivial solution I. It is necessary to clarify the temporal evolution of this fluctuation, determined by the properties of system (1) - (3). Substitute expressions (6), (7) into (1) - (3) and linearize the equations obtained in the neighborhood of solution (4)

$$\frac{\partial}{\partial t}\begin{pmatrix}\nu_1\\ \nu_2\end{pmatrix} = L_1\begin{pmatrix}\nu_1\\ \nu_2\end{pmatrix}. \tag{8}$$

Here linearized operator L_1 has form

$$L_1 = \begin{pmatrix}D_1\partial^2 / \partial x^2 + \varphi_0; 0\\ -\varphi_0; D_2\partial^2 / x^2\end{pmatrix}. \tag{9}$$

To analyze the asymptotic behavior of the solutions of system (8) with $t \to \infty$, it suffices to find the eigenvalues λ_m and the eigenvectors $\begin{pmatrix}g_{um}\\ g_{\nu m}\end{pmatrix}$ of the operator L_1

$$\begin{pmatrix}D_1\partial^2 / \partial x^2 + \varphi_0; 0\\ -\varphi_0; D_2\partial^2 / x^2\end{pmatrix}\begin{pmatrix}g_{um}\\ g_{\nu m}\end{pmatrix} = \lambda_m\begin{pmatrix}g_{um}\\ g_{\nu m}\end{pmatrix}. \tag{10}$$

The sought solution expresses by the eigenvectors so

$$\begin{pmatrix}\nu_1\\ \nu_2\end{pmatrix} = \sum_m a_m e^{\lambda_m t}\begin{pmatrix}g_{um}\\ g_{\nu m}\end{pmatrix}. \tag{11}$$

From boundary condition (3) it is follows, that

$$\begin{pmatrix}g_{um}\\ g_{\nu m}\end{pmatrix} = \begin{pmatrix}c_1\\ c_2\end{pmatrix}\cos\frac{m\pi x}{l}; m = 1,2,... \tag{12}$$

Included (12) into (10) one obtained the characteristic equation

$$\lambda_m = -D_1\pi^2 m^2 / l^2 + \varphi_0. \tag{13}$$

From the characteristic equation (13) it is follows, that if $\varphi_0 < 0$, so $\lambda_m < 0$ and solution (4) is stable. If $\varphi_0 > 0$, so $\lambda_m < 0$ at $\varphi_0 < D_1 m^2\pi^2 / l^2$.

Thus, from (13) it is follows, that if

$$\varphi_0 < D_1\pi^2 / l^2, \tag{14}$$

so all eigenvalues negative and solution (4) is asymptotic stable.

Theorem 1 it is proved.

From the expression (10) it can be seen that in the linear approximation the equation for ν_1 is separated from the equation for ν_2. This reflects the decisive role in the evolution of solution (10) of the fluctuations of the active component of the mixture.

From Theorem 1 it follows that if the concentration of the passive component in the trivial solution (4) is less than or equal to the equilibrium concentration u_{2s}, then the trivial solution is always stable. The instability of the trivial solution (4) can occur with large fluctuations, when the concentration u_2 significantly exceeds the equilibrium concentration u_{2s}. In this case, the first modes become unstable, and the modes with $m \to \infty$ stabilize the solution.

Now consider the solution (5).

Theorem 2: Solution II is the asymptotically stable trivial stationary solution of system (1) - (3).

Proof: Consider the solution of system (1) - (3), lying in the neighborhood of solution II

$$u_1 = u_{10} + \nu_3(t,x), \tag{15}$$

$$u_2 = u_{2s} + \nu_4(t,x). \tag{16}$$

Substitute expressions (15), (16) into (1) - (3) and linearize the equations obtained in the neighborhood of solution (5)

$$\frac{\partial}{\partial t}\begin{pmatrix}\nu_3\\ \nu_4\end{pmatrix} = L_2\begin{pmatrix}\nu_3\\ \nu_4\end{pmatrix}. \tag{17}$$

Here linearized operator L_2 has form

$$L_2 = \begin{pmatrix} D_1\partial^2 / \partial x^2; u_{10}(d\varphi / du_2)_s \\ 0; D_2\partial^2 / x^2 - u_{10}(\mathrm{d}\varphi / du_2)_s \end{pmatrix}. \tag{18}$$

Here $(d\varphi / du_2)_s$ is value of the derivative $d\varphi / du_2$ for $u_2 = u_{2s}$.

To analyze the asymptotic behavior of the solutions of system (17) with $t \to \infty$, it suffices to find the eigenvalues λ_n and the eigenvectors $\begin{pmatrix} g_{un} \\ g_{\nu n} \end{pmatrix}$ of the operator L_2

$$\begin{pmatrix} D_1\partial^2 / \partial x^2; u_{10}(d\varphi / du_2)_s \\ 0; D_2\partial^2 / x^2 - u_{10}(d\varphi / du_2)_s \end{pmatrix} \begin{pmatrix} g_{un} \\ g_{\nu n} \end{pmatrix} = \lambda_n \begin{pmatrix} g_{un} \\ g_{\nu n} \end{pmatrix}. \tag{19}$$

The sought solution expresses by the eigenvectors so

$$\begin{pmatrix} \nu_3 \\ \nu_4 \end{pmatrix} = \sum_m b_n e^{\lambda_n t} \begin{pmatrix} g_{un} \\ g_{\nu n} \end{pmatrix}. \tag{20}$$

From boundary condition (3) it is follows, that

$$\begin{pmatrix} g_{un} \\ g_{\nu n} \end{pmatrix} = \begin{pmatrix} c_3 \\ c_4 \end{pmatrix} \cos \frac{n\pi x}{l}; n = 1, 2, ... \tag{21}$$

Included (21) into (19) one obtained the characteristic equation

$$\lambda_n = -D_1\pi^2 n^2 / l^2 - u_{10}(d\varphi / du_2)_s. \tag{22}$$

From the characteristic equation (22), given that $(d\varphi / du_2)_s > 0$, it follows that $\lambda_n < 0$ for any *n*, i.e. solution (5) is asymptotically stable. Theorem 2 is proved.

As can be seen from expression (18) in the linear approximation, the equations of system (17) are divided and the equation for variable ν_4 does not contain variable ν_3 .These separation of variables in the neighborhood

of solutions (4), (5) is a consequence of the orthogonality of these solutions (Figure 1).

Nontrivial stationary solutions of system (1) - (3) are from the system

$$D_1 d^2 u_1 / dx^2 + u_1 \varphi(u_2) = 0, \tag{23}$$

$$D_2 d^2 u_2 / dx^2 - u_1 \varphi(u_2) = 0. \tag{24}$$

Integrating expressions (23), (24) two times, taking into account the boundary conditions (3), can to obtain

$$D_1(u_1 - u_{10}) + D_2(u_2 - u_{20}) = 0. \tag{25}$$

Here $u_{10} = u_1(x = 0), u_{20} = u_2(x = 0)$.

Express u_1 through u_2 on the basis (25) and substitute this function in equation (24)

Figure 1. Trivial solutions I, II of system (1) – (3)

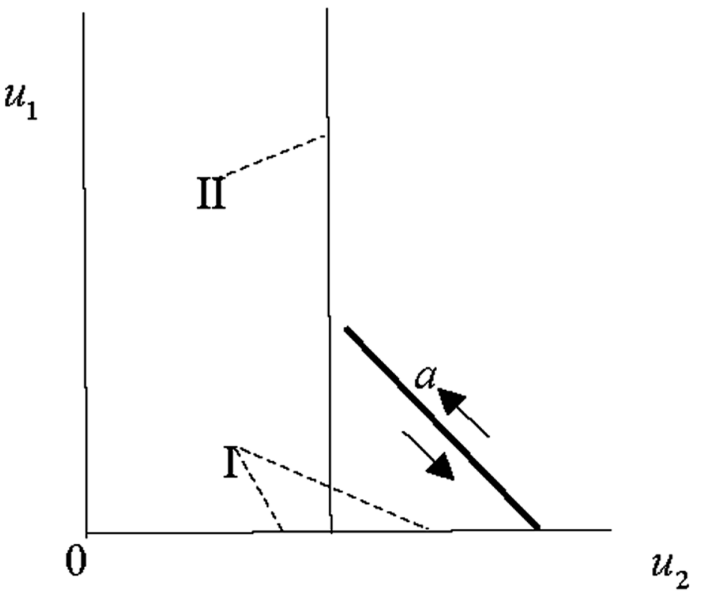

$$D_2 d^2 u_2 \,/\, dx^2 = (u_{10} - D_2(u_2 - u_{20}) \,/\, D_1)\varphi(u_2). \tag{26}$$

One write the expression (26) in the form of a system

$$du_2 \,/\, dx = Y, \tag{27}$$

$$dY \,/\, dx = (D_2^{-1} u_{10} - D_1^{-1}(u_2 - u_{20}))\varphi(u_2). \tag{28}$$

System (27), (28) is autonomous, its solutions can be represented by trajectories in the phase plane (Y, u_2) . It has two equilibrium positions

$a : Y = 0, u_2 = u_{2s};$
$b : Y = 0, u_2 = u_{200};$
$u_{200} = u_{20} + u_{10} D_1 \,/\, D_2.$

Linearizing system (27), (28) in a neighborhood of point *a*, can to find the eigenvalues at this point

$$\lambda_{a1,2} = \pm\sqrt{(D_2^{-1} u_{10} - D_1^{-1}(u_{2s} - u_{20}))(d\varphi \,/\, du_2)_s}. \tag{29}$$

Linearizing system (27), (28) in a neighborhood of point *b*, can to find the eigenvalues at this point

$$\lambda_{b1,2} = \pm\sqrt{-D_1^{-1}\varphi(u_{200})}. \tag{30}$$

The values of the eigenvalues depend on the relations between u_{20}, u_{2s}, u_{200}. Naturally, this ratio: $u_{200} \geq u_{20} \geq u_{2s}$. In this case, the special point *a* has the type of saddle, and the special point *b* has the type of center. There is no need to calculate the follow - up function in this case to clarify the type of the special point *b* (Andronov et al., 1966), due to the symmetry of system (27), (28) about the axis u_2 (Zhizhin, 2004a). The phase diagram of system (27), (28) is shown in Figure 2.

Among the trajectories of this figure, by virtue of the set boundary conditions, only closed ones located inside the separatrix *S*, surrounding the

Figure 2. Phase diagram of system (27), (28)

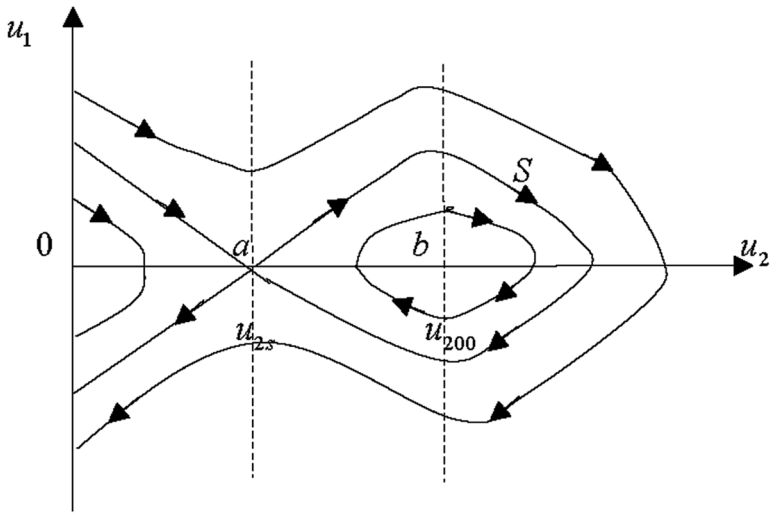

special point *b*, are of interest. In this case, it is reasonable to set $u_{10} = 0$. Then $u_{200} = u_{20}$ and at $u_2 = u_{20}$ the system is located a certain time (or on a section of a certain length) in the trivial steady state I. The value $x = 0$ can be put at the beginning of this section. Then the trajectory moves to the left part of the closed trajectory (to the left of point *b* in the negative half - plane) and moves on. During this movement, the concentration u_2 first decreases, and the concentration u_1 increases. After reaching the axis u_2, the concentration u_2 increases, and the concentration u_1 decreases. To the right of point *b* in the phase plane (Y, u_2), the value u_1 is negative (see (25)), and the solution on a closed sector loses its meaning. Therefore, the motion along a closed trajectory occurs until u_2 reaches u_{20}, and u_1, respectively, becomes equal to zero. After that, the system again goes into a trivial steady state I and stays in it until the closed trajectory crosses the perpendicular to the axis u_2 at the point $u_2 = u_{20}$. Thus, a nontrivial stationary solution consists of glued pieces of solutions I, III, and has the form shown in Figure 3 (one denote this solution I-III).

In the plane (u_1, u_2) (Figure 1), this solution corresponds to the movement in a straight line from the trivial stationary solution I in the $u_2 > u_{2s}$ towards the trivial stationary solution II and, without reaching the decision II returning along the same straight line to the solution I, as well as repeated movement

Figure 3. Integral curves of a nontrivial solution I-III

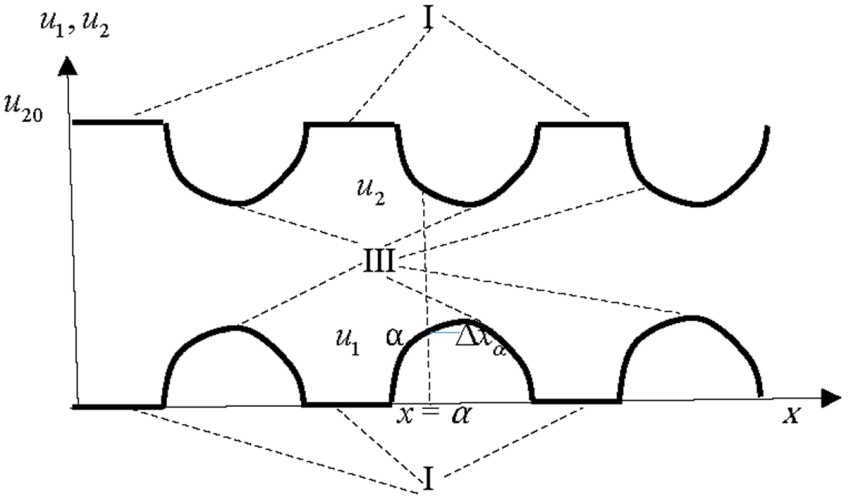

along the straight line to the solution II . This corresponds to the rhythmically - striped concentration distribution in the medium, i.e. spatial dissipative structure.

A stationary solution I-III will be called locally asymptotically stable if it is asymptotically stable in a neighborhood of each point of this solution. This condition of solution I was formulated in Theorem 1. It remains to find the condition of locally asymptotic stability of solution III, in order to determine the condition of asymptotic stability of solution I-III.

Theorem 3: Solution III is locally asymptotically stable at x = α, if $(D_1 + D_2)\pi^2(\Delta x_\alpha)^{-2} > (\varphi(u_2) - u_1 d\varphi / du_2)_{x=\alpha}$, here Δx_α is fluctuation size in the vicinity of a point x =α.

Proof: Choose an arbitrary point on solution III (a point α, see Figure 3). Suppose that in a neighborhood of this point there is a fluctuation from solution III of size Δx_α . Can to present the solution of system (1), (2) in a neighborhood of a point α as

$$u_1 = u_{1III\alpha}(x) + \nu_{1\alpha}(t, x), \tag{31}$$

$$u_2 = u_{2III\alpha}(x) + \nu_{2\alpha}(t, x). \tag{32}$$

And

$$\nu_{1\alpha} = 0, \nu_{2\alpha} = 0 \tag{33}$$

on the borders of the site Δx_{α} .

Substitute expressions (31), (32) into (1), (2) and linearize the equations obtained in the neighborhood of point α of solution III

$$\frac{\partial}{\partial t}\begin{pmatrix}\nu_{1\alpha}\\ \nu_{2\alpha}\end{pmatrix} = L_3\begin{pmatrix}\nu_{1\alpha}\\ \nu_{2\alpha}\end{pmatrix}. \tag{34}$$

Here linearized operator L_3 has form

$$L_3 = \begin{pmatrix}D_1\partial^2 \,/\, \partial x^2 + \varphi(u_{2\alpha}); u_{1\alpha}(d\varphi \,/\, du_2)_{\alpha}\\ -\varphi(u_{2\alpha}); D_2\partial^2 \,/\, x^2 - u_{1\alpha}(\mathrm{d}\,\varphi \,/\, du_2)_{\boldsymbol{\alpha}}\end{pmatrix}. \tag{35}$$

To analyze the asymptotic behavior of the solutions of system (34) with $t \to \infty$, it suffices to find the eigenvalues λ_k and the eigenvectors $\begin{pmatrix}g_{uk}\\ g_{\nu k}\end{pmatrix}$ of the operator L_k

$$\begin{pmatrix}D_1\partial^2 \,/\, \partial x^2 + \varphi(u_{2\alpha}); u_{1\alpha}(d\varphi \,/\, du_2)_{\alpha}\\ -\varphi(u_{2\alpha}); D_2\partial^2 \,/\, x^2 - u_{1\alpha}(\mathrm{d}\,\varphi \,/\, du_2)_{\alpha}\end{pmatrix}\begin{pmatrix}g_{uk}\\ g_{\nu l}\end{pmatrix} = \lambda_k\begin{pmatrix}g_{uk}\\ g_{\nu k}\end{pmatrix}. \tag{36}$$

The sought solution expresses by the eigenvectors so

$$\begin{pmatrix}\nu_{1\alpha}\\ \nu_{2\alpha}\end{pmatrix} = \sum_k d_k e^{\lambda_k t}\begin{pmatrix}g_{uk}\\ g_{\nu k}\end{pmatrix}. \tag{37}$$

From boundary condition (33) it is follows, that

$$\begin{pmatrix}g_{uk}\\ g_{\nu k}\end{pmatrix} = \begin{pmatrix}c_5\\ c_6\end{pmatrix}\sin\frac{k\pi x}{\Delta x}; \mathrm{k} = 1, 2, \ldots \tag{38}$$

Included (38) into (36) can to obtain the characteristic equation

$$\lambda_k^2 + \lambda_k(\xi_1 + \xi_2) + \xi_1\xi_2 + \varphi_\alpha u_{1\alpha}\varphi_\alpha^{'} = 0. \tag{39}$$

Here

$$\xi_1 = D_1k^2\pi^2(\Delta x_\alpha)^{-2}, \xi_2 = D_2k^2\pi^2(\Delta x_\alpha)^{-2}, \varphi_\alpha = \varphi(u_{2\alpha}), \varphi_\alpha^{'} = (d\varphi / du_2)_\alpha.$$

Solving equation (39), one have

$$\lambda_{k1,2} = -0.5(\xi_1 + \xi_2) \pm \sqrt{0.25(\xi_1 - \xi_2)^2 - \varphi_\alpha u_{1\alpha}\varphi_\alpha^{'}}. \tag{40}$$

From expressions (39), (40) it follows that the term in front of the root in (40) is negative if

$$D_1 + D_2k^2\pi^2(\Delta x_\alpha)^{-2} + u_{1\alpha}\varphi_\alpha^{'} > \varphi_\alpha. \tag{41}$$

This will be the condition of stability of the mode k. If $k = 1$ in the expression (41), then can to get

$$D_1 + D_2\pi^2(\Delta x_\alpha)^{-2} + u_{1\alpha}\varphi_\alpha^{'} > \varphi_\alpha. \tag{42}$$

Condition (42) is a condition for the stability of all modes, which proves Theorem 3. It is clear that when the fluctuations Δx_α tend to zero, the condition of local asymptotic stability of solution III is always satisfied.

Thus, the solutions obtained in this generalized model of fixed dissipative structures in an excitable medium do not fall into any of the known classes of solutions of the parabolic equations of mathematical physics (Ladyzhenskaya et al., 1967) and population biology (Fisher, 1937, 1950; Hess, 1991). Since these solutions are, firstly, composite, and secondly, one of the component parts of solutions drastically goes into the negative range of values of variables.

However, such solutions correspond to the observed Liezegang bands (Auchuty et al., 1986; Ortaleva, & Shmidt, 1988) and the distribution of concentrations in populations (Zhizhin, 2005).

SPATIAL DISSIPATIVE STRUCTURE OF PLANKTON

The considered generalized model of the spatial dissipative structure can be considered the simplest model of the spatial dissipative structure of plankton. However, the source terms in the generalized model do not take into account certain characteristic features specific to plankton. They were discussed in detail in the local approximation in the previous Chapter. One take into account these features. The equations of plankton consisting of phytoplankton and zooplankton, (2), (3) of Chapter 3 in the stationary approximation in the absence of convective terms have the form

$$d^2u_1 / dx^2 = -D_1^{-1}M(u_1) + D_1^{-1}E(u_1, u_2), \tag{43}$$

$$d^2u_2 / dx^2 = -kD_2^{-1}E(u_1, u_2) + D_2^{-1}\mu(u_2)u_2. \tag{44}$$

Considering that for all models of plankton considered earlier, the function $E(u_1, u_2) = u_1 f(u_2)$, where $f(u_2)$ is different functions in different models, the system (43), (44) can be written as

$$du_1 / dx = \nu_1, \tag{45}$$

$$du_2 / dx = \nu_2, \tag{46}$$

$$d\nu_1 / dx = -D_1^{-1}M(u_1) + D_1^{-1}u_1 f(u_2), \tag{47}$$

$$d\nu_2 / dx = -kD_2^{-1}u_1 f(u_2) + D_2^{-1}\mu(u_2)u_2. \tag{48}$$

Since the right sides of equations (47), (48) coincide, up to a sign, with the right sides of the corresponding equations of local models and do not contain variables ν_1, ν_2, the system (45) - (48) has equilibrium positions in four - dimensional phase space (u_1, u_2, ν_1, ν_2) with finite coordinates u_{1s}, u_{2s}

that coincide with the coordinates u_{1s}, u_{2s} of the corresponding local models. The coordinates ν_{1s}, ν_{2s} in this equilibrium position are obviously zero. Linearizing the right -hand sides of equations (47), (48) in the neighborhood of the equilibrium state, can to obtain

$$d\nu_1 / dx = A_1(u_1 - u_{1s}) + A_2(u_2 - u_{2s}), \tag{49}$$

$$d\nu_2 / dx = A_3(u_1 - u_{1s}) + A_4(u_2 - u_{2s}), \tag{50}$$

$$A_1 = D_1^{-1}[f(u_{2s}) - (dM / du_1)_s], A_2 = D_1^{-1}u_{1s}(df / du_2)_s, A_3 = -kD_2^{-1}f(u_{2s}),$$
$$A_4 = D_2^{-1}[-ku_{1s}(df / du_2)_s + \mu(u_{2s}) + u_{2s}(d\mu / du_2)_s].$$

The characteristic equation of the system (45), (46), (49), (50) is

$$\lambda^4 - \lambda^2(A_4 + A_1) + A_1A_4 - A_1A_2 = 0. \tag{51}$$

From equation (51) it follows that the Routh - Hurwitz condition for the equilibrium position *S* is not necessarily fulfilled for any of the plankton models. The fact is that the polynomial (51) does not contain the terms of the third and first degrees of the eigenvalue, while for the stability of the equilibrium position so that all coefficients of the characteristic equation are greater than zero.

Since for any considered models of plankton the equilibrium position at finite values of phytoplankton and zooplankton concentrations is unstable at any values of the parameters, there is no loss of stability and there can be no limit cycle production. Therefore, Medvedinsky's claims (Medvedinsky et al., 2002, 2003) that there is a Hopf bifurcation in distributed plankton models are incorrect. However, this does not mean that in system (45) - (48) there can be no dissipative structure at all. In order to be convinced of this, one consider a particular model of plankton (with given functions) in a one - dimensional approximation. Let us choose for this purpose the most complete model of plankton, built according to the study of the Kandolaksha Bay of the White Sea.

Equations (2), (3) of Chapter 3 in the stationary approximation with the source terms corresponding to the plankton model with phytoplankton sedimentation at $x_1 > 1$:

$$D_1 d^2u_1 / dx^2 = -(\alpha - s)u_1 + \gamma f(u_1)u_2, \tag{52}$$

$$D_2 d^2u_2 / dx^2 = -k\gamma f(u_1)u_2 + \mu u_2. \tag{53}$$

In the variables of Chapter 3, equations (52), (53) can be written as a system

$$dx_1 / d\chi = x_3, dx_2 / d\chi = x_4, dx_3 / d\chi = -\alpha_1 x_1 + x_2(x_1 - 1)(x_1 + \alpha_3)^{-1},$$
$$dx_4 / d\chi = -\alpha_4^{-1} x_2(x_1 - 1)(x_1 + \alpha_3)^{-1} + \alpha_2\alpha_4^{-1}x_2, \chi = x(k\gamma / D_1)^{1/2}, \alpha_4 = D_2 / D_1. \tag{54}$$

The equilibrium positions of system (54) with final values of phase variables x_1, x_2 have coordinates $x_1 = x_{1s}, x_2 = x_{2s}, x_3 = 0, x_4 = 0$. Linearizing system (54) in the vicinity of this equilibrium state, from the discriminant of the system can to obtain the characteristic equation

$$\lambda^4 - \lambda^2 2A + \alpha_1\alpha_4^{-1}(\alpha_3 + 1)^{-1}(1 - \alpha_2)(1 + \alpha_2\alpha_3) = 0. \tag{55}$$

Here

$$A = \alpha_1(1 - 2\alpha_2 - \alpha_2^2\alpha_3)0.5\alpha_2^{-1}(\alpha_3 + 1)^{-1}.$$

Since in the equation (55) there are no terms of a polynomial in λ of the first and third order the Routh – Hurwitz condition is not satisfied for any values of the parameters, i.e. the equilibrium position is always unstable. This fundamentally distinguishes the equilibrium position with the final values of the phase variables in the stationary model from the specified equilibrium position in the local model. Thus, in the stationary model there is no bifurcation of the birth of the limit cycle with the loss of stability of the equilibrium position.

Solving equation (55) can be obtain

$$\lambda_{1,2,3,4} = \pm\sqrt{A \pm \sqrt{B}}. \tag{56}$$

Here

$$B = A^2 - \alpha_1\alpha_4^{-1}(1-\alpha_2)(1+\alpha_2\alpha_3)(1+\alpha_3)^{-1}.$$

Using equation (56) it is possible to construct a bifurcation diagram of the equilibrium state (Figure 4).

Four areas of parameter values in space $(\alpha_2, \alpha_3, \alpha_1\alpha_4)$ are formed, which are formed by surfaces $A = 0$ and $B = 0$ (arrows at the surfaces indicate areas of positive values A and B, respectively). In area 1 $A > 0, B > 0$, all eigenvalues are real $\lambda_{1,3} > 0, \lambda_{2,4} < 0$. Equilibrium positions are of saddle type. The

Figure 4. Bifurcation diagram of the equilibrium state of system (54): In area 1 eigenvalues are real $\lambda_{1,3} > 0, \lambda_{2,4} < 0$, equilibrium positions are of saddle type; In areas 2 and 3, the eigenvalues form two pairs of conjugate complex numbers, the trajectories have the form of a spiral, emerging from the equilibrium position and entering into the equilibrium position; In area 4 are two pairs of conjugate purely imaginary eigenvalues; In area 5 the equilibrium position is located in the negative part of the phase space.

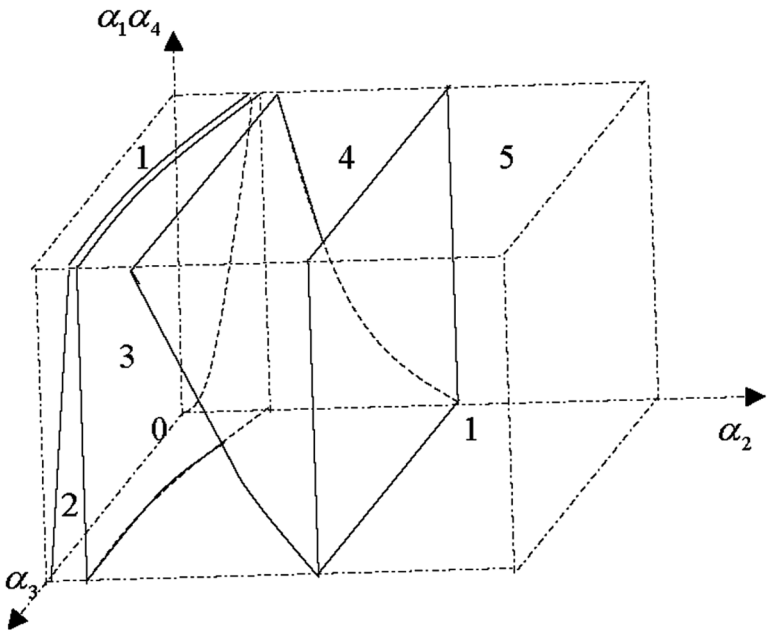

trajectories entering and exiting from equilibrium positions form two two-dimensional surfaces in phase space.

In area 2

$$A > 0, B < 0, \lambda_1 = \beta_1 + \beta_2 i, \lambda_2 = -\beta_1 + \beta_2 i, \lambda_3 = -\beta_1 - \beta_2 i, \lambda_4 = \beta_1 - \beta_2 i,$$
$$\beta_1 = \left|B\right|^{1/2} 2^{-1/2}(-A + \sqrt{A^2 + \left|B\right|})^{-1/2}, \beta_2 = 2^{-1/2}(-A + \sqrt{A^2 + \left|B\right|})^{1/2}.$$

In area 3

$$A < 0, B < 0, \lambda_1 = \beta_3 + \beta_4 i, \lambda_2 = -\beta_3 + \beta_4 i, \lambda_3 = -\beta_3 - \beta_4 i, \lambda_4 = \beta_3 - \beta_4 i,$$
$$\beta_3 = \left|B\right|^{1/2} 2^{-1/2}(\left|A\right| + \sqrt{A^2 + \left|B\right|})^{-1/2}, \beta_4 = 2^{-1/2}(\left|A\right| + \sqrt{A^2 + \left|B\right|})^{1/2}.$$

In regions 2 and 3, the eigenvalues form two pairs of conjugate complex numbers. The trajectories in the vicinity of the equilibrium position in these cases have the form of a spiral, both emerging from the equilibrium position and entering into the equilibrium position.

In area 4 $A < 0, B > 0, \lambda_{1,2} = \pm i\sqrt{\left|A\right| - \sqrt{B}}, \lambda_{3,4} = \pm i\sqrt{\left|A\right| + \sqrt{B}}$ - two pairs of conjugate purely imaginary eigenvalues.

Area 5 is of no interest, since at $\alpha_2 > 1$ the equilibrium position is located in the negative part of the phase space.

Of particular interest is the behavior of the system with the values of the parameters belonging to region 4, since in the well - known classifications of singular points in four - dimensional phase spaces (Tondl, 1973) there are no singular points with two pairs of pure imaginary eigenvalues. Lyapunov stability studies also exclude such points from analysis. A numerical investigation of system (54) for the values of parameters in region 4 revealed the existence of a strange attractor of a form that was not previously known. It consists of several layers, each of which is an attractor from a set of trajectories with two points, characteristic of a given layer, common to all trajectories of this layer. When moving away from the equilibrium position, the next layer of the general attractor gradually degenerates, turning into a single trajectory, which leads to the destruction of plankton. Figures 5 - 10 show the results of calculating the changes in the concentrations of phytoplankton and zooplankton in the layers of the attractor when moving

Figure 5. Changes in the concentrations of phytoplankton x and zooplankton y in the vicinity of the equilibrium position of system (54) with coordinates at x_s = 19 and y_s = 126.66, y(0)=128, x(0)=30

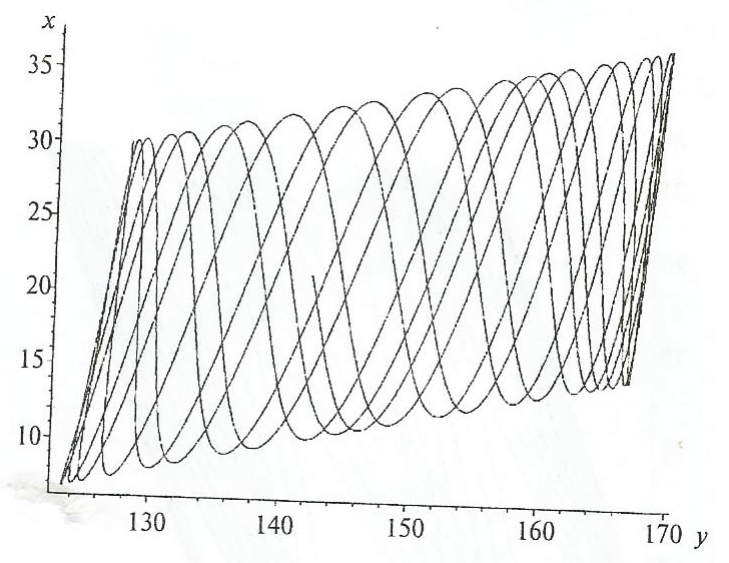

Figure 6. Changes in the concentrations of phytoplankton x and zooplankton y in the vicinity of the equilibrium position of system (54) with coordinates at x_s = 19 and y_s = 126.66, y(0)=128, x(0)=18

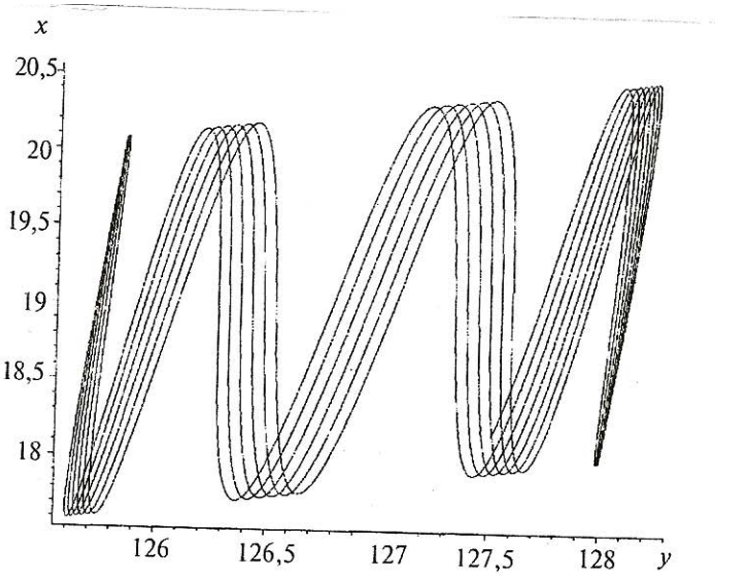

Figure 7. Changes in the concentrations of phytoplankton x and zooplankton y in the vicinity of the equilibrium position of system (54) with coordinates at x_s *= 19 and* y_s *= 126.66, y(0)=128, x(0)=17*

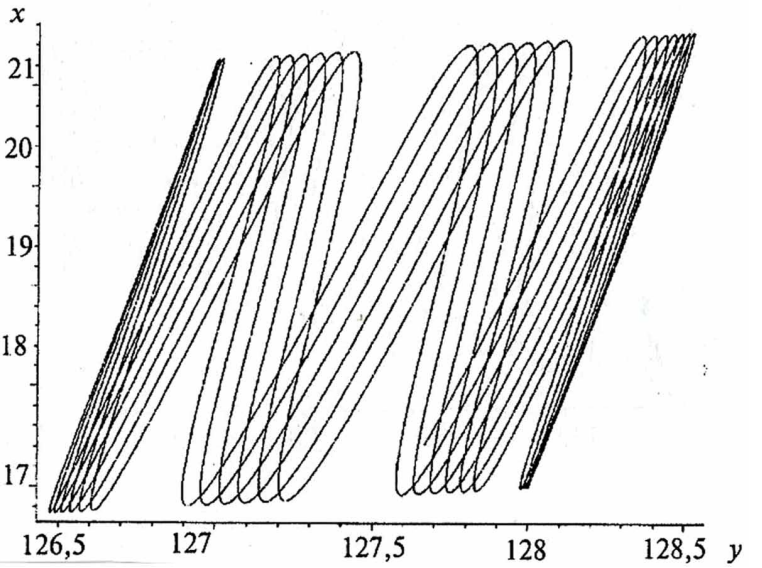

Figure 8. Changes in the concentrations of phytoplankton x and zooplankton y in the vicinity of the equilibrium position of system (54) with coordinates at x_s *= 19 and* y_s *= 126.66, y(0)=128, x(0)=16.3*

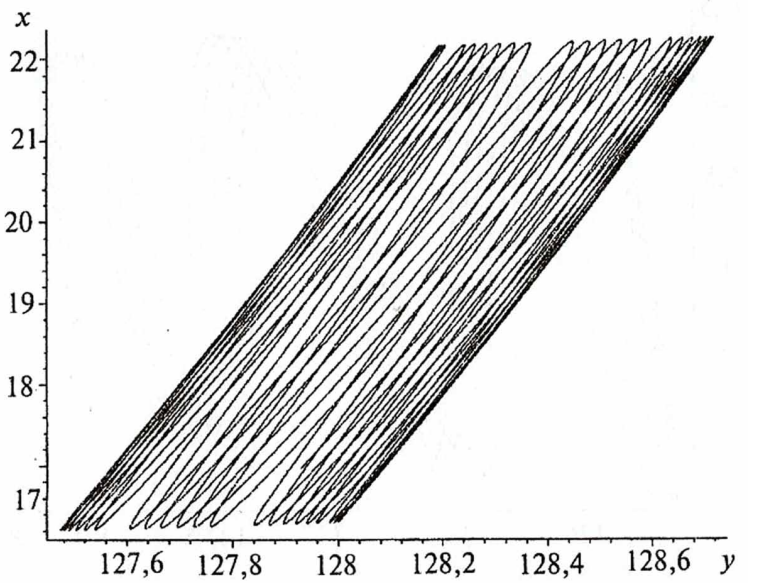

Figure 9. Changes in the concentrations of phytoplankton x and zooplankton y in the vicinity of the equilibrium position of system (54) with coordinates at x_s = 19 and y_s = 126.66, y(0)=128, x(0)=16

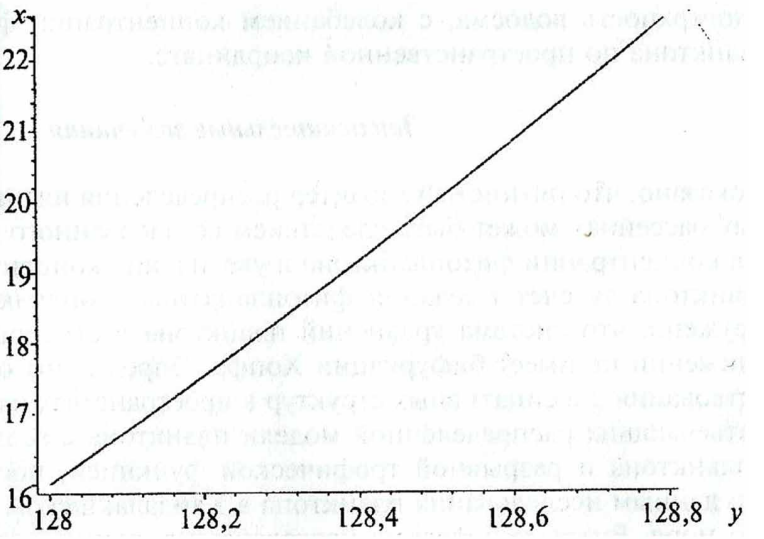

Figure 10. Changes in the concentrations of phytoplankton x and zooplankton y in the vicinity of the equilibrium position of system (54) with coordinates at x_s = 19 and y_s = 126.66, y(0)=128, x(0)=15

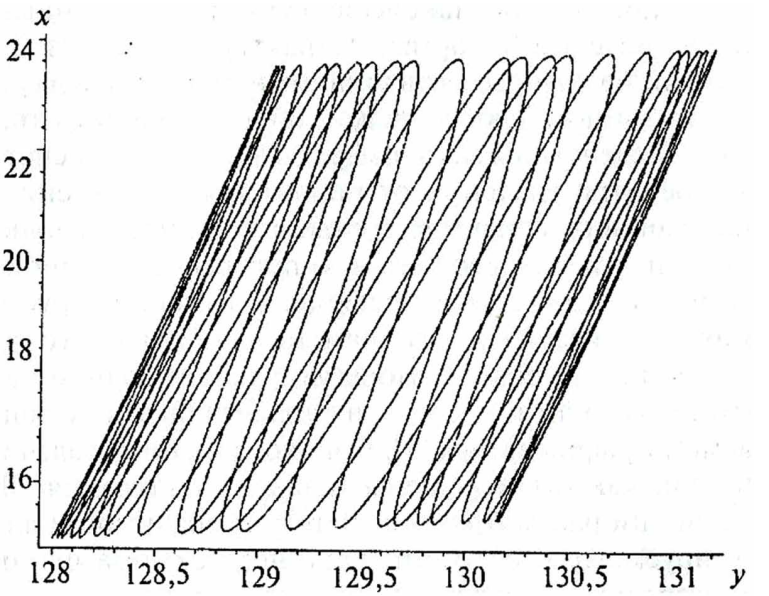

away from the equilibrium position with the values of the parameters $\alpha_2 = 0.9, \alpha_3 = 1, \alpha_1\alpha_4 = 6$ belonging to area 4 of the bifurcation diagram (Figure 4).

The results of the calculation are presented in the plane $(x = x_1, y = \alpha_4 x_2)$. Each of the six calculation options differs in value $x(0)$, from which the calculation started, and has the same value $y(0) = 128$. The chosen value of y_s *=126.66* differs slightly from the coordinate of the equilibrium position (for given values of parameters). The coordinate x_s *=19*. The selected values $x(0)$ range from 30 to 15. For each of the selected values, the system has a solution (layer) in the form of a strange attractor with two characteristic points common to all trajectories of the layer. It can clearly see how the attractor changes its shape as $x(0)$ changes. As $x(0)$ decreases, the attractor shrinks, turns into a line segment and then expands again. However, with a further decrease in $x(0)$, the closure of the trajectories of the attractor is destroyed and the solution leads to the destruction of phytoplankton and zooplankton. For the given values of the parameters, this occurs with $x(0) < 4$. An increase in $x(0)$ also leads to the destruction of the closedness of the trajectories of the layer. When $x(0) > 30$ attractor does not exist.

The existence of an attractor corresponds to the existence in the system of a spatial dissipative structure occupying the surface of a water body, with variations in the phytoplankton and zooplankton concentrations along the spatial coordinate.

MOTIONLESS DISSIPATIVE STRUCTURES FROM SOIL BACTERIA

Currently, in the study and modeling of the structures of bacteria in the soil, the processes of transfer in the soil are not taken explicitly into account. Although it is known, that it is the transfer processes that lead to the formation of self - regulating (dissipative) structures in various open physicochemical and biological systems (Nikolis, & Prigogine, 1971; Polak, & Mikhailov, 1983; Kerner, & Osipov, 1991; Field, & Burger, 1988; Svirezhev, 1987). Soil transport processes are varied. Among them, can to distinguish the filtration of the soil solution, the mobility of soil microorganisms, and the diffusion of substrate, which is feed on bacteria. Taking into account the diffusion

of the substrate and the mobility of bacteria in the mathematical modeling of processes in the soil inevitably leads to systems of parabolic equations (Zhizhin, 2004; Kolmogorov et al., 1937; Wolpert, 1987). The present attempts to take into account the transfer processes in analyzing the structures of soil bacteria were reduced only to the simplest differential equations of the first order (Kozhevin, 1989; Zelenev et al., 2000), in which there were no terms corresponding to the transfer processes. Dissipative structures emerging in excitable media under the action of the transfer processes can be divided into two classes: various traveling waves (Zhizhin, 2004c) and immobile dissipative structures in space, such as Lisegang bands (Lisegang, 1896). In 1896, Lisegang experimentally detected that the ion - exchange reactions to yield a slightly soluble substance in a vertical vessel result in the formation of deposit layers alternating in height. The first attempts to explain this phenomenon were made in terms of thermodynamics, and the effect of the kinetics of chemical reactions was underestimated. Further, it was supposed (Fein et al., 1978; Lovett et al., 1978; Ortoleva, & Schmidt, 1988) that the formation of Lisegang bands is governed by a combination of the process kinetics and the transfer processes. A detailed analytical and numerical study of Lisegang bands formed has been performed in works of Zhizhin (Zhizhin, 2004a, b, 2005a). Such a study is carried out to explore the formation of immobile dissipative structures by soil bacteria (Zhizhin, 2005b). The data of Dobrovol'skya et al. (Dobrovol'skya et al., 1997) were used, who showed that, in marsh ecosystems, structures are formed from bacteria with a dominant trophic group of copiotrophs characterized by motility (the bacteria have flagella). The numerical study used the values obtaind by Nikolaevskii (Zelenev et al., 2000) for the kinetic parameters of the growth of copiotrophs, their death, and consumption of a carbon - containing substrate.

The set of unsteady - state equations describing the changes in the bacterial concentration n and the nutrient substrate concentration s in the flow of the filtering soil solution in a one -dimensional approximation can be written as

$$\frac{\partial n}{\partial t} = -\frac{\nu \partial n}{\partial x} + \frac{\mu \partial^2 n}{\partial x^2} + n(\tau_r^{-1} - \tau_e^{-1}), \tag{57}$$

$$\frac{\partial s}{\partial t} = -\frac{\nu \partial s}{\partial s} + \frac{D \partial^2 s}{\partial x^2} - n(\eta_b \tau_r^{-1} - \eta_s \tau_e^{-1}), \tag{58}$$

where t is time, x is the coordinate in the water filtration direction, ν is the filtration velocity, τ_r is the effective bacterial lifespan, η_b is the coefficient of conversion of the substrate to the bacterial biomass, η_s is the coefficient of conversion of the bacterial biomass to the substrate by the cell lysis, μ is the bacterial motility, and D is the diffusion coefficient.

In equation (57), the effective bacterial reproduction time τ_r is given by the Monod equation (Monod, 1950)

$$\tau_r = \tau_{r0} \frac{K_s + s}{s}, \tag{59}$$

where τ_{r0} is the effective bacterial reproduction time in excess of the substrate and K_s is a constant that is equal to the substrate concentration at which $\tau_r = 2\tau_{r0}$.

Let us suppose that the effective bacterial lifespan depends on the substrate concentration and that this dependence is describe by the inverse Monod equation (Zelenev at al., 2000)

$$\tau_e = \tau_{e0} \frac{K_d + s}{K_d}, \tag{60}$$

where τ_{e0} is the effective bacterial lifespan in the absence of the substrate and K_d is a constant that is equal to the substrate concentration at which $\tau_e = 2\tau_{e0}$.

Of interest is the result of the unsteady - state process, i.e. the formation of a non-uniform steady - state distribution of components of the medium – a steady - state dissipative structure in the soil. Therefore, to find the characteristics of this structure, it is necessary to equate the partial time derivatives in equations (57) and (58) to zero and to solve the obtained total differential equations. In a steady - state approximation, equations (57) and (58) with allowance for equations (59) have the form

$$\nu \frac{dn}{dx} = \mu \frac{d^2 n}{dx^2} + n\left(\frac{s\tau_{r0}^{-1}}{K_s + S} - \frac{K_d \tau_{e0}^{-1}}{K_d + S}\right), \tag{61}$$

$$\nu \frac{ds}{dx} = D \frac{d^2x}{dx^2} - n(\frac{s\tau_{r0}^{-1}\eta_b}{K_s + S} - \frac{K_d\tau_{e0}^{-1}\eta_s}{K_d + S}). \tag{62}$$

Since the conversion of the substrate to the population biomass and the conversion of the population biomass to the substrate are opposite process, let us assume for simplicity that the product of the corresponding coefficients is unity: $\eta_b\eta_s = 1$. Then, set (61), (62) has the first integral

$$\nu n = \mu \frac{dn}{dx} + D\eta_b^{-1} \frac{ds}{dx} - \nu\eta_b^{-1}(s - s_0). \tag{63}$$

The integration constant in expression (63) is determined under the boundary condition

$$n = 0, s = s_0, \frac{dn}{dx} = 0, \frac{ds}{dx} = 0 \text{ at } x = -\infty. \tag{64}$$

This boundary condition models the ingress of the substrate at initial concentration s_0 to the spatial region under consideration.

Let introduce dimensionless variables and parameters

$$N = h_b n / K_s, c = s / K_s, K = K_d / K_s, z = x\nu / D, e = \tau_{e0} / \tau_{r0}, w = \nu(\tau_{e0} / D)^{1/2}. \tag{65}$$

In terms of them, equations (61) and (63) take the form

$$\frac{dN}{dz} = \frac{\mu}{D} \frac{d^2N}{dz^2} + \frac{N}{w^2}(\frac{\varepsilon c}{1 + c} - \frac{K}{K + c}), \tag{66}$$

$$\frac{\mu}{D} \frac{dN}{dz} + \frac{dc}{dz} = N + c - c_0, c_0 = s_0 / K_s. \tag{67}$$

Set (66), (67) has two equilibrium positions: the initial equilibrium position *A*, in which $N = 0$ and $c = c_0$, and the final equilibrium position *B,* in which $N = c_0 - c_+ = N_+$ and

$$c = c_{+} = (0.5(1-\varepsilon) + \sqrt{0.25(1-\varepsilon)^2 + \varepsilon / K})K / \varepsilon$$

is the positive root of the equation $\varepsilon c / (1+c) = K / (K+c)$.

In the vicinity of the initial equilibrium position *A*, equation (66) is written as

$$\frac{dN}{dz} = \frac{\mu}{D}\frac{d^2N}{dz^2} + N\frac{\varepsilon}{w^2}\frac{c_0^2 + c_0K(1-\varepsilon^{-1}) - K/\varepsilon}{(1+c_0)(K+c_0)}. \tag{68}$$

Its solution depends on the eigenvalues λ obtained from equation (68) after substituting $N \sim \exp(\lambda z)$:

$$\lambda_{(1,2)0} = \frac{D}{\mu}\left(0.5 \pm \sqrt{0.25 + \frac{\mu}{D}\frac{\varepsilon}{w^2}\frac{c_0K(\varepsilon^{-1}-1) + K\varepsilon^{-1} - c_0^2}{(1+c_0)(K+c_0)}}\right). \tag{69}$$

If $0.25 + \frac{\mu}{D}\frac{\varepsilon}{w^2}\frac{c_0K(\varepsilon^{-1}-1) + K\varepsilon^{-1} - c_0^2}{(1+c_0)(K+c_0)} < 0$, then the eigenvalues are complex - valued and the equilibrium position *A* is an unstable focus. In this case, the solution of equation (68) has form

$$N = A_1\exp(\lambda_{10}z) + A_2\exp(\lambda_{20}z), \tag{70}$$

where A_1 and A_2 are integration constants.

Substitution of solution (70) to equation (67) yields the expression for the substrate concentration as a function of the spatial coordinate:

$$c = c_0 + A_1\frac{\lambda_{10}\mu/D - 1}{1-\lambda_{10}}\exp(\lambda_{10}z) + A_2\frac{1-\lambda_{20}\mu/D}{\lambda_{20}-1}\exp(\lambda_{20}z). \tag{71}$$

If $0.25 + \frac{\mu}{D}\frac{\varepsilon}{w^2}\frac{c_0K(\varepsilon^{-1}-1) + K\varepsilon^{-1} - c_0^2}{(1+c_0)(K+c_0)} \geq 0$, then eigenvalues (69) are real - valued and the solution leaves the point *A* in the direction corresponding to the positive eigenvalue. This solution is written as

$$N = A_3\exp(\lambda_{10}z). \tag{72}$$

Substitution of solution (72) to equation (67) yields the expression for the substrate concentration as a function of the spatial coordinates in this case:

$$c = c_0 + A_3 \frac{1 - \lambda_{10}\mu / D}{\lambda_{10} - 1} \exp(\lambda_{10} z). \tag{73}$$

In the vicinity of the final position *B,* equations (66) and (67) have the form

$$\frac{dN}{dz} = \frac{\mu}{D}\frac{d^2N}{dz^2} + N\frac{\varepsilon}{w^2}\frac{(c - c_+)(c_+ - c_-)}{(1 + c_+)(K + c_+)}, \tag{74}$$

$$\frac{\mu}{D}\frac{dN}{dz} + \frac{dc}{dz} = N - N_+ + c - c_+, \tag{75}$$

where $c_- = (0.5(1-\varepsilon) - \sqrt{0.25(1-\varepsilon)^2 + \varepsilon / K})K / \varepsilon$ is the negative root of the equation $\varepsilon c / (1 + c) = K / (K + c)$.

Representing the solution of the equations in the form

$$N = B_1 \exp(\lambda_+ z) + N_+, \tag{76}$$

$$c = B_2 \exp(\lambda_+ z) + c_+, \tag{77}$$

and substituting solutions (76) and (77) into equations (74) and (75), one can find the eigenvalues in the final equilibrium position:

$$\lambda_{1+} = D / \mu, \lambda_{(2,3)+} = 0.5 \pm \sqrt{0.25 + \frac{N_+ \varepsilon (c_+ - c_-)}{w^2 (1 + c_+)(K + c_+)}}. \tag{78}$$

Of eigenvalues (78) only λ_{3+} is negative. It is this eigenvalues gives the solution tending to the final equilibrium position *B:*

$$N = N_+ + B_1 \exp(\lambda_{3+} z), \tag{79}$$

$$c = c_+ + B_1 \frac{\lambda_{3+}\mu / D - 1}{1 - \lambda_{3+}} \exp(\lambda_{3+} z). \tag{80}$$

The solution of set (61), (63) consists of the solutions in the vicinities of the points *A* and *B*, which continuously transform into each other. Obviously, solution (72), (73) in the vicinity of the point *A* with real - valued eigenvalues, which continuously transforms into solution (79), (80) in the vicinity of the point *B*, cannot give rise to a dissipative structure, because both solution (72), (73) and solution (79), (80) are monotonic. A dissipative structure can result only from solution (70), (71) with complex - valued eigenvalues at the point *A*, because a part of the solution is in the negative concentration range. Imposing the conditions that, at the boundary between solution (70), (71) and solution (79), (80), the values of *N*, *c*, and $d N / d z$ should be respectively equal and also $z = 0$, one can find the equations for the remaining integration constants:

$$A_2 = \frac{N_+ \lambda_{10} \lambda_{3+} (1 - \lambda_{20})}{(\lambda_{20} - \lambda_{30})(\lambda_{20} - \lambda_{10})}, \tag{81}$$

$$A_1 = A_2 \frac{\lambda_{3+} - \lambda_{20}}{\lambda_{10} - \lambda_{3+}} - \frac{N_+ \lambda_{3+}}{\lambda_{10} - \lambda_{3+}}, \tag{82}$$

$$B_1 = A_1 + A_2 - N_+. \tag{83}$$

The numerical study used the kinetic data on the growth and death of copiotrophic bacteria that were obtained in investigating the dynamics of a population of these bacteria in the soil near the wheat roots (Zelenev et al., 2000). Comparing the Monod equation and the inverse Monod equation (59) with (60), one can obtain the following values of parameters in equations (59) and (60):

$$\tau_{r0} = 15.873 \ h, \tau_{e0} = 3.846 \ h, K_s = 0.69 \ (kg \ \mathrm{s})/\mathrm{m}^3, K_d = 3.335 \ (kg \ \mathrm{s})/\mathrm{m}^3.$$

Hence, the values of the dimensionless parameters that are necessary for the numerical study are found:

$$\varepsilon = 0.2423; K = 4.833. \tag{84}$$

As follows from the previous section, to find the conditions for the zonal distribution of bacteria in the soil, the following inequality should be valid:

$$(K / \varepsilon) + c_0 K(\varepsilon^{-1} - 1) - c_0^2 < 0,$$

where c_0 is the initial scaled substrate concentration. This inequality implies that, at certain values of the parameters ε and K, which are characteristic of copiotrophic bacteria, c_0 should meet the condition $c_0 > 16.335$. Let $c_0 = 17$. Moreover, as follows from the previous, for the zonal distribution of bacteria in the soil to take place, it is necessary that

$$0.25 + \frac{\varepsilon\mu}{Dw^2} \frac{K\varepsilon^{-1} + c_0 K(\varepsilon^{-1} - 1) - c_0^2}{(1 + c_0)(K + c_0)} < 0. \tag{85}$$

This inequality at the accepted values of c_0, ε and K implies that the ratio $\mu / (Dw^2)$ should exceed 32.247. Let $\mu / (Dw^2) = 500$. Let the ratio $\mu / D = 2$ (bacteria owing to their inherent motility are more capable of self - transfer than molecules). Then, the dimensionless velocity of filtration of the soil solution is $w = 0.06324$. Substitution the obtained parameter values into expression (69) gives the eigenvalues of the initial equilibrium position: $\lambda_{(1,2)0} = 0.25 \pm i0.952$, and the eigenvalue and the varying parameter values for the final equilibrium position: $\lambda_{3+} = -0.975, c_+ = 16.335, N_+ = 0.6646$.

The parameter values obtained allow one to calculation the change of the bacterial concentration along the spatial coordinate in the soil from the analytical solution. The calculation results are illustrated in Figure 11 (solid line).

It is seen that, under the accepted conditions, which characterize specific features of copiotrophic bacteria, there is an alternating-band distribution of bacteria in the soil that transforms to a continuous distribution with constant concentration. If, at the same $c_0 = 17, \mu / (Dw^2)$ is decreased so that it approaches the limiting value 32.247, provided that $\mu / D = 2$, then the dimensionless filtration velocity increases. For example, if $\mu / (Dw^2) = 35$, then $w = 0.239$. In this case, the values of c_+ and N_+ remain the same

Figure 11. Soil bacterial concentration distribution along the spatial coordinate at $c_0 = 17, \mu / D = 2,$ *and w = 0.0632 (solid line) and 0.239 (dashed line)*

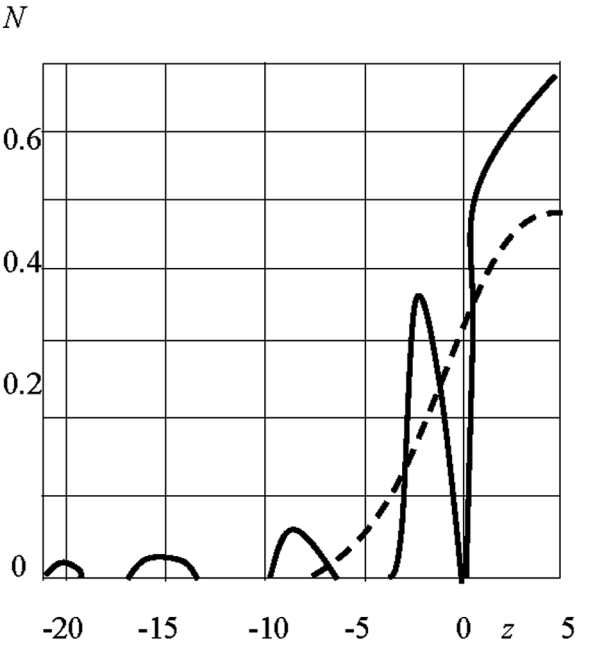

and the eigenvalues of the equilibrium positions change: $\lambda_{(1,2)0} = 0.25 \pm i0.073, \lambda_{3+} = -0.12.$

The bacterial concentration profile calculated from the analytical solution in this case is shown in Figure 11 (dashed line). One can see that, with an increase in the velocity of filtration of the soil solution, the dissipative structure in the form of alternating bands can vanish, with a single semi - infinite region inhabited with bacteria being left.

Let us increase the initial concentration of the nutrient substrate I the flow of the filtering liquid. Let, e.g. $c_0 = 32$. Let us retain the filtration velocity $w = 0.239$, at which, in the case

$c_0 = 17$, there is no alternating - band distribution of bacteria. At the same ratio $\mu / D = 2$, this corresponds to $\mu / (Dw^2) = 35$. Then, the alternating - band distribution of bacteria takes place again. In this case, the maximal bacteria concentration in the bands increase by more than an order of magnitude (Figure 12, solid line).

Figure 12. Soil bacterial concentration distribution along the spatial coordinate at $c_0 = 32, \mu / D = 2,$ *and w = 0.239 (solid line) and 0.343 (dashed line)*

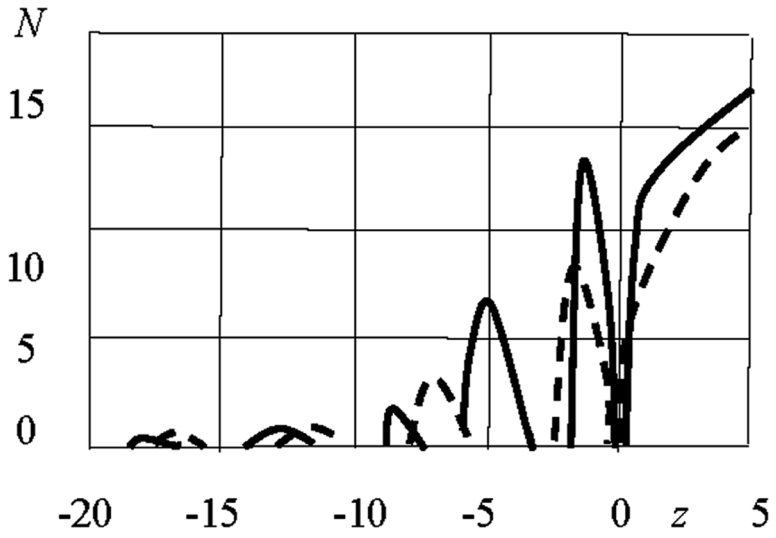

The calculated parameter values under these conditions are the following: $c_+ = 16.335, N_+ = 15.6646, \lambda_{(1,2)0} = 0.25 \pm i1.838, \lambda_{3+} = -1.351.$

If the filtration velocity is now somewhat increased again, the bacteria concentrations in the bands decrease and the non-uniformity of the structure is somewhat smoothed. Figure 12 (dashed line) presents the results of the calculating the bacterial concentration distribution at the following parameter values:

$c_0 = 32, \mu / (Dw^2) = 17, \mu / D = 2, w = 0.343, c_+ = 16.335, N_+ = 15.6646,$
$\lambda_{(1,2)0} = 0.25 \pm i1.23, \lambda_{3+} = -0.8392.$

The calculated bacterial concentration distributions along the spatial coordinate in Figures 11 and 12 characterize the bacterial distributions in the soil (Dobrovol'skaya et al., 1997). To construct the bacterial distributions in the soil in dimensional variables, it is necessary to know specific values of the substrate diffusion coefficient, the bacterial mobility, and the filtration velocity under actual conditions in the soil of a given land. Here, in particular, it should be taken into account that the diffusion coefficients in porous media

are much lower (Nikolaevskii, 1996), and so may be the bacterial mobility in such media. In dimensionless variables, the equation for the boundary of the region of the existence of the alternating - band dissipative structure can be obtained by zeroing the left - hand side of inequality (85):

$$\frac{w^2 D}{4\varepsilon\mu} = \frac{c_0^2 - c_0 K(\varepsilon^{-1} - 1) - K\varepsilon^{-1}}{(1 + c_0)(K + c_0)}. \tag{86}$$

For copiotrophic bacteria, the values of the parameters K and ε are given by expressions (84). The calculated boundary is presented in Figure 13; i.e. Figure 13 is thus a bifurcation diagram of the considered system of copiotrophic bacteria.

The results of the qualitative and numerical study suggest some conclusions about the causes of the formation of the immobile dissipative structure in the form of the alternating - band bacterial concentration distribution in the filtering soil solution. Figures 11 – 13 show that the band (zonal) dissipative

Figure 13. Bifurcation diagram: (1) region of existence of the alternating - band dissipative structure and (2) region of a continuous bacterial concentration distribution

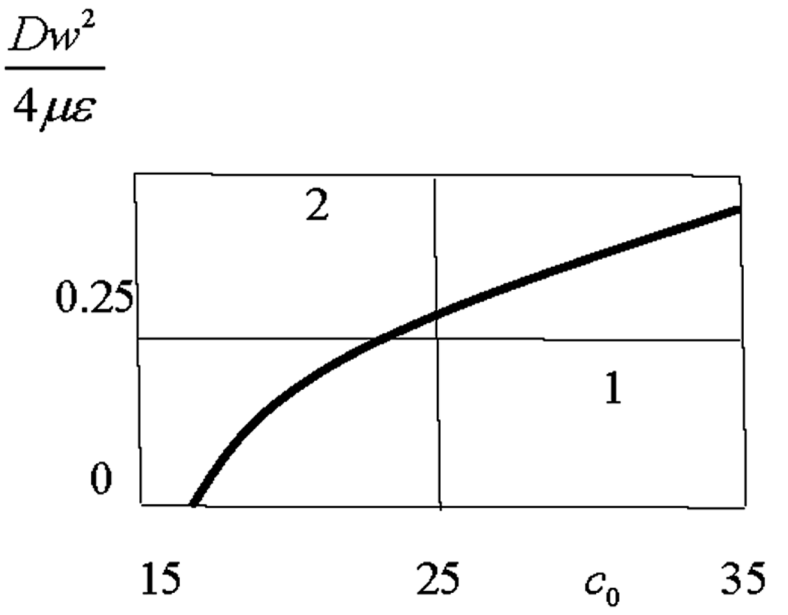

structure emerges at low velocities of the filtering flow, i.e., when the contributions of the substrate diffusion and the bacterial mobility to the transfer processes are significant. With an increase in the velocity of the convective flow, the bands initially (as the boundary of the region of existence of the dissipative structure is approached) merge to form a single semi-infinite band, which then (as this boundary is crossed) transforms into a continuous spatial distribution with the spatial coordinate raging from $-\infty$ to $+\infty$.

REFERENCES

Andronov, A. A., Leontovich, E. A., Gordon, I. I., & Mayer, A. G. (1967). *Theory of bifurcations of dynamical systems on the plane*. Moscow: Science.

Auchmuty, G., Chadam, J., Merino, E., Ortaleva, P., & Riplev, E. (1986). The structure and stability of propagating redox fronts. *SIAM Journal on Applied Mathematics*, *46*(6), 588–604. doi:10.1137/0146040

Bradford, S. C. (1916). Adsorptive stratification in dells. *The Biochemical Journal*, *10*(2), 169–176. doi:10.1042/bj0100169 PMID:16742633

Dobrovol'skaya, T. G., Chernov, N. Yu., & Zvyagintsev, D. G. (1997). About the indicator of the structure of bacterial communities. *Mikrobiologiya*, *66*, 408.

Dobrovol'skii, G. V. (2001). Evgeny Nikolaevich Mishustin - an outstanding microbiologist and soil scientist. In *Perspectives of soil biology* (pp. 5–9). Moscow: Ed. Moscow State University.

Dogadkin, V. A. (1928). *About a curious phenomenon (Liesegang's Rings)*. Moscow: Ed. State Timiryazevsky Research Institute.

Field, R. J., & Burger, M. (Eds.). (1985). *Oscillations and Traveling Waves in Chemical Systems*. New York: Wiley-Interscience.

Fisher, R. A. (1937). The wave of advance of an advantageous gene. *Annals of Eugenics*, *7*(4), 355–369. doi:10.1111/j.1469-1809.1937.tb02153.x

Fisher, R. A. (1950). Gene frequencies in a cline determined by selection and diffusion. *Biometrics*, *6*(4), 353–361. doi:10.2307/3001780 PMID:14791572

Hatschek, E. (1911). A study of some reactions in gels. *Journal of the Society of Chemical Industry*, *30*, 256–258.

Hatschek, E. (1914). Zur Theorie der Liesegang'shen Schichtuntur. *Kolloid Z.*, *14*(3), 115–122. doi:10.1007/BF01433292

Hell, P. (1905). Studien über Diffusionsvorgänge wässerriger Lüsungen in gelatin. *Ann. Der. Physik.*, *18*, 323–347.

Hess, P. (1991). *Periodic - parabolic Boundary Value Problems and Positivity*. New York: John Wiley.

Ivanitsky, G. R. (1998). The spatial structure of the population *Dictyostelium discoideum* in conditions that ensure the occurrence of Liezegang rings in the environment. *Reports RAS*, *360*(6), 827–830.

Jablczyuski, M. C. K. (1923). Laformation rythmique despre'cipite's. Les anneaux de Liesegang.

Kerner, B. S., & Osipov, V. V. (1991). *Autosolitons: localized strongly nonequilibrium regions in homogeneous dissipative systems*. Moscow: Science.

Kogevin, P. A. (1989). *Microbial populations in nature*. Moscow: Ed. Moscow State University.

Kolmogorov, A. N., Petrovsky, I. G., & Piskunov, N. S. (1937). The study of the diffusion equation, combined with an increase in the amount of substance, and its application to a single biological problem. *MSU Bulletin, series A. Mathematics and Mechanics*, *1*(1), 1–26.

Kravchenko, V. V., Medvinsky, A. B., Aslanidi, K. B., Deev, A. A., & Ivanitsky, G. R. (1998a). The emergence of ring structures in the nutrient medium around the population *Dictyostelium discoideum. Reports RAS*, *360*(5), 694–696.

Kravchenko, V. V., Medvinsky, A. B., Aslanidi, K. B., Deev, A. A., & Ivanitsky, G. R. (1998b). The spatial structure of the population *Dictyostelium discoideum* in conditions that ensure the occurrence of Lysigang rings in the environment. *Reports RAS*, *363*(6), 827–830.

Kravchenko, V. V., Medvinsky, A. B., Reshetilov, A. N., & Ivanitsky, G. R. (1998). The acidification of the substrate, initiated by the population *Dictyostelium discoideum*, contributes to the formation of Liezegang rings. *Reports RAS*, *364*(5), 687–689.

Ladyzhenskaya, O. A., Solonnikov, V. A., & Uraltseva, N. N. (1967). *Linear and quasilinear equations of parabolic type*. Moscow: Science.

Liesegang, R. E. (1896). Über einige Eigenshaften von Gallerten. *Naturw. Worhschr*, *11*(30), 353–363.

Liesegang, R. E. (1911a). Über die bei Diffusionen anftretenden Schichtungen. *Zeitschrift für Physikalische Chemie*, *75*, 444–448.

Liesegang, R. E. (1911b). Zur Übersättigungstheorie einiger scheinbar rhytmischer Reaktionen. *Zeitschrift für Physikalische Chemie*, *75*, 371–373.

Liesegang, R. E. (1923). *Beiträge zu einer Kolloidchemie des Lebens*. Leipzig: Biologische Diffusionen.

Liesegang, R. E. (1924). *Chemische Reaktionen in Gallerten*. Leipzig.

Manod, J. (1950). La technique de culture continue, theorie et applicationes. *Ann. Inst. Paster*, 79.

Mishustin, E. N. (1982). Development of the theory of coenosis of soil microorganisms. *Advances in Microbiology*, *17*, 117–136.

Nicolis, G., & Prigogine, I. (1977). *Self-Organization in Nonequilibrium Systems: from Dissipative Structures to Order through Fluctuations*. New York: Wiley.

Nikolaevskii, V. N. (1996). *Geomechanics and Fluid Dynamics*. Moscow: Nedra. doi:10.1007/978-94-015-8709-9

Ortoleva, P. J., & Schmidt, S. L. (1985). Variety and properties of chemical waves. In R. J. Field & M. Burger (Eds.), *Oscillayions and Traveling Waves in Chemical Systems*. New York: Wiley-Interscience.

Ostwald, W. (1899). *Lehrbuch der Allgemeinen Cheme*. Leipzig: Engelman.

Polak, L. S., & Mikhailov, A. S. (1983). *Self - organization in non - equilibrium physicochemical systems*. Moscow: Science.

Svirezhev, Yu. M. (1987). *Nonlinear waves, dissipative structures and disasters in ecology*. Moscow: Science.

Tondl, A. (1970). *Domains of attraction for non - linear systems. Bechovice*. National Research Institute for Machine Design.

Volpert, A. I. (1987). On the propagation of waves described by nonlinear parabolic equations. In Petrovsky I.G. Selected Works. Differential Equations. Probability theory. Moscow: Science.

Zelenev, V. V., van Bruggen, A. H. C., & Semenov, A. M. (2000). "Bakwave", a spatial - temporal model for traveling waves of bacterial populations in response to a moving carbon source in soil. *Microbial Ecology*, *40*, 260–272. PMID:11080383

Zhizhin, G. V. (2004a). Simulation of Liezegang bands formed during the filtration of chemically active liquids. *Chemical Physics*, *1*, 82–89.

Zhizhin, G. V. (2004b). Simulation of Liezegang bands formed in ion exchange reactions. *Chemical Physics*, *10*, 54–61.

Zhizhin, G. V. (2004c). *Self - regulating waves of chemical reactions and biological populations*. St. Petersburg: Science.

Zhizhin, G. V. (2005a). Motionless dissipative structures from soil bacteria. *Biophysics*, *50*(2), 323–328. PMID:15856992

Zhizhin, G. V. (2005b). *Dissipative structures in chemical, geological and ecological systems*. St. Petersburg: Science.

KEY TERMS AND DEFINITIONS

Attractor: A compact subset of the phase space of a dynamic system, all trajectories from a certain neighborhood of which tend to it at a time tending to infinity.

Copitrophic Bacteria: Bacteria living in water that can grow at low nutrient concentrations.

Dissipative Structures: The structures in various mediums that exist in nature are stationary due to the consumption (dissipation) of energy from the environment.

Separatrix: A trajectory separating from each other the trajectories of the phase space of a qualitatively different type.

Strange Attractor: A attracting set of unstable trajectories in the phase space of a dissipative dynamical system.

Chapter 5
Dimension of Molecules of Compounds of Biogenic Elements

ABSTRACT

Chemical compounds of biogenic elements are considered (i.e., chemical elements present in living organisms and ensuring the successful functioning of their various organs and systems). Biogenic elements are divided into s-, p-, and d-elements, in which respectively are completed with s-, p-, and d-electronic orbitals. In each of these groups, the structure of compounds of biogenic elements is investigated, and the dimension of the corresponding molecules is determined. It is proved that s- and d-biogenic elements exhibit increased chemical activity (higher than the standard valence) due to participation in the formation of a chemical bond of electrons of the preceding level. This leads to the creation of complex molecules of higher dimension. The chemical compounds of biogenic p-elements, which are the building blocks for the formation of biomolecules (elements of life), will be specifically investigated in subsequent chapters.

BIOGENIC ELEMENTS

In living organisms, one can find almost all the elements that exist in the earth's crust and in sea's water. Ways of receipt of elements in organisms are diverse. According to Vernadsky's (2012) biogeochemical theory, there is a biogenic migration of atoms along a chain of air, soil, water, food, man. As a result, almost all the elements surrounding a person in the environment, to

DOI: 10.4018/978-1-5225-9651-6.ch005

a greater or lesser extent, penetrate into the body. The chemical elements necessary for living organisms to build and live the activity of cells and organs are called biogenic elements. According to the concentration in the body, biogenic elements are divided into macro - elements, micro - elements, and ultra - micro - elements. Biogenic elements whose content exceeds 0.01% of body weight are called macro - elements. These include 12 elements C, H, O, N, P, S, Na, K, Ca, Mg, Cl, and Fe. Biogenic elements, the total content of which is about 0.01% of body weight is called micro - elements. The content of each of them ranges from 10^{-3} % to 10^{-5} %. The micro - elements include, for example, active transition metal atoms in the centers of enzymes and hormones. Some micro - elements exhibit affinity for certain tissues (iodine - to the thyroid gland, fluorine - to the enamel of the teeth, zinc - to the pancreas, molybdenum - to the kidneys, etc.). Elements whose content is less than 10^{-5} % are classified as ultra - micro - elements.

The current state of knowledge about the biological role of elements can be characterized as a superficial touch to the problem. A lot of evidence has been accumulated on the content of elements in various components of the biosphere, the body's response to their excess and deficiency. Compiled maps of biogeochemical zoning and biogeochemical provinces. There is no general theory of the examining function of the mechanism of action and the role of biogenic elements in the biosphere.

In this Chapter, based on the previous monographs of the author (Zhizhin, 2017a, 2018), the question is being considered that a possible mechanism of the action of biogenic elements is the creation of molecules with higher dimension in their neighborhood. What exactly in the space of higher dimension the main processes of creation and development of living matter occurs.

It is known that with insufficient intake of one or another biogenic element in the body, the growth and development of the organism slows down significantly. This happens, for example, by reducing the activity of enzymes that contain this biogenic element. With an increase in the dose of this element, the response of the body increases and reaches the norm (the biotic concentration of the element). The greater the width of the plateau in this function, the less toxic the element, since a further increase in dose leads to a negative effect of the element due to its taxis. Elements vary in their taxing power. The elements Hg, Pb, Be, Cu, Cd, Cr, and Ni differ by special taxability and prevalence. They compete with other trace elements and can displace them from biological complexes.

Biogenic elements are divided into three groups: *s* -, *p* -, and *d* - elements, i.e. elements in which building *s* -, *p* -, and *d* - are sublevels of the external level of the electronic structure of the atom, respectively. The monograph (Zhizhin, 2017a) investigated in detail the chemical compounds of almost all existing elements and showed that the majority of the molecules of these compounds have a higher dimension. Can one now select the compounds of biogenic elements from them and some elements with special taxability.

MOLECULES OF CHEMICAL COMPOUNDS OF BIOGENIC S – ELEMENTS

S - elements there are in 1A and 2A subgroups of the periodic table. The 1A subgroup contains alkali metals, among which potassium and sodium are biogenic. These are elements of the electrolyte background in living organisms. Alkali metals have an external electron shell ns^1 . They easily give bake one electron exhibiting a degree of oxidation +1. In subgroup 2A are alkaline - earth biogenic elements Mg, Ca, Sr, and Ba, as well as the toxic element beryllium Be and the radioactive element radium Ra. Alkaline - earth elements have an external electron shell ns^2. Alkaline - earth elements can release their two external electrons, showing an oxidation state of + 2. This allows for the formation of linear molecules. However, alkaline - earth elements may exhibit a valence (oxidation state) of a significantly larger group number. This happens due to the participation in the formation of chemical bonding of electronic pairs of the pre - outer level. This is most pronounced in magnesium, whose electrons are closer to the nucleus of the atom, compared to other alkaline - earth elements. The pre - outer level of Mg includes two *s* – electrons and six *p* – electrons. These four electron pairs, starting from each other, create tetrahedral coordination around the magnesium atom. Taking vacant quantum cells of ligands, they increase the possible value of valence of magnesium to six (which in turn leads to the formation of molecules of higher dimension (Zhizhin, 2017a). This gives magnesium more chemical activity especially important for living organisms. Magnesium is one of the main elements of the cell. It is called the structural element of a living organism. Magnesium participates in the coordinated work of all body systems, especially the work of the central and peripheral nervous systems. It participates in more than 300 enzymatic reactions, stimulating the work of enzymes, including in energy - saving reactions (ADP). Magnesium is needed for

protein synthesis, nucleic acids, for the breakdown of glucose, for elimination of toxins from the body. Magnesium regulates the rhythm of the contraction of the heart muscle, lowers blood pressure, dilates blood vessels, magnesium prevents the occurrence of ischemic disease and thrombosis. Magnesium ensures the normal functioning of the brain, respiratory system, hormonal system. The absence of magnesium in the body, even for a short time, can lead to serious irreversible effects. When there is not enough magnesium in the body, it begins to actively take it out of the bone tissue, nerve cells, and endocrine glands and send it to the blood where magnesium must be present. In many cases, calcium may be involved in reactions instead of magnesium.

Even for the chemical bonds of magnesium with valence 2, compounds of higher dimension are formed. Consider a molecule of bis (neopentyl) magnesium Mg $(C_5H_{11})_2$ (Gillespie & Hargittai,, 1991). Magnesium in this molecule exhibits a valence of 2. In each group C_5H_{11}, the carbon atoms form the geometric form of a tetrahedron centered. This already gives the dimension of this form equal to 4. In addition, around each carbon atom there is also a tetrahedral coordination of other atoms (hydrogen and carbon). Each group C_5H_{11} can be represented in the form of a tetrahedron with a center in which its vertices contain functional groups CH_3, and in the fourth (attached to the magnesium atom) is a functional group CH_2. At the center of the tetrahedron is a carbon atom. Then the bis (neopentyl) magnesium molecule has the form of two tetrahedrons with a center connected to each other by a magnesium atom (Figure 1). Functional groups CH_3 are located in the vertices $a_1, c_1, d_1, a_2, c_2, d_2$; functional groups CH_2 are located in the vertices b_1, b_2 ; at the points o_1, o_2 are carbon atoms; at the point *o* there is a magnesium atom.

Valentine bonds are indicated in Figure 1 with a brown color. The remaining edges (black) serve to form a convex figure (polytope), the dimension of which must be established.

Theorem 1: The dimension of bis(neopentyl) magnesium molecule equal to 6.
Proof: For proof of theorem 1can one noted that polytope on Figure 1 is 5 – cross - polytope with centrum Figure 2.

Comparing Figures 1 and 2, can to see that these figures are topologically equivalent, that is, in Figure 2, the same vertices are shown as in Figure 1. Moreover, each of the corresponding vertices in Figure 2 is incidental to the number of edges as in Figure 1 and the connection of vertices by edges in Figure 2 is topologically the same as in Figure 1. If one denote in Figure 2

Figure 1. The structure of bis(neopentyl) magnesium molecule

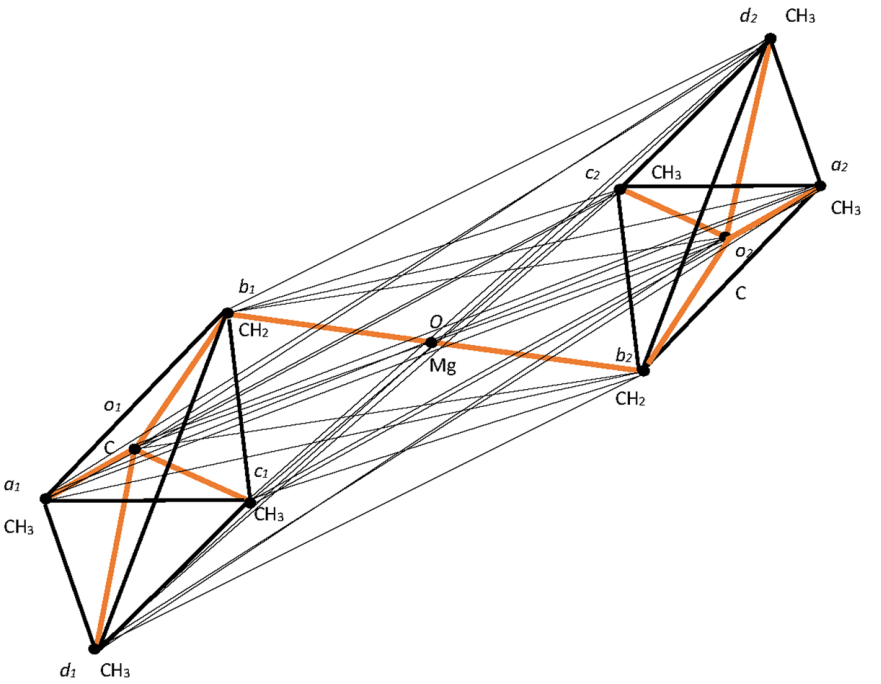

Figure 2. The 5 – cross - polytope with centrum

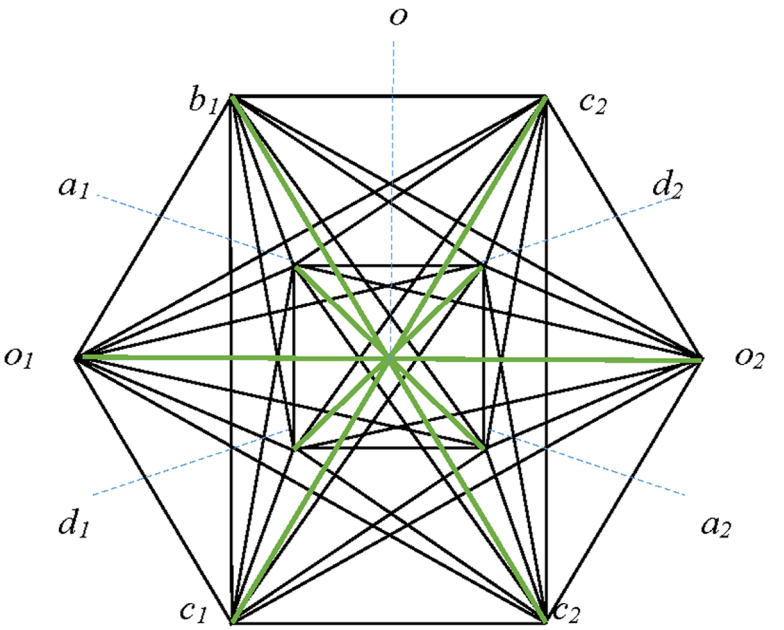

the edges issuing from vertex O to other vertices in green, the remaining figure, as can be seen, is the 5 - cross - polytope, given in the monograph by Zhizhin, (2014b). In addition, the vertex O is the center of 5 – cross - polytope. As follows from Zhizhin (2014b) 5 – cross - polytope has 10 vertices ($f_0 = 10$), 40 edges ($f_1 = 40$), 80 triangular faces ($f_2 = 80$), 80 tetrahedrons ($f_3 = 80$), 32 4 - cross - polytopes ($f_4 = 32$). The introduction of the center into the 5 – cross - polytope adds, according to Figure 2, 10 edges

$(oa_1, ob_1, oc_1, od_1, oo_1, ob_2, oa_2, oc_2, od_2, oo_2)$,

24 triangular faces

$$\begin{matrix} o_1b_1o, b_1a_1o, b_1oa_2, b_1od_2, b_1oc_2, b_1oc_1, \\ \{ c_2d_2o, c_2od_1, c_2oa_2, c_2oo_2, o_2d_2o, o_2oa_2, o_2ob_2, b_2a_2o, b_2od_2, \}, \\ b_2oc_2, b_2oc_1, b_2d_1o, c_1od_1, c_1od_2, c_1oa_2, c_1oo_1, a_1o_1o, o_1d_1o \end{matrix}$$

28 tetrahedrons

$(b_1od_2a_2, b_1c_1oo_1, b_1d_1oa_1, b_1a_1d_2o, b_1od_1a_2, b_1oa_2c_2, b_1od_1c_1, c_2oa_1d_1, c_2b_2oo_2,$

$c_2a_2od_2, c_2a_1d_2o, c_2oa_2d_1, c_2od_1b_1, c_2oa_2b_2,$
$c_1oa_2d_2, c_1a_1od_1, c_1d_1a_2o, c_1oa_1d_2, c_1od_2b_2, c_1od_1b_1,$

$o_1a_1d_1o, b_2od_1a_1, b_2d_2oa_2, b_2a_2d_1o, b_2od_2a_1, b_2oa_1c_1, b_2od_2c_2, o_2d_2a_2o)$,

18 4-siplexes

$(b_1a_1od_2c_2, b_1c_1d_1a_1o, b_1o_1a_1oc_2, b_1od_2o_2c_2, b_1od_2a_2o_2, c_1d_1oa_2b_2, c_1o_1d_1b_2o,$

$c_1oa_2o_2b_2, c_1oo_2d_2o_2, c_2b_2a_2d_2o, c_2o_2d_2ob_1, c_2oa_1o_1b_1, c_2oa_1d_1o_1, b_2a_2od_1c_1, b_2od_1o_1c_1,$

$b_2od_1a_1o_1, o_2c_2od_2a_2b_2)$,

6 5-siplexes

$(o_1b_1a_1od_1c_1, c_2od_2a_2o_2b_2, c_1od_2a_2o_2b_2, b_2oa_1o_1d_1c_1, c_2od_1a_1o_1b_1, b_1oa_2o_2d_2c_2)$.

Adding the obtained quantities of geometric figures of different dimensions connected with the center of the 5 - cross - polytope to the corresponding numbers of figures not connected with the center of the 5 - cross - polytope, can to obtain the total number of geometric figures of different dimensions in the 5 - cross - polytope with center:

$$f_0 = 11, f_1 = 50, f_2 = 104, f_3 = 108,$$

$$f_4 = 50, f_5 = 7.$$

Define dimension polytope in Figure 1 on the Euler- Poincare equation (Poincare, 1895)

$$\sum_{i=0}^{n-1}(-1)^i f_i(P) = 1-(-1)^i, \quad (1)$$

f_i is the number of the elements with the dimension *i* at polytope *P*; *n* is dimension of the polytope *P*.

Substituting the values $f_i(i = 0 \div 5)$ for Figure 1 into equation (1), can to find that the Euler-Poincare equation is satisfied for $n = 6$

11 – 50 + 104 – 108 + 50 -7 =0.

This proves that a 5 – cross - polytope with center has dimension 6. Theorem 1 is proved.

If the electron pairs of magnesium at the second energy level enter into a chemical bond, then its valence is more than two. For example, in Grignard reagent the magnesium valence is 4 and in the vicinity of magnesium atom there is tetrahedral coordination. While the nearest neighborhood of the magnesium atom has a dimension of 4, and with the account of the attached groups of atoms this dimension is even higher. An interesting example is the complex magnesium ion $Mg(OAsMe_3)_5^{2+}$, $Me = CH_3$. In this compound, magnesium exhibits a valence of 5. In this case, the nearest environment of magnesium is of dimension 5. Indeed, the nearest environment of magnesium by oxygen atoms has the form of a 4 - simplex with a center in the magnesium

atom (Figure 3). At the vertices *a, b, c, d, e* of the polytope, in Figure 3, there are oxygen atoms, in the vertex *o* there is a magnesium atom. The valence bonds are indicated in Figure 3 with a brown color, the other edges (black) are needed to create a convex figure in space. The vertices together with the connecting ribs form a 4 - simplex. The addition of a magnesium atom and valence bonds converts this polytope into a 4 - simplex with a center.

In Figure 3 can to indicate 6 vertices ($f_0 = 6$); 15 edges ($f_1 = 15$);

20 trigonal faces (abc, aeb, abo, abd, bcd, bco, bce, aeo, aed, aec, edo, edc, edb, dco, dca), $f_2 = 20$;

15 tetrahedrons (abed, abec, abcd, dbce, aecd, obcd, oecd, aoed, aoeb, aobc, boed, coae, doeb, eobc, aocd), $f_3 = 15$;

6 4-simplexes (*abcde, abedo, abeco, abcdo,dbceo, aecdo)*, $f_4 = 6$.

Substituting values f_i into equation (1), can to find that the Euler - Poincare equation is satisfied for $n = 5$

$$6 - 15 + 20 - 15 + 6 = 2.$$

This proves that a 4 - simplex with center has dimension 5. If we take into account the presence of other atoms in the ion $Mg(OAsMe_3)_5^{2+}$, then its dimension will be even higher.

Figure 3. The 4 – simplex with centrum

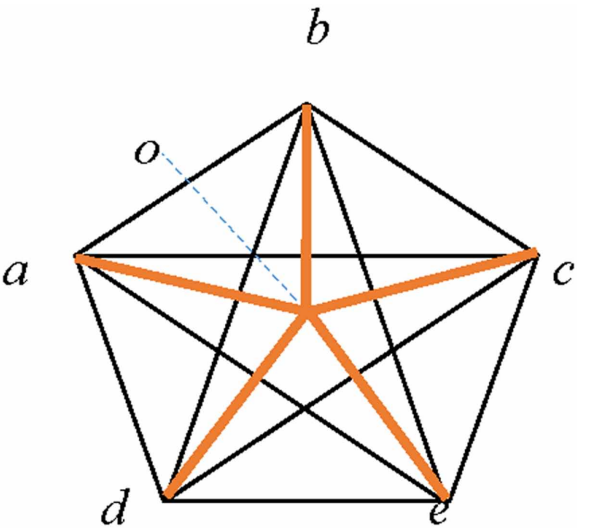

Such compounds can form other alkaline - earth elements, i. e. calcium and barium.

Note that the molecules with the participation of the toxic element of beryllium, located in the 2A subgroup of the periodic system, also have a dimension higher of three (Zizhin, 2017a).

MOLECULES OF CHEMICAL COMPOUNDS OF BIOGENIC D – ELEMENTS

In the *d* – elements are completed *d* – orbitals of the pre-outer level. All these elements form metals. It is electrons of the pre - outer level mainly determine properties of the *d* - elements. In this can to see the total of these elements with alkaline - earth metals. Since the *d* - elements are located in the periodic table between the *s* - elements and the *p* - elements, the *d* - elements are called transition elements. The valence electrons of *d* - elements in general can be written as $(n-1)d^{1-10}, ns^{1-2}$. Of the 30 *d* - elements, 12 elements are biogenic elements Cu, Zn, Ti, V, Cr, Mn, Fe, Co, Ni, Ag, Mo, and W.

Of the 12 biogenic *d* - elements of the four elements Cr, Cu, Mo, Ag there are violations in the order of filling the electron orbitals in accordance with the Hund rule (Hund, 1927) in order of increasing the electron energy. Such atoms in literature are called anomalous elements (see, for example, Arkel, 1931; Karapetyants, & Drakin, 1994). However, in the periodic table of the elements of such anomalous elements there are quite a lot - 21 elements (11 *d* - elements, 10 *f* - elements). The first analysis of the structure of filling with electrons of energy levels in anomalous elements was carried out in 1998 (Zhizhin, 1998). In 2017, rules were formulated that govern the distribution of electrons in orbitals in all the anomalous elements (Zhizhin, 2017a, b). Thus, failures in the filling of the electron orbitals of atoms by the electrons are not random. These failures follow a certain order. Moreover, these failures lead to an increase in the chemical activity of atoms. This it is especially important for biogenic elements, since an increase in the chemical activity of elements leads, as a rule, to the formation of molecules of higher dimension. To prove this statement, one consider some examples of compounds of biogenic elements.

The first anomalous biogenic element is Cr. It in consequence of the anomalies have one valence electron on the 4 *s* - orbital and five of the electrons on 3*d* - orbital. This allows have of chromium a valence equal 6

in many compounds. Since crystalline chromium oxide CrO_3 consists of chains of tetrahedrons CrO_4, united in two vertices (oxygen is also a biogenic element). Each tetrahedron has located in the center of an atom of chromium associated by double bond with each of the four oxygen atoms at the vertices of a tetrahedron. All molecules have the form of a tetrahedron with the center, as shown in (Zhizhin & Diudea, 2016; Zhizhin, Khalaj & Diudea, 2016), have a dimension of 4, i.e., crystalline chromium oxide is a chain of polytopes of dimension 4, united in two vertices (Figure 4). If instead of double bonds are one-time connection with the chromium atom monovalent groups (such as hydroxyl groups), the molecule will be the center of the octahedron, which also would have dimension 4.

There are even more complex chromium compounds (see Gillespie, 1972; Gillespie & Hargittai, 1991), the dimension of molecules, which is more than four. It is clear that all the other anomalous elements with half (or nearly half) filled *d* - orbitals of the subshell will have similar compounds having a molecular of higher dimensions.

If the anomalous elements has one electron in the outer orbital *s* and subshell *d* completely (or almost completely) filled, then the element at the expense of *s* electron forms a linear molecule, such as a linear molecule oxide X_2 O, where X is the anomalous element (Cu, Ag, Pd, Pt, Au, Rg). The first two of these elements are biogenic elements. However, due to the donor - acceptor bond linear molecule can form complex structures in the space. We choose element Cu from second group of anomalous elements. Figure 5 shows an exemplary structure formed by linear molecules Cu_2 O

Figure 4. The chain of molecules CrO_3

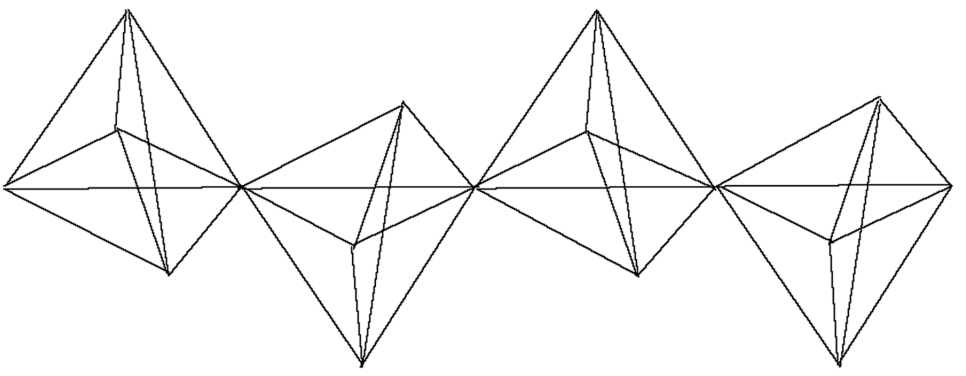

Figure 5. The structure of the compound Cu_2O. A black small circle is oxygen atom. A brown circle is copper atom.

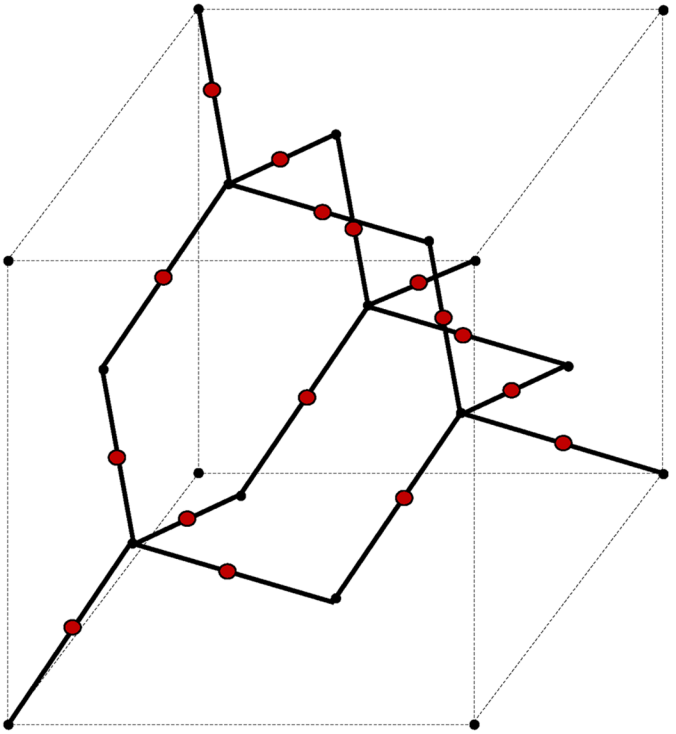

Each oxygen atom in the structure of Figure 4 bonded to four metal atoms (Cu). Two covalent bonds due to the formation of electron pairs divided: one *s* - electron metal atom and a *p* - electron atom of oxygen. In addition, there are two more donor - acceptor chemical bond due to the transfer of two electrons from the *s* - orbital and two electrons from the *p* - orbitals of the oxygen atom to vacant quantum cell of orbital metal. Thus, oxygen atom acquires valence equal four. In addition, each metal atom is linearly between two oxygen atoms.

In this structure, oxygen atoms (except oxygen atoms located at the vertices of a cube) form structure is topologically equivalent to the structure of carbon atoms (biogenic element) in the molecule of adamantane. As shown in the article of Zhizhin (2014a) on the basis the monograph Zhizhin (2014b), the dimension of this molecule is 4. However, the two molecules comprising 10 oxygen atoms have free unallocated space. Therefore, if we set the task of finding the unit cell structure of copper oxide without filling cracks and gaps

to help translation the entire space, we need to build politopic prismahedron Zhizhin (2015), with bases in the form polytopes corresponding to these molecules. Taking a line segment equal to the length of the edge of the cube, in which is inscribed the structure including 10 oxygen atoms, multiply the polytope corresponding to this structure for this segment. One obtain politopic prismahedron of dimension 5. With this politopic prismaehdron can fill space without gaps and clearances.

The various binary chemical compounds have a limited number of typical structures (Fersman, 1937). The structures of binary compounds of biogenic elements involving transition elements is considered. The simplest compound of biogenic elements with three - dimensional structure has a cubic unit cell, for example, oxides of transition elements. Since such structures form chlorides, bromides and iodides of alkali metals, one will refer to these structures rock salt structures (Table 1). Many binary chemical compounds have the structure as adamantane molecule. In work of Zhizhin (2014a) it was proved that the adamantane molecule consisting of 10 carbon atoms that make up the bulk of the unit cell of the diamond has of dimension 4. In compounds Ag_2O, Cu_2O at locations 10 of the carbon atoms are oxygen atoms, and atoms of copper and silver are arranged linearly between oxygen atoms. Many drugs are also a group of 10 carbon atoms as in the adamantane molecule. Among the inorganic and organometallic compounds have a number of structural analogues of adamantine (Table 1). All of these compounds of biogenic elements have dimension 4 or even higher.

A series of binary compounds have a structure in the form of cube with centrum as in titanium chloride at which titanium ions are arranged in the centrum of the cube bat chlorine ions are arranged in vertices of the cube. One will call these structures titanium chloride structure. How it is shown in work of Zhizhin and Diudea (2016) this structure has dimension 4.

Among the transitional elements, the biogenic element titanium is the second most abundant in the earth's crust after iron. The content of titanium in fish tissues is 10^{-4} %; in animals living on land, it is 9 10^{-4} %. Titanium is constantly contained in the human body. Its concentration is within 10^{-6} %. The study of the biological significance of titanium was carried out in a chronic experiment on plants and animals by determining the body's response to the addition of titanium. The response curve of the body to the titanium dose has a bell - shaped character similar to biogenic elements. The occurrence of a number of diseases in violation of the exchange of titanium. In the

developed form of acute leukemia, with gastrogenic iron deficiency anemia, cancer, gastric ulcer, the content of titanium in the blood decreases. Violation of the metabolism of titanium was noted also in the case of Botkin's disease, toxicosis and nephropathy of pregnant women, in patients with microbial eczema and neurodermatitis, and in burns. Titan in the body performs certain vital functions: it increases erythropoiesis, catalyzes the synthesis of hemoglobin, immunogenesis. Phosphorous complexating titanium intensifies the growth and development of plants. Titanium compounds accelerates the biosynthesis of amino acids, activate lipoxygenase activity. Resistance to various diseases increases by two times.

A series of binary compound biogenic elements have a structure of the mineral rutile TiO_2. In this compound each titanium atom is surrounded by six the oxygen atoms in the octahedral coordination. To compounds with such structure to concern for example fluorides of copper, zinc, magnesium, manganese, cobalt, nickel. One will call these structures rutile structure. In work of Zhizhin & Diudea (2016) it is shown that octahedron with centrum have dimension 4. Therefore, all these structures have dimension 4. A series of binary compounds of biogenic elements have structure of wurtzite - mineral ZnS, in which from compound ZnS with the structure of the adamantane zinc atom and sulfur atom have the tetrahedron coordination. The centrum each tetrahedron is vertex of another tetrahedron. The wurtzite structure have compounds ZnO, CdS, ZnS. The dimension of this structure remains unknown. It will be defined in the next section. A series of binary compounds of biogenic elements have a fluorite structure – mineral CaF_2 (fluorspar). Each calcium ion in this structure is in cube surrounded by fluorine ions, and each fluorine ion is in tetrahedron surrounded by calcium ions. The fluorite structure have for example chlorides of transition metals (Table 1).

Table 1. Binary compounds of the biogenic elements

N	Type of the structure	The compounds biogenic elements with this type of the structure
1	rock salt	MnO, FeO, CoO, NiO, CdO
2	Adamantane	Ag_2O, Cu_2O, ZnS, CuCl
3	titanium chloride	TiCl
4	Rutile	MnF_2, CoF_2, NiF_2, CuF_2, ZnF_2, MnO_2, MoO_2
5	Wurtzite	ZnO, CdO, ZnS
6	Fluorite	CdF_2, $MnCl_2$, $FeCl_2$, $CoCl_2$, $NiCl_2$, $ZnCl_2$, $CdCl_2$, Cu_2S

In the structure of wurtzite every atom of one component has a tetrahedral environment of the atoms of the other component. This results to arrangement of tetrahedrons with center so that vertex one tetrahedron is the center of another tetrahedron (Figure 6).

If to carry construction of atoms in Figure 6 on this principle, we obtain a spatial lattice, the unit cell the lattice is a convex shape it is shown in Figure 7 .

This figure is the unit cell structure of the wurtzite. In Figure 7, solid lines represent chemical bonds of the atoms, and the dotted lines are only geometric sense outlining contours of the figure. One define the dimension of this figure by the Euler - Poincare equation (1). The number of vertices of this figure is equal to 14, i.e. $f_0 = 14$. The number of edges is equal to 29, i.e. $f_1 = 29$. The number of two - dimensional faces is the sum of the number of triangles (8) and number of quadrangles (13), i.e. $f_2 = 21$. The number of three - dimensional faces is equal to 6. This figures are *abcghkon, gceruo, cefump, cdfulm, bcdklu,* and all shape on Figure 7 without inner partitions, i.e. $f_3 = 6$. Substituting these values $f_i, (\mathrm{i} = 0,1,2,3)$ in the Euler - Poincare equation (1), can to find that it is satisfied for $n = 4$

$$14 - 29 + 21 - 6 = 0.$$

Figure 6. The tetrahedral coordination atoms in wurtzite
A white circle is atom of one component. A black circle is atom of other component

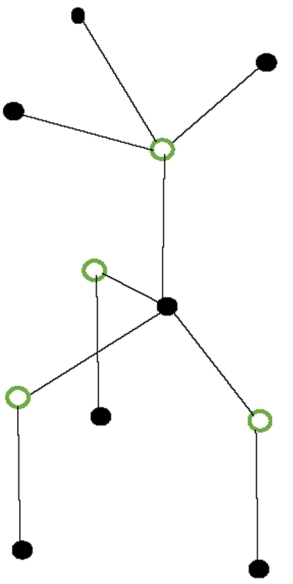

Figure 7. The unit cell of the wurtzite

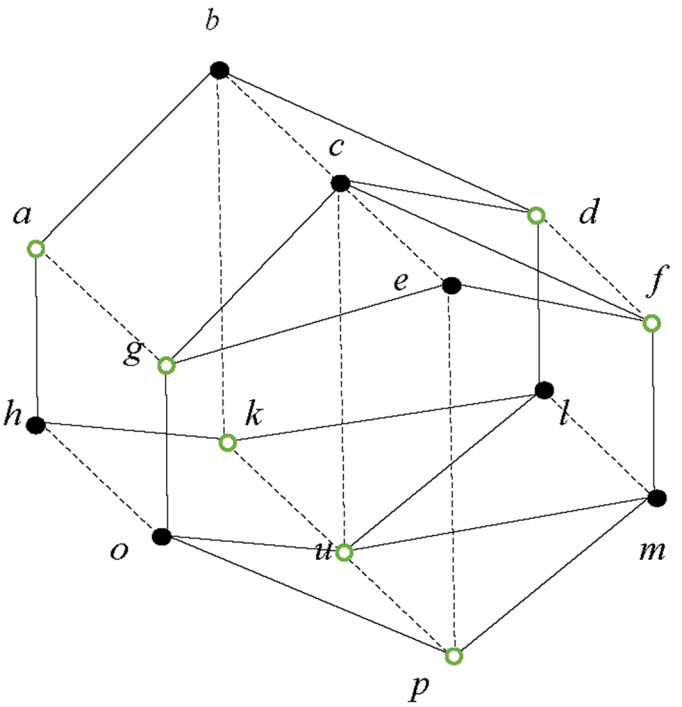

Thus, the dimension of polytope on Figure 7 is equal to 4, i.e. the unit cell structure of the wurtzite has dimension 4.

On example of compound $MnCl_2$ can to look at the structure of fluorite. Isolate magnesium atoms lying at the centers of the cube faces (•), and chlorine atoms (▲), forming a smaller cube inside the bigger cube, which are located at the vertices of magnesium atoms (Figure 8).

From Figure 8 it follows that the number of vertices is 14, i.e. $f_0 = 14$, the number of edges is 36, i.e. $f_1 = 36$, the number of flat faces is sum from number of triangles (24) and number of rectangles (6) (smaller cube faces), i.e. $f_2 = 30$. The number three dimension shape to sum up from smaller cube (1), pyramids on its faces (6) and figure (22) without inner parts (1), i.e. $f_3 = 8$ 8. Substituting these values $f_i, (\mathrm{i} = 0,1,2,3)$ in the equation (1), can to find that it is satisfied for $n = 4$

$$14 - 36 + 30 - 8 = 0.$$

Figure 8. The unit cell of the fluorite
●- *magnesium atom*
▲- *chlorine atom*

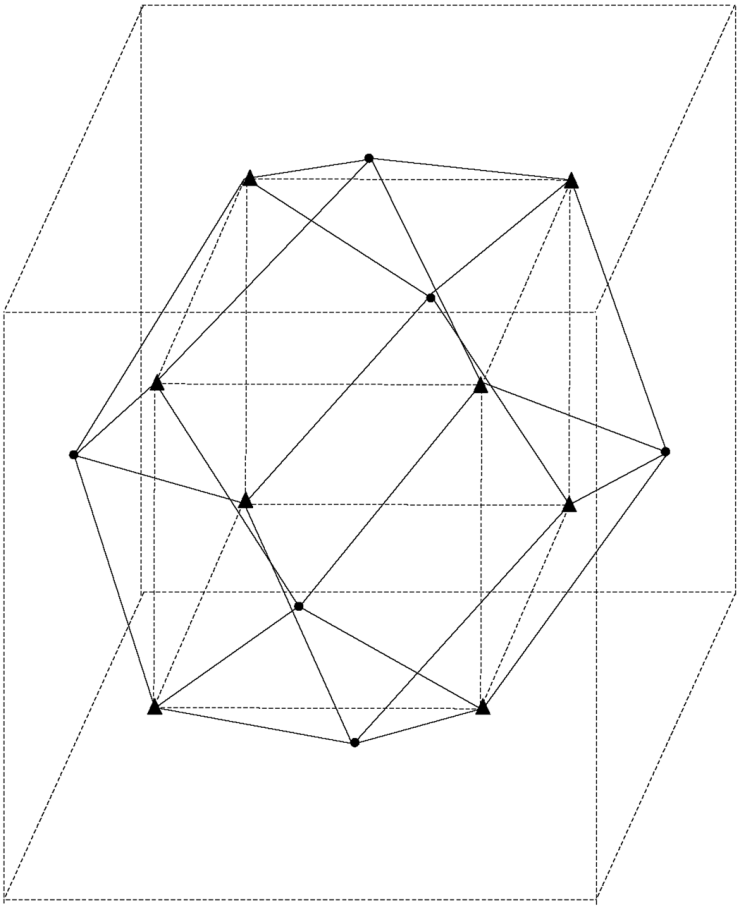

Thus, the dimension of polytope on Figure 8 is equal to 4, i.e. the unit cell structure of the fluorite has dimension 4.

MOLECULES OF CHEMICAL COMPOUNDS OF BIOGENIC P – ELEMENTS

Elements in which the completion of the p - sublevel of the outer valence level occurs are called p - elements. Electronic structure of the valence level ns^2p^{1-6} . Valence are electrons of s - and p - sublevels. Most of the p - elements

- nonmetals are biogenic elements (the exception is noble gases, tellurium and astatine). Of the *p* - elements - metals, only aluminum is considered biogenic.

The first element of group 3a of the element table is boron. Like all elements of this group, it has two *s*-electrons and one *p* - electron on the outer layer. Boron does not have vacant *d* - and *f* -orbitals, and there are not several electron pairs on the pre - existing layer, as, for example, for the atoms of alkaline - earth elements. However, the property of the collective interaction of electron pairs is manifested here also, but in a slightly different way compared to magnesium. Here pairs of electrons of the second energy level of several boron atoms interact, creating (repelling from each other) tetrahedral coordination of boron atoms. Therefore, in the compound B_4Cl_4, the boron atom has an effective valence of 4, and not three, which would correspond to the group number (Figure 9).

At the vertices *g, h, f, e* in Figure 9 boron atoms are located, and at the vertices *a, b, c, d* chlorine atoms arranged.

Figure 9. The structure of the B_4Cl_4 molecule

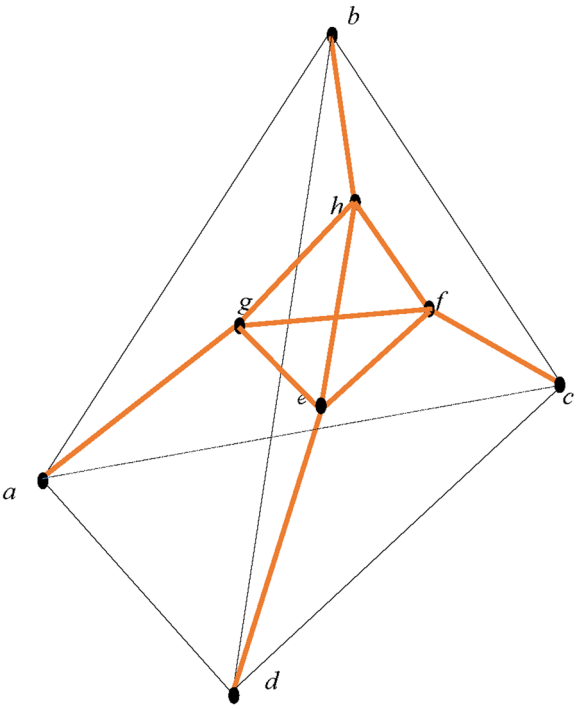

Theorem 2: The B_4Cl_4 molecule has dimension 4.

Proof: In Figure 9 there is eight vertices, $f_0 = 8$. The number of edges is 16 (*ab, bc, cd, ad, bd, ac, gh, hf,ef, he, gf, eg, bh, fc, ed, ag),* $f_1 = 16$. The number of elements of dimension 2 is 14 (triangles *abd, bcd, abc, acd, ghe, hef, ghf, gfe* and quadrangles *aghb,aged, hbed, hbfc, efcd, hfbc)*, $f_2 = 14$. The number of elements of dimension 3 is 6 (tetrahedrons *abcd, ghef* and prismatoides *abhged, hbedbfc, aghbfc, gefadc*), $f_3 = 6$. On Figure 9 the edges correspondent of chemical bounds is indicated brown, remain edges (black) it is need for creating convex body. Substituting the values of the number of elements of different dimension in the equation Euler – Poincare (1) can to obtain

$$8 - 16 + 14 - 6 = 0 .$$

One find that it holds for $n = 4$. This proves that the figure who projection is shown in Figure 9 there is polytope of dimension 4. This proves theorem 2.

Due to the interaction of electron pairs of several atoms, formation of other compounds is also possible. For example, in Figure 10. The image of the B_6Cl_6 molecule is shown. Here, also, the edges corresponding to the chemical bonds is indicated in brown, the remaining edges are necessary for obtaining a convex figure.

In the compound, both the boron atoms and the chlorine atoms have octahedral coordination. The effective valence of boron in this compound is 5. In the polytope in Figure 10, boron atoms are located at the vertices $a_1, b_1, c_1, d_1, e_1, f_1$ and hydrogen atoms are located at the vertices $a_2, b_2, c_2, d_2, e_2, f_2$.

Theorem 3: The B_6Cl_6 molecule has dimension 4.

Proof: In this case the number of elements of zero dimension is $f_0 = 12$. The number of elements of dimension one is $f_1 = 12 + 12 + 6 = 30$. The number of elements of dimension 2 is sum of the number small triangles 8 and big triangles 8, add 12 quadrangles, i. e. $f_2 = 28$. The number of elements of dimension 3 is sum two octahedrons and 8 prism, i.e. $f_3 = 10$. Substituting the values of numbers of elements of different dimensions in the equation (1) can to obtain

Figure 10. The structure of the B_6Cl_6 molecule

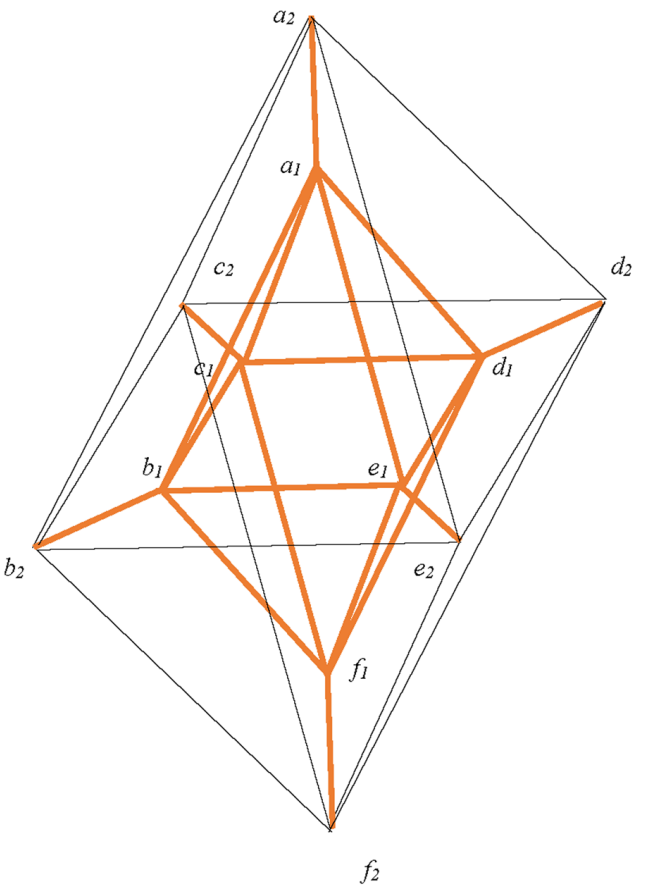

$$12 - 30 + 28 - 10 = 0.$$

One find that it holds for $n = 4$. This proves that the figure 9 is polytope of dimension 4. This proves theorem 3.

Elements Al, Ga, In and Tl have vacant *d* - and *f* - orbitals and tend to supplement their valence shell to 6 electron pairs, and in several compounds In and Tl have more than 6 electron pairs. These elements in many compounds exhibit tetrahedral coordination in the vicinity of the atom. Taking into account the possible addition of other elements to tetrahedral coordination, complex compounds with high dimensionality can arise. For example, aluminum (a biogenic element) forms a cyclic compound $[(CH_3)_2AlF]_4$ (Figure 11).

Figure 11. A cyclic compound $[(CH_3)_2AlF]_4$

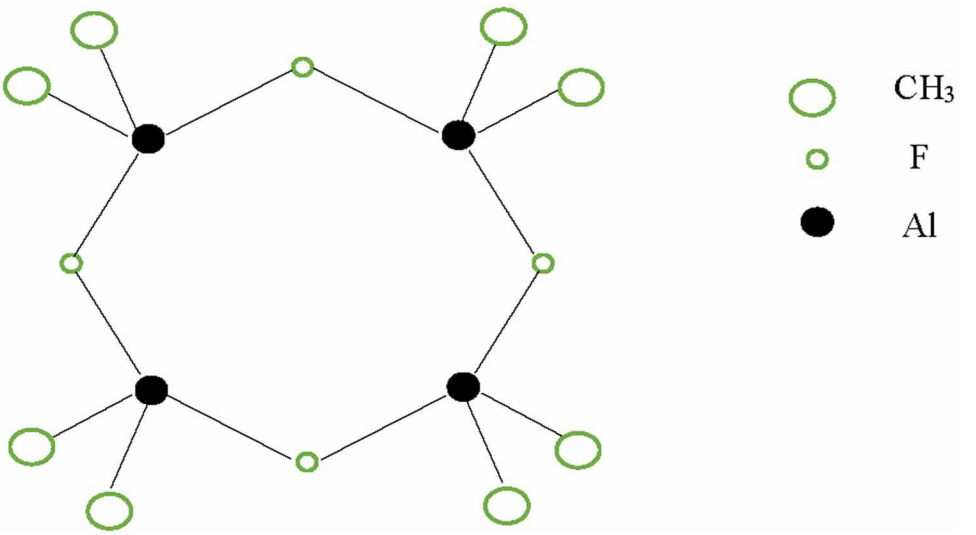

If we form a convex figure from Figure 11, one get the polytope shown in Figure 12. At the vertices of a_1, a_4, a_7, a_{10} fluorine atoms are located. At the vertices $a_{13}, a_{14}, a_{15}, a_{16}$ aluminum atoms are located. Functional groups CH_3 are located in the

$$a_2, a_3, a_5, a_6, a_8, a_9, a_{11}, a_{12}$$

vertices.

Theorem 4: The polytope of cyclic compound $[(CH_3)_2AlF]_4$ has dimension 5.

Proof: The polytope in Figure 12 has 16 vertices, $f_0 = 16$; 52 edges, $f_1 = 52$. In addition, it has 4 polytopes of dimension 4 each (tetrahedrons with a center)

$$a_1a_2a_3a_4a_{14}, a_4a_5a_6a_7a_{15},$$

$$a_7a_8a_9a_{10}a_{16}, a_{10}a_{11}a_{12}a_{13}.$$

Figure 12. The convex polytope of cyclic compound $[(CH_3)_2AlF]_4$

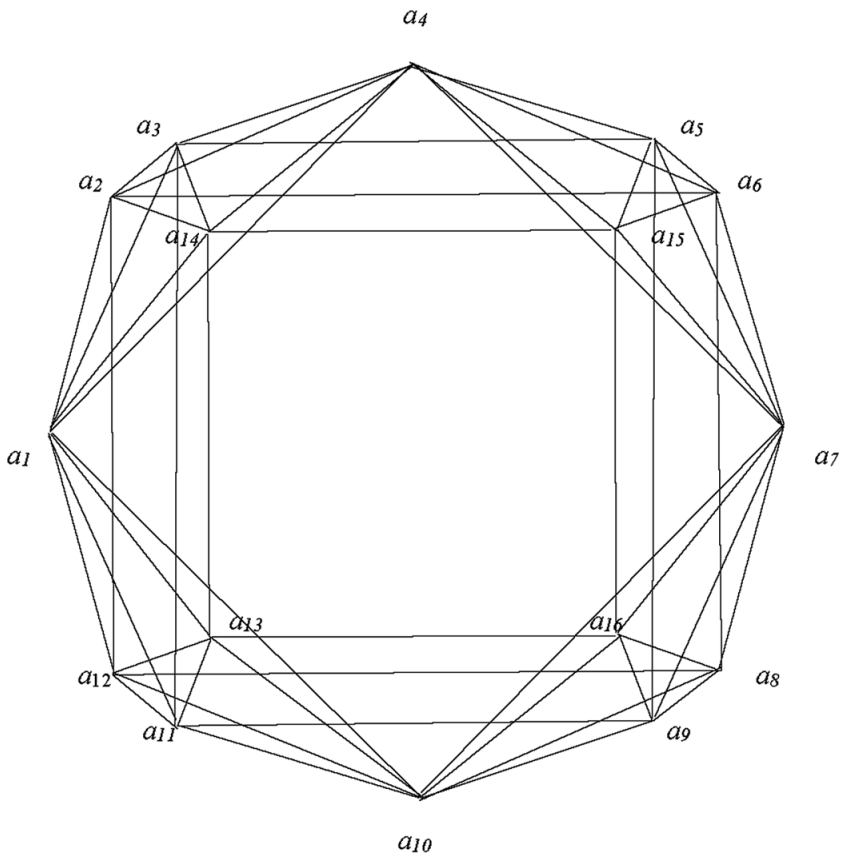

Each tetrahedron with a center has 10 triangular faces. This gives 40 triangular faces in the polytope 10. In addition, three triangular faces are formed at the vertices a_1, a_4, a_7, a_{10} with horizontal and vertical sides. This gives another $4 \cdot 3 = 12$ triangles. There are 4 more rectangular faces

$$(a_{13}a_{14}a_{15}a_{16}, a_6a_2a_8a_{12}, a_{11}a_5a_3a_9, a_1a_7a_{10}a_4)$$

and 12 trapezoids

$$(a_3a_5a_{15}a_{14}, a_3a_2a_5a_6, a_{15}a_2a_6a_{14}, a_6a_8a_{15}a_{16}, a_6a_8a_5a_9, a_{15}a_5a_9a_{16},$$

$$a_{11}a_9a_8a_{12}, a_9a_{11}a_{13}a_{16}, a_{12}a_8a_{13}a_{16},$$

$a_2a_{12}a_{14}a_{13}, a_{12}a_2a_3a_{11}, a_3a_{11}a_{13}a_{14}$).

Thus, the total number of two - dimensional faces 68, $f_2 = 68$. Each tetrahedron with a center has 5 tetrahedrons. Therefore, the total number of tetrahedrons in Figure 10 is $5 \bullet 4 = 20$. Each of the vertices a_3, a_7, a_4, a_{10} is the vertex of the three pyramids. The total number of these pyramids is 12:

$a_5a_{15}a_3a_4a_{14}, a_6a_2a_3a_4a_5, a_4a_2a_6a_{15}a_{14}, a_1a_2a_3a_{12}a_{11}, a_1a_{14}a_3a_{11}a_{13},$

$a_{10}a_{12}a_{11}a_8a_9, a_{10}a_{12}a_{13}a_8a_{16}, a_{10}a_{11}a_{13}a_{16}a_9, a_7a_8a_9a_5a_6, a_7a_9a_{16}a_5a_{15}, a_7a_8a_{16}a_6a_{15}$.

There are four triangular prisms:

$a_2a_3a_{14}a_5a_6a_{15}, a_{15}a_5a_6a_8a_9a_{16}, a_{11}a_{12}a_{13}a_8a_9a_{16}, a_2a_3a_{14}a_{11}a_{12}a_{13},$

and six quadrangular prisms:

$a_{13}a_{14}a_{15}a_{16}a_3a_5a_9a_{11}, a_{13}a_{14}a_{15}a_{16}a_2a_6a_8a_{12}, a_{13}a_{14}a_{15}a_{16}a_1a_4a_7a_{10},$

$a_2a_6a_8a_{12}a_3a_5a_9a_{11}, a_1a_2a_4a_6a_7a_8a_{10}a_{12}, a_1a_3a_4a_5a_7a_9a_{10}a_{11}$.

Than the total number of three-dimensional figures is 42, $f_3 = 42$.

In addition to the 4 tetrahedrons mentioned with the center, as four - dimensional figures, there are another four - dimensional figures. In particular, this is a figure (*F*), shown in Figure 13. Indeed, this figure has 12 vertices, $f_0(F) = 12$; 24 edges, $f_1(F) = 24$; 19 two - dimensional faces, $f_2(F) = 19$; and 7 three - dimensional figures, $f_3(F) = 7$. Substituting these values into the Euler - Poincaré equation (1) can to obtain that it is satisfied for $n = 4$

$12 - 24 + 19 - 7 = 0.$

This proofs that polytope *F* has dimension 4.

Four identical polytopes of dimension 4 exist in a neighborhood of each of the vertices a_1, a_4, a_7, a_{10}. One of these polytopes (*L*) is depicted in Figure

Figure 13. The 4 – dimension polytope F included in Figure 12

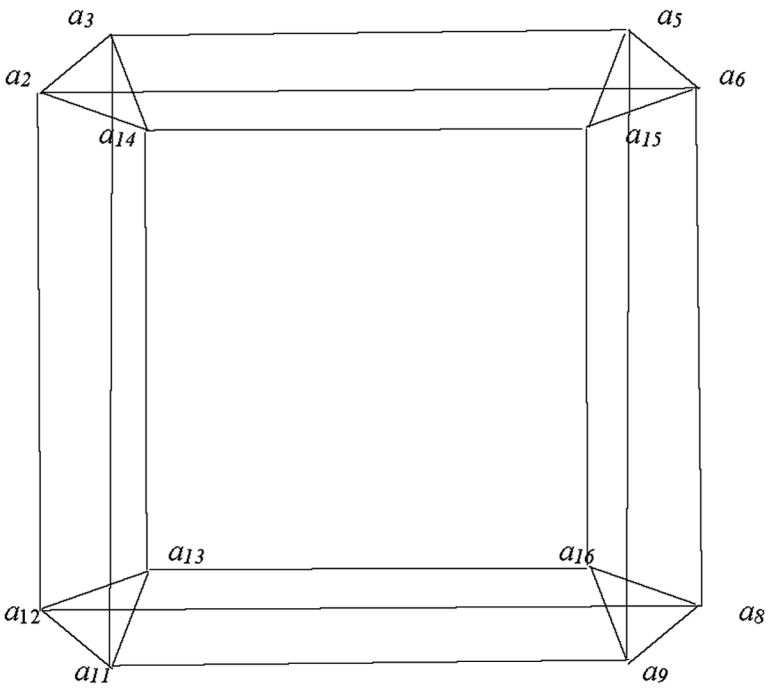

14. It has 7 vertices, $f_0\ (L) = 7$; 15 edges, $f_1(L) = 15$; 14 two - dimensional faces, $f_2(L) = 14$; and 6 $3D$ facets, $f_3(L) = 6$. Substituting these values into the Euler - Poincare equation (1) can to obtain

$$7 - 15 + 4 - 6 = 0,$$

i.e. the equation (1) hold for $n = 4$ and all the polytopes L has dimension 4.

Three more topologically equivalent polytopes of dimension 4 can be distinguished from Figure 13. Each of these polytopes consists of a rectangular prism and four tetrahedrons connected to each other in a cycle along the vertices of a_1, a_4, a_7, a_{10}. These are polytopes

$$a_1a_4a_3a_{14}a_5a_{15}a_7a_{16}a_8a_{10}a_{13}a_{12},$$
$$a_1a_2a_{14}a_4a_{15}a_6a_7a_{16}a_9a_{10}a_{11}a_{13}, a_1a_2a_3a_4a_5a_6a_7a_8a_9a_{10}a_{11}a_{12}.$$

Figure 14. The 4 – dimension polytope L included in Figure 12.

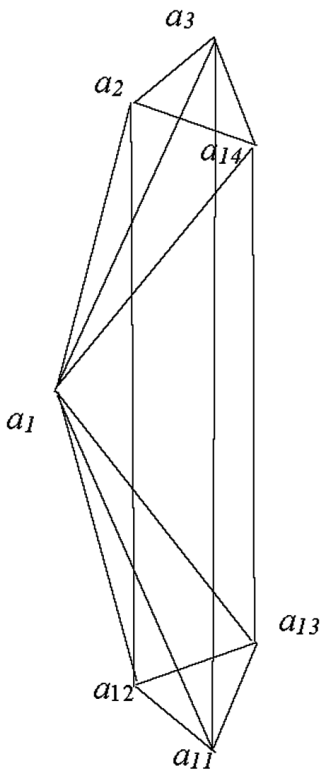

One of them (polytope *K*) is shown in Figure 15.

The *K* polytope has 12 vertices, $f_0(K) = 12$; 32 edges, $f_1(K) = 32$; 31 two - dimensional faces, $f_2(K) = 31$; and 11 3*D* facets, $f_3(K) = 11$. Substituting these values into the Euler - Poincare equation (1) can to obtain

$$12 - 32 + 31 - 11 = 0,$$

i. e. the equation (1) hold for $n = 4$ and all the polytopes *K* has dimension 4.

Thus, the polytope on Figure 12 has 11 polytopes of dimension 4. Therefore, for polytope on Figure 12 the Euler - Poincare equation (1) has face

$$16 - 52 + 68 - 42 + 11 = 2,$$

i.e. it hold for $n = 5$. This proofs theorem 4.

Figure 15. The 4 – dimension polytope K included in Figure 12.

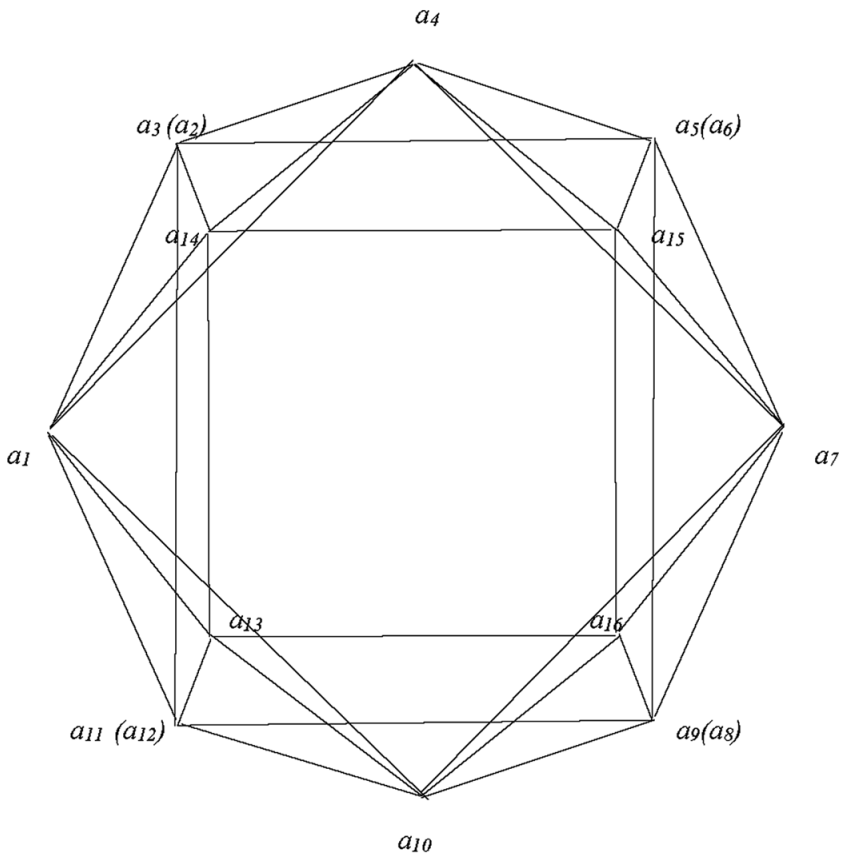

Most of the compounds known on Earth are compounds of *p* - elements. The five main (macro-biogenic) p - elements (elements of life) O, N, P, C, S are the main building material from which molecules of proteins, fats, carbohydrates and nucleic acids are composed. The structures and dimensions of these molecules will be studied in subsequent chapters.

REFERENCES

Arcel, V. (1931). *Chemical Bond*. Higher Technical School.

Fersman, A. E. (1937). *Geochemistry* (Vol. 3). Leningrad: ONTI.

Gillespie, R. J. (1972). *Molecular Geometry*. New York: Van Nostrand Reinhold Company.

Gillespie, R. J., & Hargittai, I. (1991). *The VSEPR Model of Molecular Geometry*. London: Allyn & Bacon.

Hund, F. (1927). *Linienspektren und periodisches System der Elements*. Gottingen: Springer. doi:10.1007/978-3-7091-5695-7

Karapet'yants, M. X., & Drakin, S. I. (1994). *General and Inorganic Chemistry*. Moscow: Chemistry.

Poincare, A. (1895). Analysis situs .*J. de é Ecole Polytechnique, 1,* 1 – 121.

Vernadsky, V. I. (2012). *The Biosphere*. London: Springer.

Zhizhin, G.V. (1998). *Chemistry of d – and f – elements.* Sankt-Petersburg: Nord – West Polytechnic Institute.

Zhizhin, G. V. (2014a). On the higher dimension in nature. *Biosphere*, *6*(4), 313–318.

Zhizhin, G. V. (2014b). *World – 4D*. St. Petersburg: Polytechnic Service.

Zhizhin, G. V. (2015, November). *Polytopic prismahedrons – fundamental regions of the n-dimension nanostructures.* Paper presented at The International conference "Nanoscience in Chemistry, Physics, Biology and Mathematics", Cluj-Napoca, Romania.

Zhizhin, G. V. (2016). The structure, topological and functional dimension of biomolecules. *J. Chemoinformatics and Chemical Engineering*, *5*(2), 44–58.

Zhizhin, G. V. (2017a). *Chemical Compound Structures and the Higher Dimension of Molecules: Emerging Research and Opportunities*. Hershey, PA: IGI Global.

Zhizhin, G. V. (2017b). Systematics of Anomalies in the Filling of Electron Orbitals of Chemical Elements. *J. Chemoinformatics and Chemical Engineering*, *6*(1), 44–58.

Zhizhin, G. V. (2018). *The Geometry of Higher - Dimensional Polytopes*. Hershey, PA: IGI Global.

Zhizhin, G. V., & Diudea, M. V. (2016). Space of Nanoworld. In M. V. Putz & M. C. Mirica (Eds.), *Sustainable Nanosystems, Development, Properties, and Applications* (pp. 214–236). New York: IGI Global.

Zhizhin, G. V., Khalaj, Z., & Diudea, M. V. (2016). Geometrical and topology dimensions of the diamond. In A. R. Ashrafi & M. V. Diudea (Eds.), *Distance, symmetry and topology in carbon nanomaterials* (pp. 167–188). New York: Springer. doi:10.1007/978-3-319-31584-3_12

Chapter 6
Functional Dimensions of Biomolecules

ABSTRACT

New structures of biomolecules have been constructed: carbohydrates, proteins, nucleic acids. It is shown that glucose molecules and ribose molecules have dimensions of 15 and 12, respectively. The enantiomorphic forms of biomolecules in space of higher dimension make it possible to explain the experimentally observed facts of branching of chains of biomolecules in one of the enantiomorphic forms and the absence of chain branching in another enantiomorphic form. The enantiomorphic forms of the tartaric acid molecule in a space of higher dimension reveal the cause of the reversal in different directions of the polarization plane of light in two opposite forms.

HIGHER DIMENSION OF POLYATOMIC MOLECULES FROM ELEMENTS OF LIVE AS A RESULT OF THE INTERACTION OF THE ELECTRON ORBITALS OF ATOMS IN A MOLECULES

The most common in biomolecules is a carbon atom, the main role of which to be binding in the center of biomolecules. Consider, for example, methane molecule CH_4. The carbon atom in this molecule binds around four hydrogen atoms. Geometrically, this molecule is a tetrahedron, whose vertices are located of the hydrogen atoms, and in the center is carbon atom.

DOI: 10.4018/978-1-5225-9651-6.ch006

The carbon atom in the center of the methane molecule has the valence electrons $2s2p^3$. Valence electron orbitals of carbon atoms and hydrogen atoms 1*s* overlap and form four hybrid orbitals sp^3, directed from the carbon atom to the hydrogen atoms (Gray, 1965). Let the distance from hydrogen atoms to carbon atoms is taken as unity, for the origin of coordinates to take the carbon atom, and the directions hybrid orbitals send on four coordinates *x, y, z, t.* Then the coordinates of the hydrogen atoms equal to (0, 0, 0, 1), (0, 0, 1, 0), (1, 0, 0, 0), (0, 1, 0, 0), and the carbon atom coordinates equal to (0, 0, 0, 0). So one have the integer coordinates of vertex in the four -dimensional space (Figure 1).

This is consistent with the evidence of four - dimensional convex hull of the methane molecule on the Euler – Poincare equation (1) in Chapter 5. It is easy to see that the body in Figure 1, seen in the four - dimensional space, convex, because its edges belong to the body and enter into his boundary complex (Grunboum, 1967). Polytope in Figure 1 is a 4 - simplex, since each vertex of the polytope associated edges with all the other vertices of this polytope (Zhizhin, 2014).

If in the methane molecule a hydrogen atom replaced by a hydroxyl group - OH, then can to get the simplest alcohol - methanol. If the hydroxyl group considered as the vertex of the polytope, then the dimension of this molecule will also be equal to 4. If each atom of the molecule of methanol is considered the vertex of the polytope, then connecting each vertex to all other vertices

Figure 1. The methane molecule (CH_4)

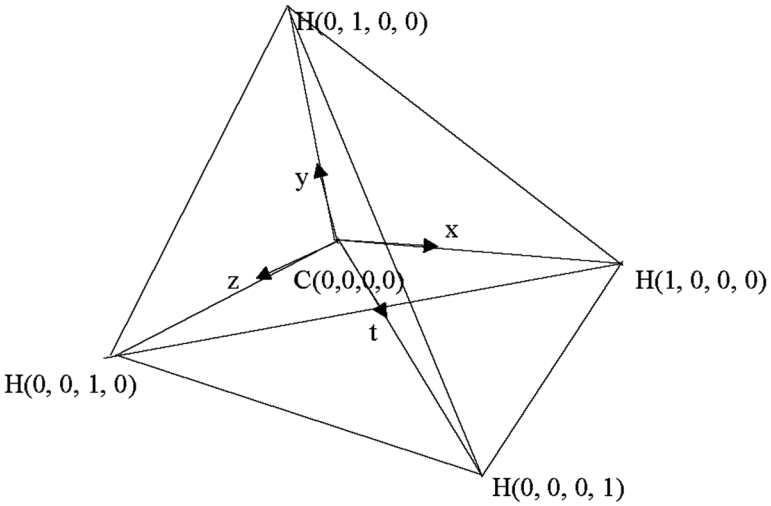

edges, it turns out that it is equal to the dimension of the polytope to 5 and one have 5 - simplex. However, here must remember that the accession of the hydroxyl group does not change the hybridization of the carbon atom, as the binding site as the place of one hydrogen atom took one oxygen atom of the hydroxyl group. Therefore, as a separate vertex in methanol molecule should take hydroxyl group entirely. Then the dimension of the methanol molecules is equal to 4 (Zhizhin, 2017).

In the biomolecules can find a lot of examples of molecules or ions in the form of a tetrahedron with the center (NH_4, PO_4, etc.). All of them have dimension 4. If the binding site appears *d* - element it is formed around the coordination sphere ligands with more than 4 of the amount due to of *d* - orbitals of the element. One can show that in this case the dimension of the molecule is equal to the number of hybrid electron orbitals directed from the center to the ligands. The ligand may act as no individual atoms or ions, and some functional groups, which may be regarded as corresponding vertices of the polytope. This is consistent with the need to describe more convenient biomolecules, molecular structures consisting of different complexity. Therefore, the dimension of the group of atoms in biomolecules, one call a functional dimension. In addition, when such descriptions of specific dimensions one will not be considered distances between atoms in molecules. Therefore, a certain dimension of the molecules so called topological dimension.

In addition, of the tetrahedron with the center in biomolecules there are complex structures of higher dimension.

CARBOHYDRATE ("CARBON COMPOUND WITH WATER")

Carbohydrates are the main source of energy for the body. All carbohydrates are made up of units that are saccharides. The simplest saccharide is an aldose monosaccharide, which contains three carbon atoms (Figure 2).

The more complex monosaccharides include 4, 5, 6 and 7 carbon atoms. Polysaccharides consist of several monosaccharides. Saccharides are part of the nucleic acids that are carried out in the cells of protein synthesis and the transfer of hereditary traits. One will try to calculate the dimension of the simplest aldose monosaccharide saccharide, since the main elements of the aldose monosaccharide construction are repeated in the more complex saccharides. From Figure 3 it follows that two carbon atoms, connected by

Figure 2. Shema of the molecule aldose monosaccharide

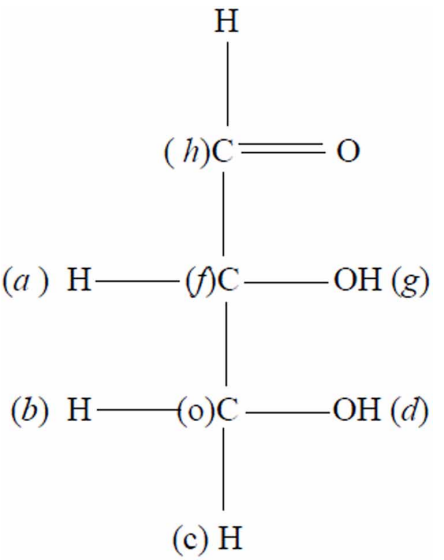

Figure 3. Spatial structure of the molecule aldose monosaccharide

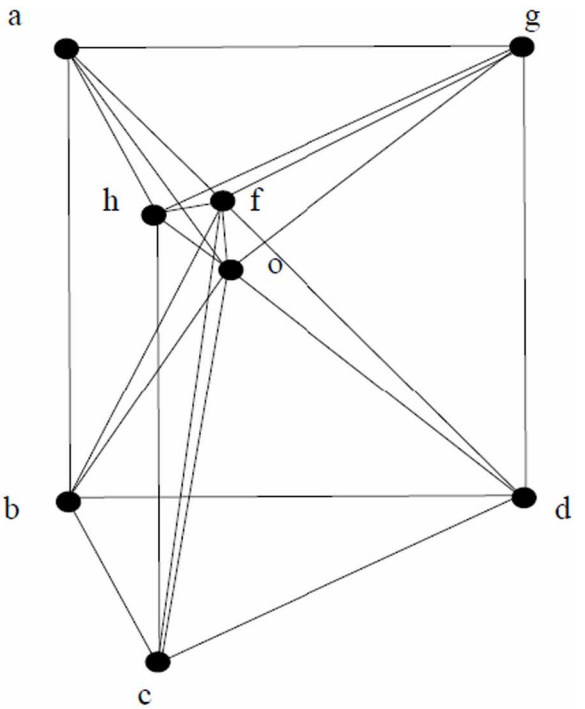

bonds to each other, hydrogen atoms projection onto the plane, this construction is shown in Figure 3.

In this figure there is a tetrahedron *bcdf* with center *o* and a tetrahedron *oahg* with center *f*. Each a tetrahedron with a center is a polytope of dimension 4.

The vertex *f* of the first tetrahedron is the center of the second tetrahedron, and the vertex *o* of the second tetrahedron is the center of the first tetrahedron. Hydrogen (H) atoms are located at the vertices *a, b, c*, hydroxyl groups (OH) are located at the vertices *g, d*, carbon atoms (C) are located at the vertices *o, f, h*. The oxygen and hydrogen atoms following the carbon atom at the vertex *h* are not shown in Figure 3 for simplification. It is necessary to determine the dimension of the polytope *bcdfahgo*. The polytope in Figure 3 has 8 vertices ($f_0 = 8$), 22 edges (*ab, ag, af, ao, ah, gh, gf, go, gd, bf, bo, bd, bc, df, do, dc, hc, hf, ho, cf, co, fo)*. Therefore, $f_1 = 22$. The polytope in Figure 3 has 29 planar faces, of which 26 are the triangles (*aho, afo, ahf, afg, ahg, aog, aob, afb, bfo, bco, bod, bfd, bfc, bcd, ghf, gho, gfo, god, gfd, dfo, dco, dfc, cof, chf, cho, hfo*) and 3 quadrangles (*abdg, hcgd, abhc*). Therefore, $f_2 = 29$. The polytope in Figure 3 has 20 three - dimensional figures, of which 13 are tetrahedrons (*bcfd, ahog, dcfo, bcdo, bfdo, cfdo, ahof, ahgf, hogf, aogf, fgod, fohc, foab*), 6 pyramids (*agbdo, ahbcf, ahbco, agbdf, Chgdf, chgdo*) and one (*ahgbcd)* prism. Therefore, $f_3 = 20$. It follows from the construction of the polytope in Figure 3 that it includes two tetrahedrons with the center *bcdfo* and *oahgf*. In addition to these two polytopes with dimension 4, five 4 - polytopes also appear in the polytope in Figure 3. Three of these polytopes have as their base three rectangular faces of the prism *ahgbcd*, whose vertices are connected with the vertices *f, o* located inside the prism. To prove their 4 - dimensionality, consider one of these polytopes *abhcfo*, since the proofs for the other two polytopes are similar. This polytope has 6 vertices ($f_0 = 6$); 13 edges (*ab, ah, hc, bc, af, hf, bf, cf, ho, ao, bo, co, fo)*, $f_1 = 13$; 13 two - dimensional faces (*ahf, aho, abo, abf, afo, bfo, boc, ahbc*), $f_2 = 13$; 6 three -dimensional faces (*hfoc, abof, bfoc, afho, ahcbf, ahcbo*), $f_3 = 13$. Substituting the obtained values of the numbers of faces of different dimensions into equation (1) in Chapter 5, can to find that equation (1) is satisfied for $n = 4$

$$6 - 13 + 13 - 6 = 0.$$

It is proved by the 4 - dimensionality of the polytope *abhcfo*.

The two polytopes of dimension 4 there are formed by the *ahgbcd* prism with the vertex *f* or *o* inside its. Consider the prism *ahgbcd* with the vertex *f* (the proof for the prism with vertex *o* is similar). The polytope *ahgbcdf* has 7 vertices, $f_0 = 7$; 15 edges (*ah, hg, ag, bd, bc, cd, ab, hc, gd, af, fh, fg, bf, fc, fd*), $f_1 = 15$; 14 two - dimensional faces (*ahg, bdc, ahf, hfg, afg, bfc, fcd, bfd, fhc, afb, fgd, ahbc, hcgd, agbd*), $f_2 = 14$; 6 three - dimensional faces (*ahgbcd, ahgf, bcdf, abdgf, hgcdf, ahbcf*), $f_3 = 6$. Substituting the values of the numbers of faces of various dimensions obtained for the polytope *ahgbcdf* into equation (1) in Chapter 5, can to find that it is satisfied for $n = 4$

$$7 - 15 + 14 - 6 = 0.$$

This proves that the polytope *ahgbcdf* has a dimension of 4.

Thus, for the polytope in Figure 3 are $f_0 = 8$, $f_1 = 22$, $f_2 = 29$, $f_3 = 20$, $f_4 = 7$. Substituting these values into equation (1) in Chapter 5, can to find that it is satisfied for $n = 5$

$$8 - 22 + 29 - 20 + 7 = 2.$$

This proves that the polytope in Figure 3 has dimension 5. Consequently, the main part of the molecule of the aldose monosaccharide also has dimension 5. Since this basic part enters into all other saccharides in the plural, their dimension is more than 5. This gives higher dimension to the molecules DNA and all carbohydrates.

There are three main classes of carbohydrates: monosaccharides, oligosaccharides, polysaccharides. The basis of the monosaccharide is an unbranched chain of the carbon atoms, connected to each other by single bonds. One of the carbon atoms has double bond to an oxygen atom to form a carbonyl group. All other carbon atoms bonded hydroxyl groups and hydrogen ions. The carbonyl group may be at the end of the carbon chain (aldose) or elsewhere (ketoses). Monosaccharides depict a Fischer projection formula (Metzler, 1980; Lehninger, 1982). For example, the most common monosaccharides with five (pentose) and six (hexoses) carbon atoms in the form of these formulas are presented in Figure 4 and Figure 5 accordingly.

However, neither the Fischer formula or formula Haworth and their modifications (e.g., conformation as a “chair”) may not reflect the spatial structure of the monosaccharides. For this target the constructs described in the form of convex polytopes with boundary elements which form boundary

Figure 4. The molecule of ribose (in RNA)

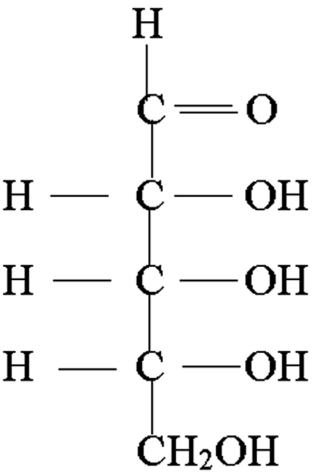

Figure 5. The molecule of D - glucose

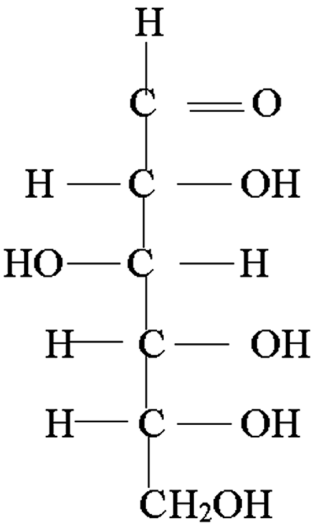

complex (Grunbaum, 1967). Only when such a representation will be to determine the dimension of these molecules. Consider a molecule of α - *D* - glucose. Closing unbranched chain of carbon atoms of monosaccharides through an oxygen atom, considering functional groups vertices, connect the each vertex by edges with each other vertices, get polytope, depicted in Figure 6.

Figure 6. The molecule of α - D – glucose

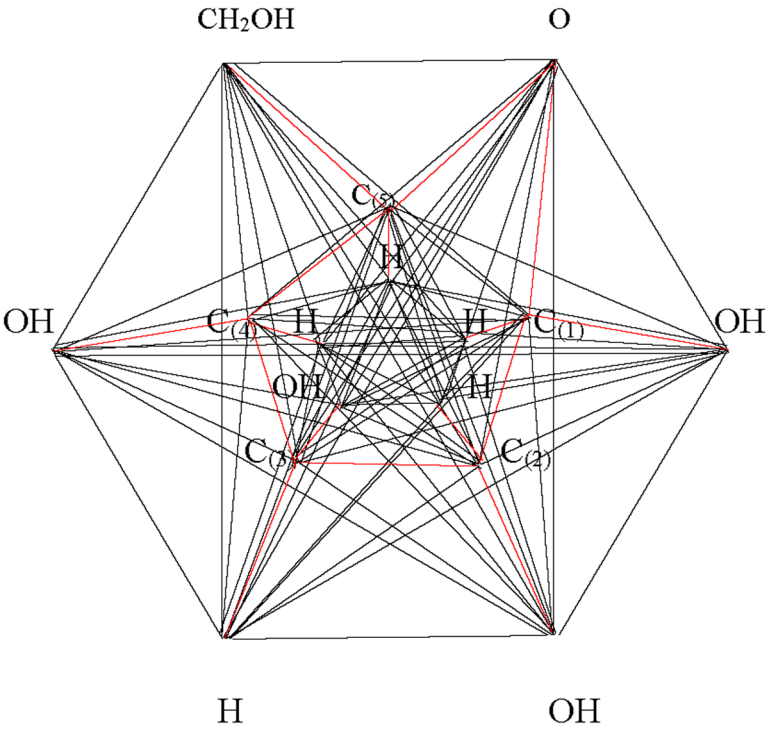

Edges marked in red in Figure 6 correspond to the chemical bonds in the molecule. The rest of the edges are only geometric sense, as the edges of the polytope.

Theorem 1: A molecule of α - D - glucose is a polytope type simplex with dimension 15 (Zhizhin, 2016).

Proof

The polytope in Figure 6 contains 16 vertices, i.e.

$f_0 = 16 = n+1$; 120 edges ($f_1 = C^2_{n+1} = 120$);
560 triangles ($f_2 = C^3_{n+1} = 560$); 1820 tetrahedrons
($f_3 = C^4_{n+1} = 1820$); 4368 4−simplexes ($f_4 = C^5_{n+1} = 4368$); 8008 5−simplexes
($f_5 = C^6_{n+1} = 8008$); 11440 6 − simplexes ($f_6 = C^7_{n+1} = 11440$); 12870 7 − simplexes

$(f_7 = C_{n+1}^8 = 12870)$; 11440 8 – simplexes $(f_8 = C_{n+1}^9 = 11440)$; 8008 9 – simplexes
$(f_9 = C_{n+1}^{10} = 8008)$; 4368 10 – simplexes $(f_{10} = C_{n+1}^{11} = 4368)$; 1820 11 – simplexes
$(f_{11} = C_{n+1}^{12} = 1820)$; 560 12 – simplexes $(f_{12} = C_{n+1}^{13} = 560)$; 120 13 – simplexes
$(f_{13} = C_{n+1}^{14} = 120)$; 16 14 – simplexes $(f_{14} = C_{n+1}^{15} = 16)$.

Substituting the values $f_i, (0 \leq i \leq 15)$ in Euler's – Poincare equation (1) in Chapter 5, can to see that it holds for $n = 15$

$$\sum_{i=0}^{14=n-1} f_i(-1)^i = 2.$$

This confirms that the polytope in Figure 6 has the dimension $n = 15$.

Theorem 1 it is proved.

High dimension of the molecule α - *D* – glucose is due to the fact that it contains a large number of differently oriented electronic atomic orbitals and, consequently, a large amount of energy. This is consistent with the established notions of large energy reserves in glucose, necessary for living organisms. Such an increase in energy and dimension occurs and other saccharides in the formation of closed loops.

In particular, the conformation of the *β* - *D* - glucose are interchanged only a hydroxyl group and a hydrogen atom bound to a carbon atom of the *C* (1) in Figure 6. Changes in the number of carbon atoms does not fundamentally change the picture of the molecule. The dimension of the polytope corresponds to the number of vertices of the polytope (not one less than the number of vertices).

Representations of the saccharide molecules in the form of polytope simplifies the understanding of the formation of polysaccharides. For example, if the molecule *α* - *D* - glucose, two molecules in accordance with Figure 6, are joined by the hydroxyl groups to form a water molecule and an oxygen atom, two molecules common *α* - *D* - glucose via α - glycoside linkages, as in simplified form shown in Figure 7.

Thus, the linear polymer of *α* - *D* - glucose has a one - dimensional translational symmetry with the translation element of higher dimension, just as quasicrystals (Shevchenko, Zhizhin & Mackay, 2013) have a multi - dimensional translational symmetry with the translation element of higher

Figure 7. The α - glycoside linkage of the molecules α – D – glucose

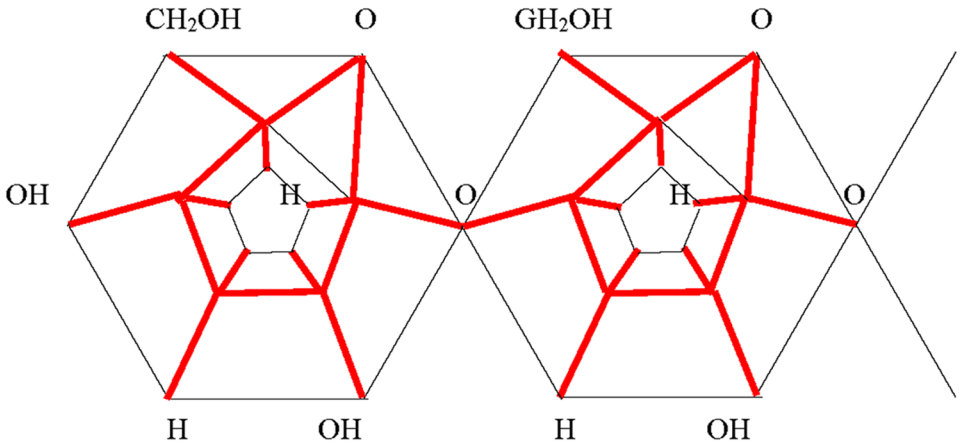

dimension. Chains with α - glycoside bond have the opportunity to branch. This is evident from Figure 5, as the functional group -CH_2OH in each molecule can be a chain branch point, to which is attached via an oxygen atom molecule of *α - D* - glucose. In the case of *β* - glycoside bond molecules *β - D* - glucose (Figure 8) such a possibility is difficult due to a denser arrangement of glucose molecules, and proximity to a functional group – CH_2OH of oxygen atom.

It seems can serve as an explanation of a chain with *β* - glycoside linkage chain branching is not observed.

Figure 8. The β - glycoside linkage of molecules β - D - glucose

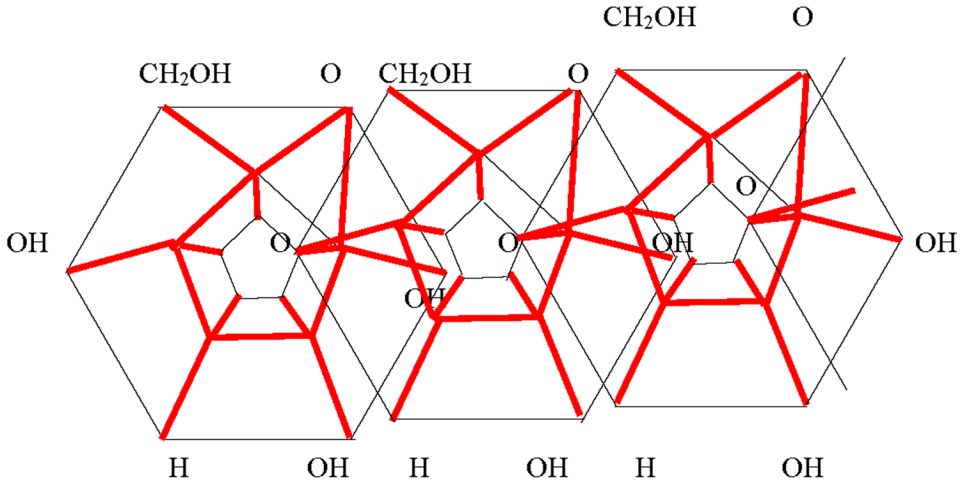

PROTEINS

Monomer units which are built of proteins are the 20 standard amino acids. These small molecules containing two different chemical functional groups capable of reacting with each other to form a covalent bond. This are amino group (-NH_2) and a carboxyl group (- COOH). Connection form of protein polymer is called a peptide bond. In the formation of such a connection by joining - COOH and -NH_2 with secretion a molecule of water. Amino acids forming two families of *D* and *L*, each of which can be represented in the form of a tetrahedron with the center in the carbon atom (Figure 9, Figure 10)

According to the ideas of this work, the amino acid is a molecular formation with topological and functional dimension of 4, regardless of the structure of the side of the functional groups represented by *R*.

Communication amino acids can be represented as a tetrahedron with the center of a peptide bond. Figure 8 shows the peptide bond the *D* - amino acids.

From geometric images of associated polytopes of dimension 4 in Figure 11 immediately implies that the peptide chain has the form of a spiral, swirling clockwise. Side functional groups *R* have different chemical nature. Sequence arrangement of functional groups and, hence, the sequence of amino acids in the chains always accurately defined genetically.

Figure 9. The molecule of D - amino acid

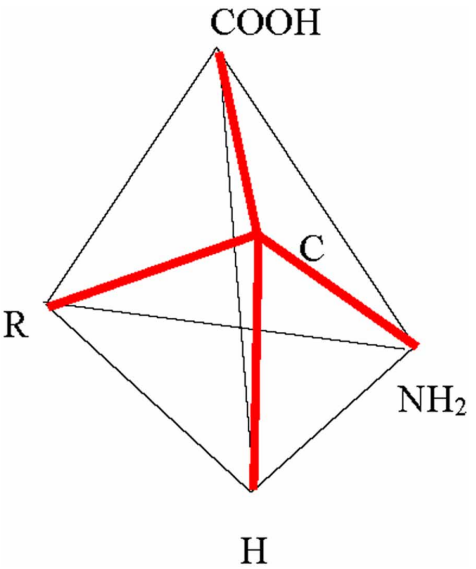

Figure 10. The molecule of L - amino acid

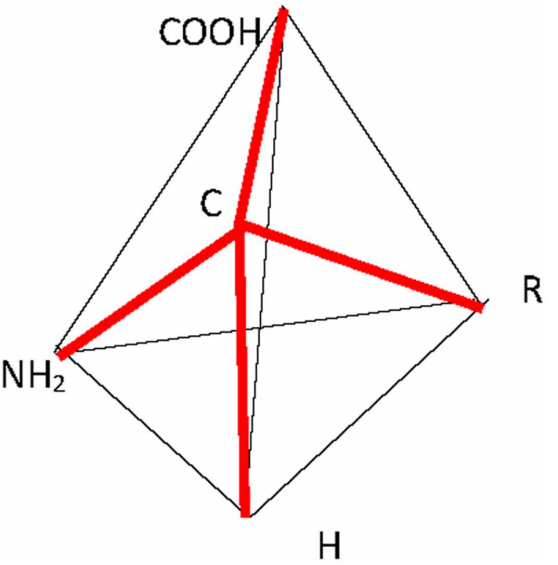

Figure 11. The peptide chain of amino acids

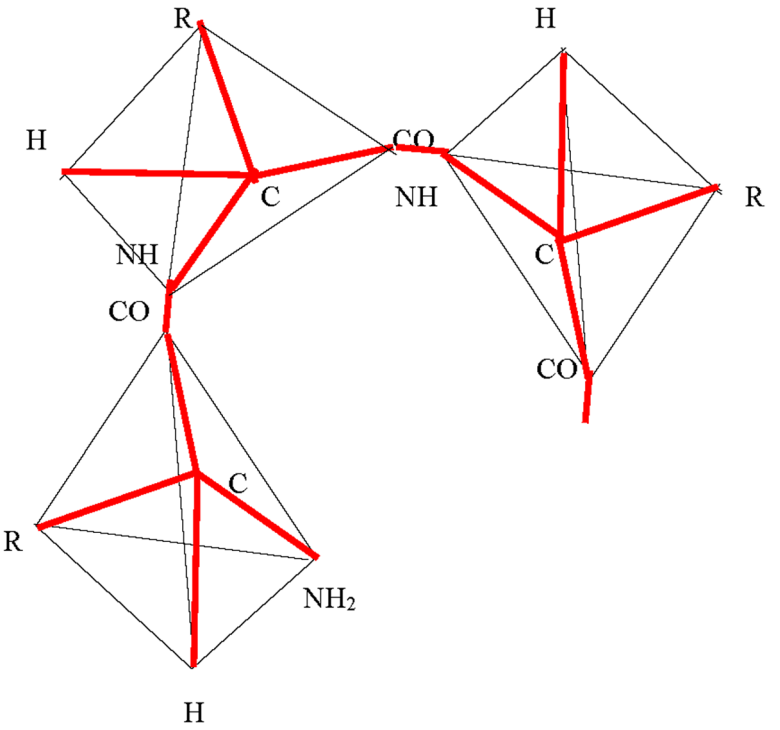

The peptide chain may form both parallel and antiparallel structure associated hydrogen bond. In addition, the peptide chain may form a compact protein globule. This class of proteins known as globular proteins that perform complex biological functions. For example, the protein is a globular myoglobin – oxygen - binding protein present in the muscles. In the center of myoglobin globule is hemo - group containing Fe - porphyrin (iron atom surrounded by five nitrogen atoms).

Theorem 2: The dimension of the Fe - porphyrin before joining the oxygen atom is equal to 5.

Proof.

Consider the first coordination sphere of the iron atom in the center of the porphyrin (Zhizhin, 2015), since only in the first coordination sphere of atoms are linked by a covalent bond, and in the following focal areas of intermolecular bonds between atoms. Before joining of the oxygen atom the first coordination sphere of Fe - porphyrin may be represented as a plane projection (Figure 12). There are the vertices *a, c, d, f* of which the nitrogen

Figure 12. The first coordination sphere of Fe - porphyrin before binding oxygen

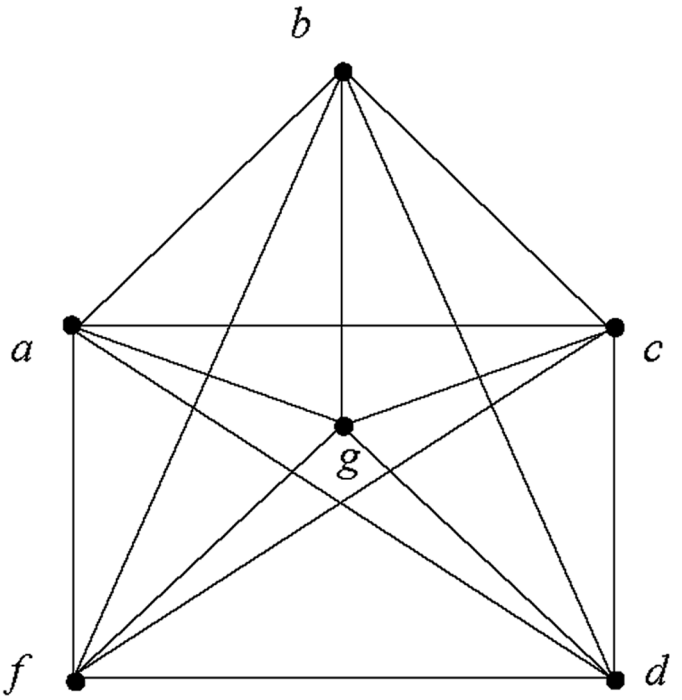

atoms of the porphyrin are located, an iron atom is located at the vertex *g*, and the nitrogen atom of the nearest histidine residue is located at the vertex *b*. The deflection of vertex *g* from the center of the rectangle *acdf* corresponds to a certain "dome" character of porphyrin (Steed & Atwwod, 2007; Lehn, 1998). The projection in Figure 12 represents some polytope (let`s denote *A* - polytope).

The *A* – polytope has six elements with dimension 0, $f_0(A) = 6$. There are vertices *a, c, d, f, g, b*. The number of elements with dimension 1 is $f_1(A) = C_6^2 = 15$. It are edges *ab, bc, bd, bf, bg, ac, cd, fd, af, fc, ad, ag, gc, fg*. The number of elements with dimension 2 is $f_2(A) = C_6^3 = 20$. It are triangles *abf*, *bfg, bgd, dbc, bga, bgc, agc, dfg, adc, acf, fcd, bgd, bcd, agd, fgc, fbc, abd, afg, gcd, afd*). The number of elements with dimension 3 is $f_3(A) = C_6^4 = 15$. It are tetrahedons *abgf, bsgd, abfc, abcd, bfcg, abdg, acfg, abdf, acdg, bfdg, abgc, fbcd, fgcd, afgd, afcd*). The number of elements with dimension 4 is $f_4(A) = C_6^4 = 6$. It are simplexes *abcdf, adcdg, abdfg, abcfg, bcdfg, acdfg*. Substituting the received numbers of elements of different dimensions in the equation (1) in Chapter 5 at a value of $n = 5$, can to obtain

6 - 15 + 20 - 15 + 2 = 2,

i.e. the Euler- Poincare equation is satisfied for *A* - polytope with $n = 5$. This is a simplex of dimension 5. This proves theorem 2.

Theorem 3: The dimension of Fe - porphyrin after joining of oxygen atom is 6.

Proof

The first coordination sphere after joining oxygen atoms is complemented by one vertex *e* (Figure 13).

"Dome" character of Fe - porphyrin after joining of oxygen atom decreases, but it is not possible to affirm that it disappears completely (Steed & Atwood, 2007). Therefore, the deflection of vertex *g* from the center of rectangle in Figure 13 quality is maintained qualitatively. Taking into account the significant difference between the geometry and mass of the groups attached to the iron atom at the top and bottom, it is shown in Figure 13 that the vertices *e* and *b* do not lie on the same line. In the polytope in Figure 13 (*B* - polytope) the number of elements of zero dimension is increased compared with to the *A*-polytope by one vertex *e*, $f_0(B) = 7$. This leads to the increase in the dimension of the polytope by 1, as the number of edges issuing from each

Figure 13. The first coordination sphere of Fe - porphyrin after joining of oxygen atom

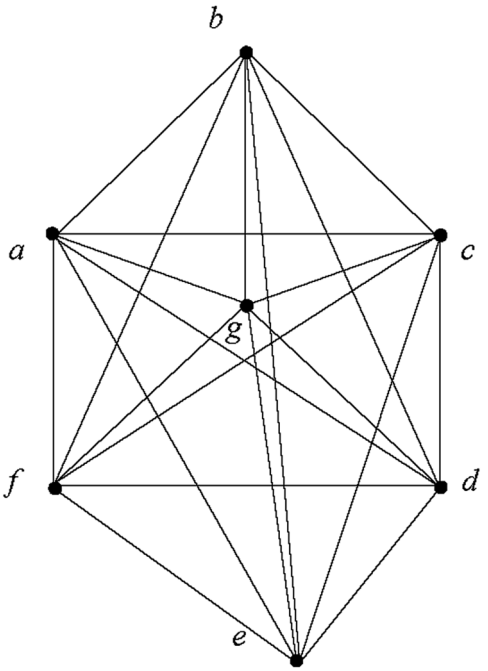

top also increases by 1. In the polytope *B* the number of elements of dimension 1 is $f_1(B) = C_7^2 = 21$ (edges). The number of elements with dimension 2 is $f_2(B) = C_7^3 = 35$ (triangles). The number of three - dimensional figures is $f_3(B) = C_7^4 = 35$ (tetrahedrons). The number of elements with dimension 4 is $f_4(B) = C_7^5 = 21$, (simplexes of dimension 4). The number of elements with dimension 5 is $f_5(B) = C_7^6 = 7$, (simplexes of dimension 5). Substituting the numbers of the elements of different dimensions in equation (1) in Chapter 5 with $n = 6$, can to get

$$7 - 21 + 35 - 35 + 21 - 7 = 0,$$

i.e. the Euler - Poincare equation for *B* - polytope is satisfied when $n = 6$. Therefore, *B* - polytope is a simplex of dimension 6. This proves theorem 3.

The dimensions of molecules increase with an increase of its energy again. It is shown that myoglobin is associated coil circuit elements of higher dimension (4) and, moreover, in the center of the coil is a group of atoms even greater dimension.

NUCLEIC ACIDS, ATP

Nucleic acids (DNA and RNA) are polynucleotide. These monomer units (nucleotides) consists of pyrimidine and purine bases, *D* - ribose (or *D* -2-deoxyribose) and phosphoric acid. The bases are virtually flat molecules (Metzler, 1980; Lehninger, 1982), one will be denoted R_f. As follows from the analysis conducted in carbohydrates *D* - ribose molecule has a higher dimension. Phosphoric acid has the structure (Figure 14)

It follows from claim 1, which, apart from a double bond between phosphorus and oxygen atoms is edge polytope, phosphoric acid molecule a geometrically is tetrahedron with the center, thus it has dimension 4.

Let is present a molecule *D* - ribose as a polytope (Figure 15).

Theorem 4: The molecule of *D* - ribose is a convex polytope type simplex of dimension 12.

Proof

Polytope in Figure 15 has vertices 13, $f_0 = 13 - n + 1$; 78 edges ($f_1 = C_{n+1}^2 = 78$); 560 triangles ($f_2 = C_{n+1}^3 = 286$);715 tetrahedrons ($f_3 = C_{n+1}^4 = 715$); 1287 4 – simplexes ($f_4 = C_{n+1}^5 = 1287$); 1716 5 – simplexes ($f_5 = C_{n+1}^6 = 1716$); 1716 6 – simplexes ($f_6 = C_{n+1}^7 = 1716$); 1287 7 - simplexes ($f_7 = C_{n=1}^8 = 1287$); 715 8 – simplexes ($f_8 = C_{n+1}^9 = 715$); 286 9 – simplexes ($f_9 = C_{n+1}^{10} = 286$); 78 10 – simplexes ($f_{10} = C_{n+1}^{11} = 78$); 13 11 - simplexes ($f_{11} = C_{n+1}^{12} = 13$).

Figure 14. The structure of phosphoric acid

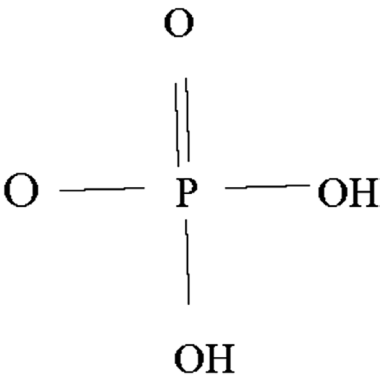

Figure 15. The molecule D – ribose

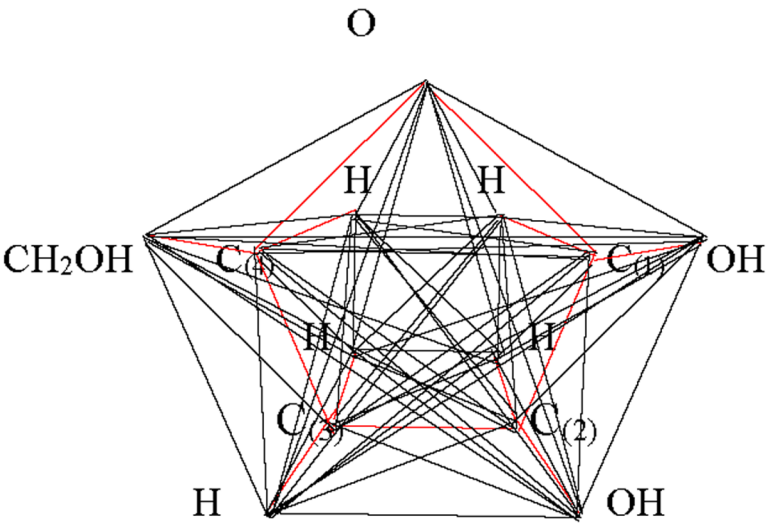

Substituting the values $f_i, (0 \leq i \leq 11)$ in Euler's - Poincare equation (1) in Chapter 5, can to see that it holds for $n = 12$

$$\sum_{i=0}^{11=n-1} f_i(-1)^i = 0.$$

Theorem 4 is proved.

The polynucleotides molecules *D* - ribose combined with phosphoric acid residues and bases R_f development of two water molecules (R_f have six kinds of alternate bases - pyrimidine, uracil, adenine, cytosine, guanine, purine). Thus, the polynucleotide chain is a sequence related to each other through oxygen atoms higher dimensional objects (simplexes)

4D - O - 12D - O - 4D - O - 12D - O - .....

Nucleotides (12 - simplex) act in some cases as a coenzyme of biochemical reactions. For example, nucleotides associated with two extra residues in the form of phosphoric acid of polyphosphoric acid to form (Figure 16) adenosine triphosphate (ATP)

Compounds of this type are readily cleaved, one or two phosphoric acid residue, which is transferred to any other radicals, - the process of so

Figure 16. The scheme of the ATP

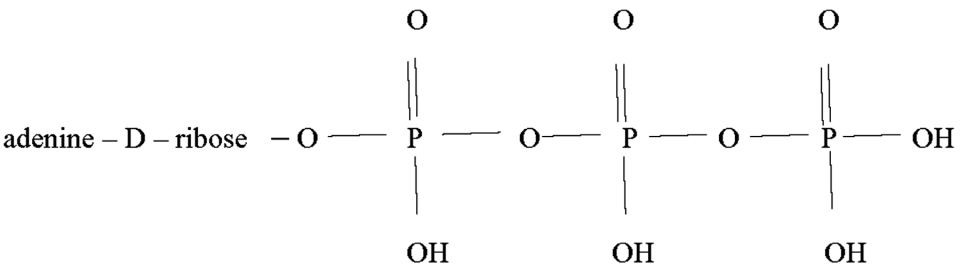

- called phosphorylation. Bond in the chain polyphosphoric rich in energy, so simultaneously with the transfer of phosphorus is carried energy transfer from one connection to another. Thus, ATP is also a chain of elements of higher dimension (simplexes)

R_f *- 12D - 4D - 4D - 4D.*

In biomolecules are essential sense transition metals. They, being in the center of the coordination spheres, provide management role in the living organisms. This is achieved due to the presence of these metals in a large number of electrons and the quantum of vacant cells in the outer shell of atoms. Due to the transition metals carried covalent and donor-acceptor chemical bonds with atoms other elements in the living organisms. A significant part of the transition metals have a deviation from the rules of filling of electron orbitals in order of increasing energy falling on the orbitals of higher energy. Currently there is no classification and analysis of the anomalous transition metals having such deviations. Considering the importance of these metals to the functioning of living organisms, it is of interest for further work to examine these anomalies in order to establish operating in these patterns and identify opportunities for their practical use.

WINE ACID

Earlier in Chapter 6, structures of two enantiomorphism forms of glucose were considered. The construction of images of their molecules in a space of dimensionality 15 made it possible to explain why the chain of molecules of α -*D* glucose has branches from the chain, and the chain of molecules of

the $\beta - D$ glucose molecule does not have a branch from the chain. Earlier in Chapter 6, the structure of the aldose monosaccharide in the configuration of *D* is considered (Metzler, 1980). The aldose monosaccharide also has an enantiomorphism configuration of *L*. We will consider the difference in these configurations by the example of a closely related tartaric acid, which played a major role in the development of biology, starting with Pasteur's well - known works (Pasteur, 1960). However, instead of the known images of these molecules in the form of Fisher's projections (Figure 17, Figure 18), we will use images of space of higher dimension for their images.

Comparing Fisher images of aldose monosaccharide (Figure 2) and tartaric acid (Figure 17, Figure 18), can to see that these compounds have the same main part of the design. It has the form of two tetrahedrons with a center, and the center of each of them is simultaneously the vertex of another tetrahedron. There is some difference in functional groups of compounds. Enantiomorphism forms of tartaric acid differ in the mirror image of hydrogen ions and hydroxyl groups in the main part of the molecule's structure. The dimension of this construction how it is shown earlier equal 5. Thus, the dimension of the molecules tartaric acid in both forms is 5. Images of polytopes corresponding to a molecule of tartaric acid in the form *D* and form *L* are presented in Figures 19 and Figure 20.

Figure 17. Shema of the molecules D - wine acid

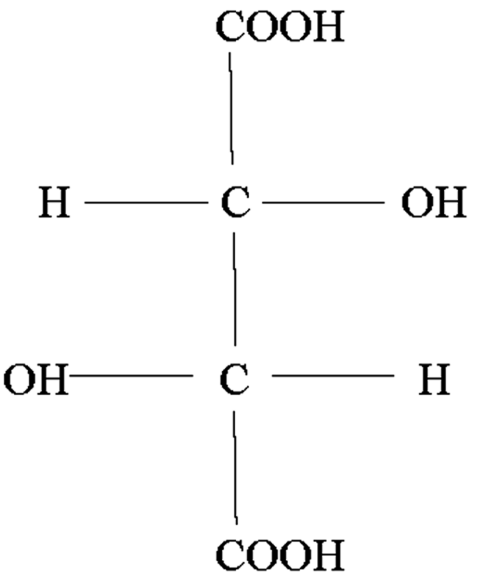

Figure 18. Shema of the molecules L – wine acid

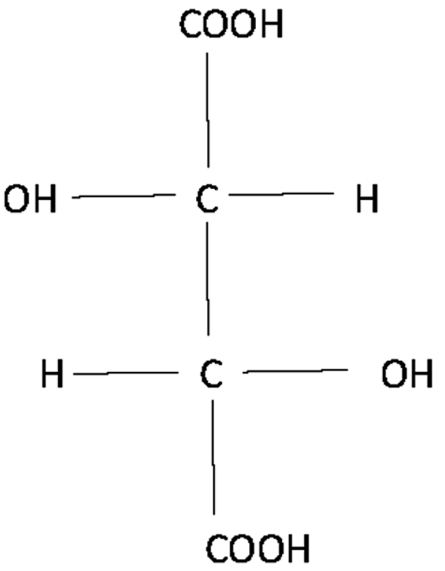

Figure 19. Spatial structure of the D – wine acid

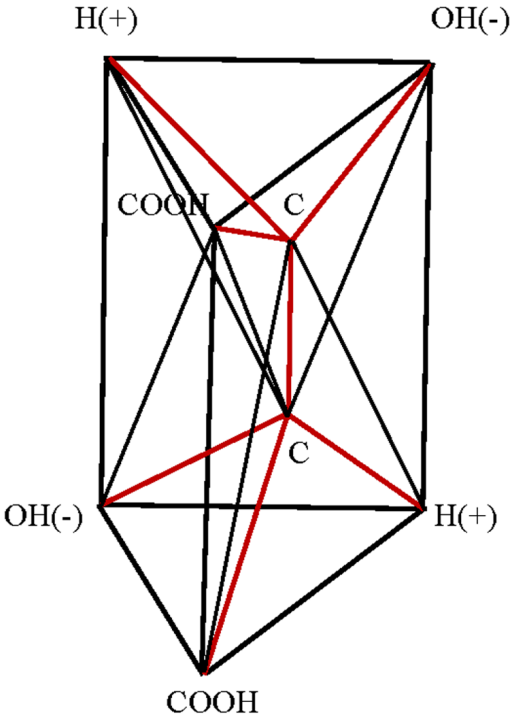

**For a more accurate representation see the electronic version.*

Figure 20. Spatial structure of the L – wine acid

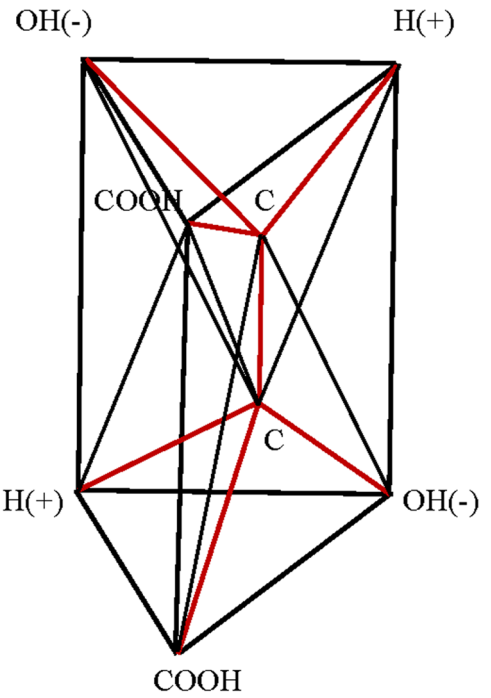

**For a more accurate representation see the electronic version.*

The brown color in Figures 19, 20 denotes the edges corresponding to the chemical bonds between the atoms. The black color in these figures denotes the edges that have values only as the edges of the convex body. The outer contour of both molecules in three-dimensional space is a triangular prism. There are two carbon atoms within these prisms. These two carbon atoms and lead to an increase in the dimension of the molecule to five. On the outer contour, two enantiomorphism forms have the opposite arrangement of hydrogen ions and a hydroxyl group. The images obtained make it possible to explain the main property of tartaric acid - rotation of the plane of polarization of the incident light in different directions: in the case of the *D* form to the right, in the case of the *L* form to the left. It are known devices for rotating the plane of polarization of light, having the appearance of two folded triangular prisms, the boundary between which serves to reflect light (Wood, 1936). Can to say that the molecule of tartaric acid is a natural device for rotating the plane of light polarization. Two carbon atoms play the role of the reflecting partition in the molecule. The rotation occurs in the forms *D* and *L* in different directions because of the opposite arrangement of the charges of the hydrogen ions (+)

and the hydroxyl group (-) in these forms. Thus, the reason for the different rotation of the plane of polarization of light lies not in the different forms of the crystals of *D* - tartaric acid and *L*-tartaric acid, as Pasteur suggested, but in different forms of molecules, clearly visible in the image in the space 5*D*.

A number of serious works on the use of spaces of higher dimension in the analysis of the structure of viruses belongs to the authors Janner and Twarock (Janner, 2006, 2008, 2011, 2016; Keef & Twarock, 2009; Twarock & Dykeman, 2010). However, it should be noted, that in these works, especially in the works of Janner, the notion of polytopes of higher dimension is often used incorrectly. The quantities of elements of different dimensions are not determined and the feasibility of the Euler - Poincare equation is not checked. Therefore, the results of these studies require verification.

REFERENCES

Gray, H. B. (1965). *Electrons and chemical bonding*. New York: W.A. Benjamin INC.

Grunbaum, B. (1967). *Convex Polytopes*. London: Springer.

Janner, A. (2006). Towards a classification of icosahedral viruses in term of indexed polyhedral. *Acta Crystallographica. Section A, Foundations of Crystallography*, *62*(Pt5), 319–330. doi:10.1107/S0108767306022227 PMID:16926480

Janner, A. (2008). Comparative architecture of octahedral protein cages. II. Interplay between structural elements. *Acta Crystallographica. Section A, Foundations of Crystallography*, *64*(Pt4), 503–512. doi:10.1107/S0108767308012051 PMID:18560167

Janner, A. (2011). Form, symmetry and packing of biomacromolecules. Shells with boundaries at anti - nodes of resonant vibration in icosahedral RNA viruses. *Acta Crystallographica. Section A, Foundations of Crystallography*, *67*(Pt6), 521–532. doi:10.1107/S010876731103577X PMID:22011468

Janner, A. (2016). Symmetry - adapted digital modeling III, Coarse - grained icosahedral viruses. *Acta Crystallographica. Section A, Foundations of Crystallography*, *72*(Pt3), 324–337. doi:10.1107/S205327331600276X PMID:27126109

Keef, T., & Twarock, R. (2009). Affine extensions of the icosahedral group with applications to the three - dimensional organization of simple viruses. *Journal of Mathematical Biology*, *59*(3), 287–313. doi:10.100700285-008-0228-5 PMID:18979101

Lehn, J. M. (1998). *Supramolecular chemistry. Concept and perspectives*. Novosibirsk: Science.

Lehninger, A. L. (1982). *Principles of Biochemistry* (Vol. 1-3). New York: Worth Publisher, Inc.

Metzler, D. E. (1980). *Biochemistry. The Chemical Reactions of Living Cells* (Vol. 1-3). New York: Academic Press.

Pasteur, L. (1960). *Selected works*. Moscow: Publishing House of the Academy of Sciences of the USSR.

Shevchenko, V. Ya., Zhizhin, G. V., & Mackay, A. (2013). On the Structure of Quasicrystals in a Higher - Dimensional Space. In M. V. Diudea & C. L. Nagy (Eds.), *Diamonds and related nanostructures* (pp. 311–320). New York: Springer. doi:10.1007/978-94-007-6371-5_17

Steed, J. V., & Atwood, J. L. (2000). *Supramolecular chemistry*. Chichester, UK: John Wiley and Sons.

Twarock, R., & Dykeman, E. C. (2010). Al-atom normal-mode analysis reveals an RNA-induced allostery in a bacteriophage coat protein. *Physical Review. E*, *81*(3), 1–10.

Wood, R. (1936). *Researches in physical optics*. Wentworth Press.

Zhizhin, G. V. (2014). On the higher dimensions in nature. *Biosphere*, *6*(4), 313–318.

Zhizhin, G. V. (2015). The dimensions of supramolecular compounds. *Biosphere*, *7*(2), 149–154.

Zhizhin, G. V. (2016). The structure, topological and functional dimension of biomolecules. *J. Chemoinformatics and Chemical Engineering*, *5*(3), 44–58.

Zhizhin, G.V. (2017). Dimensions of compounds in supramolecular chemistry. *International Journal Chemical Modeling, 5*(2).

Zhizhin, G. V., & Diudea, M. V. (2016). Space of nanoworld. In M. V. Putz & C. M. Marius (Eds.), *Sustainable nanosystems, development, properties, and applications* (pp. 214–235). New York: IGI Global.

Zhizhin, G. V., Khalaj, Z., & Diudea, M. V. (2016). Geometrical and topology dimensions of the diamond. In A. R. Ashrafi & M. V. Diudea (Eds.), *Distance, symmetry and topology in carbon nanomaterials* (pp. 167–187). New York: Springer. doi:10.1007/978-3-319-31584-3_12

KEY TERMS AND DEFINITIONS

Branching of the Chain of the *D*-Glucose Molecule: The formation of branches in a chain of carbon atoms in the molecule of *α–D*-glucose. Such branches in a chain of the carbon atoms of the molecule *β–D*-glucose are impossible. This follows from the representation of glucose molecules in the form of a polytope of higher dimension.

Enantiomorphism (Chirality) of Biomolecules: The possibility of changing the mutual arrangement of hydrogen atoms and hydroxyl groups in biomolecules (polytopes of higher dimension), leading to a change in their properties.

First Coordination Sphere of Fe-Porphyrin: A set of nitrogen atoms bound by a covalent bond to an iron atom. The dimension of the coordination sphere upon addition of the oxygen atom increases from 5 to 6.

Functional (Topological) Dimension of a Molecule: The dimension of a convex polytope, as a model of a molecule, at the vertices of which not only individual atoms but also functional groups of the molecule can be located.

Hybridization of Electronic Orbitals: This is the interaction of the electronic orbitals of atoms entering the molecule, leading under certain conditions to the formation of higher dimensionality of molecules.

Spiral Peptide Chain: The formation of a spiral chain of protein molecules, as a consequence of the higher dimension of protein molecules.

Chapter 7
Three-Dimensional Models of a Five-Carbon Sugar Molecule and Nucleic Acids

ABSTRACT

Three-dimensional images of five-carbon sugar molecules and single-stranded nucleic acid molecules (DNA and RNA) were obtained. The geometrical cause of the formation of different form by molecules nucleic acids (right and left spirals with different number of D-ribose and ribose molecules in the period, including closed chains) has been determined. Substituting the known effective values of the lengths of chemical bonds (carbon-carbon, oxygen-oxygen, phosphorus-oxygen) into the structure of polytopes, the values of the characteristic geometric parameters of molecules nucleic acids were calculated: their effective diameter and period. It turned out that the calculated values of these parameters are in good agreement with their values, determined earlier experimentally. It is shown that the set of single-stranded nucleic acids (both DNA and RNA) is broken into two sets of chiral forms. Each form in one set contains a chiral form in another set. Moreover, in each set there are possible rotation of the spirals both in the right and in the left direction.

DOI: 10.4018/978-1-5225-9651-6.ch007

THREE-DIMENSIONAL MODEL OF A FIVE-CARBON SUGAR MOLECULE

Deoxyribonucleic acid (DNA), as a chemical substance, it was isolated by Johann Friedrich Micher in 1869 from the remains of cells contained in the pus. He singled out a substance that includes nitrogen and phosphorus. When Misher determined that this substance has acid properties, the substance was called nucleic acid (Dahm, 2005). Gradually it was proved that it was DNA, and not proteins, as previously thought, and which is the carrier of genetic information. One of the first decisive proofs was the experiments of Oswald Avery, Colin MacLeod and McLean McCarthy (1944) on the transformation of bacteria.

The structure of the double helix DNA it was proposed by Francis Crick and James Watson in 1953 on the base of the X-ray structural data obtained by Maurice Wilkins and Rosalind Franklin and the "Chargaff rules" according to which in each DNA molecule the strict relationships connecting the quantity of nitrogenous bases of different (Watson, & Crick, 1953a, b). For outstanding contributions to this discovery, Francis Crick, James Watson and Maurice Wilkins were awarded the 1962 Nobel Prize in Physiology or Medicine. Deoxyribonucleic acid (DNA) is a biopolymer, the monomer of which is the nucleotide (Albert, et al., 2002; Butler, 2005). Each nucleotide consists of a phosphoric acid residue attached to sugar deoxyribose, to which one of the four nitrogen bases is attached also. The bases that make up the nucleotides are divided into two groups: purines (adenine [A] and guanine [G]) and pyrimidines (cytosine [C] and thymine [T]) are formed by combined five - and six - membered heterocycles.

They managed to show that the DNA isolated from the pneumococci corresponds to the so -called transformation (the acquisition of pathogenic properties by a harmless culture as result of the addition of dead pathogenic bacteria to it). The experiment of American scientists Alfred Hershey and Martha Chase (Hershey - Chase experiment, 1952) with radioactively labeled proteins and bacteriophage DNA showed that only the phage nucleic acid is transmitted to the infected cell, and the new generation of phage contains the same proteins and nucleic acid, as the initial phage (Hershey & Chase, 1952). Deciphering the structure of DNA (1953) has become one of the turning points in the history of biology.

In 1986, Frank - Kamenetskiy in Moscow showed how a double - stranded DNA folds into a so -called H - shape, composed not of two but three strands of DNA (Frank – Kamenetskiy, 1986, 1988). Deoxyribonucleic acid (DNA) is a biopolymer, the monomer of which is the nucleotide (Albert et al., 2002; Butler, 2005).

Nucleotides are long polynucleotide chains covalently linked. These chains in the overwhelming majority of cases (except for some viruses possessing single - stranded DNA genomes) are combined pairwise by means of hydrogen bonds into a secondary structure, called the double helix (Watson & Crick, 1953 a, b; Berg, Tymoczko & Stryer, 2002). Each base on one of the chains is connected to one definite base on the second chain. This specific binding is called complementary. Purines are complementary to pyrimidines (that is, they are capable of forming hydrogen bonds with them): adenine forms bonds only with thymine, and cytosine - with guanine. In a double helix, chains are also linked by hydrophobic interactions and stacking, which do not depend on the DNA base sequence (Ponnuswamy & Gromiha, 1994). Complementarity of the double helix means that the information contained in one chain is also contained in another chain. Different base pairs form a different number of hydrogen bonds. In the future, the existence of nucleic acids differing in the length of the period and shape with rotation of the spiral both to the right and to the left was experimentally established (Ha, et al., 2005; Cantor, & Schimmel, 1980; Frank – Kamenetskiy, 2010).

Watson and Crick postulated the spiral form of the DNA molecule, but they did not discuss the reasons for the formation of such a DNA molecule. Until now there have been no works explaining the existence of a spiral in the DNA molecule.

Another nucleic acid (RNA), essential for protein sieve, transferring genetic information from DNA to protein, is chemically similar to DNA. There are two differences in the RNA chain from a single DNA chain: 1) five - carbon sugar (pentose) in RNA is represented by ribose, and in DNA - by D - ribose; 2) one of the two pyrimidine nucleotides in RNA is represented by the uridyl residue (U), instead of its methylated derivative T in DNA. RNA is formed as a flexible single - stranded polymer, in contrast to the rigid double helix of DNA. In the second half of the 1950 it has already been established (Spirin, 2019) that the synthesis of proteins in living cells is carried out by ribosome and that RNA represents the main part of the ribosomes. At the same time, the interaction of nitrogenous bases leads to the fact that the single - stranded RNA polymer coagulates onto itself, short double - helix regions, where the regions paired with nitrogenous bases are antiparallel. An essential low

molecular weight component of ribosomes are divalent metal ions, mainly magnesium ions (Spirin, & Gavrilova, 1971). It is they, who ensure the stability of the ribosomes by binding together the negative charges of phosphoric acid residues in RNA molecules.

In the book (Zhizhin, 2017), the molecules of practically all the elements of the periodic system were studied in detail and it was shown that many of them, including magnesium and calcium, form compounds of higher dimension (see also Zhizhin, 2015 a, b; Zhizhin, & Diudea, 2016; Zhizhin, Khalaj, & Diudea, 2016). In the Chapter 6 (Zhizhin, 2016; Zhizhin, 2017), the structures of biomolecules, which also form compounds of higher dimension, are also studied. It is shown that the molecule of five - carbon sugar in nucleic acids has the shape of a polytope of the type simplex of dimension 12. Its image is presented in the form of a projection on a two - dimensional plane. A simplified image of this projection was used to construct the nucleotide chain (Zhizhin, 2019a). It was found that the alternation of this projection with the image of a phosphoric acid residue in the form of a polytope of dimension 4 leads to a geometric proof of the need to form a helix in the nucleotide chain. Moreover, depending on the possible location of the phosphoric acid residue relative to the ribose molecule (or *D* - ribose), right - or left - twisted spirals are formed. Given the extreme importance of nucleic acids in the processes of heredity and the clarity of three - dimensional images of geometric formations, it would be useful for further research to obtain three - dimensional images of nucleic acids. As noted in the last monography academician A.S. Spirin (Spirin, 2019), until now, no one has managed to build a three - dimensional image of nucleic acid molecules. An attempt to build such an image was undertaken in this Chapter. This will be taken into account (Zhizhin, 2018) that, whatever the dimension of the polytope, if it is surrounded by three - dimensional space, then the outer boundary of the polytope will be a three – dimensional bodies with two – dimensional sides. It should be noted, that the existence of polytope of higher dimension inside a three – dimensional space does not contradict Riemann`s geometry (Riemann, 1854), which assumes the boundedness of a space of higher dimension (Zhizhin, 2014).

The deoxyribose (or the *D* – ribose) is molecule of carbohydrate with five atoms carbon. There are two enantiomer forms of this molecule. Its images in the form of Fisher's formula (Metzler, 1980) are shown in Figure 1 A, B.

In the DNA molecule, *D* - ribose as a component enters with a closed carbon chain. The closed chain of the molecule in Figure 1 is formed due to the rupture of the double bond between oxygen and carbon (considering it the first in the chain), the liberation of the water molecule, and the addition

Figure 1. A, B: Two enantiomer forms of the molecule D – ribose (formulas of Fisher`s)

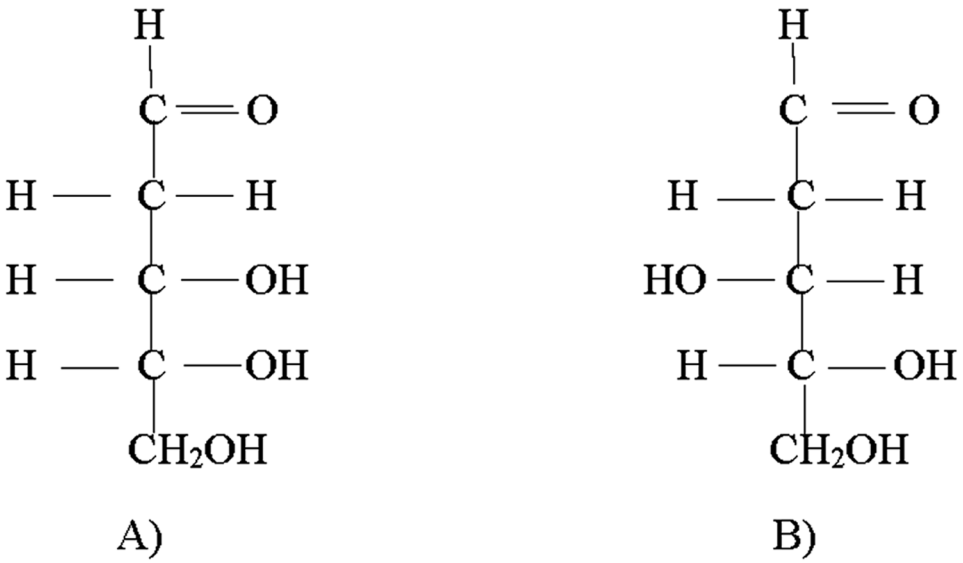

of this oxygen atom to the penultimate (fourth) carbon atom in the carbon chain. The Fischer formula or formula Haworth and their modifications (Metzler, 1980; Lehninger, 1982) may not reflect the spatial structure of the *D* – ribose molecule. For this target the constructs described in the form of convex polytopes with boundary elements which form boundary complex (Grunbaum, 1967). Only when such a representation will be to determine the dimension of these molecules (Zhizhin, 2016; 2017). Figure 2 shows the result of the closure of a chain of four carbon atoms through an oxygen atom correspondent Figure 1 A. Chemical bonds are marked as before with red color.

It is easy to see that, in addition to the form of the *D* - ribose molecule in Figure 2 (a form of *A*), there is another enantiomer form of this molecule. It connected by a symmetry transformation with respect to a straight line passing through an oxygen atom separating the projection of the form of *A* in half (we shall assume that it is a *B* shape). Form *B* of the *D* - ribose molecule is shown in Figure 3.

The ribose is molecule of carbohydrate with five atoms carbon. There are two enantiomer forms of this molecule. Its images in the form of Fisher's formula (Metzler, 1980) are shown in Figure 4 A, B.

In the RNA molecule, ribose as a component enters with a closed carbon chain. The closed chain of the molecule in Figure 4 is formed due to the

Figure 2. The molecule D – ribose with closed a chain of carbon atoms (the form A)

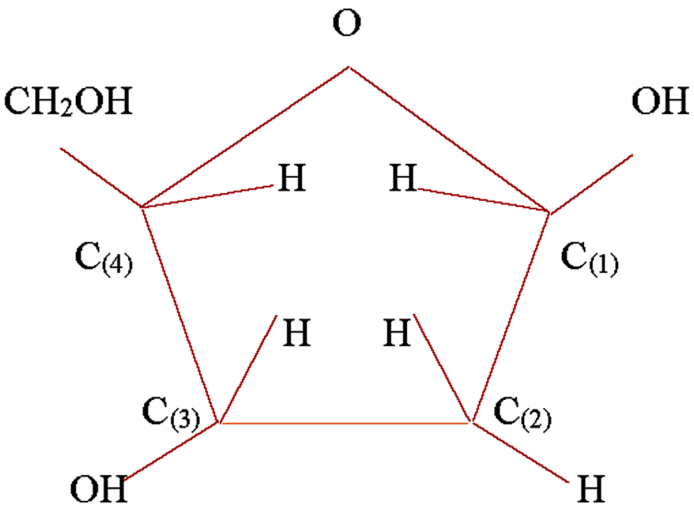

Figure 3. The molecule D – ribose with closed a chain of carbon atoms (the form B)

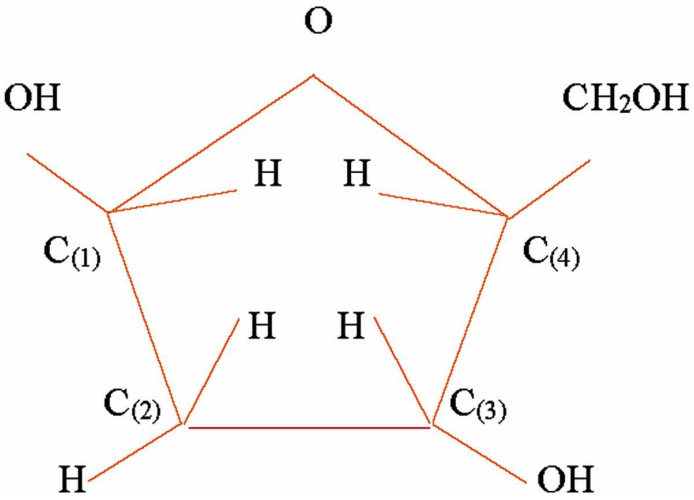

rupture of the double bond between oxygen and carbon (considering it the first in the chain), the liberation of the water molecule, and the addition of this oxygen atom to the penultimate (fourth) carbon atom in the carbon chain. Figure 5 shows the result of the closure of a chain of four carbon atoms through an oxygen atom correspondent Figure 4 A. Chemical bonds are marked as before with red color.

Figure 4. A, B: Two enantiomer forms of the molecule ribose (formulas of Fisher`s)

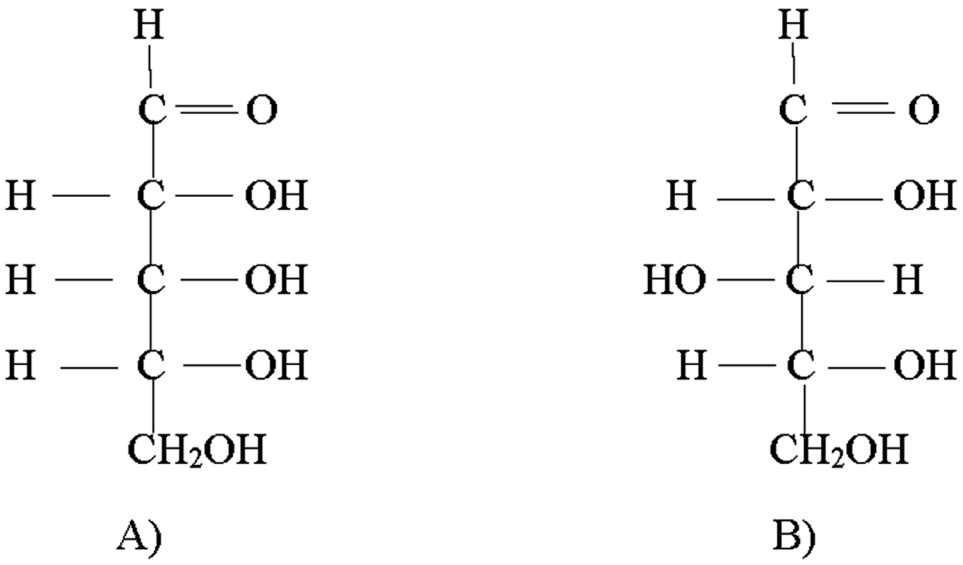

Figure 5. The molecule ribose with closed a chain of carbon atoms (the form A)

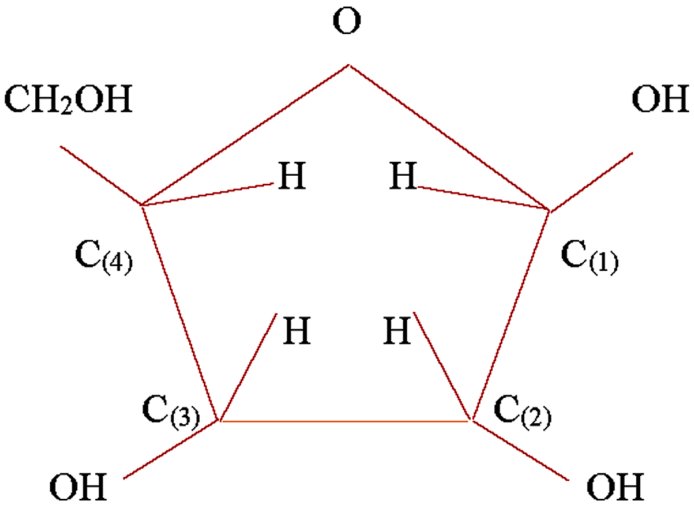

It is easy to see that, in addition to the form of the ribose molecule in Figure 4 (a form of *A*), there is another enantiomer form of this molecule. It connected by a symmetry transformation with respect to a straight line passing through an oxygen atom separating the projection of the form of *A*

Figure 6. The ribose molecule with closed a chain of carbon atoms (the form B)

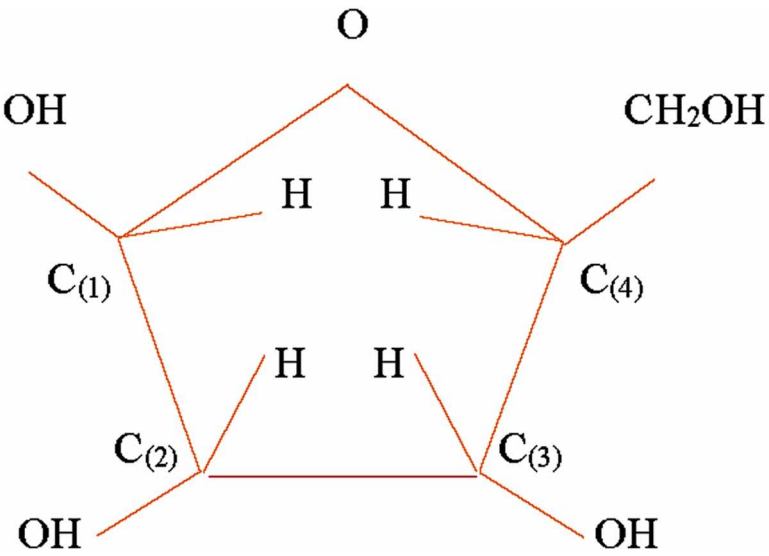

in half (we shall assume that it is a *B* shape). Form *B* of the ribose molecule is shown in Figure 6.

To determine the dimension of the molecules *D* - ribose and ribose of both enantimorphic forms (A, B), it is necessary to connect each vertex (each atom or functional group) with all other vertices of a given molecule. Obviously, due to the use of the functional dimension, in all four cases the topological view of the resulting polytope will coincide with the topological view of the polytope presented in Figure 15 of Chapter 6. Performing the transformations carried out in Chapter 6 for the polytope in Figure 15, can to obtain that the functional dimension of each of the four polytopes corresponding to *D* - ribose and ribose molecules with closed - chain are equal to 12.

Earlier it was shown that a five - carbon sugar molecule is a polytope of type simplex of dimension 12. One of the two enantiomeric forms is presented in Figure 7.

The image in Figure 7 is a topological projection of polytope 12 - simplex on a two - dimensional plane. If a hydroxyl group OH is attached to the carbon atom $C_{(2)}$ on the outer contour of the image, this corresponds to a five - carbon sugar molecule (ribose B) in the RNA molecule. If a hydrogen atom H is attached to the carbon atom $C_{(2)}$ on the outer contour of the image, this corresponds to a five - carbon sugar molecule (D – ribose B) in the DNA molecule. If to simplify the image in Figure 7, discard all the blue lines that

Figure 7. The five – carbon molecule sugar

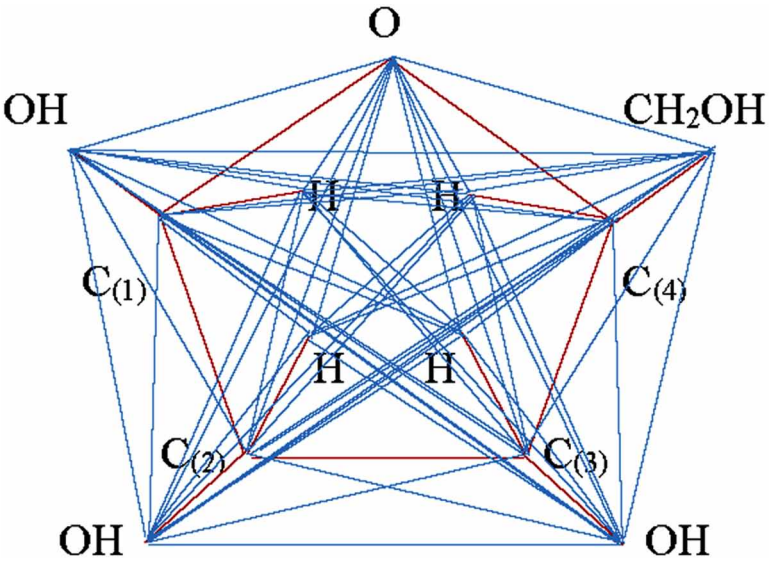

Figure 8. Simplified image of a molecule of five - carbon sugar (ribose B)

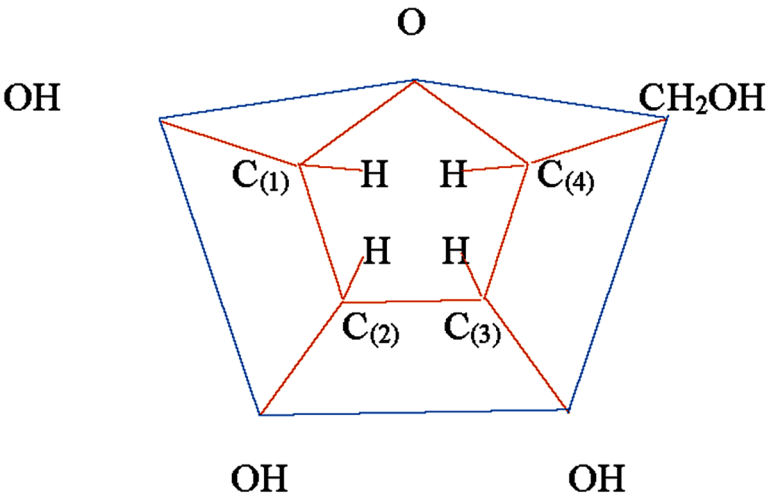

have only the geometric meaning of the edges of the convex polytope, with the exception of the outer contour, the image in Figure 8 will be obtained.

Since Figure 8 is a topological projection of a spatial figure, then by this projection it is possible to restore qualitatively the corresponding three - dimensional figure, the projection of which is Figure 8. If one take the carbon

– carbon bond length and carbon – oxygen bond $a = 0.15$ nm, then the length of the edges in the carbon – oxygen pentagonal cycle is equal to a. One can assume that the chemical bonds emanating from the four carbon atoms of this cycle are spaced symmetrically relative to the chemical bonds of this cycle and have a certain angle φ with the plane of the cycle. Since the number of valence bonds emanating into the space of four carbon atoms of the oxygen - carbon cycle is eight, it should be assumed from the symmetry condition that four valence bonds extend into a half space above the cycle plane, and four valence bonds proceed into the half space under the cycle plane. Consider a half - space above the plane of the oxygen - carbon cycle (Figure 9).

Then the length of the projection of these links on the plane of the cycle is equal to $a\cos\varphi$, and the height of the figure is equal to $h = a\sin\varphi$. In Figure 9, the orange segments are solid and dashed are valence bonds, their length is assumed to be a. Fat solid black segments together with orange segments (dotted and solid) define a part of the three - dimensional shape of the sugar molecule.

Figure 9. The half - space above the plane of the oxygen - carbon cycle

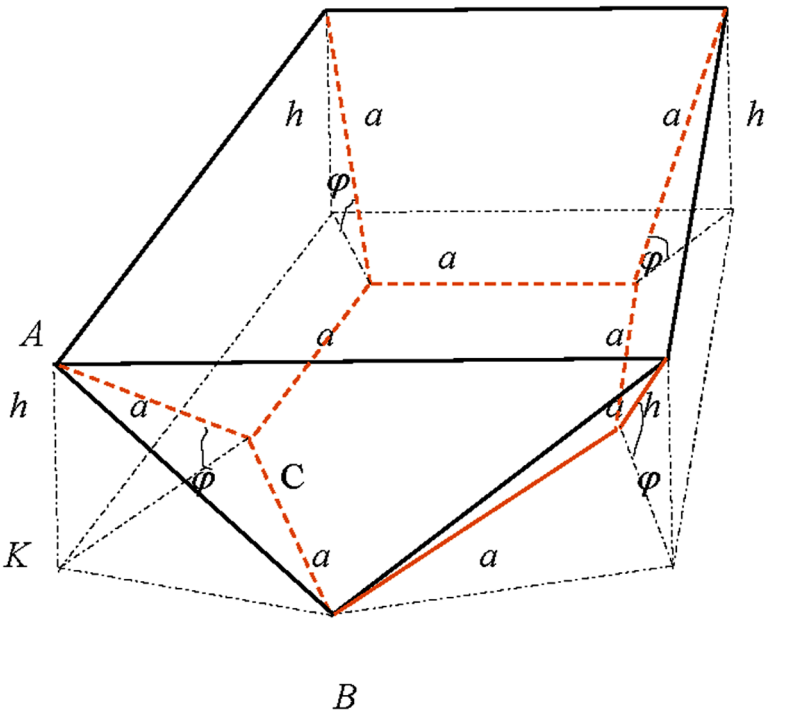

In this figure, the lower pentagonal face and the upper quadrilateral face are parallel to each other.

In Figure 9, the angle φ is unknown. One define it from two triangles *ACB* and *AKB*, equating the length of the segment *AB* from each triangle. Note that the angle *ACB* linearly depends on the angle φ : $\angle ACB = \alpha\varphi + \beta$. One take into account that the angle $KCB = 126^\circ$ due to the correctness of the lower pentagonal base of the polyhedron and the division of the external angle at the vertex *C* by the segment *KC* in half. Since $\angle ACB = 126^\circ$ for $\varphi = 0$ and $\angle ACB = 90^\circ$ for $\varphi = 90^\circ$, so $\angle ACB = 126^\circ = -\frac{2}{5}\varphi$ Since *ACB* triangle is isosceles, so

$$AB = 2a\sin\left(63^\circ - \frac{1}{5}\varphi\right) \tag{1}$$

From triangle *KCB* one have $KB = a\sqrt{1+\cos^2\varphi - 2\cos\varphi\cos 126^\circ}$. Since the *AKB* triangle is rectangular, so

$$AB^2 = a^2 2\left(1 - \cos\varphi\cos 126^\circ\right) \tag{2}$$

From (1) and (2) one have

$$1 - \cos\varphi\cos 126^\circ = 2\sin^2\left(63^\circ - \frac{1}{5}\varphi\right) \tag{3}$$

This is the equation for finding the φ angle. The equation (3) have two roots: $\varphi = 0$ and $\varphi = 90^\circ$. The first root corresponds to the flat shape of the sugar molecule. This does not correspond to the earlier proof of the multidimensionality of this molecule. One can want to find a three - dimensional view of the outer contour of the sugar molecule. This goal corresponds to the second root of equation (3), i.e. $\varphi = 90^\circ$. The second part of the three – dimensional figure is under flat of oxygen – carbon cycle. Obviously, here also the valence bonds emanating from carbon atoms are located at an angle $\varphi = 90^\circ$ to the cycle plane. The parts below the cycle plane and above the cycle plane together form a three - dimensional model of the sugar molecule ribose B (Figure 10).

Figure 10. The three – dimensional model of the sugar molecule ribose B

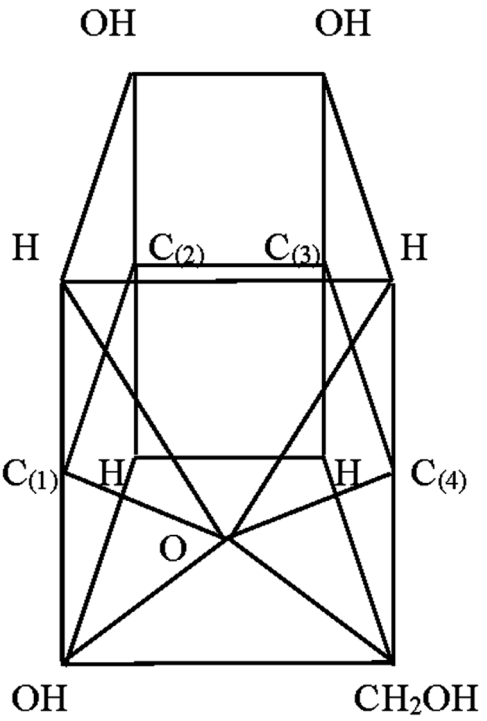

The resulting model of a five - carbon sugar molecule can be viewed as a development of the Haworth formula, since in the Haworth formula and the resulting sugar model, the valence bonds are perpendicular to the plane of the pentagonal cycle. The essential difference from Haworth's formula, however, is that the resulting model of a five - carbon sugar molecule is a convex closed polyhedron.

Similarly, three - dimensional models of five - carbon sugar molecules can be obtained ribose A (Figure 11), *D* - ribose A (Figure 12), *D* - ribose B (Figure 13).

The arrangement of atoms in the sugar molecule in Figures 10 - 13 is determined by their arrangement in the previously obtained Figures 1 – 9. These options for the arrangement of atoms and functional groups in three - dimensional models of five - carbon sugar molecules will be taken into account when analyzing the possibilities of sequential connection of five - carbon sugar molecules and phosphoric acid residues in the formation of a chain of nucleic acids.

Figure 11. The three – dimensional model of the sugar molecule ribose A

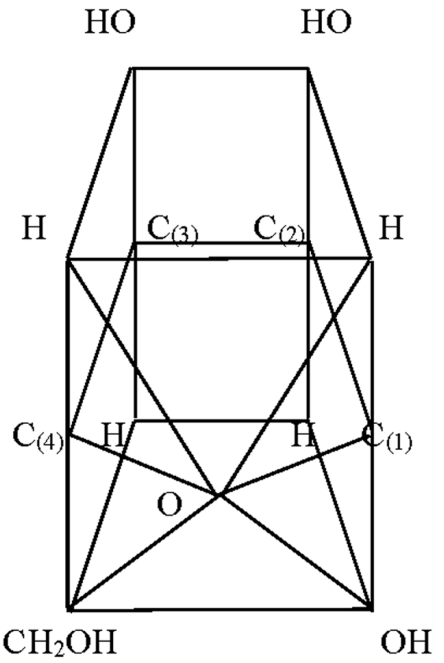

Figure 12. The three – dimensional model of the sugar molecule D - ribose A

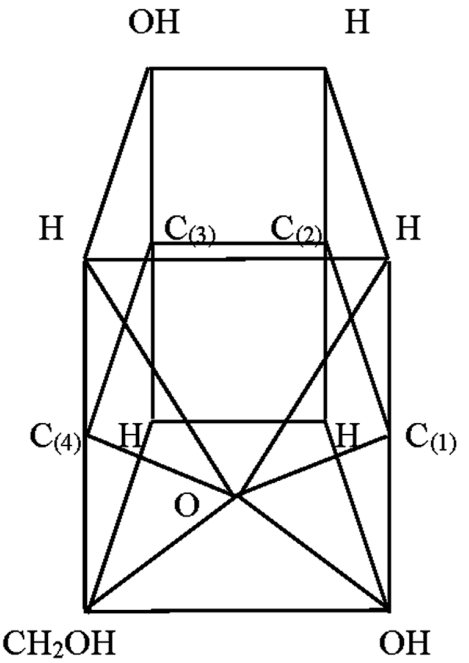

Figure 13. The three – dimensional model of the sugar molecule D - ribose B

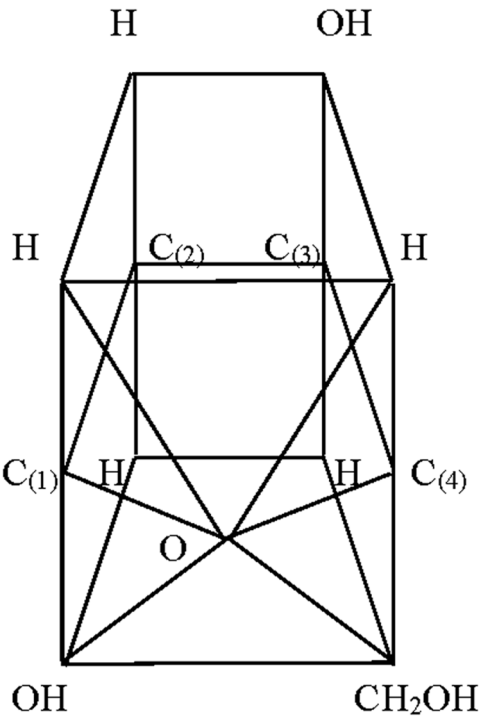

THE DIMENSION OF PHOSPHORIC ACID AND ITS RESIDUE

The phosphoric acid H_3PO_4 has the following building (see, for example, Karapetians & Drakin, 1994) (Figure 14).

On the Figure 15 is presented Fisher`s formula of phosphoric acid.

It is obvious that, used in the DNA and RNA molecules, the phosphoric acid residue obtained by detaching one hydrogen atom from it has the building also. In this case, instead of one of the hydroxyl groups attached to the phosphorus atom, there will be a negatively charged oxygen atom. To determine the functional topological dimension of phosphoric acid and its residue, it is necessary to connect the vertices, atoms and functional groups entering into these compounds (Zhizhin, 2016, 2017). Then the structure of phosphoric acid and its residue is represented in the form of a polytope in Figure 16.

Figure 14. Special structure of phosphoric acid

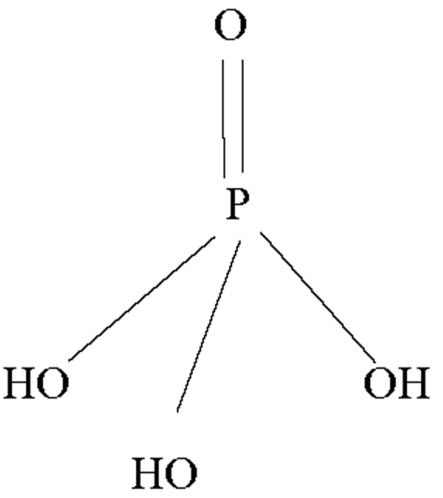

Figure 15. Fisher`s formula of phosphoric acid

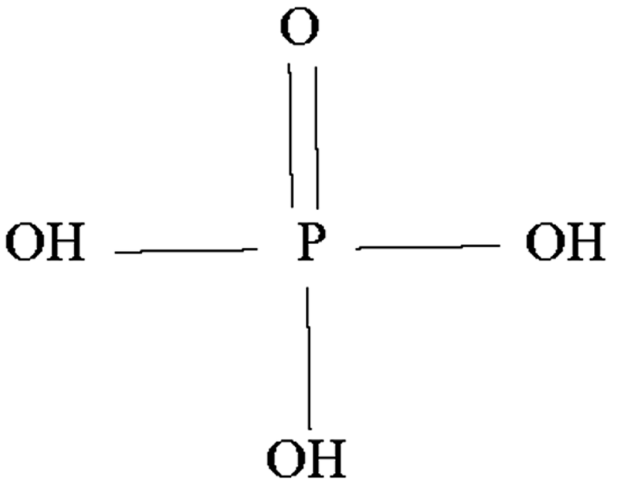

In Figure 16 in vertices *a* dispose atom phosphoric; in vertices *c* dispose atom of oxygen with double bond; in vertices *b, d, e* dispose atoms of oxygen with free bond.

Calculation of the functional topological dimension by the Euler - Poincaré equation (Poincaré, 1895) does not require specifying the exact lengths of polytope edges, and for a given number of the vertices does not depend on the groups of atoms in these vertices (Zhizhin, 2016). In Figure 16, the edges

Figure 16. The polytope of the phosphoric acid and its residue

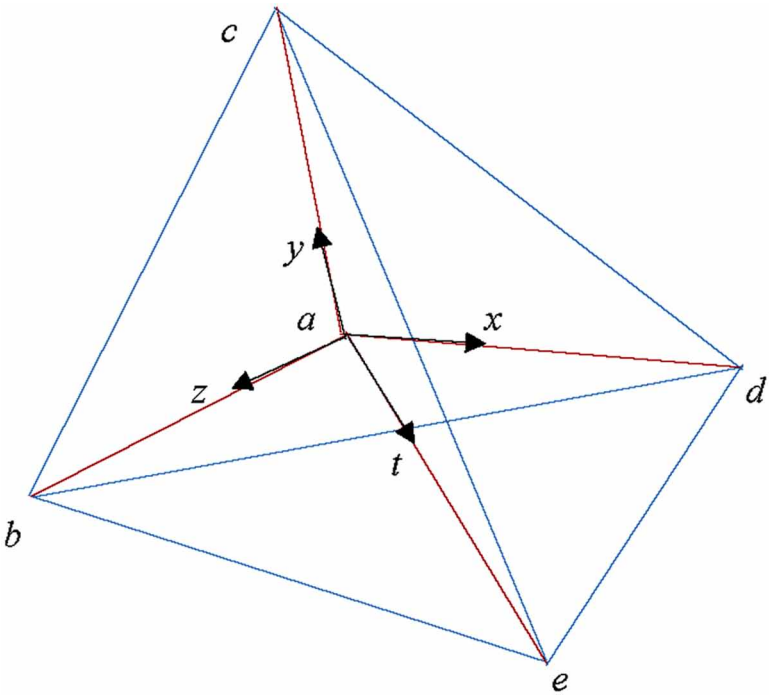

corresponding to the covalent chemical bonds are marked in red, and the edges that carry only the geometric function, delineating the closed geometric figure, are marked in blue.

It follows from Figure 16 that the polytope of phosphoric acid has five vertices (*a*, *b, c, d, e*), ten edges(*ac, ab, ad, ae, cd, de, be, ce, cb, bd*), ten plane triangular faces (*cbe, cda, cea, dab, dbe, dce, bae, dae, bce, dcb*), and five three - dimensional faces in the form of tetrahedron (*cbae, caed, cbad, abde, cebd*). These values of elements of different dimensions we must substitute into the Euler - Poincare equation

$$\sum_{i=0}^{n-1} f_i(-1)^i = 1-(-1)^i \tag{4}$$

where f_i is the number of elements with dimension i in polytope with dimension *n*. In this case there are $f_0 = 5, f_1 = 10, f_2 = 10, f_3 = 5$.

Substituting these values into equation (4), can to obtain

$5 - 10 + 10 - 5 = 0.$

Thus, equation (4) is satisfied for $n = 4$. This proves that the polytope of phosphoric acid and its residue has a dimension of four. It is worth emphasizing that the polytope of phosphoric acid and its residue is topologically equivalent to a convex polytope of the simplex type with dimension four, since these polytopes completely coincide with the values of the numbers of elements of different dimensions (Zhizhin, 2014). The origin of the four - dimensional space can be placed in one of the vertices with sending coordinates along the edges connecting this vertex to other vertices (see Figure 16).

THE THREE – DIMENSIONAL MODEL OF THE NUCLEIC ACID MOLECULE

A nucleic acid molecule is a chain of residues of phosphoric acid (a tetrahedron with a center) and sugar molecules (a prism with a pyramid). The chain (for molecules ribose A and *D* – ribose A) of successively alternating sugar molecules and residues of phosphoric acid in a three - dimensional form is shown in Figure 17.

A nucleic acid molecule with sugar molecules ribose B or D – ribose B is shown in Figure 18.

At the junctions of the phosphoric acid residue with sugar, due to the separation of water molecules, an oxygen atom and the functional group CH_2 are formed (Figure 17, Figure 18). In addition, one of the four nitrogenous bases is attached to the $C_{(1)}$ carbon atom instead of the hydroxyl group at the $C_{(1)}$ carbon atom (Figure 17, Figure 18). The yellow color in Figure 17, Figure 18 indicates the covalent bond lines connecting the phosphoric acid residues and the sugar molecules.

Figures 17 and 18 represent two chiral forms of nucleic acids (two chiral forms of DNA and two chiral forms of RNA), since not only five - carbon sugar molecules participate in them in specular reflections, but also phosphoric acid residues are also in specular reflections. Let us consider in more detail one of these forms, presented, for example, in Figure 17. It is significant that the communication lines connecting the tetrahedron with the sugar molecule form, by repulsing the electron pairs, uniform straight segments perpendicular to the bases of the prism. In the center of the tetrahedron, the chemical bond lines form a kink, since in the center of the tetrahedron there

Figure 17. A nucleic acid molecule with sugar molecules ribose A or D – ribose A

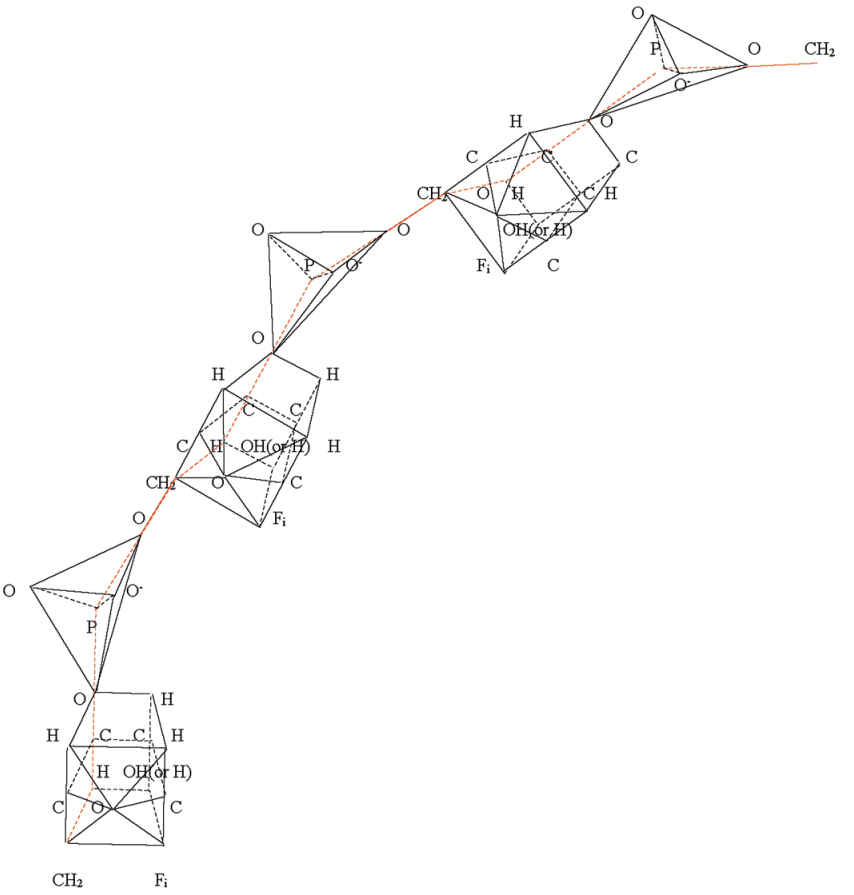

are straight lines connecting the center with the vertices of the tetrahedron. Ultimately, this fracture with simultaneous movement along the vertical coordinate leads to the formation of a helix of a nucleic acid molecule. In the projection on the plane of the figure, the covalent bond segments form a broken line close to the circle (polygon). The radius of the circle describing this polygon will be determined by the angle between the projections on the plane of the chemical bonds of the phosphorus atom with the oxygen atoms at its vertices belonging to the polygon. The tetrahedron with the center (the residue of phosphoric acid), connecting with the top of the base of the prism, has a degree of freedom. It can be rotated relative to the connection between the vertex of the prism and the center of the tetrahedron at an arbitrary angle.

Figure 18. A nucleic acid molecule with sugar molecules ribose B or D – ribose B

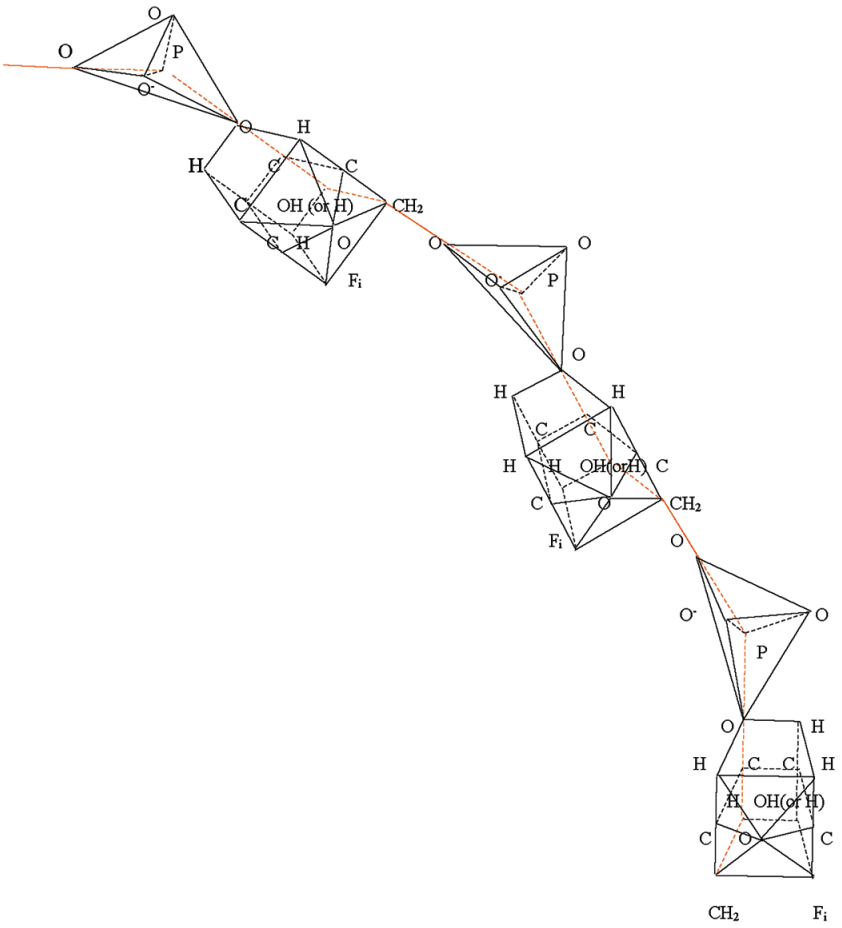

Therefore, even in the projection on the plane perpendicularity to axes of rotation, the angle between the chemical bonds emanating from the center of the tetrahedron can be arbitrary (Figure 19).

Let this angle be γ. Then the broken line between the centers of the tetrahedrons closes when the product of the number of these rotations n and the angle $\pi - \gamma$ is equal to 2π. (On projection in Figure 19 edge of low bases of prism in visible due to the perpendicularity of the generators and bases.) You can find the period of the spiral, given that there is still movement along a line perpendicular to the projection plane. Thus, to determine the radius of a circle, we have the equality

Figure 19. The projection of spiral on the plane perpendicularity to axes of rotation

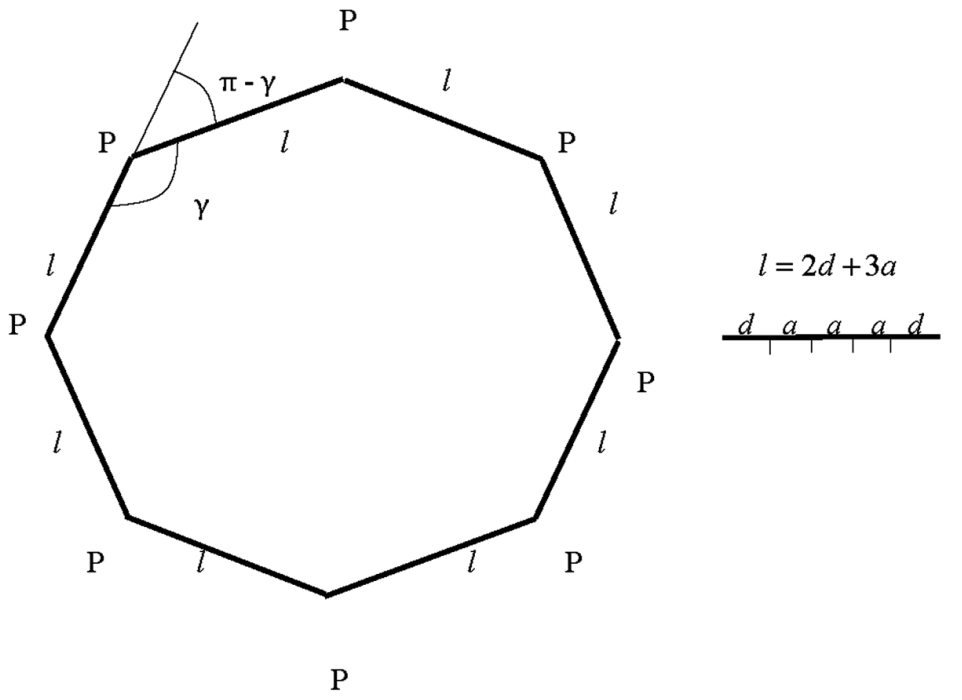

$$(\pi - \gamma)n = 2\pi$$

Since the number of turns equals the number of segments that make up a polygon, one have approximately the equality

$$\frac{2\pi}{\pi - \gamma} = \frac{2\pi R}{l}$$

R is radius of the circle, and *l* is length of the segment between centers of tetrahedrons.

From the last equality can to find the radius of the circle

$$R = \frac{l}{\pi - \gamma}$$

From Figure 17 and Figure 19 it follows that $l = 3a + 2d$. Subject to the accepted values *a* and *d* can to get

$$R = \frac{0.81}{\pi - \gamma} \text{ nm.}$$

For example, in case $\gamma = 140^{\circ}$ is *R*=1.16 nm.

This radius value is close to the experimental helix radius of nucleic acids measured by Watson and Crick. At this angle between the chemical bonds in the projection of the phosphoric acid residue, the number of nucleotides in the period $\frac{2\pi}{\pi - \gamma} = 9$. The number is in satisfactory agreement with the experimental number of nucleotides 10, given that the helix of the helix in the period is somewhat greater than the circumference of the same radius. This confirms the correctness of the three - dimensional model of the nucleic acid molecule.

The helix surface is formed due to the fact, that in a tetrahedron with a center the valence bonds connecting the center with the vertices do not lie in the same plane (Zhizhin, 2019b). Therefore, the valence bonds connecting the two sugar molecules do not lie together in the plane passing through the edge of the prism. The bond leaving the phosphorus atom, approximately 23 degrees, retreats from the plane in which the bond lies, which is part of the phosphorus atom. This causes a chain to shift along a coordinate perpendicular to the circle. The equation of the helix surface in this case can be written as $h = n\Delta h, \Delta h = l\tan(\Delta\alpha), \Delta\alpha$ is the angle between the previous segment *l* and the subsequent segment *l*, *n* is the number of turns, *h* is the height of the period. Thus, $\Delta h = 0.343nm, h = 3.43nm$. This period height value is close to the value found in the Watson and Crick experiments (3.46 nm).

If the valence bond in the tetrahedron connecting its center with the next sugar molecule is rejected in the projection to the left of the valence bond connecting the center of the tetrahedron with the previous sugar molecule, i.e. it is $\gamma > 180^{\circ}$ the nucleic acid is a left - handed helix. If is $\gamma = 180^{\circ}$, then the nucleic acid has a linear appearance.

In ribonucleic acids, a helix return in one molecule is observed (Spirin, 2019). This is possible if the angle γ is variable, i.e. in the chain, the angle γ increases to 180 degrees and the achievement of even larger values of this

angle. This means that along the chain there is a sequential rotation of the tetrahedron around the valence bond connecting its center with the previous sugar molecule.

Obviously, a similar consideration can be made for the single - stranded nucleic acid molecule shown in Figure 18. The difference between Figure 17 and Figure 18 is that the chain helix in Figure 17 rotates to the right, the chain helix in Figure 18 rotates to the left. In this case, the residues of phosphoric acid at the corresponding positions in the chains are mirrored to each other. Since the phosphoric acid residue has a degree of freedom (rotation around the axis connecting it to the five - carbon sugar molecule), with a different initial state of the phosphoric acid residue in Figure 17, there will be another state of the phosphoric acid residue in Figure 18. This leads to the set of single - stranded nucleic acids (both DNA and RNA) is broken into two sets of chiral forms. Each form in one set contains a chiral form in another set. Moreover, in each set there are possible rotation of the spirals both in the right and in the left direction.

REFERENCES

Albert, B. (2002). *Molecular Biology of the Cell* (4th ed.). New York: Garland Science.

Berg, J., Tymoczko, J., & Stryer, L. (2002). *Biochemistry*. San Francisco: W.H. Freeman & Co Ltd.

Butler, J. M. (2005). *Forensic DNA Typing*. London: Gardners Books.

Cantor, C. R., & Schimmel, P. R. (1980). *Biophysical Chemistry. Part I. The Conformation of Biological Macromolecules*. San Francisco: W.H. Freeman & Co Ltd.

Dahm, R. (2005). Friedrich Miescher and the discovery of DNA. *Developmental Biology*, *278*(2), 274–288. doi:10.1016/j.ydbio.2004.11.028 PMID:15680349

Frank-Kamenetskiy, M. (1986). DNA structure: A simple solution to the stability of the double helix? *Nature, 324*, 325.

Frank-Kamenetskiy, M. (1988). H – form DNA and the hairpin – triplex model. *Nature, 333*, 214.

Frank-Kamenetskiy, M. (2010). Queen of a living cell. From the structure of DNA to the biotechnological revolution. Moscow: Act Press.

Grunbaum, B. (1967). *Convex Polytopes*. London: Springer.

Ha, S. C., Lowenhaupt, K., Rich, A., Kim, Y.-G., & Kim, K. K. (2005). Cristal structure of a junction between B – DNA and Z – DNA revels two extruded bases. *Nature*, *437*(7062), 1183–1186. doi:10.1038/nature04088 PMID:16237447

Hershey, A., & Chase, M. (1952). Independent functions of viral protein and nucleic acid in growth of bacteriophage. *The Journal of General Physiology*, *36*(1), 39–56. doi:10.1085/jgp.36.1.39 PMID:12981234

Karapet'yants, M. X., & Drakin, S. I. (1994). *General and Inorganic Chemistry*. Moscow: Chemistry.

Lehninger, A. L. (1982). *Principles of Biochemistry* (Vol. 1-3). New York: Worth Publisher, Inc.

Metzler, D. E. (1980). *Biochemistry. The Chemical Reactions in Living Cells* (Vol. 1-3). New York: Academic Press.

Oswald, A. T., MacLeod, C. M., & McCarty, M. (1944). Studies on the Chemical Nature of the Substance Inducing Transformation of Pneumococcal Types: Induction of Transformation by a Desoxyribonucleic Acid Fraction Isolated from Pneumococcus Type III. *The Journal of Experimental Medicine*, *79*(2), 137–158. doi:10.1084/jem.79.2.137 PMID:19871359

Poincare, A. (1895). Analysis situs. *J de e'Ecole Polytechnique.*, *1*, 1–121.

Ponnuswamy, P., & Gromiha, M. (1994). On the conformational stability of oligonucleotide duplexes and tRNA molecules. *Journal of Theoretical Biology*, *169*(4), 419–432. doi:10.1006/jtbi.1994.1163 PMID:7526075

Riemann, G. F. B. (1854). *On the Hypotheses Which Lie at the Foundations of Geometry*. Gottingen: Gottingen Observatory.

Spirin, A. S. (2019). *Molecular biology. Structure of the ribosome and protein biosynthesis*. Moscow: Knowledge Lab.

Spirin, A. S., & Gavrilova, L. P. (1971). *The Ribosome*. Moscow: Science.

Watson, J. D., & Crick, F. H. C. (1953a). Molecular structure of nucleic acids. *Nature*, *171*(4356), 738–740. doi:10.1038/171737a0 PMID:13054693

Watson, J. D., & Crick, F. H. C. (1953b). Genetical implications of the structure of deoxyribose nucleic acid. *Nature*, *171*(4361), 964–967. doi:10.1038/171964b0 PMID:13063483

Zhizhin, G. V. (2014). *World 4D*. St. Petersburg: Polytechnic Service.

Zhizhin, G. V. (2015a). The dimensions of supramolecular compounds. *Biosphere*, *7*(2), 149–154.

Zhizhin, G. V. (2015b). Dimensions of compounds in supramolecular chemistry. *Int. J. Chem. Modeling*, *7*(2), 215–238.

Zhizhin, G. V. (2016). The structures, topological and functional dimension of biomolecules. *J Chemoinformatics and Chemical Engineering*, *5*(2), 44–58.

Zhizhin, G. V. (2017). *Chemical Compound Structures and the Higher Dimension of Molecules: emerging Research and Opportunities*. Hershey, PA: IGI Global.

Zhizhin, G. V. (2018). *The Geometry of Higher – Dimensional Polytopes*. Hershey, PA: IGI Global.

Zhizhin, G. V. (2019a). The Structures of DNA taking into account the Higher Dimension of its Components. In Kosrapohr (Ed.), Encyclopedia of Organizational Knowledge, Administration, and Technologies. Hershey, PA: IGI Global. (in press)

Zhizhin, G. V. (2019b). To the Question of the Geometry of the Structure of Nucleic Acids. *Journal of the European Society of Mathematical Chemistry*, *1*(1), 1–11.

Zhizhin, G. V., & Diudea, M. V. (2016). Space of nanoworld. In M. V. Putz & C. M. Marius (Eds.), *Sustainable nanosystems, development, properties, and applications* (pp. 221–245). Hershey, PA: IGI Global.

Zhizhin, G. V., Khalaj, Z., & Diudea, M. V. (2016). Geometrical and topology dimensions of the diamond. In A. R. Ashrafi & M. V. Diudea (Eds.), *Distance, symmetry and topology in carbon nanomaterials* (pp. 167–188). New York: Springer. doi:10.1007/978-3-319-31584-3_12

KEY TERMS AND DEFINITIONS

Deoxyribonucleic Acid: A biopolymer, the monomer of which is the nucleotide.

Dimension of the Space: The number of independent parameters needed to describe the change in position of an object in space.

Nucleotide: A phosphoric acid residue attached to sugar deoxyribose, to which one of the four nitrogen bases is attached also.

Polytope: A polyhedron in the space of higher dimension.

Simplex: A convex polytope, any two vertices of which are joined by an edge.

Chapter 8
The Geometry of the Structure of Nucleic Acids With Regard to the Higher Dimension of the Components

ABSTRACT

Using three-dimensional visualization of nucleic acid molecules, obtained in the previous chapter, an analysis of the geometry of nucleic acid molecules in the space of higher dimension is carried out. It is shown that phosphoric acid residues and five-carbon sugar molecules in a double-stranded nucleic acid form polytopes of higher dimension with anti-parallel edges. These polytopes are of type n-cross-polytope (n = 5 for phosphoric acid residues, n = 13 for sugar molecules). It was found that these n-cross-polytopes located in right- and left-twisted spirals are enantiomorphic. It has been found that in cross-polytopes constructed of two sugar molecules there are 12 coordinate planes, each of which may contain a bond of nitrogenous bases (one of the 12 known ones). The formation of codons (triplets) corresponds to the separation in space of the highest dimension of nucleic acids of three-dimensional regions. This also occurs in the ribosomes upon contact with transport and adapter RNA during protein synthesis.

DOI: 10.4018/978-1-5225-9651-6.ch008

POLYTOPES WITH ANTIPARALLEL EDGES

In single - stranded and double - stranded nucleic acids (RNA, DNA), the constituents of acids (residues of phosphoric acid and sugar molecules) interact with each other (Watson & Crick, 1953a, b; Spirin & Gavrilova, 1971; Frank – Kamenetskiy, 1986, 1988). Phosphoric acid residues are connected by divalent metal ions, mainly magnesium ions, due to the interaction of negative charges of phosphoric acid residues with positive charges ions (Spirin & Gavrilova, 1971). This interaction is essential for the stability of nucleic acid structures, especially in the ribosomes. Sugar molecules interact with each other due to the hydrogen bond between the nitrogenous bases attached to the sugar molecules. Being geometric forms, the constituents of nucleic acids interact with each other to form new geometric forms - new polytopes. Nitrogenous bases are known to be flat structures. However, it is not known how nitrogenous bases are oriented in space, whether their orientation depends on the type of nitrogenous base. Currently there is no information on this. There is also no information on how exactly the metal ions are located, connecting the phosphoric acid residues. It should be remembered here that the adopted three - dimensional model of the components and the nucleic acid molecule itself is only a model for visual perception. As it was shown earlier, the phosphoric acid residue is a polytope of dimension 4, and the sugar molecule has a dimension of 12. When two phosphoric acid residues or two sugar molecules are combined, the dimension of formation in each case increases by one. In this case, as will be shown, the arrangement of flat nitrogenous bases in the space of higher dimension will become clear.

The movement of triangles along a helix leads to the formation of polytopes with antiparallel edges. Consider an arbitrary triangle *ABC* on the plane. Choose some point O' on the plane outside the triangle to his left. Let this point be the base of the axis of the helix passing through the triangle. Rotate the *ABC* triangle 180 degrees to the right, moving it up the helix, parallel to the initial plane. In the projection on the plane, both triangles *ABC* and the displaced triangle $A'B'C'$ will be located as shown in Figure 1.

It is easy to see that the edges of the triangle *ABC* and $A'B'C'$ are antiparallel. It can now connect in space the vertices of the triangle *ABC* with the vertices of the triangle $A'B'C'$ so that there are no connections of the vertices with the same letters. In a projection on the plane the connection are represented by dotted segments. It can be seen that the connecting segments also break

Figure 1. Polytopes of dimension 3 with anti – parallel edges

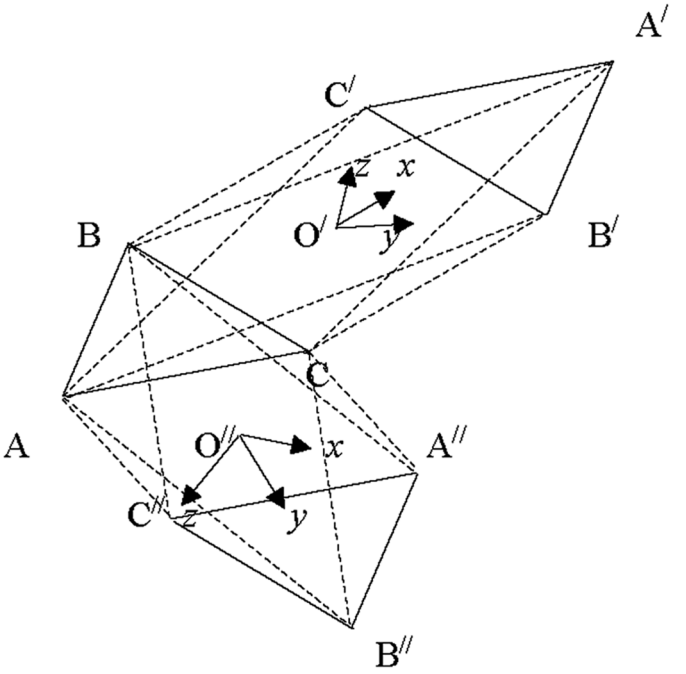

up into pairs of anti - parallel segments. Let us now verify that the image $ABCA'B'C'$ in Figure 1, along with the dotted segments, is a projection of a three - dimensional convex polytope. One use the Euler – Poincaré equation (Poincaré, 1895) for this aim

$$\sum_{k=0}^{n}(-1)^k f_k(n) = (-1)^k + 1, \tag{1}$$

f_k is the number of elements of dimension *k* in polytope of dimension *n.*

The shape $ABCA'B'C'$ in Figure 1 has 6 vertices, 12 edges, 8 triangular faces (rectangles are not faces by construction, since connecting, for example, vertex *A* with vertices B', C' it turns out to be exactly the triangle $AB'C'$). Substituting these values of elements of different dimensions into equation (4), can to find

6 – 12 +8 = 2,

i.e. the Euler – Poincaré equation holds in this case for $n = 3$. This proves that the resulting figure is a convex polytope of dimension 3 (if the figure were not convex, the Euler – Poincaré equation would be violated).

The point O' in Figure 1 coincides with the center of the three - dimensional figure $ABCA'B'C'$ as diagonal figures pass through it and point O' located on the axis of the helix. Point O' can be considered as the origin of three - dimensional space. Coordinate axes *x, y, z* in this direction emanate from directions AA', BB', CC' respectively. Three pairs of these axes define the coordinate planes of the space of this shape.

Choose some point O'' on the plane outside the triangle below it. Let this point be the base of the axis of the helix passing through the triangle. Rotate the *ABC* triangle 180 degrees to the left, moving it up the helix, parallel to the initial plane. In the projection on the plane, both triangles *ABC* and the displaced triangle $A''B''C''$ will be located as shown in Figure 1.

It is easy to see that the edges of the triangle *ABC* and $A''B''C''$ are antiparallel. It can now connect in space the vertices of the triangle *ABC* with the vertices of the triangle $A''B''C''$ so that there are no connections of the vertices with the same letters. In a projection on the plane the connection are represented by dotted segments. It can be seen that the connecting segments also break up into pairs of anti - parallel segments. Let us now verify that the image $ABCA'B'C'$ in Figure 1, along with the dotted segments, is a projection of a three - dimensional convex polytope. Obviously, a shape $ABCA''B''C''$ has as many vertices, edges, and flat faces as a shape $ABCA'B'C'$. Therefore, it satisfies the Euler – Poincaré equation (4) with dimensionality $n = 3$, i.e. it is a convex three - dimensional polyhedron. The point O'' in Figure 1 coincides with the center of the three - dimensional figure $ABCA''B''C''$ as diagonal figures pass through it and point O'' located on the axis of the helix. Point O' can be considered as the origin of three - dimensional space. Coordinate axes *x, y, z* in this direction emanate from directions AA'', BB'', CC'' respectively. The order of the coordinate axes *x, y, z* in the figures $ABCA'B'C'$ and $ABCA''B''C''$, as can be seen from Figure 1, coincide. This suggests that both figures $ABCA'B'C'$ and $ABCA''B''C''$ are topologically one and same figure - the wrong octahedron.

Interestingly, to transform an arbitrary tetrahedron $ABCD$ into a tetrahedron $A'B'C'D'$ with anti-parallel edges, it is not enough to rotate it along a helix by 180 degrees. To do this, you must turn the helix together with the tetrahedron and move the tetrahedron along the helix in the opposite direction, also rotating it 180 degrees. In the initial state, the tetrahedron on the initial helix

and the tetrahedron on the reversed helix, after its rotation by 180 degrees, will have anti -parallel edges. Both tetrahedrons can *ABCD* and $A^{/}B^{/}C^{/}D^{/}$ be present by the Figure 2 for rotation to the right. On Figure 2 the point $O^{/}$ is the point of rotation.

Now connect the vertices of the tetrahedrons so that the connecting edges (dotted segments) do not have the same letters. The resulting figure (along with dotted edges) has 8 vertices ($f_0 = 8$), 24 edges ($f_1 = 24$), 24 triangular faces ($f_2 = 24$), and 8 tetrahedrons ($f_3 = 8$). Substituting these values into equation (4), can to find

$$8 - 24 + 24 - 8 = 0.$$

Consequently, the Euler – Poincaré equation is satisfied in this case for $n = 4$. Thus, the polytope $ABCD\,A^{/}B^{/}C^{/}D^{/}$ in Figure 2 has dimension 4. It is easy to see (Zizhin, 2018) that this is 4 - cross – polytope (Grunbaum, 1967; Zhizhin, 2014; Zhizhin & Diudea, 2016).

The point $O^{/}$ in Figure 2 coincides with the center of the forth - dimensional figure $ABCD\,A^{/}B^{/}C^{/}D^{/}$ as diagonal figures pass through it and point $O^{/}$ located on the axis of the helix. Point $O^{/}$ can be considered as the origin of forth - dimensional space. Coordinate axes *x, y, z, t* in this direction emanate from directions $AA^{/}, BB^{/}, CC^{/}, DD^{/}$ respectively. Six pairs of these axes define the coordinate planes of the space of this shape.

Choose some point $O^{//}$ on the plane outside the tetrahedron *ABCD* below it. Let this point be the base of the axis of the helix passing through the tetrahedron. Rotate the *ABCD* tetrahedron 180 degrees to the left, moving it up the helix, parallel to the initial plane. In the projection on the plane, both

Figure 2. Polytope of dimension 4 with anti - parallel edges

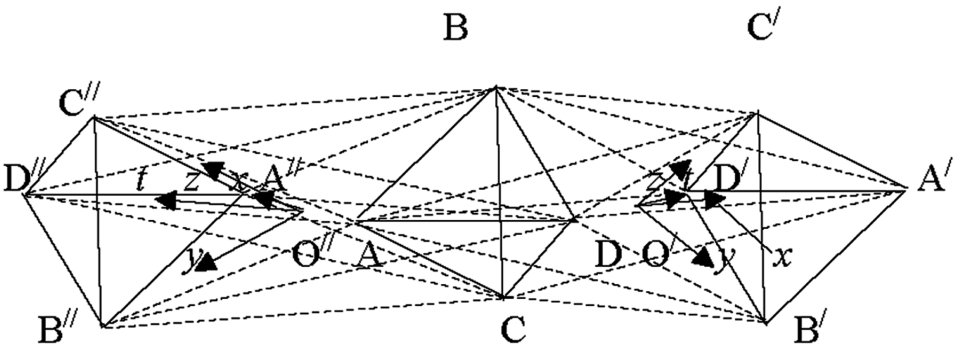

tetrahedrons *ABCD* and the displaced tetrahedron $A^{//}B^{//}C^{//}D^{//}$ will be located as shown in Figure 2.

It is easy to see that the edges of the tetrahedrons *ABCD* and $A^{//}B^{//}C^{//}D^{//}$ are antiparallel. It can now connect in space the vertices of the tetrahedron *ABCD* with the vertices of the tetrahedron $A^{//}B^{//}C^{//}D^{//}$ so that there are no connections of the vertices with the same letters. In a projection on the plane the connection are represented by dotted segments. It can be seen that the connecting segments also break up into pairs of anti - parallel segments. Let us now verify that the image *ABCD* $A^{//}B^{//}C^{//}D^{//}$ in Figure 2, along with the dotted segments, is a projection of a forth - dimensional convex polytope. Obviously, a shape *ABCD* $A^{//}B^{//}C^{//}D^{//}$ has as many vertices, edges, and flat faces as a shape *ABCD* $A^{/}B^{/}C^{/}D^{/}$. Therefore, it satisfies the Euler – Poincaré equation (4) with dimensionality $n=4$. Thus, the polytope *ABCD* $A^{//}B^{//}C^{//}D^{//}$ in Figure 2 has dimension 4. It is easy to see (Zizhin, 2018) that this is 4 - cross - polytope.

The point O'' in Figure 2 coincides with the center of the 4 – cross - polytope as diagonal figures pass through it and point $O^{//}$ located on the axis of the helix. Point $O^{//}$ can be considered as the origin of forth - dimensional space. Coordinate axes *x, y, z, t* in this direction emanate from directions $AA^{//}, BB^{//}, CC^{//}, DD^{//}$ respectively. From Figure 2 it follows that the sequence of alternation of coordinate axes *x, y, z, t* in a 4 - cross – polytope *ABCD* $A^{/}B^{/}C^{/}D^{/}$ differs from the sequence of alternation of coordinate axes *x, y, z, t* in a 4 - cross – polytope *ABCD* $A^{//}B^{//}C^{//}D^{//}$. Thus, a surprising fact emerged: the figures *ABCD* $A^{/}B^{/}C^{/}D^{/}$ and *ABCD* $A^{//}B^{//}C^{//}D^{//}$, being 4 - cross - polytopes, are topologically different from each other. It is impossible to move from one of them to another by continuous transformation, since they have a different order of alternation of vertices.

Let us now consider the figure, which is formed by two tetrahedrons with a center, which model the residues of phosphoric acid. Interestingly, to transform an arbitrary tetrahedron with a center $ABCDF$ into a tetrahedron with center $A^{/}B^{/}C^{/}D^{/}F^{/}$, which has the anti - parallel edges, it is not enough to rotate it along a helix by 180 degrees. To do this, you must turn the helix together with the tetrahedron and move the tetrahedron along the helix in the opposite direction, also rotating it 180 degrees. In the initial state, the tetrahedron with a center on the initial helix and the tetrahedron with center on the reversed helix, after its rotation by 180 degrees, will have anti -parallel

edges. Both tetrahedrons can *ABCDF* and $A^{/}B^{/}C^{/}D^{/}F^{/}$ be present by the Figure 3 for rotation to the right. On Figure 3 the point $O^{/}$ is the point of rotation.

Now connect the vertices of the tetrahedrons with center so that the connecting edges (dotted segments) do not have the same letters. The resulting figure (along with dotted edges) has 10 vertices ($f_0 = 10$), 40 edges ($f_1 = 40$), 80 triangular faces ($f_2 = 80$), 80 tetrahedrons ($f_3 = 80$) and 32 4 – cross – polytopes ($f_4 = 32$). Substituting these values into equation (4), can to find

$$10 - 40 + 80 - 80 + 32 = 2.$$

Consequently, the Euler – Poincaré equation is satisfied in this case for $n = 5$. Thus, the polytope *ABCDF* $A^{/}B^{/}C^{/}D^{/}F^{/}$ in Figure 3 has dimension 5. It is easy to see (Zizhin, 2018) that this is 5 - cross - polytope.

Figure 3. Polytope of dimension 5 with anti - parallel edges

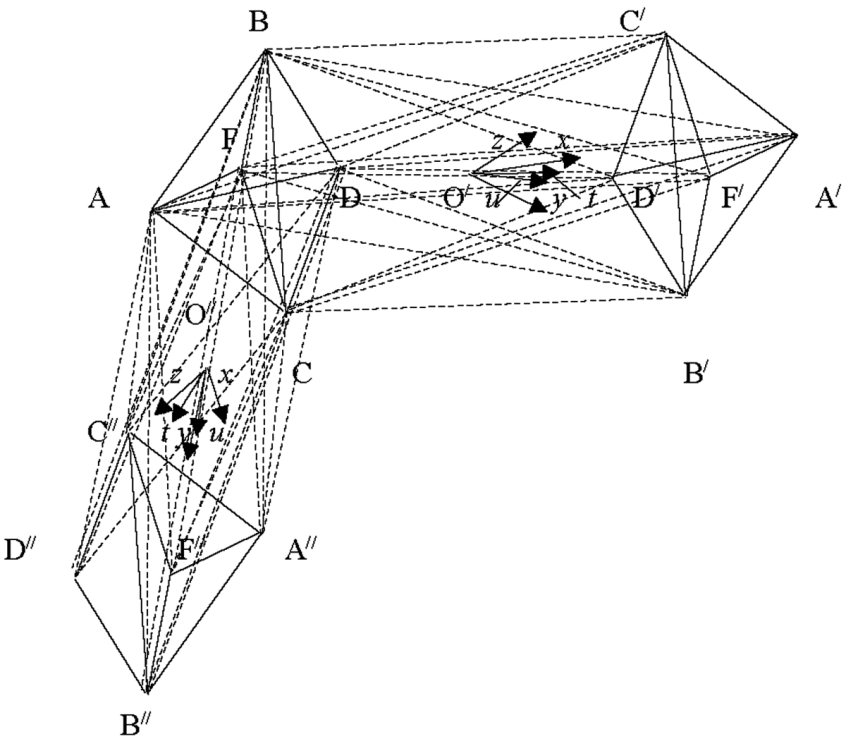

The point O' in Figure 3 coincides with the center of the five - dimensional figure *ABCDF* $A'B'C'D'F'$ as diagonal figures pass through it and point O' located on the axis of the helix. Point O' can be considered as the origin of five - dimensional space. Coordinate axes *x, y, z, t, u* in this direction emanate from directions AA', BB', CC', DD', FF' respectively.

Choose some point O'' on the plane outside the tetrahedron with a center *ABCDF* below it. Let this point be the base of the axis of the helix passing through the tetrahedron. Rotate the *ABCDF* tetrahedron with a center on 180 degrees to the left, moving it up the helix, parallel to the initial plane. In the projection on the plane, both tetrahedrons with a center *ABCDF* and the displaced tetrahedron with a center $A''B''C''D''F''$ will be located as shown in Figure 3.

It is easy to see that the edges of the tetrahedrons with a center *ABCDF* and $A''B''C''D''F''$ are antiparallel. It can now connect in space the vertices of the tetrahedron with a center *ABCDF* with the vertices of the tetrahedron with a center $A''B''C''D''F''$ so that there are no connections of the vertices with the same letters. In a projection on the plane the connection are represented by dotted segments. It can be seen that the connecting segments also break up into pairs of anti - parallel segments. Let us now verify that the image *ABCDF* $A''B''C''D''F''$ in Figure 3, along with the dotted segments, is a projection of a five - dimensional convex polytope. Obviously, a shape *ABCDF* $A''B''C''D''F''$ has as many vertices, edges, and flat faces as a shape *ABCDF* $A'B'C'D'F'$. Therefore, it satisfies the Euler – Poincaré equation (4) with dimensionality $n = 5$. Thus, the polytope *ABCDF* $A''B''C''D''F''$ in Figure 3 has dimension 5. It is easy to see (Zizhin, 2018) that this is 5 - cross - polytope.

The point O'' in Figure 3 coincides with the center of the 5 – cross - polytope as diagonal figures pass through it and point O'' located on the axis of the helix. Point O'' can be considered as the origin of five - dimensional space. Coordinate axes *x, y, z, t, u* in this direction emanate from directions $AA'', BB'', CC'', DD'', FF''$ respectively. From Figure 3 it follows that the sequence of alternation of coordinate axes *x, y, z, t, u* in a 5 - cross – polytope *ABCDF* $A'B'C'D'F'$ differs from the sequence of alternation of coordinate axes *x, y, z, t, u* in a 5 - cross – polytope *ABCDF* $A''B''C''D''F''$. Thus, also as in 4 – cross – polytope, a surprising fact emerged: the figures *ABCDF* $A'B'C'D'F'$ and *ABCDF* $A''B''C''D''F''$, being 5 - cross - polytopes, are topologically different from each other. It is impossible to move from one of

them to another by continuous transformation, since they have a different order of alternation of vertices.

Among the ten coordinate planes in the vicinity center of 5 – cross - polytope, only 4 coordinate planes have the opportunity to locate bivalent magnesium ions within themselves. These are planes based on coordinate axes passing through two vertices of a tetrahedron with a center containing an O^- ion. The second pair of vertices coordinate axes is pair of vertices coinciding with one of the four remaining vertices of a tetrahedron with a center in which there are three oxygen atoms and a phosphorus atom.

CONNECTION OF TWO FIVE – CARBON SUGAR MOLECULES IN A DOUBLE – STRADED NUCLEIC ACID MOLECULE

Let us consider in detail the formation of a polytope of dimension 13 of two sugar molecules with anti - parallel edges.

Here, as in the case of the tetrahedron, to form a polytope with antiparallel edges from two sugar molecules, you must have one sugar molecule on one helix to turn this helix together with the sugar molecule and move the sugar molecule along this reversed helix in opposite direction to the original helix direction. When the sugar molecule rotates 180 degrees to the right while moving, then the original sugar molecule and the sugar molecule on the reversed helix are two polytopes with anti - parallel edges. Both of these sugar molecules in a simplified form are represented in Figure 4 by black solid lines.

When the five - carbon sugar molecule is rotated to the left by 180 degrees, the nitrogenous bases are on opposite sides of both molecules, so that for their connection it is necessary to cross the entire set of atoms of two molecules. This is unrealistic, therefore this option is not considered. When the sugar molecule is rotated 180 degrees to the left, it is possible to connect the sugar molecules through nitrogenous bases only between two different chains of nucleic acids or in the case of turning the chain itself in the opposite direction.

In full, the sugar molecules have a dimension of 12, in the corresponding polytope each vertex must have an edge connection with all the other vertices. Knowledge of this now one need. For the formation of a polytope of dimension 13, it is necessary to connect each vertex of one polytope with the vertices of another polytope so that there are no vertex connections with the same letters. All connecting edges break into pairs of antiparallel edges. At the

Figure 4. The polytope of dimension 13 with anti – parallel edges

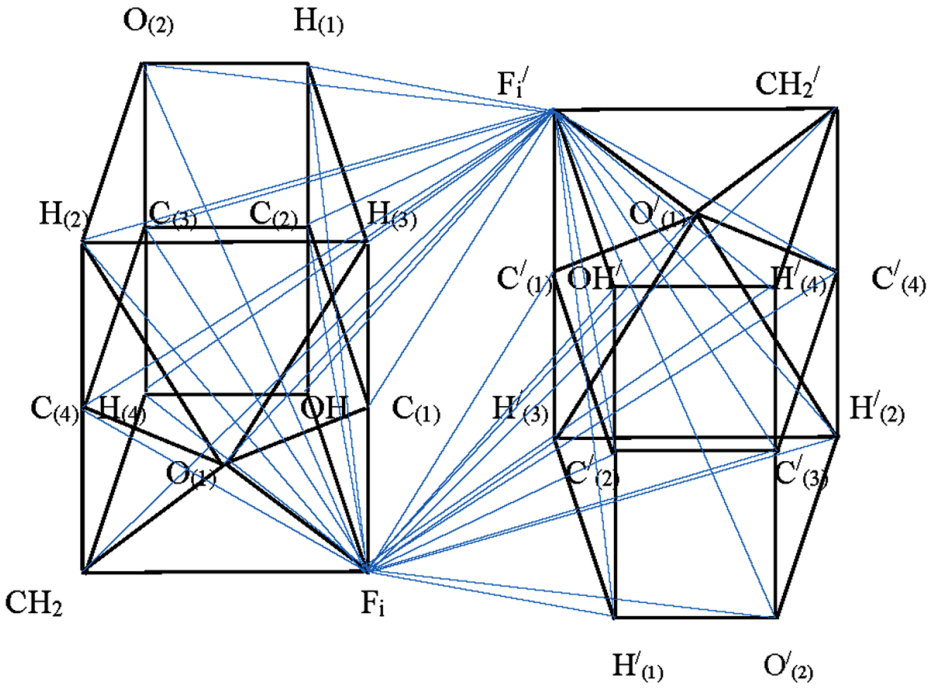

same time, a set of coordinate two - dimensional planes emanates from the center of the formed polytope as from the origin of coordinates. Their number is equal to the number of combinations from 13 to 2, i.e. 48 coordinate planes. In order to clarify the possible geometrical circumstances of the connection of helices in double - helix nucleic acid molecules with nitrogenous bases, we are primarily interested in the coordinate planes containing these nitrogenous bases $F_i, F_i^{/}$. There are exactly 12 such coordinate planes in the obtained polytope of dimension 13. They are depicted in Figure 4 by blue solid lines and are indicated below by the vertices of the polytopes contained in them

$$F_i^{/}H_{(1)},\ F_i^{/}O_{(2)},\ F_i^{/}H_{(2)},\ F_i^{/}C_{(3)},\ F_i^{/}C_{(2)},\ F_i^{/}H_{(3)},$$
$$H_{(1)}^{/}F_i,\ O_{(2)}^{/}F_i,\ H_{(2)}^{/}F_i,\ C_{(3)}^{/}F_i,\ C_{(2)}^{/}F_i,\ H_{(3)}^{/}F_i,$$

$$F_i^{/}C_{(4)},\ F_i^{/}H_{(4)},\ F_i^{/}OH,\ F_i^{/}C_{(1)},\ F_i^{/}O_{(1)},\ F_i^{/}CH_2$$
$$C_{(4)}^{/}F_i,\ H_{(4)}^{/}F_i,\ (OH)^{/}F_i,\ C_{(1)}^{/}F_i,\ O_{(1)}^{/}F_i,\ (CH_2)^{/}F_i.$$

Other edges of the polytope of dimension 13 are not shown in Figure 4, so as not to ignite the figure. In the center of each parallelogram, indicated by its four vertices, is the origin of coordinates and the corresponding pair of coordinate axes (they are not shown). To identify the different hydrogen and oxygen atoms at vertices of polytope, they indicated by numbers in brackets at the lower indices.

It is surprising that the number of coordinate planes containing vertices is exactly equal to the number of possible compounds of nitrogenous bases 12 (Spirin, 2019)

$$A:U, U:A, G:C, C:G, G:U, G:A, U:U, U:C, A\cdot A, A\cdot C.$$

Since each coordinate plane designated by the vertices of the parallelograms has a specific atomic environment, it can be assumed that each of the 12 possible compounds of nitrogenous bases is located on one particular coordinate plane out of 12 possible. This solves the question of the possible orientation of the bond of nitrogenous flat bases in nucleic acids using ideas about the high dimensionality of the constituent nucleic acids. It is also surprising that in order to create 13 – cross - polytopes, providing the connection with nitrogenous bases $F_i, F_i^{/}$, nature specially created double - stranded nucleic acids with oppositely directed spirals. This is realized in DNA and RNA when creating regions with inverted helices.

In a variety of nucleic acid molecules, the issue of chain interaction is important. In ribosomes, RNA interacts with each other due to bivalent metal ions (mainly magnesium ions). Positively charged magnesium ions attract negative charges of phosphoric acid residues, ensuring the stability of the ribosomes. In double - stranded nucleic acids, the helices are connected to each other by means of nitrogenous bases complementarily interacting with each other by a hydrogen bond. However, the magnesium ions and nitrogen bases in nucleic acids could not be specifically located. It has been established that magnesium ions and flat nitrogenous bases can be located inside special polytopes of higher dimension. Here knowledge is needed of the higher dimension of phosphoric acid residues and sugar molecules. Such polytopes are polytopes with anti - parallel edges, i.e. cross - polytopes of higher dimension. Binding agents are located on the free coordinate planes of these polytopes in the vicinity the center of the polytope.

In this case, the two - dimensional coordinate plane on the boundary of the polytope should contain the objects to be joined. In the case of magnesium

ions, there are four specific coordinate planes inside the 5 – cross - polytope, in which an ion can accommodate, combining negative charges. In the case of nitrogenous bases, the existence of 12 coordinate planes inside a cross - polytope of dimension 13, in which flat nitrogenous bases can be located, connecting the helix of nucleic acids, was discovered. Exactly as much as there are options for combining nitrogenous bases. It is given, that each coordinate plane of these 12 planes has a specific environment of atoms. It should be assumed that only one of the 12 possible compounds of nitrogenous bases is placed in each of these planes. It is surprising that the existence of higher - dimensional polytopes with anti - parallel edges is possible only in the case of the opposite direction of interacting helices, and this is exactly what nature provides in the double - helix DNA and in the RNA segments with self - inversion of the helix in the opposite direction.

GENETIC CODE IN HIGHER DIMENSION SPACE

The evidence of the higher dimension of biomolecules and nucleic acid molecules requires clarification and revision of the adopted laws of the transfer of genetic information, taking into account the higher dimension of molecules and their components. According to this view, hereditary information is encoded in a double - stranded DNA molecule by a sequence of nucleotides, more precisely, by a sequence of nitrogen bases attached to five - carbon sugar molecules. The sequence of nitrogenous bases of one of the chains of the DNA molecule in the process of transcription (or rewriting) is repeated in the process of the synthesis of the chemically related polymer RNA (single - stranded molecule). The combination of nitrogenous bases located in different helices of a double-stranded DNA molecule occurs in accordance with the principle of complementarity A (adenine) - T (thymine), T (thymine) - A (adenine), G (guanine) - C (cytosine), C (cytosine) - G (guanine). The sequence of nucleotides in the DNA molecule encodes the sequence of amino acids created in the ribosome protein. But since the number of different amino acids is 20, and the number of different nucleotides is 4, it is necessary to translate the language of nucleotides into the language of amino acids when writing these sequences. The only way of such a translation is to assign an orderly combination of several nucleotides to a particular amino acid (Gamow, 1954; Gamow et. al., 1956; Crick et. al., 1957; Crick, 1958).

It has been proven experimentally that it is triplets of nucleotides in a chain of nucleic acids that solve this problem. These triplets became known as

codons. A table of these codons has been established, numbering 64 different triplets (Nirenberg et. al., 1963; Morgan et. al., 1966; Brenner et. al., 1961). Of the 64 codons, there are semantic codons, i.e. they encode one or another amino acid, and the 3 codons do not encode any of the known amino acids. The genetic code was thus highly degenerate: most amino acids are encoded by more than one codon (Spirin, 2019).

One of the most significant achievements in biology is the experimental decoding of the genetic code, i.e. establishing a specific nucleotide composition and sequence of nucleotide triplets for all 20 amino acids that make up proteins.

Taking into account the fact of formation in this chapter of dimension 13 polytopes with antiparallel ribs as a result of the interaction of nitrogenous bases in double - stranded DNA, it can be said that each triplet distinguishes in this space a three - dimensional region bounded by coordinate planes on which are bound flat nitrogenous bases. Moreover, if the DNA molecule in the 12 - cross - polytope contains 4 coordinate planes corresponding to the standard compounds of nitrogenous bases A: T, T: A, G: C, C: T, then other of the 12 possible variants of the connection of nitrogenous bases can be found in messenger RNA (Spirin, 2019). The formation of the secondary structure of RNA due to paired interactions of adjacent regions of the same chain (Spirin, 2019) can be explained by the existence of nitrogenous bases in the nucleotide chain, located not in the region adjacent to the center of the helix, but in the peripheral region. This was shown in the previous sections of the chapter. Such arrangements of nitrogenous bases occur when the direction of rotation of the helix changes, in particular, due to the rotation of phosphoric acid residues (an object of dimension 4) around its internal degree of freedom (Zhizhin, 2019a, b).

The complementary interaction of nucleotides occurs in ribosomes during protein synthesis. Here, transport RNA and adapter RNA approach each other, and when a three - dimensional space is formed at the point of contact, surrounded by three coordinate planes containing the corresponding flat nitrogenous bases, the transfer of the corresponding amino acid to the protein chain occurs. It should be emphasized that the space in the ribosome and due to the presence of adapter RNA in it, and due to their crosslinking with divalent magnesium ions, has a sufficiently large dimension, which allows placing objects of higher dimensionality (amino acids and all protein chains, Zhizhin, 2016, 2017) in the ribosome. Note that, in accordance with the ideas of Riemann geometry, space is not infinite (Riemann, 1854). Therefore, a combination of objects of different dimensions, separated by a boundary, is possible.

REFERENCES

Brener, S., Jacob, F., & Meselson, M. (1961). An unastable intermediate carring information from genes to ribosomes for protein synthesis. *Nature*, *190*(4776), 576–581. doi:10.1038/190576a0 PMID:20446365

Crick, F. H. C. (1959). The present position of the coding problem. *Brookhaven Symposia in Biology*, *12*, 35–39. PMID:13812855

Crick, F. H. C., Griffith, J. S., & Orgel, L. E. (1957). Codes without commas. *Proceedings of the National Academy of Sciences of the United States of America*, *47*(5), 416–421. doi:10.1073/pnas.43.5.416 PMID:16590032

Frank-Kamenetskiy, M. (1986). DNA structure: A simple solution to the stability of the double helix? *Nature, 324*, 325.

Frank-Kamenetskiy, M. (1988). H – form DNA and the hairpin – triplex model. *Nature, 333*, 214.

Gamov, G. (1954). Possible relation between deoxyribonucleic acid and protein structures. *Nature*, *173*(4398), 318. doi:10.1038/173318a0

Gamov, G., Rich, A., & Ycas, M. (1956). The problem of information transfer from the nuckeic acids to proteins. *Advances in Biological and Medical Physics*, *4*, 23–68. doi:10.1016/B978-1-4832-3110-5.50006-6 PMID:13354508

Grunboum, B. (1967). *Convex Polytopes*. London: Springer.

Morgan, A. R., Wells, R. D., & Khorana, Y. G. (1966). Studies on polynucleotides, lix. further codon assignments from amino acid incorporations directed by ribopolynucleotides containing repeating trinucleotide sequences. *Proceedings of the National Academy of Sciences of the United States of America*, *56*(6), 1899–1906. doi:10.1073/pnas.56.6.1899 PMID:16591436

Nirenberg, M. W., Jones, O. W., Leder, P., Clark, B. F. C., Sly, W. S., & Pestka, S. (1963). On the coding of genetic information. *Cold Spring Harbor Symposia on Quantitative Biology*, *28*(0), 549–557. doi:10.1101/SQB.1963.028.01.074

Poincare, A. (1895). Analysis situs. *J de e'Ecole Polytechnique.*, *1*, 1–121.

Riemann, G. F. B. (1854). *On the Hypotheses Which Lie at the Foundations of Geometry*. Gottingen: Gottingen Observatory.

Spirin, A. S. (2019). *Molecular biology. The ribosomes and protein biosynthesis*. Moscow: Knowledge Lab.

Spirin, A. S., & Gavrilova, L. P. (1971). *The Ribosome*. Moscow: Science.

Watson, J. D., & Crick, F. H. C. (1953a). Molecular structure of nucleic acids. *Nature*, *171*(4356), 738–740. doi:10.1038/171737a0 PMID:13054693

Watson, J. D., & Crick, F. H. C. (1953b). Genetical implications of the structure of deoxyribose nucleic acid. *Nature*, *171*(4361), 964–967. doi:10.1038/171964b0 PMID:13063483

Zhizhin, G. V. (2014). *World 4D*. St. Petersburg: Polytechnic Service.

Zhizhin, G. V. (2016). The structures, topological and functional dimension of biomolecules. *J Chemoinformatics and Chemical Engineering*, *5*(2), 44–58.

Zhizhin, G. V. (2017). *Chemical Compound Structures and the Higher Dimension of Molecules: emerging Research and Opportunities*. Hershey, PA: IGI Global.

Zhizhin, G. V. (2018). *The Geometry of Higher – Dimensional Polytopes*. Hershey, PA: IGI Global.

Zhizhin, G. V. (2019a). The Structures of DNA taking into account the Higher Dimension of its Components. In Kosrapohr (Ed.). Encyclopedia of Organizational Knowledge, Administration, and Technologies. Hershey, PA: IGI Global. (in press)

Zhizhin, G. V. (2019b). To the Question of the Geometry of the Structure of Nucleic Acids. *Journal of the European Society of Mathematical Chemistry*, *1*(1), 1–11.

Zhizhin, G. V., & Diudea, M. V. (2016). Space of nanoworld. In M. V. Putz & C. M. Marius (Eds.), *Sustainable nanosystems, development, properties, and applications* (pp. 221–245). Hershey, PA: IGI Global.

KEY TERMS AND DEFINITIONS

Deoxyribonucleic Acid: A biopolymer, the monomer of which is the nucleotide.

Dimension of the Space: The number of independent parameters needed to describe the change in position of an object in space.

N-Cross-Polytope: A convex polytope of dimension n in which every two vertices opposite to the center of the polytope have no connection by an edges, and the remaining vertices joined by edges.

Nucleotide: A phosphoric acid residue attached to sugar deoxyribose, to which one of the four nitrogen bases is attached also.

Polytope: A polyhedron in the space of higher dimension.

Ribosome: The most important non-membrane organelle of a living cell, which serves for protein biosynthesis from amino acids in a given matrix based on genetic information provided by messenger RNA (mRNA).

Simplex: A convex polytope, any two vertices of which are joined by an edge.

Related Readings

To continue IGI Global's long-standing tradition of advancing innovation through emerging research, please find below a compiled list of recommended IGI Global book chapters and journal articles in the areas of molecular biology, genetics, and big data. These related readings will provide additional information and guidance to further enrich your knowledge and assist you with your own research.

Agarwal, P., & Mehta, S. (2019). Subspace Clustering of High Dimensional Data Using Differential Evolution. In H. Banati, S. Mehta, & P. Kaur (Eds.), *Nature-Inspired Algorithms for Big Data Frameworks* (pp. 47–74). Hershey, PA: IGI Global. doi:10.4018/978-1-5225-5852-1.ch003

Agarwalla, P., & Mukhopadhyay, S. (2018). Selection of Pathway Markers for Cancer Using Collaborative Binary Multi-Swarm Optimization. In M. Lytras & P. Papadopoulou (Eds.), *Applying Big Data Analytics in Bioinformatics and Medicine* (pp. 337–363). Hershey, PA: IGI Global. doi:10.4018/978-1-5225-2607-0.ch014

Agarwalla, P., & Mukhopadhyay, S. (2019). Wolf-Swarm Colony for Signature Gene Selection Using Weighted Objective Method. In H. Banati, S. Mehta, & P. Kaur (Eds.), *Nature-Inspired Algorithms for Big Data Frameworks* (pp. 170–195). Hershey, PA: IGI Global. doi:10.4018/978-1-5225-5852-1.ch007

Al Mazari, A. (2018). Computational and Data Mining Perspectives on HIV/AIDS in Big Data Era: Opportunities, Challenges, and Future Directions. In A. Al Mazari (Ed.), *Big Data Analytics in HIV/AIDS Research* (pp. 81–116). Hershey, PA: IGI Global. doi:10.4018/978-1-5225-3203-3.ch004

Andrade, S. F., & Modesto, L. M. (2017). Architecture with Multi-Agent for Environmental Risk Assessment by Chemical Contamination. In D. Adamatti (Ed.), *Multi-Agent-Based Simulations Applied to Biological and Environmental Systems* (pp. 180–211). Hershey, PA: IGI Global. doi:10.4018/978-1-5225-1756-6.ch008

Ansari, M. T., & Pandey, D. (2018). Risks, Security, and Privacy for HIV/AIDS Data: Big Data Perspective. In A. Al Mazari (Ed.), *Big Data Analytics in HIV/AIDS Research* (pp. 117–139). Hershey, PA: IGI Global. doi:10.4018/978-1-5225-3203-3.ch005

Arora, A., Srivastava, A., & Bansal, S. (2019). Graph and Neural Network-Based Intelligent Conversation System. In H. Banati, S. Mehta, & P. Kaur (Eds.), *Nature-Inspired Algorithms for Big Data Frameworks* (pp. 339–357). Hershey, PA: IGI Global. doi:10.4018/978-1-5225-5852-1.ch014

Ballet, P., Rivière, J., Pothet, A., Theron, M., Pichavant, K., Abautret, F., ... Rodin, V. (2017). Modelling and Simulating Complex Systems in Biology: Introducing NetBioDyn – A Pedagogical and Intuitive Agent-Based Software. In D. Adamatti (Ed.), *Multi-Agent-Based Simulations Applied to Biological and Environmental Systems* (pp. 128–158). Hershey, PA: IGI Global. doi:10.4018/978-1-5225-1756-6.ch006

Bansal, A., & Srivastava, P. A. (2018). Transcriptomics to Metabolomics: A Network Perspective for Big Data. In M. Lytras & P. Papadopoulou (Eds.), *Applying Big Data Analytics in Bioinformatics and Medicine* (pp. 188–206). Hershey, PA: IGI Global. doi:10.4018/978-1-5225-2607-0.ch008

Banu, P. K., & Samraj, S. A. (2017). Swarm-Based Clustering for Gene Expression Data. In D. Acharjya & A. Mitra (Eds.), *Bio-Inspired Computing for Information Retrieval Applications* (pp. 123–149). Hershey, PA: IGI Global. doi:10.4018/978-1-5225-2375-8.ch005

Belayachi, N., Amrani, F., & Bouamrane, K. (2018). A Decision-Making Tool for the Optimization of Empty Containers' Return in the Liner Shipping: Optimization by Using the Genetic Algorithm. *International Journal of Decision Support System Technology*, *10*(3), 39–56. doi:10.4018/IJDSST.2018070103

Ben Halima, N. (2019). *Unique Sequence Signatures in Plant Lipolytic Enzymes: Emerging Research and Opportunities*. Hershey, PA: IGI Global. doi:10.4018/978-1-5225-7482-8

Biswas, R. N., Saha, A., Mitra, S. K., & Naskar, M. K. (2019). PSO-Based Antenna Pattern Synthesis: A Paradigm for Secured Data Communications. In H. Banati, S. Mehta, & P. Kaur (Eds.), *Nature-Inspired Algorithms for Big Data Frameworks* (pp. 218–245). Hershey, PA: IGI Global. doi:10.4018/978-1-5225-5852-1.ch009

Born, M. B., Adamatti, D. F., Sanchotene de Aguiar, M., & Schiavon de Souza, W. (2017). Use SUMO Simulator for the Determination of Light Times in Order to Reduce Pollution: A Case Study in the City Center of Rio Grande, Brazil. In D. Adamatti (Ed.), *Multi-Agent-Based Simulations Applied to Biological and Environmental Systems* (pp. 227–240). Hershey, PA: IGI Global. doi:10.4018/978-1-5225-1756-6.ch010

Briot, J., Irving, M. D., Filho, J. E., Mendes de Melo, G., Alvarez, I., Sordoni, A., & Pereira de Lucena, C. J. (2017). Participatory Management of Protected Areas for Biodiversity Conservation and Social Inclusion: Experience of the SimParc Multi-Agent-Based Serious Game. In D. Adamatti (Ed.), *Multi-Agent-Based Simulations Applied to Biological and Environmental Systems* (pp. 295–332). Hershey, PA: IGI Global. doi:10.4018/978-1-5225-1756-6.ch013

Celik, S., Albayrak, A. T., Akyuz, S., & Ozel, A. E. (2019). The Importance of Ionic Liquids and Applications on Their Molecular Modeling. In C. Chen & S. Cheung (Eds.), *Computational Models for Biomedical Reasoning and Problem Solving* (pp. 206–230). Hershey, PA: IGI Global. doi:10.4018/978-1-5225-7467-5.ch008

Celik, S., Ozkok, F., Akyuz, S., & Ozel, A. E. (2019). The Importance of Anthraquinone and Its Analogues and Molecular Docking Calculation. In C. Chen & S. Cheung (Eds.), *Computational Models for Biomedical Reasoning and Problem Solving* (pp. 177–205). Hershey, PA: IGI Global. doi:10.4018/978-1-5225-7467-5.ch007

Chakraborty, H. J., Gangopadhyay, A., Ganguli, S., & Datta, A. (2018). Protein Structure Prediction. In M. Lytras & P. Papadopoulou (Eds.), *Applying Big Data Analytics in Bioinformatics and Medicine* (pp. 48–79). Hershey, PA: IGI Global. doi:10.4018/978-1-5225-2607-0.ch003

Corrêa, L. D., & Dorn, M. (2017). Multi-Agent Systems in Three-Dimensional Protein Structure Prediction. In D. Adamatti (Ed.), *Multi-Agent-Based Simulations Applied to Biological and Environmental Systems* (pp. 241–278). Hershey, PA: IGI Global. doi:10.4018/978-1-5225-1756-6.ch011

Cortés, A. J. (2018). Prevalence in MSM Is Enhanced by Role Versatility. In A. Al Mazari (Ed.), *Big Data Analytics in HIV/AIDS Research* (pp. 140–148). Hershey, PA: IGI Global. doi:10.4018/978-1-5225-3203-3.ch006

Costa, A. C. (2017). Ecosystems as Agent Societies, Landscapes as Multi-Societal Agent Systems. In D. Adamatti (Ed.), *Multi-Agent-Based Simulations Applied to Biological and Environmental Systems* (pp. 25–43). Hershey, PA: IGI Global. doi:10.4018/978-1-5225-1756-6.ch002

Dara, S., & Tiwari, A. K. (2017). Application of Optimization Techniques for Gene Expression Data Analysis. In P. Kumar & A. Tiwari (Eds.), *Ubiquitous Machine Learning and Its Applications* (pp. 168–180). Hershey, PA: IGI Global. doi:10.4018/978-1-5225-2545-5.ch008

Das, S., & Das, A. K. (2018). Probability Based Most Informative Gene Selection From Microarray Data. *International Journal of Rough Sets and Data Analysis*, *5*(1), 1–12. doi:10.4018/IJRSDA.2018010101

Elrashedy, A. A. (2018). HIV-Associated Neurocognitive Disorder: The Interaction Between HIV-1 and Dopamine Transporter Structure. In A. Al Mazari (Ed.), *Big Data Analytics in HIV/AIDS Research* (pp. 171–205). Hershey, PA: IGI Global. doi:10.4018/978-1-5225-3203-3.ch008

Elsayad, D., Ali, A., Shedeed, H. A., & Tolba, M. F. (2017). PAGeneRN: Parallel Architecture for Gene Regulatory Network. In A. Hassanien & T. Gaber (Eds.), *Handbook of Research on Machine Learning Innovations and Trends* (pp. 762–786). Hershey, PA: IGI Global. doi:10.4018/978-1-5225-2229-4.ch034

Fonseca de Moraes, M., Adamatti, D. F., Oliveira de Borba, A., Werhli, A. V., & von Groll, A. (2017). Using Probability Distributions in Parameters of Variables at Agent-Based Simulations: A Case Study for the TB Bacillus Growth Curve. In D. Adamatti (Ed.), *Multi-Agent-Based Simulations Applied to Biological and Environmental Systems* (pp. 333–355). Hershey, PA: IGI Global. doi:10.4018/978-1-5225-1756-6.ch014

Gallo, C. (2018). Building Gene Networks by Analyzing Gene Expression Profiles. In M. Khosrow-Pour, D.B.A. (Ed.), Encyclopedia of Information Science and Technology, Fourth Edition (pp. 440-454). Hershey, PA: IGI Global. doi:10.4018/978-1-5225-2255-3.ch039

Gangopadhyay, A., Chakraborty, H. J., & Datta, A. (2018). Protein Docking and Drug Design. In M. Lytras & P. Papadopoulou (Eds.), *Applying Big Data Analytics in Bioinformatics and Medicine* (pp. 207–241). Hershey, PA: IGI Global. doi:10.4018/978-1-5225-2607-0.ch009

Goswami, S. (2018). Proteomics in Personalized Medicine: An Evolution Not a Revolution. In M. Lytras & P. Papadopoulou (Eds.), *Applying Big Data Analytics in Bioinformatics and Medicine* (pp. 80–98). Hershey, PA: IGI Global. doi:10.4018/978-1-5225-2607-0.ch004

Goyal, M., & Krishnamurthi, R. (2019). Pedagogical Software Agents for Personalized E-Learning Using Soft Computing Techniques. In H. Banati, S. Mehta, & P. Kaur (Eds.), *Nature-Inspired Algorithms for Big Data Frameworks* (pp. 319–338). Hershey, PA: IGI Global. doi:10.4018/978-1-5225-5852-1.ch013

Gutiérrez, J. M., Sánchez-Alonso, S., Sicilia, M., & Barriocanal, E. G. (2018). Predicting Patterns in Hospital Admission Data. In M. Lytras & P. Papadopoulou (Eds.), *Applying Big Data Analytics in Bioinformatics and Medicine* (pp. 322–336). Hershey, PA: IGI Global. doi:10.4018/978-1-5225-2607-0.ch013

Hao, Y., Weiss, G. M., & Brown, S. M. (2018). Identification of Candidate Genes Responsible for Age-related Macular Degeneration using Microarray Data. *International Journal of Service Science, Management, Engineering, and Technology*, *9*(2), 33–60. doi:10.4018/IJSSMET.2018040102

Hertzberg, L., Yitzhaky, A., & Pasmanik-Chor, M. (2018). GEView (Gene Expression View) Tool for Intuitive and High Accessible Visualization of Expression Data for Non-Programmer Biologists. *International Journal of Knowledge Discovery in Bioinformatics*, *8*(1), 94–105. doi:10.4018/IJKDB.2018010107

Hiremath, N. B., & Dayananda, P. (2019). Machine Learning Techniques for Analysis of Human Genome Data. *International Journal of Smart Education and Urban Society*, *10*(1), 49–63. doi:10.4018/IJSEUS.2019010105

Idowu, P. A., & Balogun, J. A. (2019). Development of a Classification Model for CD4 Count of HIV Patients Using Supervised Machine Learning Algorithms: A Comparative Analysis. In C. Chen & S. Cheung (Eds.), *Computational Models for Biomedical Reasoning and Problem Solving* (pp. 149–176). Hershey, PA: IGI Global. doi:10.4018/978-1-5225-7467-5.ch006

Jarouliya, U., & Keservani, R. K. (2017). Genomics and Proteomic Approach in the Treatment of Various Human Diseases: Applications of Genomics and Proteomics. In R. Keservani, A. Sharma, & R. Kesharwani (Eds.), *Recent Advances in Drug Delivery Technology* (pp. 97–123). Hershey, PA: IGI Global. doi:10.4018/978-1-5225-0754-3.ch004

Jayarathna, S., Jayawardana, Y., Jaime, M., & Thapaliya, S. (2019). Electroencephalogram (EEG) for Delineating Objective Measure of Autism Spectrum Disorder. In C. Chen & S. Cheung (Eds.), *Computational Models for Biomedical Reasoning and Problem Solving* (pp. 34–65). Hershey, PA: IGI Global. doi:10.4018/978-1-5225-7467-5.ch002

Ji, B., Zhang, W., Li, R., & Ji, H. (2019). Deep Learning Models for Biomedical Image Analysis. In C. Chen & S. Cheung (Eds.), *Computational Models for Biomedical Reasoning and Problem Solving* (pp. 128–148). Hershey, PA: IGI Global. doi:10.4018/978-1-5225-7467-5.ch005

Jyothi, S., & P, B. (2018). Data Science and Computational Biology. In S. Karthik, A. Paul, & N. Karthikeyan (Eds.), *Deep Learning Innovations and Their Convergence With Big Data* (pp. 152-172). Hershey, PA: IGI Global. doi:10.4018/978-1-5225-3015-2.ch009

Kasemsap, K. (2018). Bioinformatics: Applications and Implications. In M. Lytras & P. Papadopoulou (Eds.), *Applying Big Data Analytics in Bioinformatics and Medicine* (pp. 26–47). Hershey, PA: IGI Global. doi:10.4018/978-1-5225-2607-0.ch002

Kashyap, R. (2019). Computational Healthcare System With Image Analysis. In C. Chen & S. Cheung (Eds.), *Computational Models for Biomedical Reasoning and Problem Solving* (pp. 89–127). Hershey, PA: IGI Global. doi:10.4018/978-1-5225-7467-5.ch004

Kaur, P., & Sharma, M. (2017). A Survey on Using Nature Inspired Computing for Fatal Disease Diagnosis. *International Journal of Information System Modeling and Design*, *8*(2), 70–91. doi:10.4018/IJISMD.2017040105

Kaushik, A., Indu, S., & Gupta, D. (2019). Nature-Inspired Algorithms in Wireless Sensor Networks. In H. Banati, S. Mehta, & P. Kaur (Eds.), *Nature-Inspired Algorithms for Big Data Frameworks* (pp. 246–275). Hershey, PA: IGI Global. doi:10.4018/978-1-5225-5852-1.ch010

Khatri, N., & Madan, A. K. (2017). Path Pendeccentric Connectivity Indices: Detour Matrix Based Molecular Descriptors for QSAR/QSPR Studies, Part 2: Development of Models for TTK Inhibitory Activity of Acetamide/Carboxamide Analogs. *International Journal of Quantitative Structure-Property Relationships*, *2*(2), 75–89. doi:10.4018/IJQSPR.2017070107

Konagala, P. (2019). Big Data Analytics Using Apache Hive to Analyze Health Data. In H. Banati, S. Mehta, & P. Kaur (Eds.), *Nature-Inspired Algorithms for Big Data Frameworks* (pp. 358–372). Hershey, PA: IGI Global. doi:10.4018/978-1-5225-5852-1.ch015

Kumar, D., Kumar, S., Bansal, R., & Singla, P. (2017). A Survey to Nature Inspired Soft Computing. *International Journal of Information System Modeling and Design*, *8*(2), 112–133. doi:10.4018/IJISMD.2017040107

Kumar, H., Chandramohan, V., Simon, S. M., Yadav, R., & Kumar, S. (2018). Big Data Analysis Techniques for Visualization of Genomics in Medicinal Plants. In R. Segall & J. Cook (Eds.), *Handbook of Research on Big Data Storage and Visualization Techniques* (pp. 749–781). Hershey, PA: IGI Global. doi:10.4018/978-1-5225-3142-5.ch026

Machado, D. O., Adamatti, D. F., & Gonçalves, E. M. (2017). Microbial Fuel Cells Using Agent-Based Simulation: Review and Basic Modeling. In D. Adamatti (Ed.), *Multi-Agent-Based Simulations Applied to Biological and Environmental Systems* (pp. 212–226). Hershey, PA: IGI Global. doi:10.4018/978-1-5225-1756-6.ch009

Magessi, N. T., & Antunes, L. (2017). Ignition of Algorithm Mind: The Role of Energy in Neuronal Assemblies. In D. Adamatti (Ed.), *Multi-Agent-Based Simulations Applied to Biological and Environmental Systems* (pp. 1–24). Hershey, PA: IGI Global. doi:10.4018/978-1-5225-1756-6.ch001

Mehta, S., & Kaur, P. (2019). Scheduling Data Intensive Scientific Workflows in Cloud Environment Using Nature Inspired Algorithms. In H. Banati, S. Mehta, & P. Kaur (Eds.), *Nature-Inspired Algorithms for Big Data Frameworks* (pp. 196–217). Hershey, PA: IGI Global. doi:10.4018/978-1-5225-5852-1.ch008

Michalek, A. M., Jayawardena, G., & Jayarathna, S. (2019). Predicting ADHD Using Eye Gaze Metrics Indexing Working Memory Capacity. In C. Chen & S. Cheung (Eds.), *Computational Models for Biomedical Reasoning and Problem Solving* (pp. 66–88). Hershey, PA: IGI Global. doi:10.4018/978-1-5225-7467-5.ch003

Mittal, R., & Bhatia, M. P. (2019). Analysis of Multiplex Social Networks Using Nature-Inspired Algorithms. In H. Banati, S. Mehta, & P. Kaur (Eds.), *Nature-Inspired Algorithms for Big Data Frameworks* (pp. 290–318). Hershey, PA: IGI Global. doi:10.4018/978-1-5225-5852-1.ch012

Mohapatra, C., Acharya, B., Rautaray, S. S., & Pandey, M. (2018). Usage of Big Data Prediction Techniques for Predictive Analysis in HIV/AIDS. In A. Al Mazari (Ed.), *Big Data Analytics in HIV/AIDS Research* (pp. 54–80). Hershey, PA: IGI Global. doi:10.4018/978-1-5225-3203-3.ch003

Montagna, S., & Omicini, A. (2017). Agent-Based Modelling in Multicellular Systems Biology. In D. Adamatti (Ed.), *Multi-Agent-Based Simulations Applied to Biological and Environmental Systems* (pp. 159–178). Hershey, PA: IGI Global. doi:10.4018/978-1-5225-1756-6.ch007

Mukhopadhyay, S., & Das, S. (2019). Application of Nature-Inspired Algorithms for Sensing Error Optimisation in Dynamic Environment. In H. Banati, S. Mehta, & P. Kaur (Eds.), *Nature-Inspired Algorithms for Big Data Frameworks* (pp. 124–169). Hershey, PA: IGI Global. doi:10.4018/978-1-5225-5852-1.ch006

Munugala, S., Brar, G. K., Syed, A., Mohammad, A., & Halgamuge, M. N. (2018). The Much Needed Security and Data Reforms of Cloud Computing in Medical Data Storage. In M. Lytras & P. Papadopoulou (Eds.), *Applying Big Data Analytics in Bioinformatics and Medicine* (pp. 99–113). Hershey, PA: IGI Global. doi:10.4018/978-1-5225-2607-0.ch005

Nawaz, M. S., Mustafa, R. U., & Lali, M. I. (2018). Role of Online Data from Search Engine and Social Media in Healthcare Informatics. In M. Lytras & P. Papadopoulou (Eds.), *Applying Big Data Analytics in Bioinformatics and Medicine* (pp. 272–293). Hershey, PA: IGI Global. doi:10.4018/978-1-5225-2607-0.ch011

Nishiwaki, K., Kanamori, K., & Ohwada, H. (2017). Gene Selection from Microarray Data for Alzheimer's Disease Using Random Forest. *International Journal of Software Science and Computational Intelligence*, *9*(2), 14–30. doi:10.4018/IJSSCI.2017040102

Papadopoulou, P., Lytras, M., & Marouli, C. (2018). Bioinformatics as Applied to Medicine: Challenges Faced Moving from Big Data to Smart Data to Wise Data. In M. Lytras & P. Papadopoulou (Eds.), *Applying Big Data Analytics in Bioinformatics and Medicine* (pp. 1–25). Hershey, PA: IGI Global. doi:10.4018/978-1-5225-2607-0.ch001

Pinheiro, P. R., Pinheiro, M. C., Damasceno, V. C., Marques, M. C., Araújo, R. S., & Branco, L. M. (2018). Applying Bayesian Networks in the Early Diagnosis of Bulimia and Anorexia Nervosa in Adolescents: Applying Bayesian Networks in Early Diagnosis in Adolescents. In M. Lytras & P. Papadopoulou (Eds.), *Applying Big Data Analytics in Bioinformatics and Medicine* (pp. 364–379). Hershey, PA: IGI Global. doi:10.4018/978-1-5225-2607-0.ch015

Porcellis, D. D., Adamatti, D. F., & Abreu, P. C. (2017). Biomass Variation Phytoplanktons Using Agent-Based Simulation: A Case Study to Estuary of the Patos Lagoon. In D. Adamatti (Ed.), *Multi-Agent-Based Simulations Applied to Biological and Environmental Systems* (pp. 279–294). Hershey, PA: IGI Global. doi:10.4018/978-1-5225-1756-6.ch012

Portegys, T., Pascualy, G., Gordon, R., McGrew, S. P., & Alicea, B. J. (2017). Morphozoic, Cellular Automata with Nested Neighborhoods as a Metamorphic Representation of Morphogenesis. In D. Adamatti (Ed.), *Multi-Agent-Based Simulations Applied to Biological and Environmental Systems* (pp. 44–80). Hershey, PA: IGI Global. doi:10.4018/978-1-5225-1756-6.ch003

Ralha, C. G., & Abreu, C. G. (2017). Mase: A Multi-Agent-Based Environmental Simulator. In D. Adamatti (Ed.), *Multi-Agent-Based Simulations Applied to Biological and Environmental Systems* (pp. 106–127). Hershey, PA: IGI Global. doi:10.4018/978-1-5225-1756-6.ch005

Ramamoorthy, S., & Sivasubramaniam, R. (2018). Image Processing Including Medical Liver Imaging: Medical Image Processing from Big Data Perspective, Ultrasound Liver Images, Challenges. In M. Lytras & P. Papadopoulou (Eds.), *Applying Big Data Analytics in Bioinformatics and Medicine* (pp. 380–392). Hershey, PA: IGI Global. doi:10.4018/978-1-5225-2607-0.ch016

Rocha, V., & Brandão, A. A. (2017). A Scalable Multiagent Architecture for Monitoring Biodiversity Scenarios. In D. Adamatti (Ed.), *Multi-Agent-Based Simulations Applied to Biological and Environmental Systems* (pp. 81–105). Hershey, PA: IGI Global. doi:10.4018/978-1-5225-1756-6.ch004

Roy, A. G., & Peyada, N. K. (2019). Aircraft Aerodynamic Parameter Estimation Using Intelligent Estimation Algorithms. In H. Banati, S. Mehta, & P. Kaur (Eds.), *Nature-Inspired Algorithms for Big Data Frameworks* (pp. 276–288). Hershey, PA: IGI Global. doi:10.4018/978-1-5225-5852-1.ch011

Roy, A. G., & Rakshit, P. (2019). Motion Planning of Non-Holonomic Wheeled Robots Using Modified Bat Algorithm. In H. Banati, S. Mehta, & P. Kaur (Eds.), *Nature-Inspired Algorithms for Big Data Frameworks* (pp. 94–123). Hershey, PA: IGI Global. doi:10.4018/978-1-5225-5852-1.ch005

Sajja, P. S., & Akerkar, R. (2019). Deep Learning for Big Data Analytics. In H. Banati, S. Mehta, & P. Kaur (Eds.), *Nature-Inspired Algorithms for Big Data Frameworks* (pp. 1–21). Hershey, PA: IGI Global. doi:10.4018/978-1-5225-5852-1.ch001

Sarigiannis, D. A., Gotti, A., Handakas, E., & Karakitsios, S. P. (2018). Informatics and Data Analytics to Support Exposome-Based Discovery: Part 2 - Computational Exposure Biology. In M. Lytras & P. Papadopoulou (Eds.), *Applying Big Data Analytics in Bioinformatics and Medicine* (pp. 145–187). Hershey, PA: IGI Global. doi:10.4018/978-1-5225-2607-0.ch007

Sarigiannis, D. A., Karakitsios, S. P., Handakas, E., Papadaki, K., Chapizanis, D., & Gotti, A. (2018). Informatics and Data Analytics to Support Exposome-Based Discovery: Part 1 - Assessment of External and Internal Exposure. In M. Lytras & P. Papadopoulou (Eds.), *Applying Big Data Analytics in Bioinformatics and Medicine* (pp. 115–144). Hershey, PA: IGI Global. doi:10.4018/978-1-5225-2607-0.ch006

Sedkaoui, S. (2018). Statistical and Computational Needs for Big Data Challenges. In A. Al Mazari (Ed.), *Big Data Analytics in HIV/AIDS Research* (pp. 21–53). Hershey, PA: IGI Global. doi:10.4018/978-1-5225-3203-3.ch002

Settouti, N., Daho, M. E., Bechar, M. E., & Chikh, M. A. (2018). An Optimized Semi-Supervised Learning Approach for High Dimensional Datasets. In M. Lytras & P. Papadopoulou (Eds.), *Applying Big Data Analytics in Bioinformatics and Medicine* (pp. 294–321). Hershey, PA: IGI Global. doi:10.4018/978-1-5225-2607-0.ch012

Singh, D., Sisodia, D. S., & Singh, P. (2019). Genetic Algorithm Based Pre-Processing Strategy for High Dimensional Micro-Array Gene Classification: Application of Nature Inspired Intelligence. In H. Banati, S. Mehta, & P. Kaur (Eds.), *Nature-Inspired Algorithms for Big Data Frameworks* (pp. 22–46). Hershey, PA: IGI Global. doi:10.4018/978-1-5225-5852-1.ch002

Spruit, M., & Lammertink, M. (2018). Effective and Efficient Business Intelligence Dashboard Design: Gestalt Theory in Dutch Long-Term and Chronic Healthcare. In M. Lytras & P. Papadopoulou (Eds.), *Applying Big Data Analytics in Bioinformatics and Medicine* (pp. 243–271). Hershey, PA: IGI Global. doi:10.4018/978-1-5225-2607-0.ch010

Subramanian, A. A. (2019). Nature Inspired Feature Selector for Effective Data Classification in Big Data Frameworks. In H. Banati, S. Mehta, & P. Kaur (Eds.), *Nature-Inspired Algorithms for Big Data Frameworks* (pp. 75–92). Hershey, PA: IGI Global. doi:10.4018/978-1-5225-5852-1.ch004

Unissa, A. N., & Hanna, L. E. (2018). Computational Analysis of Reverse Transcriptase Resistance to Inhibitors in HIV-1. In A. Al Mazari (Ed.), *Big Data Analytics in HIV/AIDS Research* (pp. 1–20). Hershey, PA: IGI Global. doi:10.4018/978-1-5225-3203-3.ch001

Unissa, A. N., & Hanna, L. E. (2018). Dissection of HIV-1 Protease Subtype B Inhibitors Resistance Through Molecular Modeling Approaches: Resistance to Protease Inhibitors. In A. Al Mazari (Ed.), *Big Data Analytics in HIV/AIDS Research* (pp. 149–170). Hershey, PA: IGI Global. doi:10.4018/978-1-5225-3203-3.ch007

Vimal, M. (2017). Gene, Genomics and Networks. *International Journal of Actor-Network Theory and Technological Innovation*, *9*(1), 1–12. doi:10.4018/IJANTTI.2017010101

Wambuguh, O. J. (2019). *Examining the Causal Relationship Between Genes, Epigenetics, and Human Health* (pp. 1–603). Hershey, PA: IGI Global. doi:10.4018/978-1-5225-8066-9

Welch, K. C., Lahiri, U., Warren, Z. E., & Sarkar, N. (2019). A System to Measure Physiological Response During Social Interaction in VR for Children With ASD. In C. Chen & S. Cheung (Eds.), *Computational Models for Biomedical Reasoning and Problem Solving* (pp. 1–33). Hershey, PA: IGI Global. doi:10.4018/978-1-5225-7467-5.ch001

Yoshida, R., Hara, H., & Saluke, P. M. (2019). Sequential Importance Sampling for Logistic Regression Model. In C. Chen & S. Cheung (Eds.), *Computational Models for Biomedical Reasoning and Problem Solving* (pp. 231–255). Hershey, PA: IGI Global. doi:10.4018/978-1-5225-7467-5.ch009

Yu, X., Li, X., Deng, H., Tang, Y., Hou, Z., & Kong, Q. (2019). The Research on the Osmotic Stress Gene Mining Model Based on the Arabidopsis Genome. *Journal of Information Technology Research*, *12*(1), 117–132. doi:10.4018/JITR.2019010109

Zhang, G., Gong, X., & Chen, X. (2017). PID Control Algorithm Based on Genetic Algorithm and its Application in Electric Cylinder Control. *International Journal of Information Technology and Web Engineering*, *12*(3), 51–61. doi:10.4018/IJITWE.2017070105

Zhizhin, G. V. (2018). *Chemical Compound Structures and the Higher Dimension of Molecules: Emerging Research and Opportunities*. Hershey, PA: IGI Global. doi:10.4018/978-1-5225-4108-0

Zhizhin, G. V. (2019). *The Geometry of Higher-Dimensional Polytopes*. Hershey, PA: IGI Global. doi:10.4018/978-1-5225-6968-8

Index

R

S

T

Z